ROYAUME DU MAROC
Université Mohammed V - RABAT -
جامعة محمد الخامس – الرباط –
Faculté des sciences
كلية العلوم
CENTRE D'ETUDES DOCTORALES - SCIENCES ET TECHNOLOGIES

N° d'ordre: **3404**

THESE

In order to obtain the title of : ***Doctor of Philosophy***

Research Center: Center of Materials Science
Laboratory: Laboratory of Materials, Nanotechnologies and Environment
Research Group: ***Composite Materials, Polymers and Environment***
Discipline: Chemistry
Specialty: Materials sciences

Dissertation Defended in 24/12/2020

by:

Maryama HAMMI

Studies of lead phosphate glass based composites in bulk and thin films forms: Promising materials for thermo-electricity and photovoltaic applications

JURY

Ahmed EL YAHYAOUI	PES	Faculté des Sciences, Université Mohammed V – Rabat – Maroc	Président
Abdelkrim MAAROUFI	PES	Faculté des Sciences, Université Mohammed V – Rabat – Maroc	Directeur de thèse
M'Hamed TAIBI	PES	École Normale Supérieure, Université Mohammed V – Rabat – Maroc	Rapporteur / Examinateur
Rachid BENCHRIFA	PES	Faculté des Sciences, Université Mohammed V – Rabat – Maroc	Rapporteur / Examinateur
Mohammed BENAISSA	PES	Faculté des Sciences, Université Mohammed V– Rabat – Maroc	Rapporteur / Examinateur
Aumeur EL AMRANI	PH	École Supérieure de Technologie Université Moulay Ismaïl – Meknès –Maroc	Rapporteur / Examinateur
Mouloud EL MOUDANE	PH	Faculté des Sciences, Université Mohammed V – Rabat – Maroc	Rapporteur / Examinateur
Abdelkader BEN ALI	PA	Faculté des Sciences, Université Mohammed V – Rabat – Maroc	Invité
Omar OABI	Dr.	Office Chérifien des Phosphates – Khouribga – Maroc	Invité

Academic year : 2019-2020

✉ Faculté des Sciences, avenue Ibn Battouta, BP. 1014 RP, Rabat –Maroc
☎ 00212(05) 37 77 18 76 🖷 00212(05) 37 77 42 61; http://www. fsr.um5.ac.ma

Acknowledgements

This thesis has been carried out at the Research Group: Composite Materials, Polymers and Environment (**LMCPE**), Laboratory of Materials, Nanotechnologies and Environment (LMNE), Faculty of Science, the University of Mohammed V– Rabat, under the supervision of **Prof. Abdelkrim MAAROUFI.**

First, praises and thanks go to Allah, the Almighty, for his unlimited and uncountable blessings in my whole life and throughout my research work especially.

I would like to take this opportunity to express my thanks and gratitude to the many people who have in so many ways helped and supported me throughout my thesis study.

I would like to express my deepest sense of **G**ratitude (with a capital and bold g) to my supervisor

Prof. Abdelkrim MAAROUFI, professor of higher education, from the University of Mohammed V– Rabat, Faculty of Sciences, who offered his continuous advices and encouragement throughout the course of this thesis. I thank him for the systematic guidance and great efforts he put into training me in the scientific field. I am especially thankful to him for his fruitful discuss, help, encouraging and most of all patience throughout the entire process. A sincere thank you my supervisor.

I wish to thank my committee members who were more than generous with their expertise and precious time.

A bundle of thanks goes to the president of this thesis, **Prof. Ahmed EL YAHYAOUI,** professor of higher education, from the University of Mohammed V– Rabat, Faculty of Sciences, who honored me by accepting to chair the examination committee of this thesis and for his enthusiastic interest in my work.

I would like to thank **Prof. M'Hamed TAIBI,** professor of higher education, from the University of Mohammed V– Rabat, École Normale Supérieure (ENS), for reviewing and reporting this thesis. I am grateful to him for his collaboration, time and assistance.

Also, I would like to extend my thanks to **Prof. Rachid BENCHRIFA**, professor of higher education, from the University of Mohammed V– Rabat, Faculty of Sciences, for reviewing and reporting this thesis. I am grateful to him for honoring me by being among the members of jury.

I would like to thank **Prof. Mohammed BENAISSA,** professor of higher education, from the University of Mohammed V– Rabat, Faculty of Sciences, who openly accepted to be a member of thesis examination committee.I am grateful to him for honoring me by reviewing and reporting this thesis.

I would like to extend my gratitude to **Prof. Aumeur EL AMRANI**, qualified professor, from University of Moulay Ismaïl–Meknès, Ecole supérieure de technologie (EST) to honor me by kindly accepting to be among the members of the thesis examination committee, and for traveling a long distance in order to take part into it. I thank him also for reviewing and reporting this thesis.

Many very thanks go to **Prof. Mouloud EL MOUDANE,** qualified professor, from the University of Mohammed V– Rabat, Faculty of Sciences, who honored me by accepting to evaluate my work.I am grateful to him for reviewing and reporting this thesis.

I would like to thank **Prof. Abdelkader BEN ALI**, assistant professor, from the University of Mohammed V– Rabat, Faculty of Sciences, who honored me by accepting to take part of the thesis examination committee; I thank him for reviewing and reporting this thesis.

Special thanks goes to **Dr. Omar OABI**, projects' manager, from Cherifian Office of Phosphates (OCP), Khouribga, who honored me by kindly accepting to be among the members of the thesis examination committee, and for traveling a long distance in order to take part into it.

Special thanks should be given to my family members for their support and encouragement whenever i was in need. Finally, my thanks also go to my colleagues at Research Group: Composite Materials, Polymers and Environment **(LMCPE)**.

Résumé

Le but de cette thèse est la valorisation éminente des matériaux phosphatés dans le secteur énergétique. Ainsi, des verres à base de phosphate de plomb (PbP) : $PbO-P_2O_5$ chargés de particules conductrices (Ni, Co, Cr et Zn) ont été élaborés sous forme massive et en couches minces, en utilisant respectivement la technique de trempe et la voie sol-gel. Pour les composites massives, les propriétés structurales et thermiques ont été étudiées par les mesures de la densité, la diffraction des rayons X (DRX), la microscopie électronique à balayage (MEB), l'analyse calorimétrique différentielle (DSC) et l'angle de contact.

Ensuite, l'évolution de la conductivité électrique en fonction de la charge à l'ambiante a été interprétée par la théorie de la percolation. Les mesures de la conductivité électrique en fonction de la température ($300 \leq T \leq 715$ K) ont été entreprises au-dessus du seuil de percolation indiquant une transition de phase conducteur-isolant, nommée Coefficient de Température Positif (PTC). Enfin un comportement semi-conducteur a été décelé en dessous du seuil de percolation, montrant ainsi des mécanismes de conduction multiples, interprétés par la théorie des polarons à haute température et celle de VRH de Mott (Mott's variable range hopping theory) à basse température.

Les films obtenus ont été caractérisés par DRX, MEB-EDAX, UV-visible et des mesures de résistivité respectivement. De plus, la résistivité électrique des couches minces semi-conductrices a été mesurée en fonction de la température. Tous les résultats ont été décrits en détail et ils ont indiqué que les couches minces préparées dans cette étude sont utiles dans le domaine optoélectronique.

Mots clefs : composites ; verres de phosphate ; couches minces ; structure ; optoélectronique ; conductivité électrique ; Angle de contact ; percolation ; PTC ; Polarons; VRH theory.

Abstract

The aim of this thesis is the eminent valorization of phosphate materials in the energy field. Thus, lead phosphate glasses (PbO-P2O5) filled with conductive particles (Ni, Co, Cr and Zn) were elaborated in bulk and thin film forms, using melt quenching technique and low-cost sol gel technique, respectively.

For bulk forms, the structural and thermal properties of the elaborated composites have been studied by density measurements, X-ray diffraction technique (XRD), scanning electron microscopy (SEM) and differential scanning calorimetry (DSC) analysis. Afterward, the electrical conductivity as function of filler content at room temperature were investigated and have been interpreted on the basis of percolation theory framework, the outcomes related to percolative models were assessed by surface analysis trough the calculation of composites' surfaces tension via contact angle measurements.

The electrical conductivity temperature dependence ($300 \leq T \leq 715K$) was undertaken on heating and cooling above the percolation threshold indicating a Positive Temperature Coefficient (PTC). Furthermore, bellow percolation threshold, a semiconducting behavior is fairly discussed with polarons theory at high temperature and with Mott's Variable Range Hopping (VRH) mechanism theory frame at low temperature.

The thin film forms composites were elaborated by filling the matrix with conducting particles ranging from 0 wt % - 16wt %. Then, the effect of fillers on structural, morphological, optical and electrical properties of glass thin films were investigated by XRD, SEM-EDAX, UV-VIS and DC electrical resistivity measurements respectively. Moreover, electrical resistivity of the semiconducting thin films was measured versus temperature. Taking into account the dc resistivity depending on the concentration of free carriers and the absorption coefficient, the figure of merit was calculated.

All results were described in details and they indicated that the films prepared in this study could be useful for opto-electronic applications.

Keywords: composites; phosphate glasses; thin film; structure; opto-electronic; electrical conductivity; contact angle; percolation; PTC; Polarons; VRH theory.

List of publicatios and communications

➢ *List of publications*

- **M. Hammi**, G. Aziate,G. Pinto, and A. Maaroufi, Electrical and Thermoelectrical Behavior of Binary Composites of Phosphate Glass Loaded with Zinc Fillers:Promising Materials forPhotovoltaic's(Received: Jun. 11, 2015; Accepted: Aug. 16, 2015;Published Online: Nov. 6,2015; DOI: 10.1002/jccs.201400254), Journal of the Chinese Chemical society.
- **M.Hammi**, A.Maaroufi, On optical properties of phosphate glass thin films, Materials Letters, 182(2016)227–230.
- **M. Hammi** , A. Maaroufi *, and G. Pinto b, Structural, thermal and electrical properties of new composite materials of lead phosphate glass filled with conducting particles, (to be submitted).
- **M. Hammi**, A. Maaroufi a,*,Morphology and contact angle of metallic particles-lead phosphate glass composites, (to be submitted).
- **M. Hammi**, A. Maaroufi*, Lead phosphate glass based composites with variable range hopping - small polaron hopping conduction mechanisms' transition and interesting positive temperature coefficient, (to be submitted).
- **M. Hammia**, A. Maaroufia,*, Structural and morphological characterizations of unloaded and loaded PbO-P_2O_5 glass thin films, (to be submitted).
- **M. Hammi**, A. Maaroufi,*,Studies on optical,electrical and thermo-electrical properties of sol gel deposited PbO-P_2O_5 thin films loaded with transition metal, (to be submitted).

➢ *Communications*

- O. Oabi, **M. Hammi**, A. Maaroufi, G. Pinto, M. Ouchetto, R. Benavente, J.M. Pereña, Non - linear electronic conductivity of zinc phosphate glasses/ metal composites, the first China-Morocco Symposium on Advanced Materials Rabat, Morocco, 21&22 March 2013.
- O. Oabi, **M. Hammi**, A. Maaroufi, G. Pinto, M. Ouchetto, R. Benavente, J.M. Pereña, Non - linear electronic conductivity of zinc phosphate glasses/ metals composites, Asia Core Workshop"Fundamentals and Applications of Nano-Photonics, Photovoltaics and Bio-Photonics" Rabat, Morocco, March 7 & 8 (2013).
- **Maryama Hammi**, Omar Oabi, Abdel-Karim Maaroufi, Thermoelectricity in novel ZnO-P_2O_5 phosphate glass / metal composites, Solaire Expo, Palais des Congrès - Marrakech, Maroc, 13-16 Février 2013.
- Oabi1, **M. Hammi**, A. Maaroufi, B. Lucas, A. EL Amrani, S. Degot , Thermoelectricity in novel ZnO-P_2O_5 phosphate glass / metal composites, 12thInternational Conference on Condensed Matter and Statistical Physics (ICCMSP) October 30 - November 01, 2013, Errachidia- Morocco.
- **Maryama Hammi**, Thermo-electricity in novel ZnO-P_2O_5-Doctoriales 2014-6,7&8 February 2014.
- **M. Hammi**, A.Maaroufi, G. Pinto Phosphate glass/transition metal composites:New generation of materials with interesting non linear electrical and thermoelectrically properties, the 1st international conference on Materials and Environmental Science(ICMES 2016),Held in knowledge campus ,Oujda ,Morocco December 1-3, 2016.

Table of Contents

List of figures

List of figures

List of figures

List of tables

List of tables

General introduction

The growing demand in the sector of technological development and supply in the field of environmentally friendly energies, prompts scientists to develop new materials. Thermoelectric materials represent one of these alternatives, since they make it possible to consider the recovery of the heat into electrical energy and vice versa. These concerns have encouraged the development of new thermoelectric materials because of their many industrial applications. They are characterized by a good electrical conductivity, a high thermoelectric coefficient, and the lowest possible thermal conductivity. In this contest, our thesis work focuses on the study of electrical and thermo-electrical properties of composites based on binary phosphate glasses, in order to give new applications to these phosphate materials in the energy domain.

Phosphate glasses are of economical cost, environment friendly and relatively easy to prepare, offering a large range of compositional possibilities. It has been shown that they have lower melting temperatures, which allows optimizing the coefficients of thermal expansion (CTE), and gives facility to varying the glass transition temperature (T_g), based on the variation in the composition. Such characteristics have given to phosphate glass materials different potential applications in diverse areas of technology, such as laser glasses and optics, energy transfer materials, magneto-optical devices, glasses for sealing in electronics, biomaterials, matrix for waste confinement, battery materials for ultrafast charging and discharging, and many other interesting applications are possible ; especially in energetic field.

Indeed, this later possibility is somewhat less explored. As far as we know, with the exception of our research group, no systematic work has been presented to date on the valorization of phosphate glass in energy sector. However, phosphate glass materials are insulator and for new energy field applications, it is necessary to be transformed to semiconductors. One of the offered ways is obtained by filling the amorphous phosphate glasses with conductive particles leading to composites with many features, which are somewhat similar as in amorphous semiconductors.

Elsewhere, it should be mentioned that glasses have several advantages over the crystalline materials such as absence of grain boundaries, isotropic properties, ease of fabrication into complex and desirable shapes etc., they are known by their good optical transparency that makes them suitable for potential applications in new technology devices. They would be of great usefulness in thin film form. They are considered as promising materials for thermoelectricity as well as photovoltaic component when they are fabricated in both bulk and thin film forms.

Therefore, in this thesis, we undertake a systematic investigation of Lead phosphate glass and their based composites in bulk and thin films forms and new features are brought to light. The binary glass system, which is subjected in this study, is one of the unique glass, for which no satisfactory studies have yet been performed. Therefore, detailed experimental studies are needed on different forms of the glassy system. It has been widely accepted for decades that the design of electrically conductive materials is much easier and more economical by fabrication of composites based on amorphous matrix filled with conductive particles rather than by synthesizing intrinsically conductive materials. The properties of these random macroscopic mixtures are now relatively well known and are well explained by percolative theories. Hence, the aim of the present work is to prepare composites-based lead phosphate glass filled with conductive particles. A systematic study of various properties of these glasses by varying the concentrations of the incorporated fillers and temperature have been carried out in order to investigate conducting particles effect in the glass binary system in bulk and thin film forms.

The present thesis entitled "Studies of lead phosphate glass based composites in bulk and thin film forms: Promising materials for thermo-electricity and photovoltaic applications" contains results of elaboration and investigations of structural, morphological, spectroscopic, thermal and electrical properties such as XRD, SEM/EDS, density, infrared spectroscopy, Raman spectroscopy, differential scanning calorimetry, optical absorption and refractive index of different obtained composite materials. Moreover, electrical conductivity measurements were conducted versus filler concentrations and as function of temperature. Also, the objective of this work consists of description of the electronic conduction properties of the studied composites versus filler concentration in the light of percolation theory and the mechanism conduction as function of the temperature with polarons and Mott VRH theory

We have also synthesized similar glass composition in thin film form, for the first time at our knowledge, by wet sol-gel using precursors of the starting oxides. This method has several advantages namely a good degree of purity, a low temperature of synthesis and an ease of obtaining the final product. We have used this method in order to be able to miniaturize composites and improve their electrical properties, as well as their good transparency, which might make them a good candidate for solar cell application.

Therefore, we focused the second part of our work on obtaining thin sol-gel films with good electrical and optical properties.

The thesis is divided into eight chapters,

In the **first chapter**, an introduction to glass, stability, structural aspects and general applications of these glasses are described. This is followed by a discussion of the main properties provided

by the glasses. A brief review of the earlier work carried out on physical properties of glasses is also included in this chapter. Finally, the aim and scope of the present investigation is presented at the end of this chapter.

Chapter II of the thesis presents the theoretical concepts used and developed in this work. Topics like glass formation, thermal analysis; electronic structure, electronic transport and thermo-electricity behavior of the studied composites are included.

In **chapter III**, a brief description of glass and composites processing are discussed, and explorating the most stable and durable glass composition is performed followed by structural properties of glasses and their based composites.

Chapter IV aimed to investigations of morphological aspects of four series of bulk composites samples and the contact angle measurements were performed in order to get clear insights on the surface energy, which is a signature of matrix-fillers interactions.

Chapter V reports the obtained results of electrical and thermoelectrical investigations of lead phosphate glass/metals composites as well as detailed explanation of the electrical phenomena.

Chapter VI is concerned by structural studies of lead phosphate glass-based composites in thin film forms; it includes XRD analysis, IR/ATR, Raman spectroscopy and SEM/EDS investigations.

chapter VII is reserved to the study of optical and electrical properties of obtained films at ambient temperature and versus temperature.

Chapter VIII, is restricted to solar cell prototype fabrication based on P-N junction, and the calculation of its contact resistance evolution using three different wavelengths.

Conclusion of this work is also highlighted at the end of this chapter.

Appendix is included at the end of the manuscript. It contains samples processing, and comprehensive listing used techniques.

CHAPTER I

Brief review on chemistry and physical properties of binary phosphates glasses and their based composites

I.1 Introduction

Within this chapter, we will remind some basic notions about glasses, oxides and their classifications. Also, we will highlight some properties and applications of glasses. We are more particularly focused on binary phosphate glass, their properties and their application fields. Thus, we are going to present a brief state of the art concerning this type of material. Then we are going to discuss in details the composites based on these glasses in bulk and thin film forms. Afterward we will highlight different concepts for better understanding several physical properties given in the upcoming chapters of the manuscript.

I.2 Principal characteristics of glass materials

I.2.1 Introduction to glass notion

Solids can be generally considered as crystalline and non-crystalline or amorphous materials. [1,2,3]. A perfect amorphous material are solids in which the atomic sites are randomly arranged. They lack long range periodic ordering in their network. A clear distinction should be done between amorphous and poly-crystalline materials. Poly-crystalline materials are composed of many clusters ; each has a periodic array of atoms. Recent correlations of experimental data on electronic and optical properties in amorphous materials have demonstrated the existence of band gaps similar to crystalline semiconductor [4,5]. A gradually deep understanding of chemical bonding nature has supported the study of non-crystalline solids by contributing to the determination of short-range order around the atoms [6]. That is to say that in the absence of long-range periodic order, local order is of crucial importance in understanding the structure and properties of these materials [7]. Experimental facts evidenced that short-range order remains in amorphous network.

It should be mentioned that glassy materials play an important role in recent day technology, they are gradually involving in high-tech devices including lasers, optical fiber communications, opto-electronics [8], etc.. For this reason, they are regarded as versatile materials, which are mainly fabricated by several techniques to produce enormous variety of products. Due to their great industrial applications, such as switching and memory devices, transducers, superior insulators and dielectrics, glassy materials are widely studied through various electronic transport and spectroscopic techniques [9,10,11]. In addition, they offer a large number of advantages over crystalline materials, such as their physical isotropy [4], absence of grain boundaries, ease of thin film formation for device applications and significant thermal stability. Thus, the prime interest in glasses is due to their relatively easy and fast synthesis process compared to that of crystalline materials.

I.2.2 Definition

Glass is a non-crystalline or amorphous material; it is an isotropic solid, which is generally obtained by rapid cooling of a supercooled liquid. It presents a perfect disorder and it is distinguished from other amorphous materials by the marked glass transition phenomenon T_g. The T_g characterizes the transition from the amorphous solid state to the viscous liquid state. Thus, a much more concise definition of glass has been proposed as follows "Glass is a non-crystallized solid that exhibits the glass transition phenomenon" [12].

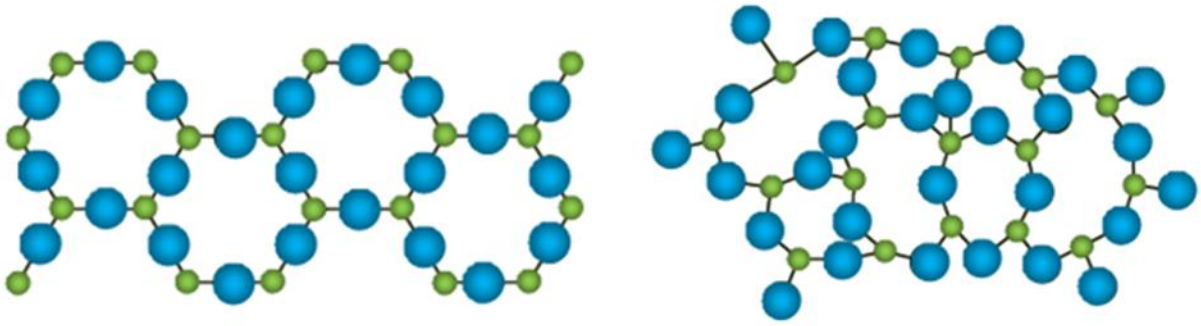

Figure I- 1 : Schematic Representation of a crystal (a) and glassy network (b) for an oxide type compound formed by an oxygen atom (in blue) and a metal atom (in green) [13].

I.2.3 History of glass

In 1932, a first theory was developed by Zachariasen [14] is called random network theory [15], which constructed hypotheses about the structure of glass and grouped into two main currents:
Atomistic models: the best known is Zachariasen, which defines glass as a continuous network.
Models based on kinetic considerations of phase transformation.

*** Random Network Theory:**

This theory is based on empirical reasoning. The initial postulate assumes that glass is a three-dimensional network with a structure composed of polyhedron bonds. The basic structure of the network is therefore the silicon-oxygen tetrahedron; silicon is connected to 4 oxygen atoms. And Zachariasen has defined criteria for joining the polyhedra so the network is similar to that of a crystal.

Within this approach an oxide must satisfy the following rules:

1. Each oxygen atom is bonded to at most two cations.
2. The number of oxygen atoms around each cation is three to four.
3. The oxygen polyhedron can have only occupied vertices and not edges or faces.

4. At least three vertices must be shared with other polyhedra. In addition to these four criteria, three other rules, which are recalled by Shelby, were defined by Zachariasen for more complex glasses [16]. These works were completed by those of Warren to arrive at the structure of the glass shown in Figure I-2.

This theory explains many properties of glass. It is valid for oxide-based glasses but not for other types of glasses such as titanium glasses. Nevertheless, this approach has prevailed for many years in the scientific world despite its lack of generality.

***Kinetic theory:**

The second theory, called kinetic, is based on the conditions of the glass formation and interatomic bonds, just like the previous theory, it is based on empirical rules. The starting point of this theory is as follows:

The covalent bonds, which define the length of the bonds and the angle, are not compatible with the random arrangements of atoms in the glass. According to this theory, the properties of silicates do not rest on the nature of the ions of the network but on the interatomic bonds. The connection between vitrification and interatomic bonds in the structure makes it possible to deduce the properties of glass [17]. This last theory leads to the conclusion that all the amorphous substances belong to glass family.

As concluding remark, these two theories are not contradicted by the experimental measurements and allow understanding the variation of the properties of the glasses according to their composition.

I.2.4 Conditions of vitrification

To explain the glasses formation, we can use a structural approach based on crystallographic considerations or the nature of the bonds. It should be known that not all oxides are able to form a vitreous network. The vitrification of $A_mO_n$network can take place if the cation or anion ionic radius ratio (r_A/r_O) is between 0.2 and 0.4 [18], but still, this is not enough to give sufficient vitrification conditions [19], because there are some oxides (for example BeO [20]), which has no ability of vitrification despite it meets the criterion.

Some rules, set out by Zachariasen on the basis of disordered network hypothesis of oxide-based glasses, define the oxides that are able to form an amorphous network. They are four in number, the first two rules (in bold characters) are the most important:

1. Oxygen surrounding the cation forms a polyhedron that must have few atoms (3 or 4)

2. Oxygen cannot be linked to more than two cations

3. Polyhedra have a common vertex, but never common edges or faces

4. Each polyhedron shares at least three vertices with its neighbors

Basically, Zachariasen defines three classes of oxides to be involved in the formation of a glass, namely; forming oxides, modifying oxides and intermediate oxides.

I.2.5 Classification of oxide glasses according to Zachariasen criteria

There are several ways to classify glasses. Zachariasen [14] was particularly interested into oxides. Indeed, he showed that an oxide forming glass should satisfy several rules:

The sample contains a sufficient percentage of cations surrounded by tetrahedra or oxygen triangles.

These tetrahedra or these triangles have only common summits.

Some oxygen atoms are simply linked to only two of these cations and do not form new bonds with other cations.

Zachariasen defines three types of cations according to the role they play in structuring the vitreous network:

-The network forming cations have higher electronegativity than the modifying cations. The bond between an oxygen and a forming cation will therefore be more covalent than that between an oxygen and a modifying cation. These cations play polymerization role of the network.

- Network modifying cations do not directly constitute the glassy network. They depolymerize it by breaking the bonds between triangles or tetrahedra.

- The intermediate cations may have a role of network former or modifier depending on the composition of the glass.

The three types of the above-mentioned oxides are gathered in tableI-1:

Table I- 1 : Classification of oxides according to their capability for vitrification according to Zachariasen [19].

Forming oxides	Modifying oxides	Intermediate oxides
SiO_2	Li2O	Al_2O_3
GeO_2	Na2O	PbO
$B2O_3$	K2O	ZnO
P_2O_5	CaO	CdO
AS_2O_3	BaO	TiO2
AS_2O_5		TeO_2
		Nb_2O_5
		Ga_2O_3

I.3 Synthesis method and some thermal characteristics of binary phosphate glass ($PbO-P_2O_5$)

Lead Phosphate glasses despite their relatively low hydrolytic resistance, they are important from a technological standing point, mainly due to their low glass transition temperature, low optical dispersions and relatively high thermal expansion coefficients [21,22]. These properties make them useful as good candidates for other important applications such as semiconducting materials when it loaded with conductive fillers, known as composites. Thus, in this ongoing work, we have selected the binary system glass ($PbO-P_2O_5$) since it is among the glasses which are hardly explored in term of physical properties.

There are different ways to synthesize a glass, but the most common is a method that freezes the structural disorder of a liquid phase from a supercooled liquid called the classic thermal quenching method. The starting products are mixed and then melted at high temperature to obtain a single liquid and homogeneous phase. The liquid is then quenched to freeze the amorphous nature of the mixture by a rapid cooling.

Within our work, the used melt-quench method consists of melting a mixture of oxide precursors in a furnace at temperatures of around 950˚C and amorphous solid is obtained by rapid quenching of the melt. When the cooling rate is sufficiently high to suppress nucleation and crystal growth, the melt's disordered state is maintained in the solid state. To achieve a high cooling rate the molten glass can be poured into a preheated mold. Since the main component in the phosphate-based glasses (phosphorus pentoxide) is highly hygroscopic, the presence of small amounts of water can promote crystallization [15]. Thus, to synthesize binary P_2O_5-PbO glass systems; $NH_4H_2PO_4$ and PbO powders can be used as the sources of phosphorus and lead oxide, respectively.

I.3.1 Bulk binary systems of Lead phosphate glasses

Before going further in this study, it is necessary to define and understand some basic notions related to our developed materials. It was stated in the literature that the included lead oxide (PbO) provides a good chemical durability to the glassy network [23], which often enlarges their usefulness in many fields [24]. Lead oxide is both modifier and network former [25], so it can be incorporated in large proportions in the glass network [26], which is P_2O_5 in our study. Let's keep in mind that phosphate compounds are composed of networks formed by interconnected tetrahedral structures [27]. The figure I-2 illustrates the formation of non-bridging oxygen (NBOs) in phosphate tetrahedra by breaking the P–O–P links (structure a), and more addition of

PbO increases the number of NBOs (structure b); structure c) and d) exhibit the formation of bridging oxygens BOs and the P-O-Pb covalent bonds, respectively .

As we notice from Figure I-2, phosphorus-oxygen-phosphorus bonds are distributed throughout the structure, forming rings and / or chains that contribute to the construction of a high phosphate network connectivity. With the increase of the modifying oxide content(PbO), the phosphate units are dispersed throughout the network in shorter chains or single phosphate tetrahedra, which terminate due to charge balancing with the cations in the structure.

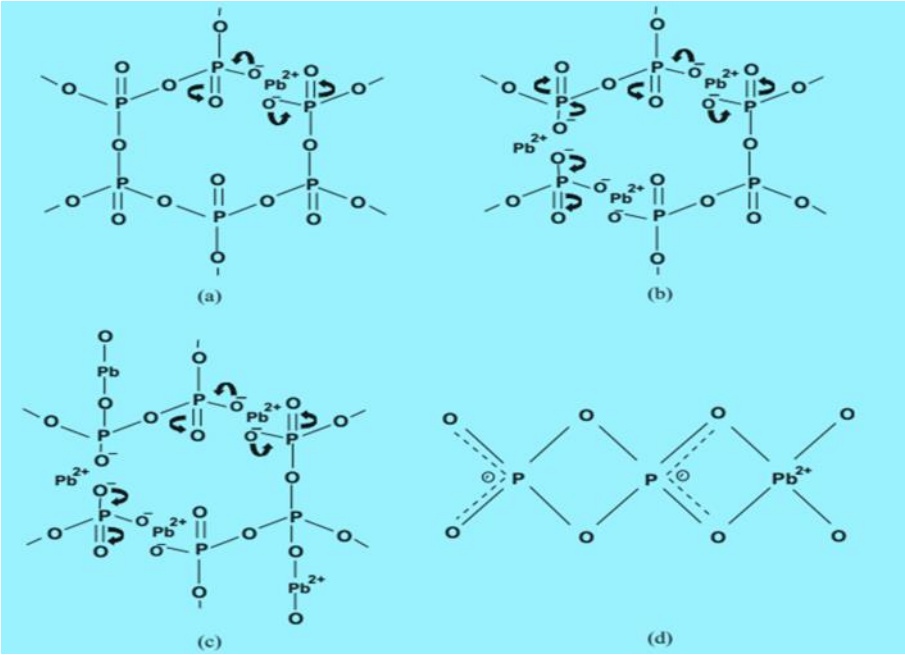

Figure I- 2 : Possible structural roles of PbO in the P_2O_5 network [28].

Several properties of phosphate glass result from the incorporation of PbO into the network. For example, PbO is useful for protecting against high-energy radiation, including nuclear radiation [29] and its addition can result in the formation of P-O-Pb bonds. These bonds lead to an improvement in the chemical durability of the phosphatized glasses [30]. So, one of the objectives of this work is the elaboration of the glasses of the binary system PbO-P_2O_5 which interests us the most.

I.3.2 Some structural and physical properties of binary phosphate glass (PbO-P_2O_5)

Several properties of phosphate glasses have been found to result from the incorporation of PbO into P_2O_5 network. Indeed, PbO decreases the glass transition temperature T_g and its addition may result in the formation of P–O–Pb bonds. These bonds lead to an improvement of the chemical durability of phosphate glasses [31]. Lead-based glasses are used in radiation

protection. Within these glasses family, PbO increases the refractive index and water resistance [32-36]. Therefore, within this section we aimed to shed more light on the role of $PbO–P_2O_5$ glass structure using IR spectroscopy. Also, we have correlated the variation of the ionic conductivity, the density and the optical properties of the studied glasses with the structural changes.

I.3.2.1 Density and molar volume of xPbO (100-x) P_2O_5

Series of glasses with the compositions $xPbO\ (100-x)P_2O_5$ (x = 25–60 mol%) were synthesized by K. El-Egili et al. [37], using melt quenching route. The obtained samples were transparent. They were investigated by density (D) measurement at room temperature using the Archimedes method. The density measurements allowed to calculate the molar volume (V_m) of the investigated glass.V_m was calculated from the following relationship [37] :

$$V_m = \sum \frac{n_i M_i}{D} \qquad \textbf{(I-1)}$$

Where M_i is the relative molecular mass of the component i and n_i is its molar fraction.

The curves of D and V_m as function of PbO content in $PbO–P_2O_5$ glasses are depicted in Figure I-3. Obviously, it was found that while density increases, the molar volume decreases, However there is a marked change in both quantities at around 50 mol% PbO.

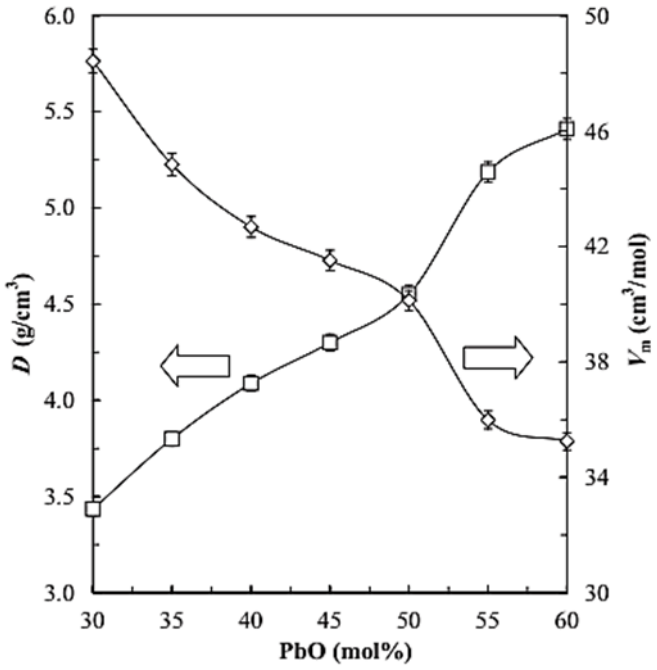

Figure I- 3 : Dependence of both the density (D) and molar volume (V_m) on the PbO content in $xPbO\ (100-x)P_2O_5$ glasses [37].

Similar findings of density and molar ratio were reported by sharaf El deen et al. [38], for xPbO–(100- x) P_2O_5 glasses where x = 5, 10, 15, 20, 25, and 30, the authors have stated the increase of density with incorporation of PbO content. This might be due to the fact that, incorporation of the PbO content serve to increase the compactness of the glass network. The ionic radius of Pb is smaller than that of phosphorus. Consequently, PbO addition leads to shorter chains and the cross-link density will increase. Both stiffer chains and the increase in strong ionic cross-link serve to increase the density of glass samples with PbO content and the glass transition temperature.

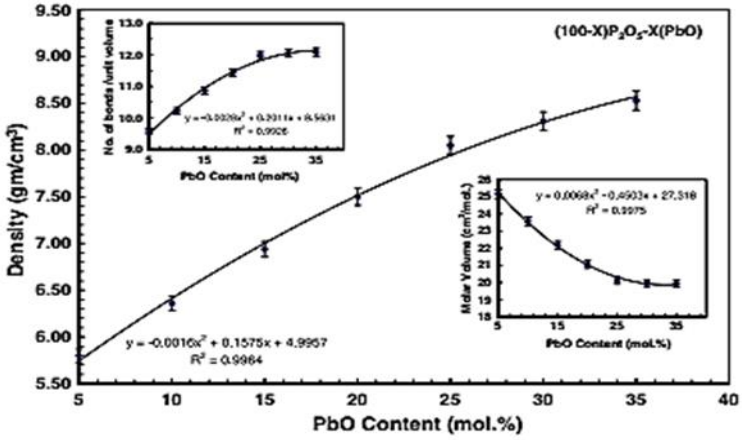

Figure I- 4 : Density, molar volume, and number of bonds per unit volume as a function of PbO content for PbO–P_2O_5 glass system. [38].

I.3.2.2 Proprieties of phosphates

From a structural point of view, the study by infrared spectroscopy showed that PbO depolymerizes the vitreous network by the appearing of shorter chains. Glasses covering a wide range of compositions where the PbO content varies between 25 and 60 mol% were investigated through FTR-IR spectroscopy. This region includes lead ultra-phosphate (30 < x < 50 mol%), lead meta-phosphate (x = 50mol%) and lead pyrophosphate glasses (50 < x < 66.6 mol%). With this identification, it would be easier to follow the trends of IR band-forming tendency or the structural modification with PbO addition within P_2O_5 matrix.

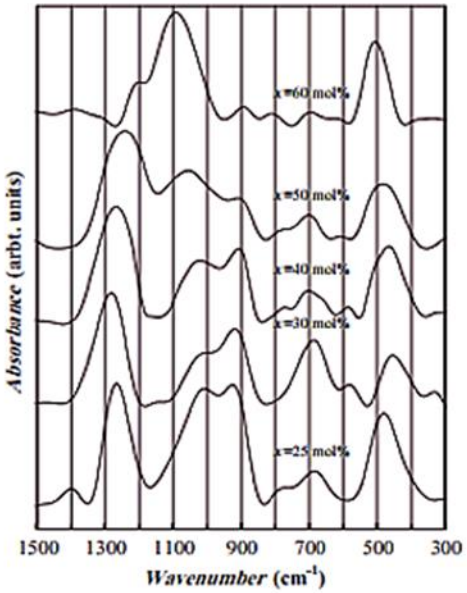

Figure I- 5 : Infrared absorption spectra of xPbO (100-x) P_2O_5 glasses [37].

As we can notice from Figure I-5, there are four main bands at ~1263, ~1010, ~920 and ~475 cm^{-1}. In addition, there are two weak bands at ~776 and 687 cm^{-1}.With the PbO content increases (x=30–60 mol%), a remarkable shift of the band is observed at ~1263 cm^{-1} occurred toward a lower wave number (1263– 1213 cm^{-1}). This band is attributed to asymmetric stretching vibration of P = O bond (υ_{as} (P = O)).

The band at ~1010 cm^{-1} is attributed to symmetric stretching vibration of PO_4^{3-} tetrahedra (P–O ionic group) [39,40]. This band has shifted to a higher wave number (1010–1090 cm^{-1}) with increasing PbO content.

Indeed, Osaka et al. [41] have shown that the PO_4 units have two bridging oxygen bonds (P–O–P) and two non-bridging bonds such as P = O and P–O, which are in resonance with each other. The shift in the position of the band of the ionic groups, PO_4^{3-} (1010–1090 cm^{-1}) and the increase of its relative area (above 40 mol% PbO) at the expense of that of P = O and P–O–P, may be considered as an indication for the formation of more non-bridging oxygen ions (NBOs).

The band at ~ 920 $cm^{-1}$is attributes to a symmetric stretching vibration of P–O–P linkages (υ_s (P–O–P)). This band is shifted to a lower wave number (920–890 cm^{-1}) and its relative area decreases until it becomes a small band.

The band at ~687 cm^{-1} is due to the asymmetric vibration of these linkages (υ_{as} (P–O–P)) [42]. This band shifts to higher wave number (687–702 cm^{-1}).

The absorption band at 480–508 cm^{-1} is assigned to harmonics of bending vibration of O = P–O linkages. The weak absorption band cited at 809–776 cm^{-1} is attributed to the bending vibration of P–O–P linkage [43]. The shift of P = O position to a lower wave number with increasing PbO content is due to the reduced force constant between P and O [44]. For PbO greater than 50 mol%, the intensity of the P = O band decreases rapidly. This means that the P=O double bond is markedly affected and is converted into bridging bonds P–O–Pb and P–O–P.

I.3.2.3 Glass transition temperature

It is worthy to mention that there are many specific characteristics of glasses. Thus, among the thermal characteristics we find :

- The glass transition temperature ($\mathbf{T_g}$), it characterizes the transition from the amorphous solid state to the viscous liquid state in a viscosity range between 10^{12} and 10^{14} Pa.s.
- The crystallization temperature ($\mathbf{T_c}$), which corresponds to the crystallization of the liquid.
- The melting temperature ($\mathbf{T_m}$), which corresponds to the melting point of the solid.

As aforementioned, the conventional way to produce a glass is to cool a liquid quickly so that the crystallization does not have time to occur. The continuous increase of the viscosity with the temperature decreasing, leads to progressive freezing of the liquid until solidification is achieved. To study and understand this process more precisely, we can follow the evolution of a thermodynamic variable such as the specific volume **V**, depending on the temperature **T** (Figure I- 6) [13].

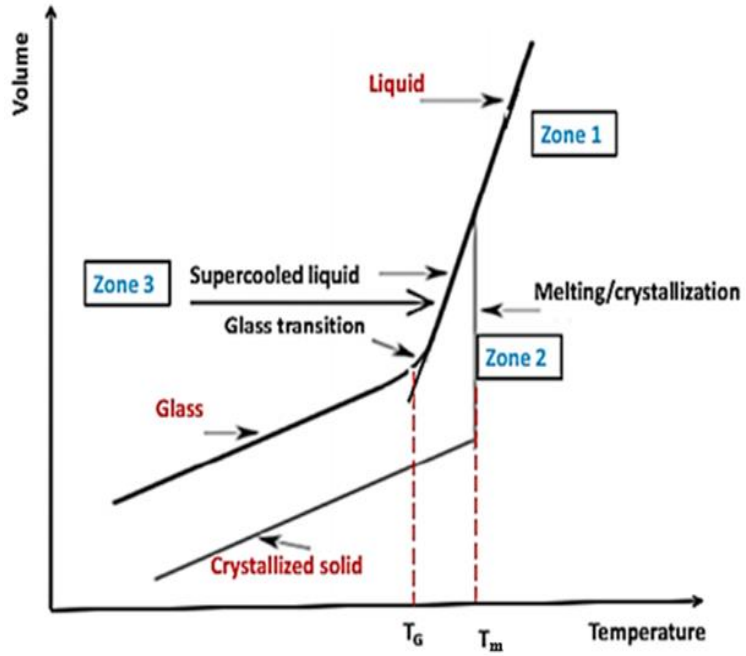

Figure I- 6 : Variation of glass specific volume as a function of temperature [13].

Starting from a liquid at high temperature, the cooling first causes a shrinking of the liquid (Zone 1). When the solidification point is reached, two phenomena might occur: The liquid can either crystallize or pass into a supercooled liquid state. The crystallization phenomenon is identified by a sudden shrinkage of the volume, giving rise to a discontinuity in the volume curve (Zone 2). Whereas, the evolution of the volume as a function of temperature during the transition to the supercooled state is in the continuity. During this cooling step (Zone 3), the supercooled liquid is shrinking linearly and maintains a coefficient of thermal expansion similar to that of the melt. It is more convenient to mention that, viscosity of the mixture also plays a predominant role in the formation of glass. During the cooling, the viscosity of the liquid and supercooled liquid has found to be increasing exponentially [13].

Definitely, the formation of glasses is essentially a kinetic phenomenon. The elaboration technique affects its properties, thus to form a glass, it is necessary from a kinetic standpoint to perform a rapid quenching in order to avoid the crystallization process. Thermal characteristics of glasses can be measured in order to check the glassy state of the studied binary systems using most known techniques such as Differential Scanning Calorimetry (DSC).

Within a work reported by Sudarsan et al [45], the characteristic glass transitions temperature (T_g) of $PbO-P_2O_5$ glasses were obtained using Shimadzu Differential Thermal Analyzer. By a simple comparison of representative DSC patterns of $PbO-P_2O_5$ glasses it was proven that the binary glass system having the formula 50mol%PbO-50mol%P_2O_5 exhibits endothermic peak at around 603K corresponding to glass transition.Elsewhere, in order to further understand the evolution of glass transition with lead oxide content, Sharaf El-Deen et al [38] have evidenced within their undertaken experimental work that T_g is increased with increasing PbO content (Figure I- 7).

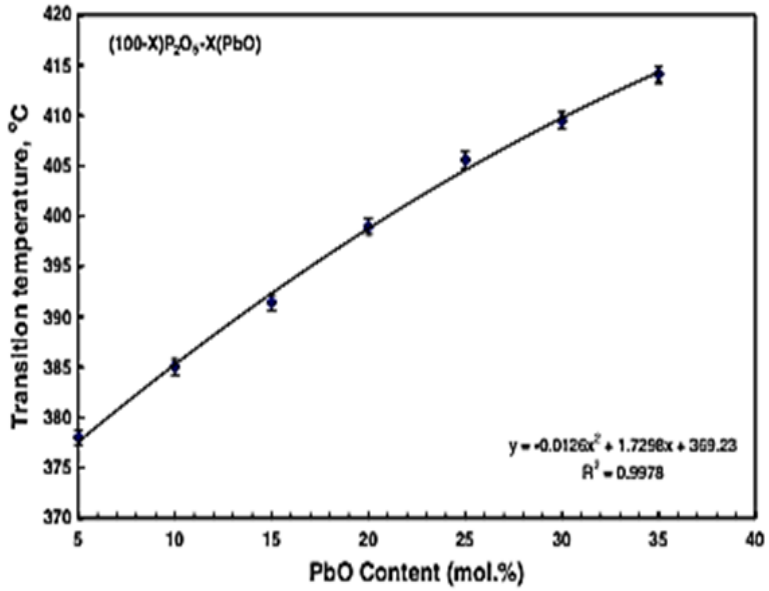

Figure I- 7 : Glass transition temperature as a function of PbO content for PbO–P_2O_5 glass system [38].

The evolution of T_g with PbO addition is more probably due the closeness of the network structure of these glasses and that is explained by the fact that of the incorporation of the PbO content serve to increase the compactness of the glas network, in a good consistence with the finding reported by sharaf El deen et al. [38] concerning Density and molar volume of xPbO (100-x)P_2O_5.

I.3.2.4 Optical properties

Optical absorption studies were performed elsewhere [45], within Figure I-8 it is indicated a decrease in slope values with increase in PbO content in the glass, this behavior has been attributed to the increase of concentration of non-bridging oxygen atoms.

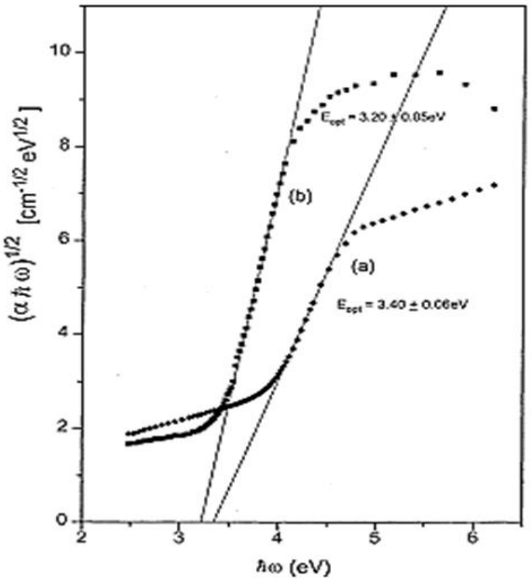

Figure I- 8 : Plot of $(\alpha h\nu)^{1/2}$ versus hν with E_{opt} values for $(a)PbO_{0.4}P_2O_{5\ 0.6}$ and $(b)PbO_{0.6}P_2O5_{0.4}$ [45].

I.3.2.5 Electrical properties

Electrical properties of the lead phosphate glasses were reviewed, and the electrical conduction of phosphate glasses containing PbO was characterized by El-Egili et al.[37]. The dependence on the PbO content of both W (the activation energy for conduction) and $ln\sigma_{423}$ (the natural logarithm of the conductivity at 423 K) were carried out for the binary glass system. Note that the system PbO-P_2O_5 is suitable for this purpose because of its wide glass-formation region. The dependence of the dc conductivity on PbO concentration in the wide range is shown in Figure I- 9

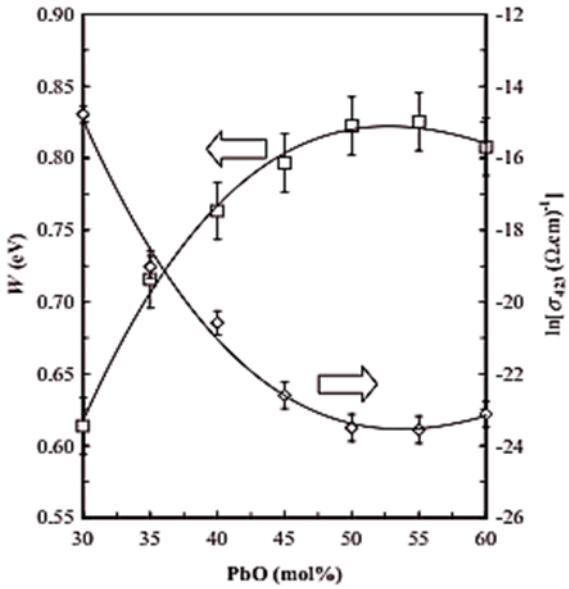

Figure I- 9 : Composition dependence of both the activation energy(W) and $ln\sigma_{423}$ (natural logarithm of the electric conductivity at 423 K) for xPbO (100-x)P_2O_5 glasses[37].

It is shown that W increases with a decreasing rate up to 50 mol% PbO. In the same region there is a decrease in $ln\sigma_{423}$. It seems that both W and $ln\sigma_{423}$ tend to have constant values or slightly change in the opposite direction above 50 mol% PbO. This feature can be attributed to the formation of PbO_4 units (network former PbO) above 50 mol% PbO. The increase in W and the decrease in $ln\sigma_{423}$ with PbO content can mainly be attributed to an increase in the strain energy because of the decrease in V_m of the studied glasses.

It is also shown that W changes nearly in symmetry with $ln\sigma_{423}$, which suggests some correlation between both quantities. This behavior reveals that the conductivity depends mainly on the mobility of charge carriers. This conclusion can also be obtained from the conductivity equation:

$$\sigma = nq\mu \qquad \textbf{(I-2)}$$

In light of the above results, we presume that Pb^{2+} ions in the studied glasses would be the charge carriers. Therefore we see the necessity to find out about correlation between $ln\sigma$ (natural logarithm of the electric conductivity) and temperature for $xPbO(100\text{-}x)P_2O_5$ glasses. The temperature dependences of dc conductivity are shown in Figure I- 10.

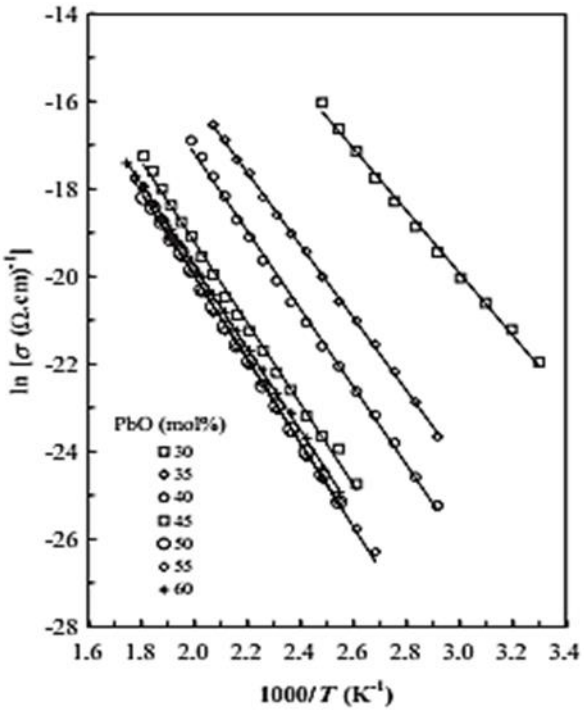

Figure I- 10 : Effect of temperature on dc conductivity [37].

Figure I- 10 shows the dependence of $ln\sigma$ on the reciprocal of temperature for $PbO–P_2O_5$ glasses. Between 30 and 60 mol% PbO there is a linear decrease in $\ln\sigma$ with increasing 1/T. This is a

characteristic behavior of the ionic conduction in glass, where the conductivity (σ) can be described by the Arrhenius equation:

$$\sigma = \sigma_0 e^{\left(-W/K_B T\right)} \quad \textbf{(I-3)}$$

Where σ_0 is a constant, which depends on the composition of glass, K_B is the Boltzmann constant, T is the absolute temperature and W is the activation energy for the conduction process. The electrical properties of the studied glasses lead to say that the conductivity of these glasses depends mainly on the mobility and is dominated by the activation energy.

I.4 Lead phosphate glass-based composites in bulk form

As shown above, the phosphate glasses are electrically insulator. To explore their electrical properties, they have beenloaded with conductive particles, called **fillers** [46-50]. The resulting materials are called **composites**; they are original and revealed new properties as PTC effects, high dielectric constants and high Seebeck coefficients.

I.4.1 Fillers

Filler is a technical name, which is meant any inert substance to be added to a neat material (matrix), and allows modifying significantly the mechanical, electrical or thermal properties and the appearance (opacity, color, texture), improving the surface appearance, or simply reducing the cost of the processed material [51] . The introduction of metal fillers in the vitreous material lead to the increase of the electrical and mechanical properties; their effect is much more marked because of their structural characteristics as well as their form factor. The form factor is defined as the product between half of the radius and the inverse of the thickness of the sample. In fact, there is a significant diversity in shapes, sizes, structure and inherent properties of fillers; hence, they can be classified in numerous ways depending on the form factor of the fillers, which is considered as an important parameter, since it contains information about the size and shape of the single particles.

A more convenient scheme proposed by Mascia [52] for classification of fillers according to specific functions, such as their ability to modify mechanical, electrical or thermal properties, flame retardancy, processing characteristics. The classification of fillers according to five primary functions are as follows:

(1) Mechanical property modifier

(2) Fire retardancy

(3) Electric and magnetic property modifiers

(4) Surface property modifier

(5) Processing aids

For a given glass matrix, the choice of fillers is determined according to the desired changes on the final processed material. In general, the utilized substances as fillers must be meet a number of requirements set out below:

1 - Compatibility with the host matrix: non-toxicity, absence of discoloration or impurities, neutrality and chemical inertness, stability to heat and light and low water absorption.

2 - Uniformity of quality and granulometry.

3- Low cost

Note that fillers are mainly distinguished from other adjuvants by a much higher incorporation rate, ranging from a few percent to more than 40% and by their mode of action within the host matrix, which is rather physico-mechanical than chemical.

I.4.2 Composites

A composite is defined as a material composed of different heterogeneous elements. The composites are, generally, made up of a matrix, which ensures the rigidity, the material's texture, and another phase called filler, which has specific properties (electrical, mechanical, thermal) that one wishes to find in the desired composite material [51].

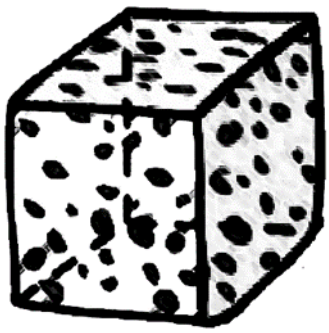

Figure I- 11 : Schematic representation of bulk composite.

Within the current study, the used fillers are in the form of metallic powders. They are incorporated in the glass matrix in order to make electricity conducting glass-based composites

useful for electronics and in particular for the solar cells (photovoltaics) and thermo-electric devices (see more details in the upcoming chapters).

In our case, the electrical conductivity of lead phosphate glasses is low. One way to improve this conductivity is to transform them into composites by inclusion of metallic fillers. These fillers were chosen to fill the electrical failure of lead phosphate glass matrix. For this reason, it would be intriguing to understand how the physicochemical properties of these new composites based on phosphate glasses can be improved?

Note that, binary phosphate glass-based composites are advantageous, because they are promising materials for the energy fields. Our team lab is a pioneer in the elaboration and the investigation of structural, thermal, electrical and thermo-electrical properties of similar materials group such as $ZnO\text{-}P_2O_5$ and $CaO\text{-}P_2O_5$ based composite [46-50]. Within the same work, authors have evidenced that an original insulating-conducting transition are prominently occurring in these types of composites.

The quality of a glass /metal conducting composite tightly depends on the qualities of the used conductive particles, in particular the nature, the shape and size of the particles. The investigated composites conductivity by Oabi et al [46,49] was found to be a function of the concentration of the conductive particles in the glass matrix. It has been found that the electrical conductivity of the phosphate glasses loaded with conductive particles increases non-linearly with volume increasing filler content ϕ, showing a percolative behavior [49,50].Critical threshold ϕc at which the conductivity sharply increases by several decades of magnitude from insulating to semiconducting or conducting range is observed [49,50].Theoretically, this phenomenon has been successively explained on the bases of different percolation models [54,55,56,57].

At low concentration, below a certain threshold called percolation threshold (by volume percent), the authors evidenced that conductivity of the elaborated composites versus temperature show typical behaviors of semiconductor materials with multiple conduction mechanisms. This mechanism will be fairly discussed and analyzed in the next chapter. At a higher concentration, the studied composites become conductor and at critical filler volume incorporation, conductor /non-conductor transition occurred. This finding has been extended by researchers of our laboratory, to the study of electrical conductivity and thermoelectric power as a function of temperature. The experimental findings indicated that for conductive composites ($\Phi > \Phi c$), a transition conductor / non-conductor known as the positive temperature coefficient (PTC) effect occurred. In the best of our knowledge this phenomenon has been first observed in such type of composites [46-50].

I.4.3 Applications of bulk composites

Similar composites types were elaborated by Oabi et al. [46, 49] in several previous works with different glasses namely zinc phosphate glass and calcium phosphate glass having high dielectric constants in comparison with silica dioxide [53]. These types of materials are dielectrics or insulators with low volume fraction. According to our co-workers' findings on phosphate glass based composites [46,47,48], these materials can be classified into two categories; dielectrics or insulators with low volume fraction of the filler, and semiconductors above percolation threshold or at higher filler volume fraction, which gives new application opportunities, using PTC effect, for example. This transition (PTC) occurs beyond the percolation threshold within these composites type. Moreover, these materials show also a high dielectric constant and high Seebeck coefficients, which can be applied in the thermoelectric field (see, fig. I-12).

Figure I- 12 : a- Dielectric capacitor b- Photovoltaic generation c- Thermoelectric effect.

They can potentially be useful in capacitor fabrications for energy storage, in the land-supply decoupling for secure signal integrity of high speed. Also, they are useful for reducing the electromagnetic interference, for cabling, for thermoelectric sensor, and auto-regulating heater, current limiters in circuit protection, thermal detector devices, divers' electronic devices, etc [46,47, 48]. Practically, these materials show different electrical phases which make the studied bulk composites as a suitable candidate for a large energy sector application field [47,48, 58]. However, for the current use, it is better to obtain these materials as thin films.

I.5 Lead phosphate glass-based composites as thin films

I.5.1 Different preparation methods

So far, several physical and chemical methods were employed for preparing thin films. The main intention of employing these techniques is to develop a material with multi properties, because every method has its own advantages and disadvantages [59]. The choice of technical deposition

is crucial step to obtain suitable properties since the preparation of the same material by different technical methods yield the different optoelectronic properties. In general, there are two main classes : vapor deposition and wet chemical methods.

I.5.1.1 Vapor deposition

Vapor deposition techniques can be classified into two main classes: Physical vapor deposition (PVD) and Chemical vapor deposition (CVD).

I.5.1.1.1 Physical Vapor Deposition (PVD)

The vapor is deposited on a substrate creating from a material source target under low-pressure conditions in a chamber [60]. The material source target can be evaporated by thermal evaporation (Vacuum evaporation) or bombarding (Sputtering) its surface with high energetic particles, often Ar+ gas. In Addition, reactive gases such as acetylene, nitrogen or oxygen might be injected into the vacuum chamber during the deposition to design different compound coating compositions. The result is a very strong bond between the coating and the tooling substrate, as well as, suitable tailored physical, structural and tribological properties of the deposited films.

I.5.1.1.2 Chemical vapor deposition (CVD)

Chemical vapor deposition involves the coating in the gas phase on a substrate within requiring vacuum [61]. It is the chemical reaction of precursors in the vapor phase, which distinguishes CVD from physical vapor deposition (PVD) processes. In this technique, the CVD sources used are mainly gases, volatile liquids, sublimable solids or a combination of these materials. This method is suitable to achieve high growth rates and produce a large variety of films and coatings with high purity and at relatively low cost.

I.5.1.2 Laser ablation technique (laser beam)

The method consists of directing a pulsed laser beam PLD (Pulse Laser Deposition) on a target of the material to be deposited [62]. The material is placed in an ultrahigh vacuum chamber.

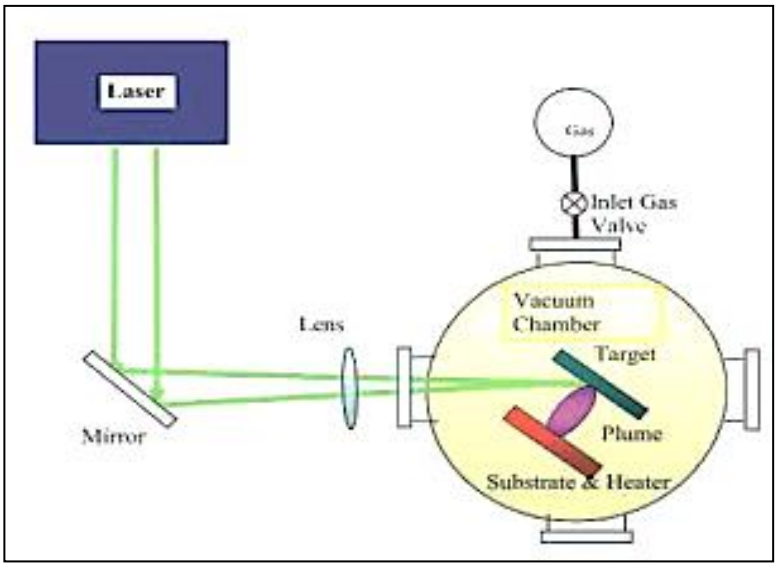

Figure I- 13 : A typical experimental setup of pulsed laser deposition technique [62].

The main advantage of this technique is that it allows the deposition at room temperature. Thus, it easily enables the coating of all types of substrates, ranging from semiconductors to polymer materials. Therefore, we find no polluting thermal source inside the main enclosure of external thermal energy.

I.5.1.3 Wet Chemical Deposition methods

Wet chemical deposition is technique in which the material species to be deposited are dispersed in a liquid medium. The advantage of this technique is reflected in its ability to produce coatings with high optical quality on different transparent substrate types.

I.5.1.3.1 Spray pyrolysis

The spray paralysis is one of the simple and inexpensive deposition method [63]. In this technique, fine droplets are sprayed onto substrates at controlled temperature. The precursor solution can be prepared by dissolving soluble salts (often metal-acetate or nitrate) in ionized water with specific molar ratio. The process is easy to perform and require only simple equipments and it is possible to coat large substrates with different geometries.

I.5.1.3.2 Sol-Gel

The sol–gel process, also called soft chemistry, allows elaborating thin films from a solution by using a sol or a gel as an intermediate step, and at much lower temperatures compared to other preparation methods [64].The synthesis of amorphous semiconductor glass thin films is carried

out by three principal steps: solution preparation, coating and heat treatment. Indeed, it involves chemical and physical processes such as hydrolysis, polymerization, drying and densification. The final solution can be also obtained by dissolving soluble salts (in our case nitrate) in a solvent and then spread across of substrates at room temperature. In general, the sol-gel method yields many advantages for synthesizing of a large variety of thin films with low cost.

I.5.1.3.3 Elaboration of binary glass thin films by sol gel route

The sol-gel method serves as a useful alternative to the conventional melt-quench method and refers to a low temperature synthesis method by using chemical precursors in liquid form to produce ceramics and glasses with high purity and homogeneity. The interest in producing glasses via sol-gel routes has been increasing very rapidly since the processing temperature is usually below the crystallization temperature of the oxide elements that allows the production of novel glass compositions [65].

Another advantage of sol-gel synthesis over the other methods is the tunable structure that allows control over the morphology, porosity, size, and the ability to modify the surface that is not achievable via the melt-quench route. The main advantages of the sol-gel synthesis are then ; High purity, Homogeneity and low processing temperature that allows incorporating different kinds of inorganic, organic, and biomolecules during the formation of a gel matrix and low energy required in comparison with the melt-quench method, also a variety of shapes and morphologies can be obtained.

The sol-gel process occurs where one or many elements are used to form a sol from which is transformed to a homogeneous and amorphous gel [66]. In this process, choosing the right precursors, temperature of the precursor, solutions and appropriate ageing time have been found to be critical processing factors [67].

At a very early stage of the development of sol-gel technology, the need for precursor compounds that have high solubility in an organic solvent that can easily transform into chemically reactive forms are essential.

For binary phosphate glass elaboration, many studies have shown that phosphoric acid (H_3PO_4) cannot be used as a phosphorus precursor because it is too reactive and leads to precipitation rather than gelation and more convenient precursors could be obtained by dissolving P_2O_5 into alcohol solutions [68 ,69]. Tang et al. [70] have successfully synthesized transparent titan-phosphate sol-gel derived glasses with high refractive index for optical applications by using triethyl phosphate as a phosphorus precursor. In another study by Carta et al. [65], quaternary

phosphate-based glasses in the P_2O_5-CaO-Na_2O-SiO_2 system with low silica content were successfully prepared by using P_2O_5 dissolved in anhydrous ethanol. Also, silicate free sol-gel glasses in the P_2O_5-CaO-Na_2O system were successfully synthesized for biomedical application purposes [71,72]. The process of reacting from the liquid may allow these sol-gel derived glasses to be drawn into fibers, micro/nano-sized glass spheres, or as a thin film on a substrate. Low processing temperatures also have direct and positive implications for biomedical applications, specifically in drug delivery systems that offer molecular control over the incorporation of active biological ingredients such as antibiotics and chemotherapeutic molecules into the glass structure [73]. A comparison between sol-gel and melt-derived glasses with similar compositions appear to have similar structure and atomic correlations [74].

I.5.2 Applications

One of the most important applications based on optical properties of glass today is in the field of information technology. Additionally, the absence of long-range order allows the modification of their optical properties to a specific technological application by continuously changing their chemical composition [75]. For instance, the use of chalcogenide glasses offers notable advantages such as remarkable optical properties like a wide transmission window (1–20 μm), high refractive index, making them suitable for sensitive detection of clinical or environmental changes [76-87]. Chalcogenide optical waveguides also play a significant role in the development of optical biosensors [88].

Elsewhere, the easy preparation and cheap cost of phosphate glasses as composites should be open a new opportunity of industrial applications. We deduce also that amorphous films are known to have properties that are sometimes different from their bulk glass counterparts.

Solar cells:

Solar cell photovoltaic technology can directly convert light energy into electric current. Until recently, the photovoltaic (PV) cells are a vital present-day commercial industry and there is a potential to grow enormously in the future [89,90]. Figure I-8 displays a typical architecture of inorganic thin films solar cell of Chalcogenide glass composite materials containing a mixture of amorphous and crystalline phases. The solar cell is generally made up from several layers each one has specific properties. If only one of these layers fails in its task, then solar cell devices yield poor efficiency. Among critical components, the amorphous semiconductor layer acts as a front electrode in the solar cell device. The electrode allows light to pass through to the active

layer, where the photo generated charge carrier occurs, and it acts as a conductor for the transfer of the charges wich are generated out of the solar cell device.

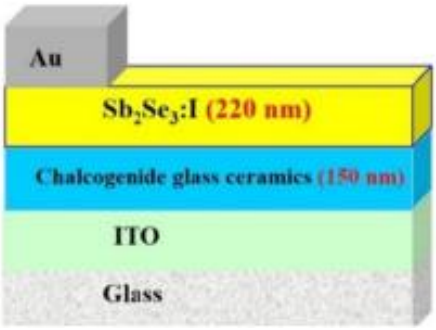

Figure I- 14 : Schematic view of chalcogenide glass/ceramics based solar cell [91].

Within the silicon industry, research continues to improve cell performance. Among the innovative structures, we find cells with silicon hetero-junctions (HET cell)

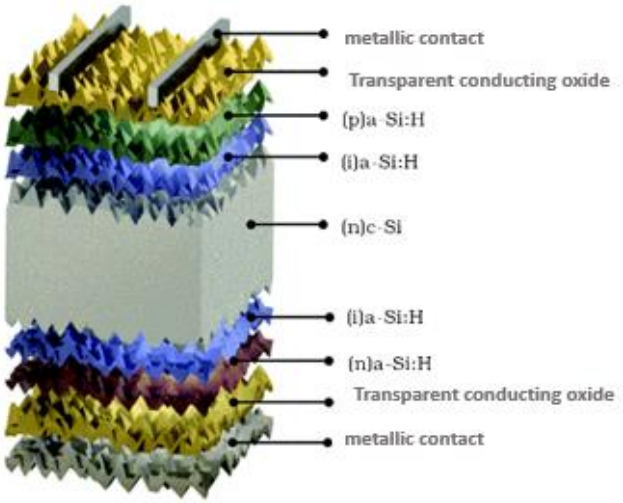

Figure I- 15 : Structure of a standard hetero-junction cell (HET) [92].

Figure I-15 shows the different layers of materials of a standard structure of a HET cell. After etching on both sides of c-Si to create texturing and decrease reflectivity, layers of amorphous hydrogenated a-Si: H silicon of around 10 nanometers are deposited. On the front face, the a-Si: H layer is made up of two parts: an intrinsic a-Si: H layer used to passivate the c-Si surface and heavily doped P-type layer that plays the role of transmitter of the P / N junction.

Flat-panel display:

Amorphous silicon thin films might be used in new indirect type a-Si flat-panel detector for medical imaging. Amorphous silicon flat-panel detector is used for digital radiography. Elsewhere [93], a prototype flat-panel detector was fabricated using a p–i–n photodiode/thin-film transistor (TFT) array [93].

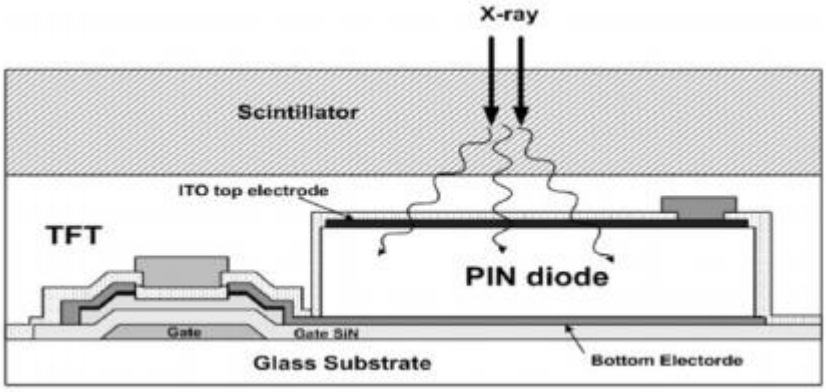

Figure I- 16 : The cross-sectional structure of an indirect-type flat panel detector [93].

A photosensor is built into each pixel and the entire array is covered by a scintillating layer, where X-ray interact and produce visible light. Electron–hole pairs are generated by this light from the scintillating layer and are collected in the photosensor.

I.6 Aim and scope of the present study

The aim and scope of the present thesis work is to prepare binary phosphate glass based composites in bulk and thin film forms and study their properties using different experimental techniques. In the best of our knowledge, no attempt was so far made, to study this glassy system in two different forms in one go. Their usefulness is mainly exhibited in the electrical and thermo-electrical properties.

The scope of the present investigation can be broadly outlined as below:

- Preparation of different glass systems as given below in bulk form. $xPbO\text{-}(1\text{-}x)P_2O_5$, (x = 20,45,60 and 80mol%).
- The one pure glass system of composition $45mol\%PbO\text{-}55mol\%P_2O_5$ has been found the most suitable for this study in terms of chemical and thermal stability as well as concerning higher transparency and amorphous nature compared to other elaborated samples,
- Determination of the physical properties like density and porosity,

- Investigation of structural (XRD) and morphological (SEM,TEM) properties for both bulk and thin film samples,
- Thermal properties using Differential Scanning Calorimetry (DSC) studies to determine glass transition temperature (T_g), onset of crystallization and peak temperature of crystallization,
- Studies of electrical and thermo-electrical properties for both bulk and thin films composites versus filler contents,
- Optical absorption studies on thin film glasses to determine refractive index, and band gap energy variation versus fillers concentrations.

Conclusion

The main goal of this chapter is to identify and justify the choice of the studied systems. It deals with the basic properties of amorphous semiconductors, namely, the basic classification, preparation, and structural properties of lead phosphate glasses in bulk and thin film forms. Thus, we have shed a light on glasses, which are considered as distinctive class of amorphous solids. They are electrically insulating, but also can be transformed into semiconductors or conductors when they are loaded with conducting particles. This has opened a new exciting field of research and many potential applications in energy field.

Since amorphous semiconductors have attracted most interest, because of their potential applications due to their fascinating properties. We focused on miniaturization of lead phosphate glass-based composites by studying their based thin films, which are found to have significant electrical conduction and optical transparency as referred to as amorphous semiconductors.

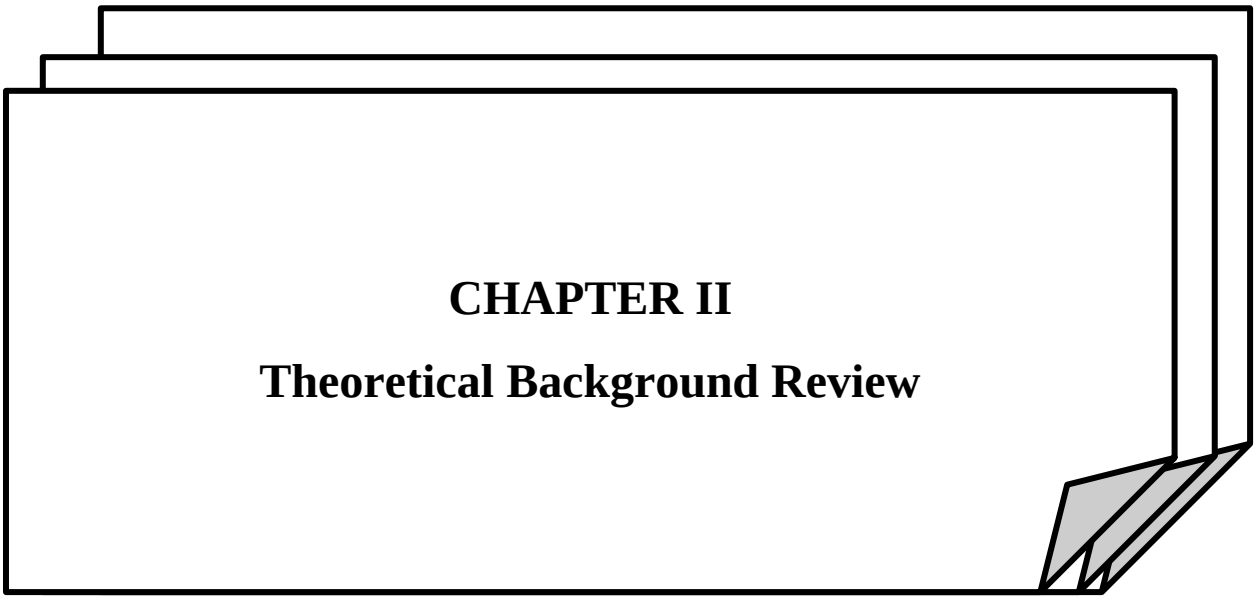

CHAPTER II

Theoretical Background Review

II.1 Introduction

As aforementioned before, the aim of this thesis work is focused on structural, thermal, electrical and optical investigations of composites based on phosphate glass filled with conductive particles in bulk and films shapes. Thus, in current chapter, we will be interested in bulk and films composites; we discuss different concepts for better understanding of several physical properties given in the upcoming chapters of the manuscript. We are mainly interested in electrical transport through disordered heterogeneous binary system using the concept of percolation theory at ambient temperature. Then, to understand different conduction mechanisms versus temperature, we have reviewed the electronic band energy of crystallized and amorphous solids.

However, it is well known that the properties of wetting and interface exchange between the matrix and the filler play an important role in the physical properties (stability, mechanical, electrical properties, etc.) of the composite material, hence it can help in modeling electrical behavior. Therefore, we firstly give the theoretical approach to determine the surface and interface energy of materials using contact angles [94, 95, 96, 97].

II.2 Contact angle, surface and interface energies

II.2.1 Contact angle studies.

Contact angle (θ) is an angle of deflection θ formed between the droplet and the surface. The contact angle is mainly determined by the tangent of the contour of the droplet deposited on the solid surface. It is the angle between these two lines as shown in the Figure II-1.

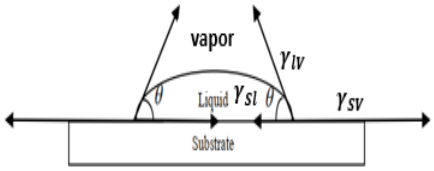

Figure II- 1 : Typical figure of contact angle formed by liquid on the substrate[98]

As can be seen, the shape of the droplet (Figure II-1) on the surface of a solid is governed by 3 parameters [99]:

- surface tensions at the liquid-vapor interface (γ_{Lv}) or γ_L,
- surface tensions at the solid-liquid interface (γ_{SL})

- surface tensions at the solid-vapor interface (γ_{SV}) or γ_S.

These surface tensions can be highlighted by a few simple observations:

• The water rises in a capillary tube above the level in the initial container.

• A paper clip can float on the surface of the water, even if it is made of steel.

• There is a meniscus on the surface of a liquid, in contact with the wall of the container.

• Soap bubbles exist!

These experiments demonstrate the existence of a force, f on the surface of a liquid. The liquid surface has its own properties, different from those of the rest of the liquid [99]:

-There is a force, f, between the interface of a liquid and another medium.

-The surface tension γ is measured by the quotient of the intensity of the force f by the length L over which it is exerted:

$$\gamma = f / L \qquad \textbf{(II-1)}$$

With γ in $N.m^{-1}$; f in N; L in m.

The surface tension depends on the liquid and the nature of the other part of the interface (gas, air, glass, metal ...); Ex: water / air $\gamma = 73\ 10^{-3}$; oil / air $\gamma = 32\ 10^{-3}$ N/m.

The surface tensions and energies therefore have respectively a force per unit of length ($N.m^{-1}$) and an energy per unit of surface ($J.m^{-2}$), they have the same dimension equation.

The contact angle can have several different values:

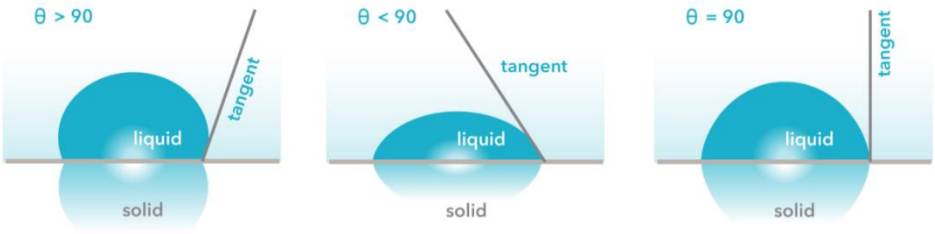

Figure II- 2 : Typical contact angle values made by liquid on the substrate [94].

Three cases are possible:

$\theta < 90$: the liquid partially wets the solid (water / dirty glass),

$\theta \geq 90$: the liquid does not wet the solid (ex: mercury / glass),

$\theta = 0$: the liquid completely wets the solid (water / clean glass).

Measuring this angle gives us three types of information [99]

-If water is used as the contact angle measurement liquid, we can deduce the hydrophobic (wide angle, low surface energy) or hydrophilic (small angle, large surface energy) nature of the surface.

-If we use several different reference liquids, we can access to the free energy of the surface, while discriminating the polar or non-polar components of this energy using the Owens -Wendt model [100]

-If we measure the hysteresis between the angle at the advancement and the withdrawal of the droplet, we obtain information on the physical non-homogeneity (roughness) or chemical non-homogeneity of the surface.

II.2.2 Solid-Liquid Adhesion work and Surface energy of solid

Surface energy of a solid is a measure of the exchange of physical interactions with other media. Young observed that, when a droplet of liquid is deposited on a flat surface, there is an interaction of the three components of surface tension (figure II-1) giving arise at equilibrium, a certain contact angle.These components are linked to the surface tension acting on the vapor/liquid interface (γ_L), the solid/liquid interface (γ_{SL}), and at the solid/vapor interface (γ_S). From a vector analysis, Young has successfully extracted the following expression [95, 100]:

$$\gamma_S = \gamma_{SL} + \gamma_L \cos\theta \qquad \textbf{(II-2)}$$

This equation is very important because it shows that γ_L is often known, θ is measurable, therefore, it is necessary to have additional relations, to determine the unknowns γ_{SL} and γ_S. Several models have been developed to estimate these parameters.

Thus, using thermodynamic considerations, Dupré [101] established a relationship with the work of adhesion (w_{sl}) between the solid and the liquid as:

$$w_{sl} = \gamma_s + \gamma_l - \gamma_{sl} \qquad \textbf{(II-3)}$$

By introducing equation (II-2) in equation (II-3), we obtain a simplified solid -liquid interfacial energy or wettability as:

$$\mathbf{w_{SL}} = \boldsymbol{\gamma_L}(1+\mathbf{cos}\theta) \qquad \textbf{(II-4)}$$

Elsewhere, Fowkes expressed free surface energy as the sum of two terms representative of the contributions of dispersive (London) and polar (Debye, Keesom, hydrogen bond) interactions [94,95] :

$$\gamma = \gamma^d + \gamma^p \quad \textbf{(II-5)}$$

Thus, the dispersive part in the adhesion work between a solid and a non-polar liquid becomes:

$$W_{SL}^d = 2\sqrt{\gamma_S^d . \gamma_L^d} \quad \textbf{(II-6)}$$

Keeble, Owens and Wendt [94,95,96] extended this relationship to polar interactions, by applying the geometric mean method and finally showed that adhesive energy can be expressed as the geometric mean of dispersive and polar component of solid and liquid interphases as :

$$W_{SL} = \gamma_L(1+cos\theta) = 2\left(\sqrt{\gamma_s^d}\sqrt{\gamma_l^d} + \sqrt{\gamma_s^p}\sqrt{\gamma_l^p}\right) \quad \textbf{(II-7)}$$

The solid-liquid interfacial free energy interaction can be written also as:

$$\gamma_{SL} = \gamma_S + \gamma_L - 2\sqrt{\gamma_S^d . \gamma_L^d} - 2\sqrt{\gamma_S^p . \gamma_L^p} \quad \textbf{(II-8)}$$

This equation can be solved by introducing a pair of polar and non-polar liquid.

Hence, the interface energy of the matrix-filler composites can be deduced [96,97]as:

$$\gamma_{mf} = \gamma_m + \gamma_f - 2\sqrt{\gamma_m^d . \gamma_f^d} - 2\sqrt{\gamma_m^p . \gamma_f^p} \quad \textbf{(II-9)}$$

The index m and f design the matrix and filler respectively.

II.2.3 Owens-Wendt method determination

As there are no direct methods for determining the surface energy of solids. Various indirect methods are considered within several previous works [95, 102-108]. The ones worth mentioning are Fowkes, Owens–Wendt and Wu methods [95, 106].

The wettability, surface energy and matrix-filler interface energy of our elaborated composites have been determined by the A. Maaroufi method [99], using the process of Owens–Wendt; by applying the following equation:

$$\gamma_L\left(1+\cos\theta\right) = 2\sqrt{\gamma_s^d \gamma_l^d} + 2\sqrt{\gamma_s^p \gamma_l^p} \quad \textbf{(II-10)}$$

This equation can be simplified as:

$$\frac{\left(1+\cos\theta\right).\gamma_L}{2\sqrt{\gamma_L^d}} = \sqrt{\gamma_S^p}.\sqrt{\frac{\gamma_L^p}{\gamma_L^d}} + \sqrt{\gamma_S^d} \quad \textbf{(II-11)}$$

It is written in the form of : $Y = ax + b$,

Where:

$$y = \frac{(1+\cos\theta).\gamma_L}{2\sqrt{\gamma_L^d}}$$

$$x = \sqrt{\frac{\gamma_L^p}{\gamma_L^d}} \; ; \; a = \sqrt{\gamma_S^p} \; ; \quad b = \sqrt{\gamma_S^d} \qquad \textbf{(II-12)}$$

The determination of the dispersive and polar components of γ_s therefore requires the measurement of the contact angle θ. The experimental measurement of θ is given in chapter IV. It is important to note that these measurements will allow the determination of surface or adhesin energy (W_{SL}) of our composites and interfacial energy (γ_{SL}) of phosphate glass/filler composites (see chapter IV).

II.2.4 The choice of liquids used for Owens-Wendt method

From the value of contact angle, one can measure the strength of interaction forces between the solid substrate and the molecules of the used liquid, with γ_L which is known. Thus, we have used series of liquids with different polarities. Different straight lines are obtained and polar and dispersive component of surface free energy of solid can be calculated from the best fit line.
In this model, surface energy of solid is divided into two elements: polar surface energy and dispersive surface energy. The summation of two energies is the total surface energy as expressed above Eqt. (II-5) and by following equations:

$$\gamma_L = \gamma_L^d + \gamma_L^P$$
$$\textit{and} \qquad \textbf{(II-13)}$$
$$\gamma_S = \gamma_S^d + \gamma_S^P$$

In order to apply this model on our samples, we used different solvents such as distilled water, ethylene of glycol and glycerol. The wettability, surface and interface matrix-filler energies of our elaborated composites are determined.

II.3 Conduction behavior as filler content (ϕ) of composites based on glass matrix loaded with conductive particles

For lead phosphate glass/metals composites (PbP/metals) being elaborated during this work,the variation of the electrical conductivity versus filler contents shows firstly that glass/metals composites are insulator phase. Then, the conductivity slowly increases until it reaches a critical

value or threshold, and then suddenly increases for decades, indicating an insulating to conducting phase transition as showed by figure II-3.

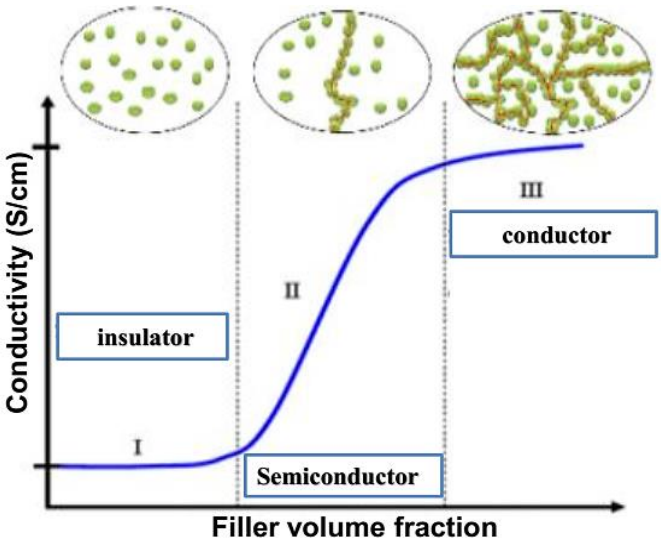

Figure II- 3 : Schematic representation of the dispersion of metallic particles in the glass matrix [109].

Indeed, as illustrated in the above figure, the metallic particles are randomly dispersed in the glass matrix. At the low loading, the filler particles are lying far apart (Part I) and cannot contact with each other just like "islands" in the sea, leading to conductivity of the composite, which is almost equal to the conductivity of the neat glass matrix. When the filler content increases and approaches the critical concentration, the fillers become relatively interconnected (Part II), and the conductivity becomes possible, which reaches the so-called percolation threshold. Any higher filler loading leads to the formation of more continuous conductive chains (paths) which are formed by contact of conducting particles with each other's (Part III). This would build greatly enhanced electrical conductivity which reaches semi- metallic or metallic behavior [109,110,111]. Hence, the observed behavior was interpreted on the basis of percolation theory.

II.4 Percolation theory and conduction

Percolation theory is a very powerful technique for dealing with physical properties associated with spatially random processes occurring in inhomogeneous systems. It deals with the effects of varying the number of interconnections and the appearance of a sharp phase transition at which a long-range connectivity suddenly appears in a random system [112, 113].
Percolation theory has a practical importance, which lies in its applicability to a wide range of physical phenomena. They include metal-insulator transitions in random binary composites,

hopping conductions in amorphous semiconductors, sol-gel transitions in polymers, electron localizations in disordered potentials, magnetic transitions in dilute ferromagnets, etc. This theory has been reviewed by many authors like Stauffer et al. [113], Shklovskii and Efros [114], Bergmann and Stroud [115]etc.

II.4.1 Percolation threshold

The percolation threshold is often used as a parameter to characterize a material, we have just shown in the previous section the existence of a critical conduction threshold, called percolation threshold, beyond which we observe a sudden and sharp increase of electrical conductivity due to the creation of conductive paths through the insulating matrix.

The existing experimental data in open literature show that the percolation threshold strongly depends on the nature of the matrix and the geometric and physical characteristics of the inclusions (size, shape, aspect ratio and electrical conductivity) [112,116]. It is also depending on the fillers-matrix interfacial interaction. This latter can be extracted from contact angle measurement [97].

II.4.2 Electrical conductivity modeling

Nonlinear conduction is a very common feature of inhomogeneous systems. However, surprisingly, barring sporadic efforts in the past, the topic did not receive sustained attention from people working with these systems. It was not appreciated that since the nonlinearity arises primarily due to randomness of the disorder itself, its systematic study could only lead to greater understanding of the effects of disorder on the transport process. Some old theories known as the "effective medium" consider the material as a mixture of two types of particles (conductive and insulating) and replace the heterogeneous medium by an equivalent homogeneous medium [117-120]. They consist in making the local properties of this mixture (conductive and insulating) homogeneous. These theories give good results far from transitions when they are observable or when the properties of the constituents are comparable. However, these theories could not take into account the position of the transitions and of the behaviors in the vicinity of the transition threshold. The weakness of these theories is that they do not take into account the existence of statistical clusters of connected particles within the medium which possibly lead to infinite clusters crossing the medium.Thus,a "good" theory is the one that describes the connectivity of particles. This is the case of percolation theory, which is being firstly as a structure theory of random media. Indeed, it offers a set of predictions in good agreement with experience. In this

context it should be noted that the first percolation process was developed by chemists P. J. Flory [121] and W. H. Stockmayer [122] to describe the polymerization of branched molecules during a sol-gel transition [123, 124]. Flory has particularly highlighted the sudden transition from the solution state to the gel state for some progress of the reaction. It shows that this transition corresponds to the appearance of a macroscopic structure of branched chains [124, 125]. Afterward, Broadbent and Hammersley introduced mathematical concept of percolation firstly in 1957 [126] to study the phenomenon of diffusion of a fluid through a porous medium. Then, it was applied to study different phenomena, in particular electrical conduction in heterogeneous media (dc conduction). As previously well detailed above, for conductor and insulator mixture, there is a critical concentration of conductive particles for which the dc conductivity is enhanced remarkably; it is the percolation threshold, which is linked to the appearance of a conductive path through the sample. Thus, the electrical conductivity modelling is desirable for allowing the prediction of electrical properties in such mixtures.

Among the parameters influencing the percolation, we found that filler distribution, filler shape, filler/matrix interactions and the processing technique are the most important ones [112,116].

For conductivity prediction based on these parameters, different models have been proposed. A few important percolation theories and models are given later within the current chapter. Most modeling of electrical properties of composites have been performed on the dc conductivity/resistivity. There are four main classes of conductivity models found in literature, and they include statistical, thermodynamic, geometrical, and structure-oriented models [116,127,128]. Each class predicts the electrical conductivity based on distinct approaches taking into account parameters described above. The most applicable models to conducting lead phosphate glass/particles composites are statistical and thermodynamic percolation models [110,111,112].

II.4.2.1 Statistical model

In the aim to adjust these experimental data, several models were suggested by different authors [19,23,35,36,37][112,116,127,128,129]. We quote those, which, in our opinion, are most significant. Since one of our objectives is to find a theoretical law, which gives the same shape, which is experimentally obtained, we will try to adjust the various parameters explaining the variation of electrical conductivity of the composites versus of conducting particles loading.

The model set out by Kirkpatrick [127] follows a power law in which the dimensionality of the medium is involved and allow describing the conductivity of composite σ beyond the percolation threshold:

$$\sigma = \sigma_0 . (\phi - \phi_c)^t \quad \textbf{(II-14)}$$

Where σ_0 is the filler conductivity, ϕ refers to volume fraction of the conductive particles, ϕ_c presents volume fraction at the percolation threshold and t is a critical exponent. This critical exponent reflects the dimensionality of the system. For an isotropic system in Mean Field Theory of the three directions of space, it is found between 1.6 and 2 [130, 131, 132].It is worthy to note that, the statistical percolation theory of Kirkpatrick has fairly described many experimental data near the critical region and thus provides the possibility to easily obtain percolation threshold value and a universal power exponent t [15,16,17][108,109,110]. It does not suppose any interactions between matrix and fillers. It allows linking the electrical conductivity behavior of composite to the growing of clusters of connected filler particles, which enable formation of the infinite conducting cluster over the boundaries of the system at critical value ϕc of filler.

II.4.2.2 Models based on the thermodynamics of percolation

II.4.2.2.1 Mamunya Model

The kirckpatrick model became the basis for numerous later conductivity models. Thus, Mamunya et al.[116,129]have established new model by taking into account the matrix-filler interface energy is follows as:

$$\sigma = \sigma_o + (\sigma_m - \sigma_o) . \left(\frac{\phi - \phi_c}{F - \phi_c} \right)^{t_{eff}} \quad \textbf{(II-15)}$$

$$\text{Where } \mathbf{t_{eff}} = \mathbf{t_1} + \mathbf{t_2} \quad \textbf{(II-16)}$$

σ is the composite conductivity, σ_0 is the filler conductivity, $\sigma_m$is the maximal conductivity of composite, ϕ is the volume fraction, ϕ_c is the percolation threshold. F is the filler packing density coefficient (equivalent to the maximal value of the filler volume fraction, which can be loaded). The value t_{eff} is effective critical exponent, which is mainly dependent on matrix-filler interaction [110,111,112].

Mamunya et al. [116].studied the composite conductivity versus filler volume fraction, allowing to evaluate the influence of many factors such as the nature of the matrix and filler's characteristics (nature, size, shape, etc). Also, the model showed that the percolation behavior is

dependent of matrix-filler interaction [112].The exponent t_1 is equivalent to the t parameter in the basic Kirkpatrick Eq.(II-14), corresponding to the universal conductivity critical exponent for three –dimensional lattices in the mean field theory [131, 132].. It takes a value near 2. The exponent t_2 is supposed to take into consideration the constituent characteristics of composites, matrix-filler interface interactions and possible interparticles tunneling exchange [133, 134]. or anisotropy effect [135]. Thus, these effects allow to t_{eff} taking higher values and breaking the universality of the critical exponent.

II.4.2.2.2 Updated Mamunya Model

In our previous studies [110,111,112]., we have used the Mamunya et al. model [116,129]., taking the interface matrix-filler interactions by using the effective exponent t_{eff}. In the present study, we are able to determine the matrix-filler interface energy (see Eqt.II-9) by using the contact angle measurements. Thus, we will use this thermodynamic model as given by Mamunya et al. [116,127].:

$$\log\sigma = \log\sigma_0 + (\log\sigma_m - \log\sigma_0).\left(\frac{\phi - \phi_c}{F - \phi_c}\right)^k \qquad \textbf{(II-17)}$$

Where $k = \dfrac{K\phi_c}{(\phi - \phi_c)^n}$ and the exponent K is expressed as a function of the interfacial energy γ_{mf} (mJ/m²)) (see Eqt.II-9) between matrix and dispersed particles as follows:

$$K = A - B\gamma_{mf} \qquad \textbf{(II-18)}$$

A and B are two adjustment constants. The value of *k* depends on the volume fraction of the inclusions, the percolation threshold and the interfacial tension.

The results will be compared with these obtained using Eqt.(II-15).

II.5 Electrical transport mechanisms in thin film and bulk composites

II.5.1 Electronic structure in order solid

The percolation theory is a macroscopic approach, which describes successfully the conductivity behavior as filler content in matrix. However, to understand the mechanisms of electronic conduction a short review on the distribution of electrons in the energy bands inside the solid state is necessary. In the case of ordered solids these bands take the following forms :

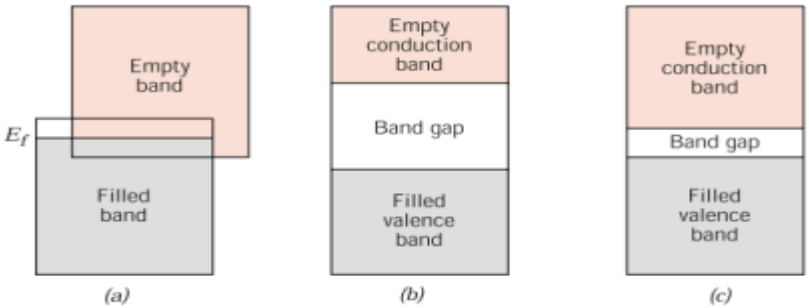

Figure II- 4 : The various possible electron band structures in solids at 0 K. (a) The electron band structure of metals. (b) The electron band structure characteristic of insulators which is relatively large band gap (> 3 eV). (c) The electron band structure of semiconductors [136]The mechanisms of electrical properties result from the distribution of electrons in the energy bands.

In metals (conductors), the conduction band and the valence band overlap. The electrons can then get closer between the atoms. Thus, the solid is fully electronic conductor (conductivity $\sigma \geq 10^{+4}$ $(\Omega.m)^{-1}$); example: cooper, silver, aluminium,…

In insulators, the band gap width separating the conduction band and the valence band is large (Eg ≈ 5 eV). There is no accessible energy level for electron. Hence, conduction is very low (conductivity $\sigma \sim 10^{-10}(\Omega.m)^{-1}$) or lower; example: quartz, diamond, …

In semiconductors, the width of forbidden band is lower (Eg ≈ 1-3 eV). Conduction remains low; however, it increases significantly with temperature, which means that conductivity is related to mobility and the number of charge carriers, $\sigma \sim 10^{-4}$ to 100 $(\Omega.m)^{-1}$; example: germanium (Ge), silicon (Si), etc.

The order magnitudes of the conductivity are given in figure II-5:

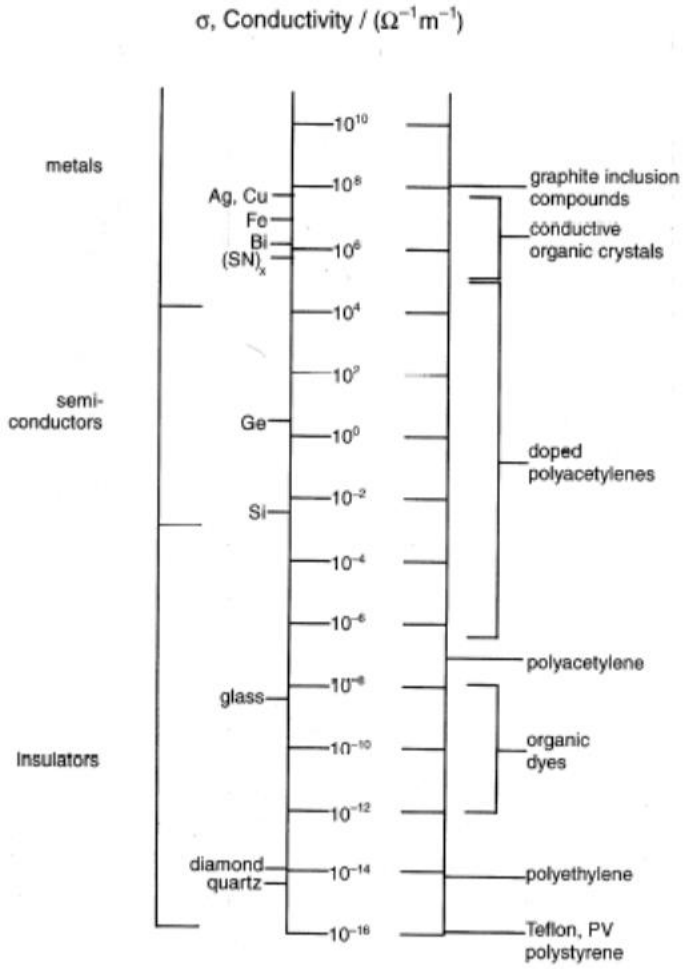

Figure II- 5 : Conductivity order magnitude of crystalline phase at room temperature [137].

In the semiconductors, electrons and holes provide the conduction phenomenon. Indeed, at ambient temperature and under illumination, when energy of photo-excited charge carrier reaches a value greater or equal to the band gap energy of the studied material, the electron can transit from the occupied states in the valence band to the un-occupied states in the conduction band, leaving one hole in the valence band (Figure II-6):

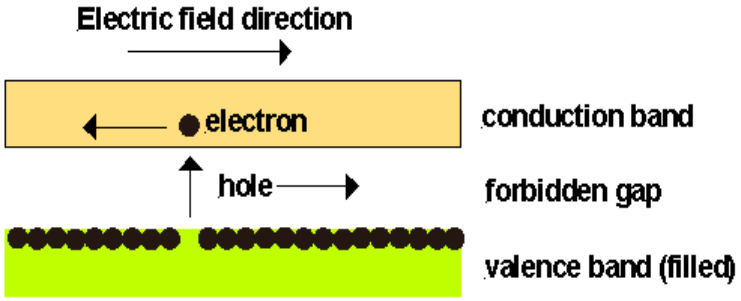

Figure II- 6 : Conduction via electrons and holes in a semiconductor [138].

This process is named a generation phenomenon. Usually, the generation phenomenon can only happen if the light energy is larger than the band gap energy of semiconductor. For a wide-band-gap semiconductor, this band gap energy is correspondent to the visible or ultraviolet spectrum excitations. The basic idea is to create free charge carriers (electrons or holes) in wide-band-gap semiconductor through appropriate charge carriers, which can be achieved by metallic incorporation (composites). This may be playing a critical role for enhancing their electrical conductivity. Generally, these charge carriers should be shallow and localized around the bottom of the conduction band. It leads to increase the electron concentrations in the conduction band and thereby improve electrical conductivity. Thus, the well-known relation for the conductivity of metallic crystal:

$$\sigma = ne\mu \qquad \textbf{(II-19)}$$

Or :

$$\boldsymbol{\sigma = \left(ne^2 \tau \right) / m_e}$$

Where $\boldsymbol{\sigma}$ denotes electrical conductivity; $\boldsymbol{n}$ denotes concentration of charge carriers; $\boldsymbol{e}$ is the electronic elementary charge; μ refers to the mobility of the charge carriers, $\boldsymbol{\tau}$ denotes the electron relaxation time, and m_e denotes the electron effective mass. The mobility is given by :

$$\mu = \frac{e\tau}{m_e} \qquad \textbf{(II-20)}$$

For the semiconductor, it is necessary to distinguish between the mobility $\mu\boldsymbol{n}$ of the electrons and that $\mu\boldsymbol{p}$ of the holes. The Eqt.(II-19) becomes:

$$\sigma_{semiconductor} = \sigma_{electrons} + \sigma_{holes} \qquad \textbf{(II-21)}$$

In amorphous semiconductor, the conduction mechanism is somewhat more complex. Indeed, the energy bands take a complicated structure.

II.5.2 Energy Band Theory and conduction in Amorphous Semiconductors

In this section, some aspects of electronic structure in amorphous solids will be briefly discussed. Like crystalline solids, there is also the band gap in amorphous solids. However, the band gap in disordered material is a bit different, because tails of valance and conduction bands are entangled. Thus, the concept of density of state g(E) and band gap are usually retained in the discussion of electronic properties of non-crystalline materials [139].

Unlike crystalline solids, the mobility associated with the band gap of amorphous materials is very low and the conduction is due to thermal activation from one localized state to another

[48][140]. A large number of parameters are required for their characterization, as the amorphous materials are disordered. Also, given that the theoretical models for amorphous solids cannot always explain the experimental data, some approximations are required.

Very often, the density of states g(E) approach is used to explain or predict the properties of a material in the band theory. It denotes the number of electron states per energy unit per electron that a material would have at an energy level. The g(E) approach was successfully used to describe several characteristics found in a crystalline semiconductor.

In fact, when it was discovered that amorphous and crystalline semiconductors shared the same basic electronic and optical properties [49] [141].. It immediately led to the thinking that the g(E) of the amorphous semiconductor might be similar to that of its crystalline counterpart and not completely different as it was thought initially. This can be clearly visualized with the three popular density of states models as shown in Figure II-7:

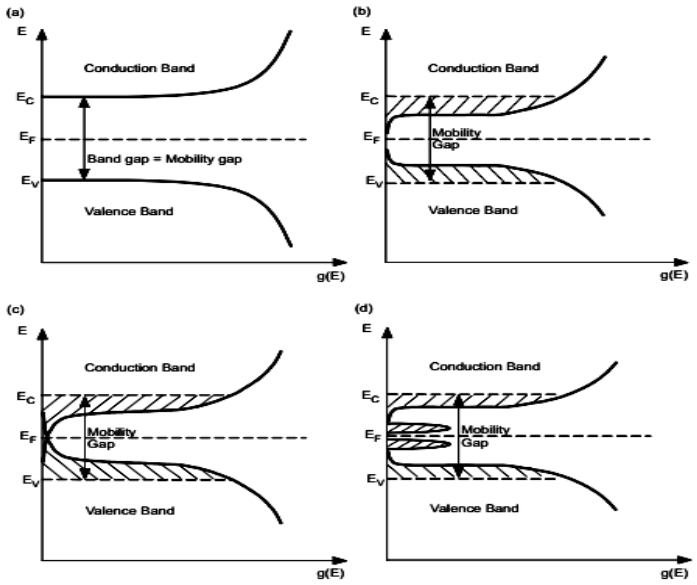

Figure II- 7 : (a): Energy-State density of a crystalline semiconductor ; (b) Energy-State density models proposed by Mott for amorphous semiconductor;(c) DOS models proposed by Cohen, Fritzsche and Ovshinski (CFO) for amorphous semiconductor (d) Energy-State density models proposed by Marshall and Ownfor amorphous semiconductor. The hatched regions denote localized states [142, 143].

As can be seen in figure II-7, the energy bands are characterized by tails, compared to the crystalized semiconductor (see Figure II-7a). In these tails, the electronic states have a localized character and their nature changes from localized to delocalized at a critical boundary called the mobility edge (Figure -II-7b, c, d) or also as shown in g(E) versus energy diagram (Figure II-8):

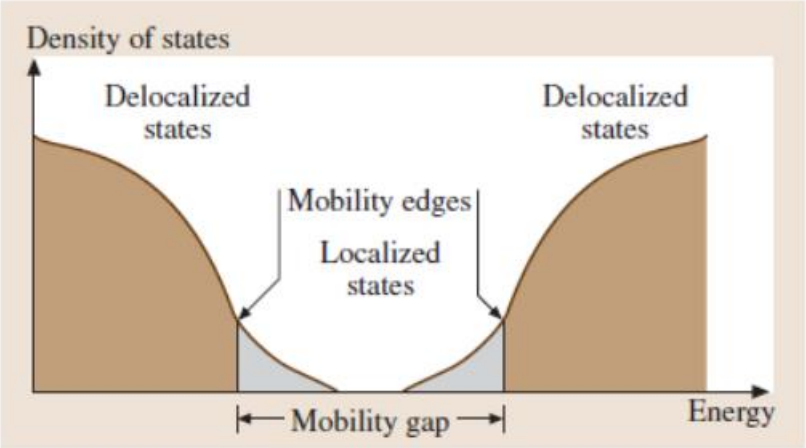

Figure II- 8 : distribution of energy states in the amorphous solid bands [144].

The energy separation between the two mobility edges of the conduction and valence bands is called the mobility gap. Also, it is referred as pseudo gap energy, Eg. Unlike the extended states found in the two principal bands, electrons in the localized states (tails) are not free to travel anywhere in the material. While some of these localized states (tails) are created by the loss of long order range existing in amorphous solids. This shows clearly the complexity of electronic transport mechanism in the amorphous systems.

For our conductive composites, the electronic structure is more complex because the final material consists of conductive particles embedded in an insulating matrix. Indeed, the analysis with XRD technique on bulk and thin film composites show some diffraction peaks after load of some percent of filler (volume percent for bulk composites and weight percent for thin films). Thus, the composites at critical loading values can be considered as poor crystalline semiconductor and the percolation phenomenon indicates a transition from insulator to semiconductor or conductor phase.

II.6 The effect of the temperature on the electrical conductivity behavior of phosphate glass/metals composites

The previous studies of our research group [109,110,111,112]. on the similar phosphate glasses/metals ($ZnO\text{-}P_2O_5$/(Ni, Co) composites show that the effect of the temperature above and below the percolation threshold is fairly different. Thus, it is very exciting to explore the electrical behavior by changing the moderator oxide (PbO) in the glass composition.

II.6.1 Temperature effect on the conductivity of phosphate glass/ metals composites above the percolation threshold ($\phi > \phi c$)

The electrical conductivity versus temperature was studied by our group [145,146] on similar bulk phosphate glasses/metals composites (ZP/(Co,Ni)) beyond the percolation threshold ($\phi > \phi c$). It was found that the conductivity of elaborated composites exhibit at higher fillers incorporation a slight decrease as a function of temperature (see, Figure II-9), in good coherence with the metallic behavior, as expressed by the relation given above Eqt.(II-19):

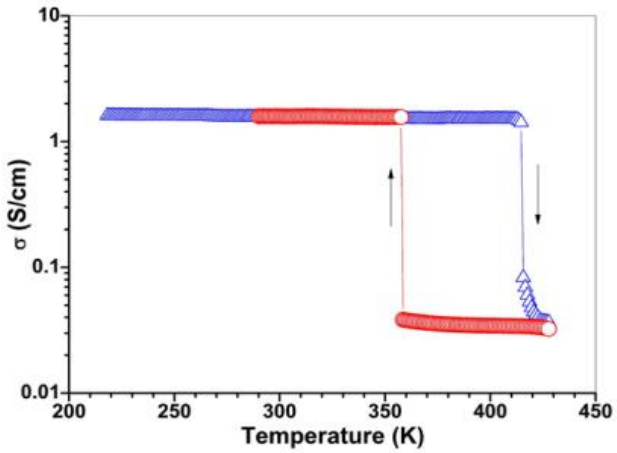

Figure II- 9 : Electrical conductivity of the (ZnO-P_2O_5/Ni (40 vol%) composite versus temperature (heating and cooling) [145].

Indeed, at high load, the filler clusters become more connected togethers to form crystal network, as confirmed by XRD measurements, showing the growing of organized system. Hence, the density of carriers increases to give a metallic behavior. However, at certain critical temperature T_c an abrupt decrease is occurred, revealing a conductive-insulating phase transition,called Positive Temperature Coefficient (PTC). This phenomenon (PTC) was for the first time explored in zinc-phosphate glass/metals composite (ZP/ (Ni,Co)) by our group [145,146]. Moreover, this transition showed small hysteresis, indicating first order phase transition.

Since this behavior originated from the 'positive temperature coefficient' (PTC) effect. It is defined by the amplitude of the conductivity jump called PTC intensity (I_{PTC}) [53, 54] [145,146] as given by the following equation:

$$I_{CTP} = \log\left(\sigma_{low} / \sigma_{RT}\right) \qquad \textbf{(II-22)}$$

Where σ_{RT} is the conductivity at room temperature and σ_{low} is the lowest conductivity after the PTC transition.

Note that the responsible mechanisms for the PTC effect are rather complex. PTC effect arise from the sudden drop of conductivity, leading to the break-up of the conducting chains, this behavior is more likely due to the expansion of the host matrix [145,146]. Within studies conducted by Maaroufi et al. [145], the PTC phase transition has been explained on the basis of volume expansion of the host glass matrix as illustrated in figure II-10:

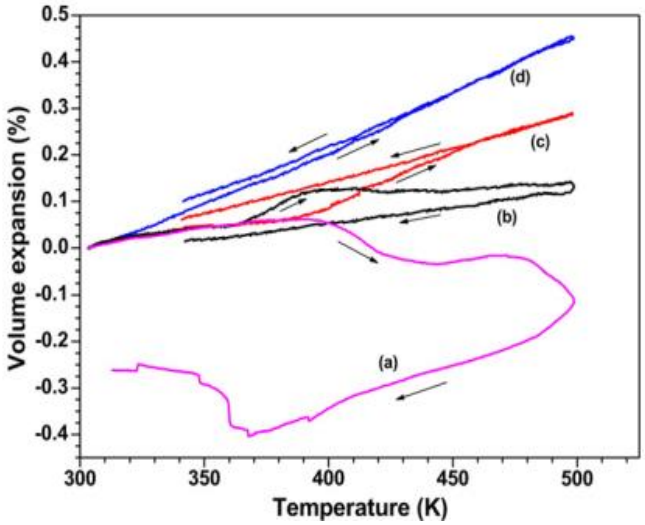

Figure II- 10 : Temperature dependence of volume expansion of ZP/Ni composites for different Ni filler loading: (a) ZP-matrix, (b) 40, (c) 36 and (d) 7 vol. % [145].

Finally, it is important to note that the observed PTC transition on this kind of binary phosphate glass-based composites (ZP/ (Ni, Co)) is reversible.This may open a new opportunities of industrials applications, as electrical switching, for example. This makes the study of these materials on a new phosphate glass matrix as the bulk shape and especially the films more exciting (see chapters V and VI)

II.6.2 Temperature on the electrical conductivity of phosphate glasses/ metals composites bellow the percolation threshold ($\phi \leq \phi c$):

The measurements of the conductivity of the phosphate glasses (ZP/metals (Ni, Co) composites, with metallic amount below the percolation threshold ($\phi \leq \phi c$) as function temperature were undertaken by our laboratory team [145,146]. The found result on ZP/Ni (26vol.%) composite is given in Figure II-11:

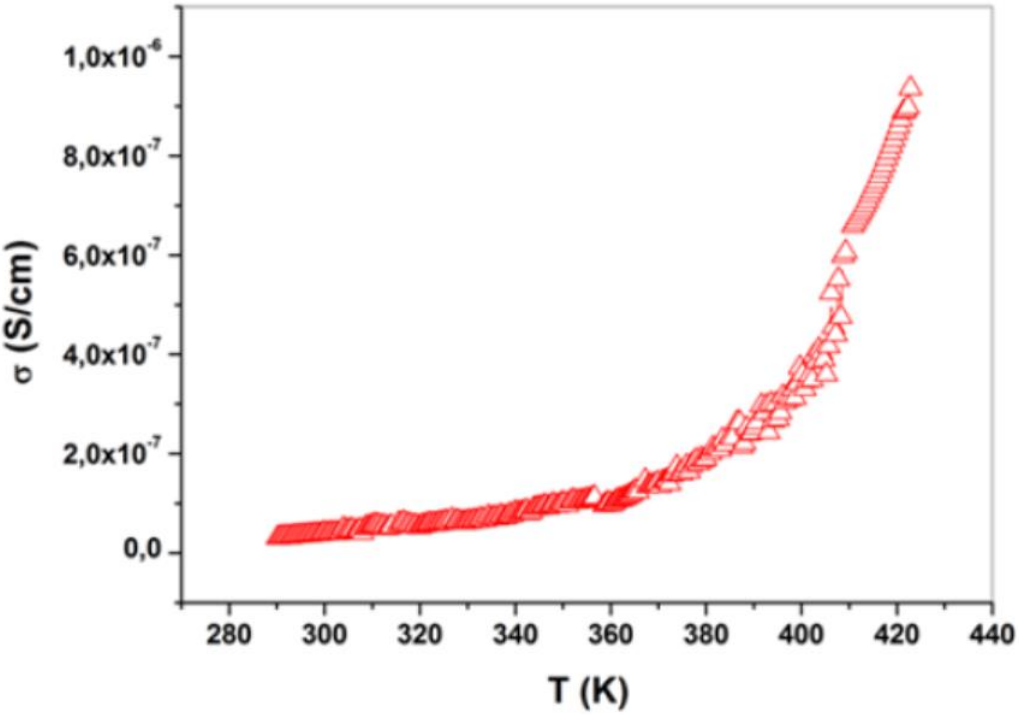

Figure II- 11 : The conductivity evolution as function of temperature of (ZnO-P_2O_5/Ni (26vol.%) composite [109]

The same behavior was obtained on (ZP/Co (19vol.%). The conductivity increases with temperature (figure II-11), showing a change in slope around 410K, which suggests that at least two conduction mechanisms occurred. Such activated behavior is typical of semiconductor materials. Indeed, it has been shown [110] that the studied composites are formed with amorphous glass matrix filled with metallic fillers. When the amount of fillers becomes critical, a crystallized network of these fillers is obtained. Hence, the investigated composites are partially ordered materials. Thus, the analysis with theoretical models which have been proposed to explain the electrical conductivity in amorphous semi-conductors, was justified. As indicated above, the most used model is the band energy model proposed by Mott-Davis [148]. In this model the electrical conduction occurs by hopping between first neighbors localized states near the Fermi level and in the tails of valence and conduction bands (see, Figures II-7 and II-8). Therefore, different behaviors can be observed as a function of temperature and depending upon the distribution of energies in these localized state bands. Hence, in order to clarify the thermally activated hopping mechanisms in localized states and in the extended states of the conduction band, the authors [109, 145,146]. firstly fitted the data with Arrhenius law :

$$\sigma = \sigma_o \exp\left(-\Delta E / kT\right) \qquad \textbf{(II-23)}$$

Where σ_o is the conductivity of the composite at room temperature, ΔE is the activation energy for hopping and k the Boltzmann constant.

The fits with Eqt.(II-23), Arrhenius law are showed in Figures II-12 and II-13 :

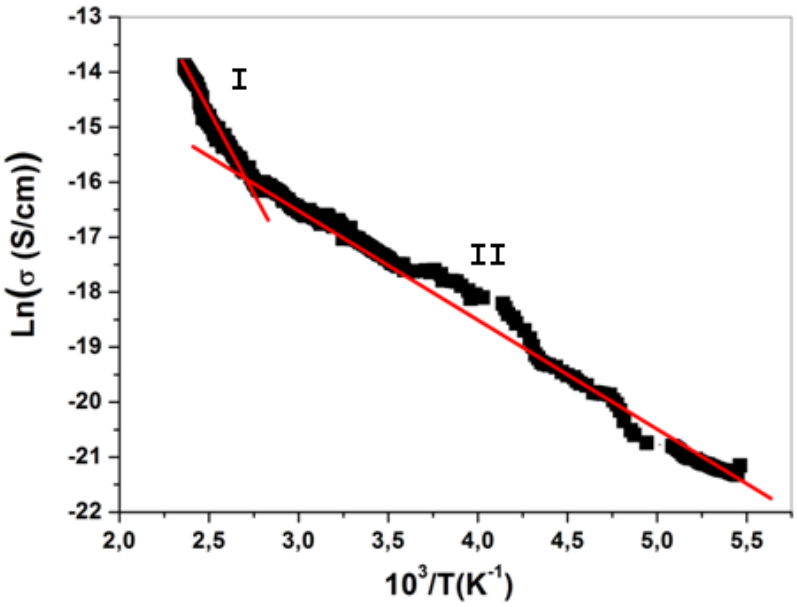

Figure II- 12 : Reciprocal temperature dependence of electrical conductivity of ZP/Ni (26 vol. %) composites; continuous line fit with Arrhenius law, Eqt.II-21 [145].

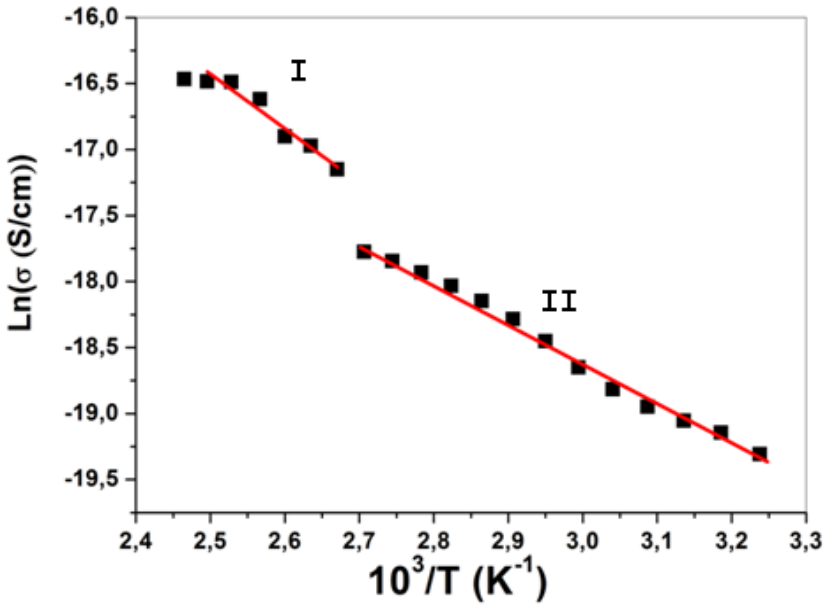

Figure II- 13 : Evolution of the electrical conductivity as function of reciprocal temperature of ZP/Co(19vol.%) composite, with Arrhenius law (solid line) [146].

As can be seen, the fits are fairly good, giving two activation energies, above and below a characteristic temperature ranging between 360 and 400K, which seems dependent of filler nature and its concentration (table II-1):

Table II- 1 : Activation Energies (ΔE_I and ΔE_{II}) *obtained with Arrhenius fit, corresponding respectively to high and low temperatures* [145,146].

Composites	Slope temperature change (K)	ΔE_I (eV)	ΔE_{II} (eV)
ZP/Ni (26vol. %)	370	0.61	0.30
ZP/Co (19vol. %)	370	0.31	0.26

This confirms two different conduction mechanisms that have been happened inside the ZP/(Ni,Co) composites materials. The authors [145,146] have successively assigned that the conduction mechanism at high temperature is associated to the movement of carriers localized states near the Fermi level E_F and delocalized states outside the gap (the tails of conduction and valence bands), as illustrated in figure II-14:

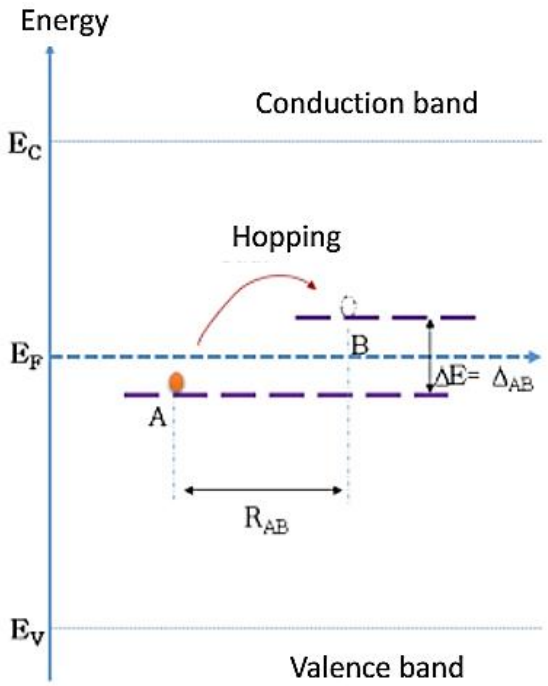

Figure II- 14 : Description of conduction mechanisms between localized states [147].

Indeed, the existing disorder implies that the electronic states are no longer considered as delocalized and the electrons then occupy states located in the forbidden band and close to the Fermi level. According to Anderson [141,143,147-151], the electronic states can be described by space-localized wave functions with a localization length. The charge transport in the disordered solids would carry out according to the following mechanisms:

High temperature (kT >> ΔE):

The conduction is ensured by hopping mechanism between localized energy states of band tails (associated with the disorder). Therefore, the observed conductivity is thermally activated; this type of conductivity is assisted by small polaron hopping mechanism at higher temperature range (kT >> ΔE = ΔAB). The obtained activation energies (Table II-1) are in good agreement with those found in similar phosphate materials [152,153,154]. The observed difference [145,146] (Table II-1) can be explained taking into account that the activation mechanism is complex and dependent of several parameters, such as the important localized states contribution in band tails or near the Fermi level [143], the initial composition of the matrix [153,154], the nature of filler and its concentartion, etc…

Low temperature (kT << ΔE):

In this case the thermal activation is low (kT << ΔE). The carriers can only jump to another level more energetically favorable, even if it is spatially distant, favoring the closest empty levels. Thus, the Hopping can occur between the nearest neighbors at variable distances, called VRH (Variable Range Hopping), for which the energy of jump is minimized. This mechanism is generally observed in intermediate temperature range [141,143,147-151].Thus, the change of slope of the thermal dependence conductivity of ZP/(Ni, Co) composites, below around 370K, was attributed to the process obeying Mott's variable range hopping law (VRH model), which is more appropriate to interpret the conductivity behavior at intermediate ranges of temperatures [148]. The electrical conductivity then follows the law of the variable distance hopping (VRH) given [143] as :

$$\sigma T^{1/2} = A\exp\left(-B/T^{1/4}\right) \qquad \textbf{(II-24)}$$

Whence,

$$A = \left[e^2/2(8\pi)^{1/2}\right]\nu_{ph}\left[N(E_F)/\alpha kT\right]^{1/2} \qquad \textbf{(II-25)}$$

$$B = 2.1\left[\alpha^3/kN(E_F)\right]^{1/4} \qquad \textbf{(II-26)}$$

$$R = \left[\frac{9}{8\pi\alpha N(E_F)kT} \right]^{1/4} \quad \textbf{(II-27)}$$

$$W_o = 3 \Big/ \left[4\pi R^3 N(E_F) \right] \quad \textbf{(II-28)}$$

A represents the conductivity at infinite temperature, T is absolute temperature and B is the characteristic temperature of system, k is the Boltzmann constant, α is the decay of the localized state wave functions (i.e. the inverse localization length of the localized wave functions), W_o is the hopping energy, R is the mean hopping distance, e is the electron charge, N(EF) is the state density at the Fermi level E_F, and ν_{ph} is optical phonon frequency, which can to be obtained from the Debye temperature θ_D as :

$$k\theta_D = h\nu_{ph} \quad \textbf{(II-29)}$$

Where, h is the Plank's constant.

As can be seen from Eqt.(II-26), larger B implies a stronger localization of the charge carriers, showed by decrease of the conductivity at low temperatures, whereas a low B implies a weak localization. The fits at low temperature using Eqt.(II-24), $Ln(\sigma T^{1/2})$ versus $T^{-1/4}$ are given in Figures (II-15) and (II-16) :

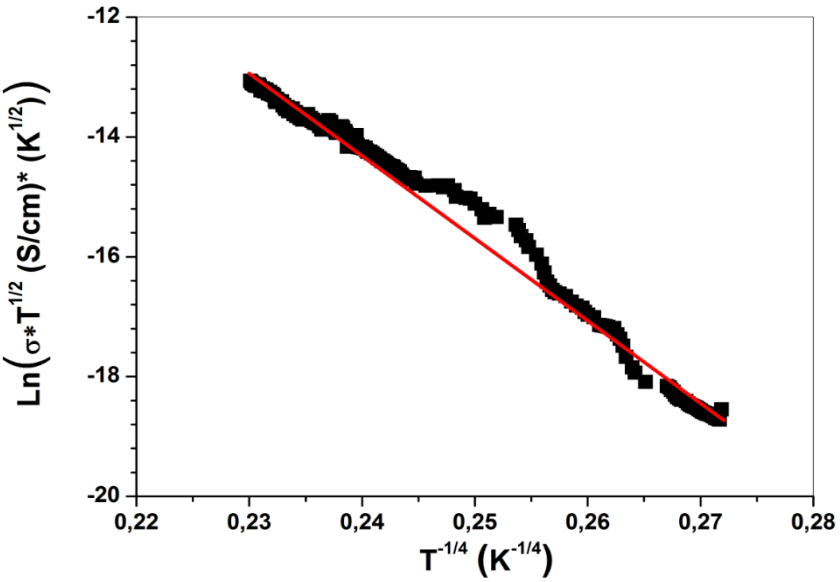

Figure II- 15 : Electrical conductivity Evolution as function of ($T^{-1/4}$) of the ZP/Ni (26vol.%) composite, fitted with Mott VRH theory (solid line) [145].

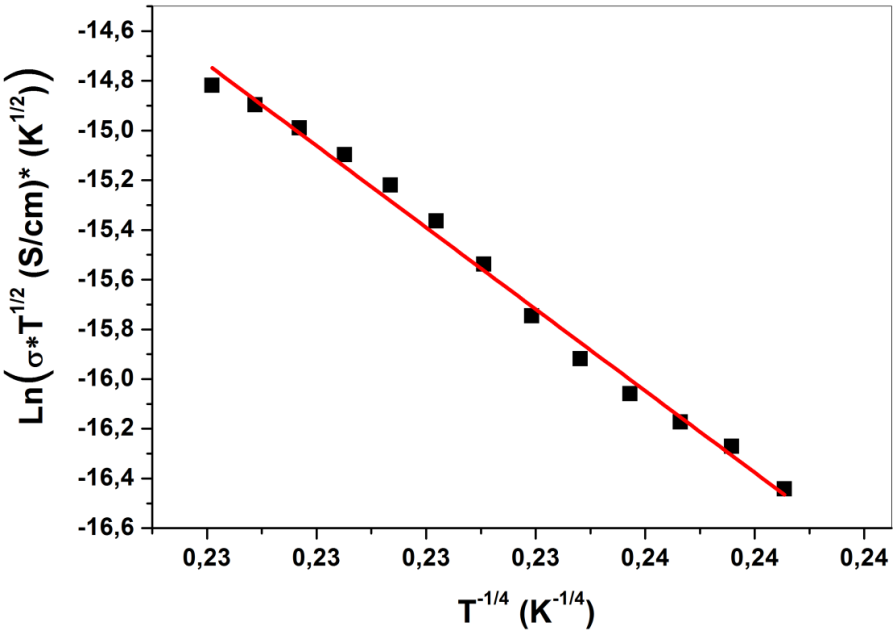

Figure II- 16 : Electrical conductivity Evolution as function of ($T^{-1/4}$) of the ZP/Co (19vol.%) composite, fitted with Mott VRH theory (solid line) [146].

The fits were obtained with good correlation factor ($R^2 \geq 0.996$), indicate a three-dimensional process of conduction, taking place in the ZP/Ni(26vol.%) and ZP/Co(19Vol.%) composites, which is in good agreement with the variable range hopping mechanism [148]. Using the Eqt.(II-25) to Eqt.(II-28) and the slopes of $Ln(\sigma T^{1/2})$ as function of $T^{-1/4}$ curves, the parameters α, N(EF), R and W_o were estimated as gathered in Table II-2:

Table II- 2 : Electrical parameters of ZP/(Ni, Co) composites extracted by fitting experimental data with VRH Mott theory [145,146].

	A ($Scm^{-1}K^{1/2}$)	B ($K^{1/4}$)	A (cm^{-1})	$N(E_F)$ ($eV^{-1}cm^{-3}$)	R (cm)	W_o (eV)	ν_{ph} (Hz)
ZP/Ni (26vol.%)	18.57	133.73	$1.1x10^9$	$1.8x10^{23}$	$1.4x10^{-8}$	0.48	$1.5x10^{13}$
ZP/Co (19vol.%)	22.74	164.34	$1.2x10^9$	$5.5x10^{23}$	$1.2x10^{-8}$	0.25	$1.5x10^{13}$

The obtained parameters for the ZP/(Ni,Co) composites [143,144] were found globally in the same order of magnitude and slightly higher than that of an amorphous material ($B \approx 10^8 K$); indicating a weak value of $N(E_F)$ [143,148].

The observed high temperature mechanisms were interpreted [143,144,145,146] with non-adiabatic small Polaron Hopping (SPH) theory [146] which predicts a change of slope at critical

temperature $\theta_D/2$ of the linear behavior of conductivity versus inverse of temperature, showing a transition from SPH to VRH (Figures II-12, II-13). At low temperatures, the Polaron binding energy becomes smaller than the disorder energy W_D [149].., which can attain approximately the values of $W_D \approx Wo \approx 0.25eV$ and 0.5eV [145,146]. Thus, taking in consideration the temperature of 370K of change in slope, θ_D may be of order 740K. Hence, from Eqt.(II-29), the value of ν_{ph} was calculated and found $\nu_{ph} \approx 1.5x10^{13}Hz$, which seems realistic because the optical phonon frequency is of order 10^{12} -10^{13}Hz. The obtained state density ($N(E_F) \approx 10^{23}$ $eV^{-1}.cm^{-3}$) [145,146] was higher than that found in semiconducting glasses (10^{21} $eV^{-1}.cm^{-3}$) [152-156]. However, these results confirmed the occurrence of VRH because the term $\alpha R >> 1$ and WD >> kT (= 0.0255eV) at T = 300K [148].

In conclusion of this part, we can say, within amorphous semiconductors, electronic conduction assisted by charge transport requires the creation of free charge carriers. In fact, insulating system tends to become semiconductor by in situ mixing of metal precursors and insulating matrix. This in situ mixing leads to the so-called composite, which owns almost the same properties of amorphous semiconductors. As we know, charge carriers are responsible of the conduction and also achieved under temperature effect by delocalization of the polaron within the material giving a rise to electrical conduction by "hopping" transport mechanism. Consequently, the thermally activated conductivity might be the sum of contributions of three types of conduction [145,146]:

• Conduction in extended states (beyond the conduction and valence bands).
• Conduction by hopping in the band tails.
• Conduction by hopping at Fermi level.

During our study, we will attempt to apply this approach to new lead phosphate glasses/metals composites, as bulk and thin films shapes.

II.7 Efficiency of amorphous semiconductors films

An important part of the project of this thesis is to elaborate and characterize conducting amorphous phosphate glass thin films by loading with metallic fillers. The studied amorphous matrix is formed with two oxides: phosphorus oxide and lead oxide. A comparison of our found results with studies of different physical properties of transparent conducting oxides (TCO) given in literature will be very important. Indeed, the solid glasses are very important because their technological applications are wide range and challenging. In recent years, the discovery of semiconducting glasses, which behave like intrinsic semiconductors, has attracted a wide attention and researchers are being much focused on electrical-conduction processes in the

glasses [159]. Spear first reported the studies on drift mobility in vitreous selenium [160] and Tauc et al. first reported physical properties of amorphous germanium [138].

Unlike transparent conducting oxides (TCO) materials, amorphous thin films are usually electrically insulating. Therefore, they are not useful as a transparent conducting material despite their high optical transparency. To ensure that the material meets required criteria for transparent conducting applications, the charge carrier's incorporation have been the popular approaches to be adopted so far. In fact, the performed heterogeneous mixture or composites lead to new physical properties such as high optical transparency and good electrical conductivity [115,139-144,147-151]. One important criterion of their possible industrial applications is their electrical figure of merit. Such efficiency is determined as a ratio of the electrical conductivity to absorption coefficient [160-164]. The figure of merit of amorphous thin film is given by:

$$\textbf{Figure of merit } = \frac{\sigma}{\alpha} \qquad \textbf{(II-30)}$$

Where σ is the electrical conductivity, given by the relation (II-19) and α is the absorption coefficient. This is typically used to describe the material's performance. Therefore, any choice of transparent and conducting material, for industrial application, should take into account the figure of merit quantity. Hence, a good material should have high electrical conductivity combined with low absorption coefficients. We show in the Table II-3 several figures of Merit for some commonly known transparent conducting oxides (TCO) as reported in the literature [56,67-71] [148,160-164]:

Table II- 3 : Figures of merit σ/α for some TCOs [161].

Material	Sheet resistance Ω/cm^2	Visible absorption coefficient α	Figure of Merit (Ω^{-1})
ZnO : F	5	0.03	7
Cd_2SnO_4	7.2	0.02	7
ZnO : Al	3.8	0.05	5
In_2O_3 : Sn	6	0.04	4
SnO_2 : F	8	0.04	3
ZnO : Ga	3	0.12	3
ZnO : B	8	0.06	2
SnO_2 :Sb	20	0.12	0.4
ZnO : In	20	0.20	0.2

Concerning our phosphate glass films, the concentration of free charge carriers was increased by metallic fillers loading, which has enhanced the electrical conductivity. We will compare the obtained figures of merit of differents thin films, which are elaborated during our study (see chapter VII).

II.8 Optical Properties of phosphate glass/metals composites

One of the most important properties of the glass is its transparency. This transparency is due to the insulating state of amorphous structure (no order at long distance) and to the absence of electronic absorption in the considered wavelength (Figure II-17):

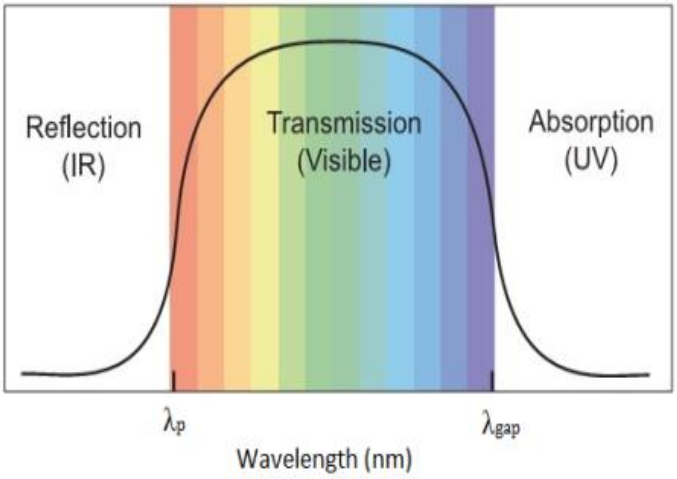

Figure II- 17 : Spectral dependent of semiconducting transparent semiconductors [165].

The optical transmission window (UV + visible + near IR) is one of the physical characteristics determining the potential applications of the glasses. Thus, optical transparency is an essential feature for transparent and conducting materials. Therefore, a good material should have high optical transparency covering the most part of the light spectrum. Usually, the optical transmission is defined as the ratio between incoming light intensity and transmitted intensity averaged over all values in the light spectrum. Moreover, the figure-II-17 is indicating the optical properties of semiconductor substrates, in UV visible and infrared spectral ranges. It is clear that in the visible range, semiconductors have considerable transmission. However, we note a very low transmission, versus wave number in IR and UV ranges. Thus, it appears that spectroscopy is an effective method for the determination of optical properties such as transmission and absorption in the UV-visible and infrared spectral interval.

In general, the optical properties of a material describe how the characteristics of light are affected when it passes through it. The two most important optical constants are refractive index n and absorption coefficient α.

The refractive index of an optical material or dielectric medium is generally defined as the ratio of the velocity of light c in vacuum to its velocity v in the considered medium:

$$n = c / v \qquad \textbf{(II-31)}$$

In materials where an electromagnetic wave can lose its energy during propagation, the refractive index becomes complex. Thus, the light propagation in materials is characterized by its complex refractive index [165]:

$$n^*(\lambda) = n(\lambda) - i\kappa(\lambda) \qquad \textbf{(II-32)}$$

The real part n, its dependence on wavelength λ is at the origin of dispersion phenomenon and usually given by Cauchy's law. The imaginary part κ is related to the absorption coefficient α by Beer's law [166,167] as:

$$\kappa = \alpha\left(\frac{\lambda}{4\pi}\right) \qquad \textbf{(II-33)}$$

The absorption edge of many amorphous semiconductors has a shape that looks like the one depicted in Figure-II-18. There will be a high absorption region A, which is also referred to the fundamental absorption edge. An exponential region B, which is usually referred to as the Urbach edge and has values that extend over 4 orders of magnitude of α, and a weak absorption tail C called the Urbach tail (to be discussed in later section).

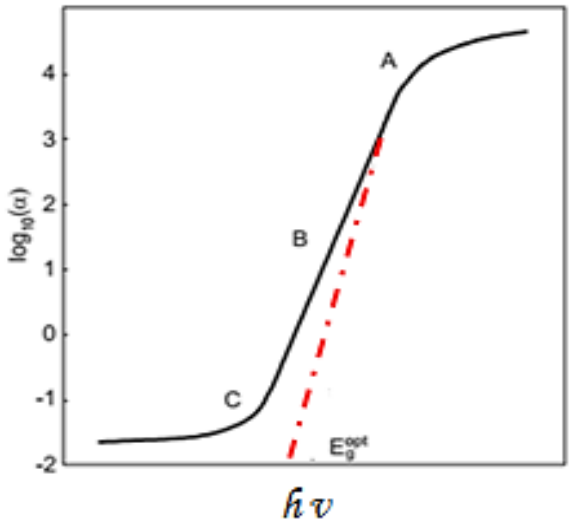

Figure II- 18 : Typical absorption edge of an amorphous semiconductor, where A represents a region called the fundamental absorption edge, B represents a region changing exponentially, which is referred to as the urbach edge, and C represents a region referred to as the weak absorption tail or Urbach tail E is the optical bandgap [148].

The absorption coefficient, dictates how readily photons will be absorbed by the material, it can be understood from the photoconductor standpoint using the following relation [166,167]:

$$\alpha = \left(\frac{1}{d}\right)\ln\left(\frac{100}{T}\right) \qquad \textbf{(II-34)}$$

With T is the measured transmittance in % and d is the thickness of the film.

II.8.1 Optical constants

The optical constants can be determined by exploiting the UV-Visible transmission spectra as a function of wavelength.To find out refractive index n, we simply use approximate method (n>>κ) of Manifacier and Swanepol *[* 166,167] .The advantage of this method is that we don't need reflectance spectra. The only condition is that we should get interference fringes. Thus, refractive index n of the film is given as:

$$n = \left[N + \left(N^2 - S^2 \right)^{1/2} \right]^{1/2} \quad \textbf{(II-35)}$$

With:

$$N = 2S\left(\frac{T_M(\lambda) - T_m(\lambda)}{T_M(\lambda) T_m(\lambda)} \right) + \left(\frac{S^2 + 1}{2} \right) \quad \textbf{(II-36)}$$

Where, S is the refractive index of the glass substrate, $T_M(\lambda)$ and $T_m(\lambda)$ represent maxima and minima of the transmittance curve.

The knowledge of index n allows the determination of the thickness d of the film as:

$$d = \left(\frac{\lambda_1 \lambda_2}{2\left(\lambda_1 n_2(\lambda_2) - \lambda_2 n_1(\lambda_1) \right)} \right) \quad \textbf{(II-37)}$$

Where, n_1 and n_2 are the refractive indices corresponding respectively to wavelength λ_1 and λ_2 extracted from two consecutive maxima of the transmittance spectra. As can be seen by Eqt.(II-37), the accuracy in the determination of the thickness d is very sensitive to the errors in n and λ. Thus, to optimize the obtention of the thickness d, average of several values should be taken [168]. The accuracy in the determination of thickness with this method is also enhanced when the film is more transparent in UV-Visible range.

II.8.2 Band gap energy

The absorption coefficient α allows the determination of extinction coefficient κ as given above. Also, the energy gap Eg near to the band edge is given by Tauc's equation [169], as:

$$(\alpha h\nu) = B\left(h\nu - E_g \right)^n \quad \textbf{(II-38)}$$

This relation can be also rewritten in logarithm scale [168]as:

$$\ln(\alpha h\nu) = \ln B + n \ln\left(h\nu - E_g \right) \quad \textbf{(II-39)}$$

Where, h is Planck's constant, α is the absorption coefficient, ν is the frequency of absorption, B is constant, and n depends on the kind of optical transition. If n = 1/2 and n=2 ,the transition will be direct and indirect allowed, respectively. To determine if the occurred electronic transition in the studied system is direct or indirect, the obtained experimental curves (αhν) as photon energy (hν) can be fitted with Eqt.(II-38) in the almost end straight region, using the mean square method, with n, B and Eg as adjusted parameters [168]. Then, to check the validity of the used method, the obtained parameters (n, B, Eg) can be introduced in Eqt.(II-39) and plotted, a good correlation between experiment and theory should be obtained [168].

II.8.3 Determination of Urbach Energy

The Urbach energy or band tail width is another important optical parameter. It is associated to the optical band gap energy. It allows estimating the effect of disorder or defects in poor crystalline or predominant amorphous phases of solid. Its measurement is achieved as width of exponential band tail energy of localized states, near band edges [170,171]. Indeed, the structural disorder is at the origin of the considered tails formation, which produce localized states extended in the forbidden band gap. This phenomenon is evidenced by the behavior of the absorption coefficient (α) versus the photon energy near the band edge, showing an exponential tail (Figure II-18). Thus, the Urbach energy is defined by involving (α) and (hν) in the following empirical equation [165]:

$$\alpha = \alpha_0 \exp\left(\frac{h\nu}{E_u}\right) \qquad \textbf{(II-40)}$$

Where α_o is a constant and E_U is Urbach energy or energy of the band tails.Urbach energy is weakly dependent upon temperature and is often interpreted as the width of the band tail due to localized states, which are mainly associated with disordered or low crystalline materials. Taking the logarithm of the two sides of equation, one can get a straight-line equation as follows:

$$\ln(\alpha) = \ln(\alpha_0) + \left(\frac{h\nu}{E_u}\right) \qquad \textbf{(II-41)}$$

Therefore, the band tail energy or Urbach energy (E_U) can be obtained from the slope of the straight-line plotting ln(α) against the incident photon energy (hν) as shown in figure II-19. Thus, the reciprocal slope of the fitted experimental straight behavior determines Eu.

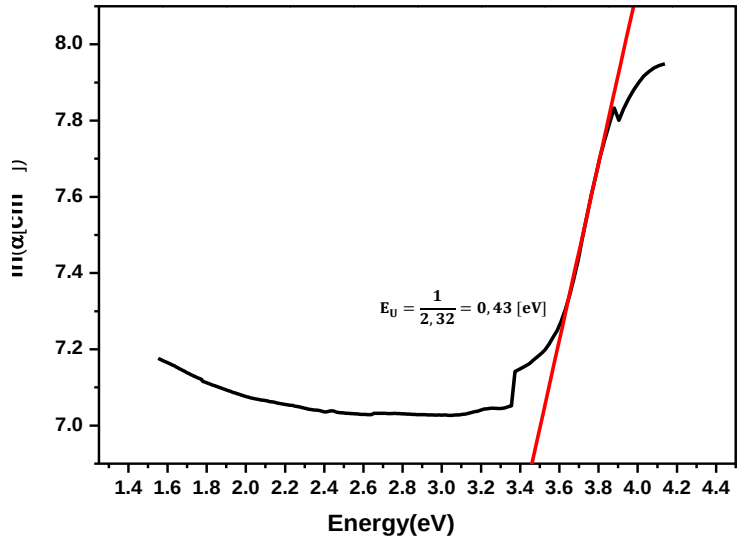

Figure II- 19 : Determination of the band tail energy from the plotting ln (α) against the incident photon energy (hν) [169].

II.9 Correlation of optical and electrical properties

The blue shift occurring in the optical band gap of amorphous semiconductor with increasing the charge carrier concentration is useful for TCO applications as demonstrated in Burstein-moss effect [170]. Optical absorption and electrical conductivity are tightly dependents. When the optical absorption increases strongly which is favorable for all optical applications, the electrical conductivity increases as well. Moreover, as reviewed above, the neat glass either in bulk or thin film form does not possess high enough electrical conductivity value.To overcome this limitation, the concentration of free charge carriers can be increased by loading approach, which leads to electrical conductivity enhancement, by increasing charge carrier's density. This type of material is currently being studied for the purposes of optoelectronic applications, in bullk or film form, such as solar cell devices, using several junctions, like p-n junction for example (see chapter VIII).

Conclusion

In this chapter, we have given some theoretical reviews of the amorphous materials investigated as composites during our thesis project. Thus, we hope to help better understanding of the phenomena encountered in next chapters and permit us to give appropriate explanations for the coming experimental findings.

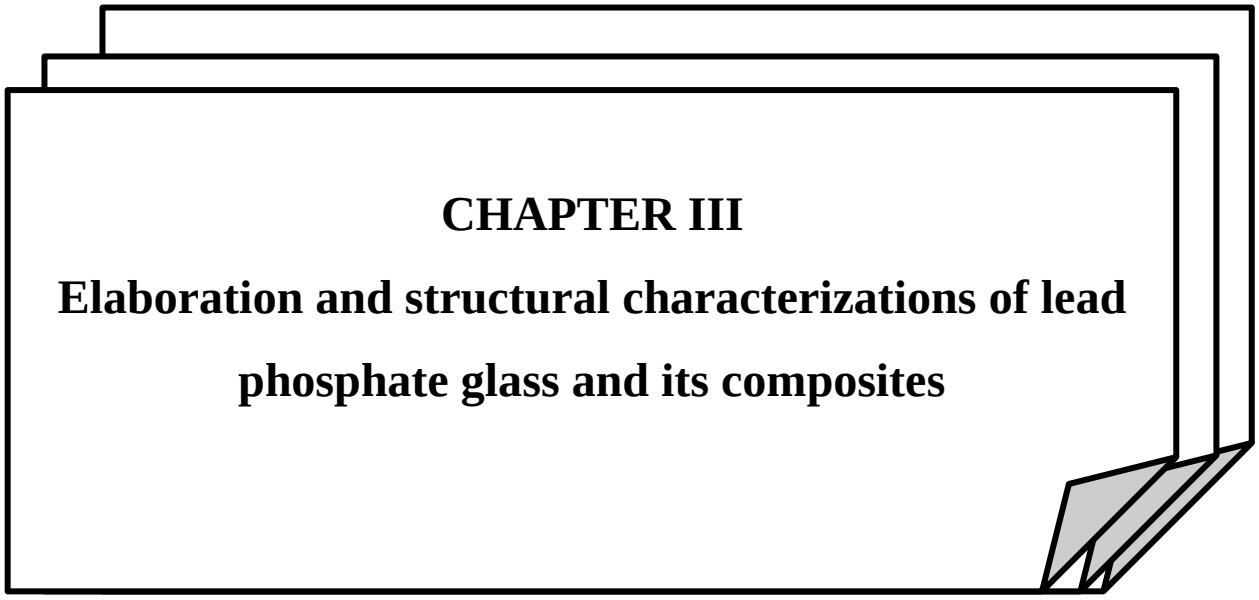

CHAPTER III

Elaboration and structural characterizations of lead phosphate glass and its composites

III.1 Introduction

Glass is considered as a frozen liquid, it retains many of the properties of its liquid precursor. Continuous and disordered atomic network provides considerable isotropy to the glass in macroscopic scale. Indeed, atomic disorder makes it difficult to describe the structure of glass since the lack of long-range periodicity precludes precise knowledge of the atomic location.

The structure of the glasses and their different properties are commonly depending on the nature of their constituents and how the atoms are placed. Therefore, one of the objectives of the present chapter is to shed more light on the role of lead oxide in the PbO-P_2O_5 binary system glass structure. Also, we aimed to correlate the variation of morphology and density of the studied glasses with the structural changes. The composition of (45mol%PbO-55 mol%P_2O_5) was found to be the most appropriate to consider for further investigations. We have then elaborated new composites based on the forementioned phosphate glass composition filled with metallic powders. We are going to describe in detail within this chapter, the techniques used to make the bulk glass samples, their based composites and the different characterizations of the obtained samples, namely XRD, density, porosity measurements, scanning electron microscopy coupled with energy of dispersive x-ray analysis(SEM/EDAX) as well as thermal analysis.

III.2 Preparation of lead phosphate glasses

III.2.1 Glass preparation

The synthesis of the glasses is carried out by melt quenching technique using reagent grade purity PbO (purity 99% from Panreac) and $NH_4H_2PO_4$. The mixture is preheated to 120°C for 12 hours. It is then brought to a temperature between 300 and 600°C to ensure the removal of NH_3 and H_2O according to the following reaction:

$$\mathbf{2\ NH_4H_2PO_4 \rightarrow P_2O_5 + 2NH_3 + 3H_2O}$$

The mechanically homogenized mixtures were melted in sintered porcelain crucible during one hour at 950°C to avoid any volatilization of P_2O_5. After 1 hour (h), the molten material was quenched at room temperature by pouring the liquid onto ceramic plate, which was already preheated at 300°C for 2 hours. The procedure for synthesizing the glass is described below in Figure III-1.

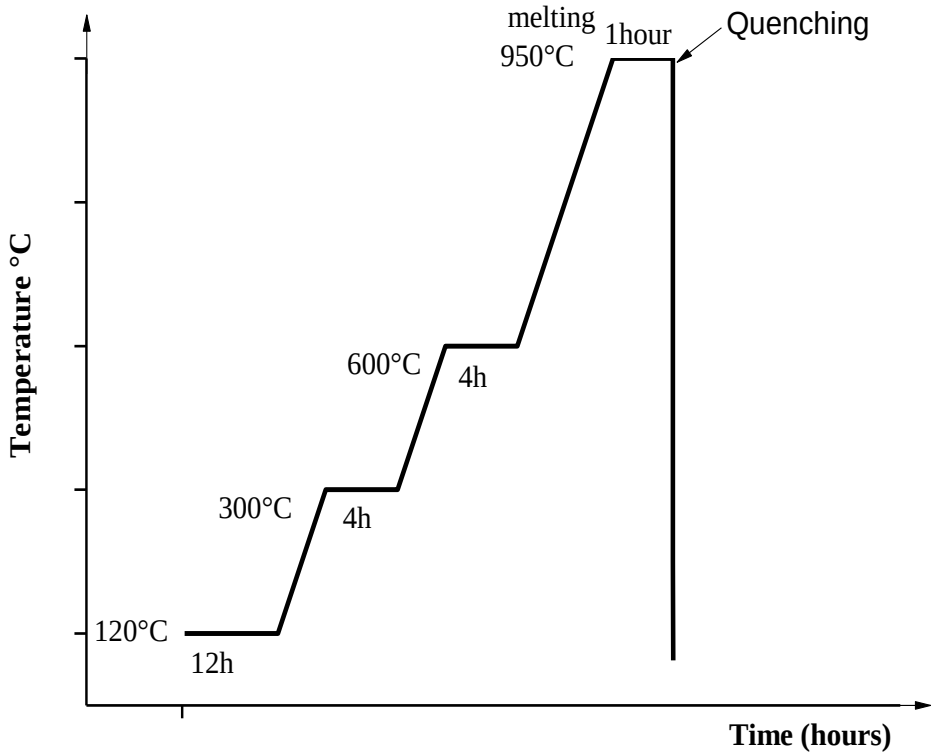

Figure III- 1 : The adopted thermal profile for the synthesis of glasses.

III.2.2 The glass formation domain of xPbO-(1-x) P_2O_5

The glassy domain in this binary system arises up to a limit of 60-mol% PbO as shown in the table below:

Table III- 1 : Phases identification of xPbO- (1-x) P_2O_5 matrix.

mol % PbO	mol % P_2O_5	State of the glass
25	75	Transparent and incolor
30	70	Transparent and incolor
35	65	Transparent and incolor
40	60	Transparent and incolor
45	55	Transparent and incolor
50	50	Barely transparent
55	45	Barely transparent
60	40	Barely transparent
70	35	Opac
85	15	Opac

In this system, we can notice the presence of quite large glass forming domain and it is similar to that of binary system xZnO-(1-x)P_2O_5 previously synthesized by Oabi et al.[1] .[173].. This suggests that ZnO and PbO oxides are among the mixed forming-modifying oxides.

III.3 Glass characterizations

III.3.1 Density and porosity measurements

The density of glasses was measured at room temperature by Archimedes method in Diethyl phthalate (from Panreac of 99.5% purity) as buoyancy liquid that got known density ; ρ_{sol} = (1.118 ± 0.001)g/cm^3, at 23 °C.

The glass samples were weighed in air (wair) and then weighed in diethyl phthalate liquid (w_{sol}.) with a Mettler Toledo (Columbus, OH) AJ 100 balance equipped with a density-determination kit. Then the experimental density d_{ex} data of the investigated glass was calculated from the equation [173]

$$d_{ex} = (W_{air} \cdot \rho_{sol}) / (W_{air} - W_{sol}) \qquad \textbf{(III-1)}$$

The main combined uncertainties (random and systematic) of obtained densities were estimated to $\Delta d_{ex} \approx \pm 0.01$ g/cm^3.

In order to verify how far the experimental density of the glass matrix is accurate, it has been found convenient to compare with theoretical density which is given by the following equation [174,175].

$$d_{ex} = \sum x_i M_i \Big/ \left(\sum x_i M_i / \rho_i \right) \qquad \textbf{(III-2)}$$

x_i denotes the molar fraction of the constituent oxides, M_i is their molar mass, ρ_i is their densities (d_{P2O5} =2.39 g/cm^3 and d_{PbO} = 9.53 g/cm^3).

The comparison between theoretical and experimental densities is given in figure III-2 :

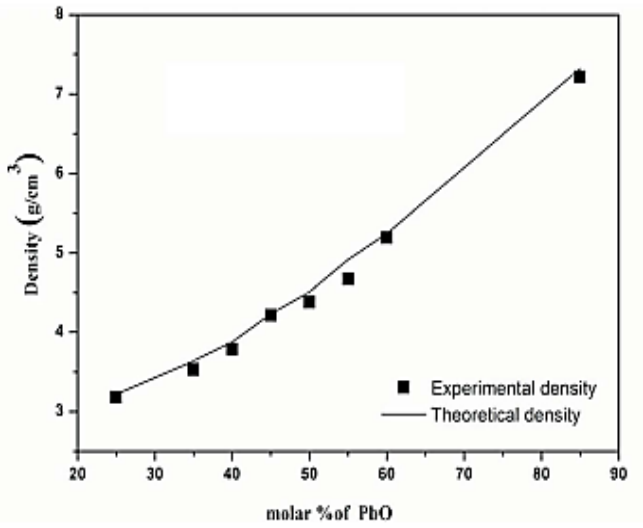

Figure III- 2 : Evolution of experimental and theoretical density versus mol% PbO within the glass network.

As can be seen from Figure III-2, the experimental and theoretical density increase steadily with the increasing of PbO content. This evolution has proved a good agreement between theoretical and experimental values of the matrix densities. This confirms that the obtained glass is truly binary system of two oxides and no important presence of impurities are detected, because the calculated density was performed considering only two oxides constituents. However, it's noticeable that experimentally determined density is slightly less than the calculated one, this is more likely due to the presence of certain porosity τ. In order to estimate the porosity, we have used the following relation [176]:

$$\tau(\%) = \frac{(d_{th} - d_{exp})}{d_{th}}.100 \qquad \textbf{(III-3)}$$

Where d_{exp} and d_{th}represent the experimental and theoretical density respectively. Curve of porosity is reported in figure III-3.

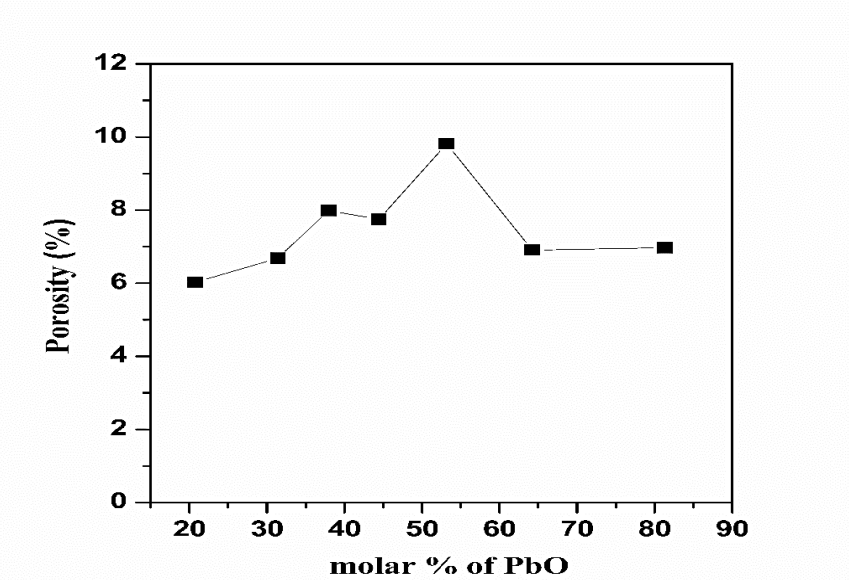

Figure III- 3 : Variation of porosity rates as function of mol% PbO.

The curve depicted in FigureIII-3 indicates that the estimated porosity is low and varies between 6 and 10%. In fact, some porosity is needed in such kind of glasses .These are known by their crucial role in thermal shrinkage and certain reversible process fitting the most to sealing applications [177,178,179].The observed porosity of glass matrix of 45mol%PbO-55mol%P_2O_5 composition, is only about 8%, this is more likely due to tight difference between experimental density value which is about 4.09±0.01g/cm^3 and theoretical value which was found to be 4.13 g/cm^3. In agreement with previous study [180]. Thus, we assume that 45 mol% PbO-55mol%P_2O_5 composition is the most chemically stable. In the contrary case, the experimental and theoretical densities would be different if the matrix has absorbed water. This point will be confirmed by weighing the mass of this same glass over a long period (see later).The depicted porosity will be also checked by SEM observations and compared. Elsewhere, the density measurements revealed that the molar concentration of PbO seems to be one of the most influencing parameters. Thus,

obtained glass compositions with different PbO molar concentrations have been analyzed through X-ray diffractions.

III.3.2 XRD characterizations

The XRD measurements were perfomed with The X-ray powder diffractometer (available to UATRS*(**(Unités d'Appui Techniques à la Recherche Scientifique du CNRST (Centre National pour la Recherche Scientifique et Technique, Maroc)***)) which uses the BRAGG - BRENTANO assembly and has a vertical goniometer of θ-θ configuration with direct optical coding allowing direct reading of the angular position on the goniometer arms. The diffractometer is equipped with an X-ray tube with copper anticathode (λ = 1.54051 Å).

III.3.2.1 Effect of lead oxide concentration

The x-ray data of the prepared glasses having composition $xPbO\text{-}(1\text{-}x)P_2O_5$ are obtained in Figure III-4.

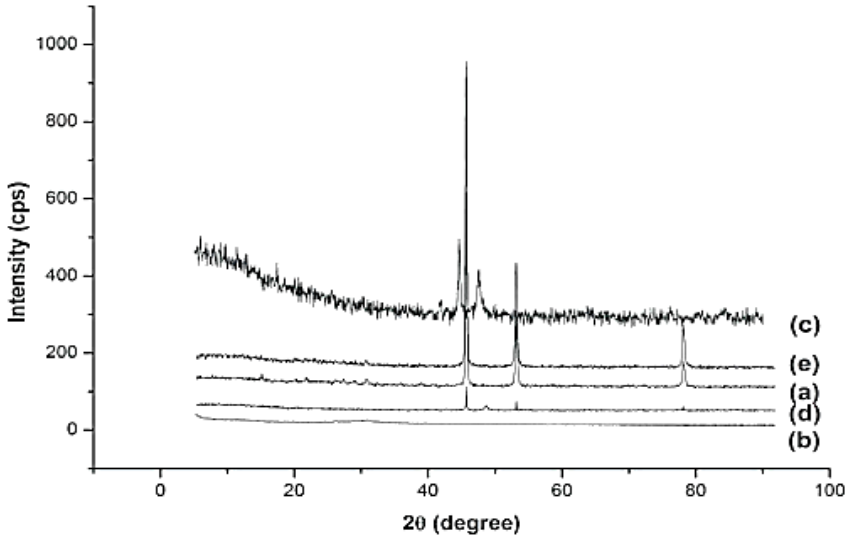

Figure III- 4 : XRD data of a) 20 mol% PbO-80 mol% P_2O_5, b) 45 mol% PbO-55 mol% P_2O_5, c) 60 mol% PbO- 40 mol% P_2O_5, d) 70 mol% PbO-30 mol% P_2O_5 and e) 85 mol% PbO-15 mol% P_2O_5.

The patterns show crystalline phase within 0mol%<x<20mol% and 60mol% < x < 100 mol% intervals, while the amorphous area is extended in the molar range of 20 mol% PbO < x < 60 mol% PbO.

Indeed, the X-ray patterns of the different binary glass compositions aims to precisely explore the vitreous domain, note that in all cases, the glasses are synthesized according to the protocol as aforementioned above.

***The concerned are gratefully acknowledged.**

As shown by diagram phase of figure, glass formation takes place when 25mol% PbO is added to the P_2O_5 oxide. In addition, up to 60mol% PbO can be introduced into the P_2O_5 glass matrix.

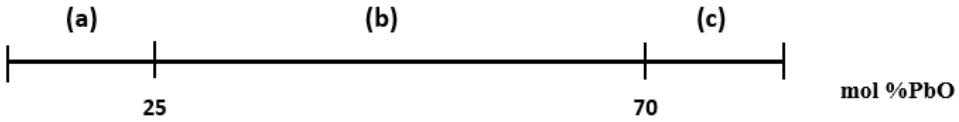

Figure III- 5 : PbO-P_2O_5 phase diagram: a: crystalline phase, b: amorphous phase, c: crystalline phase.

As we notice, the concentration of PbO plays an important role on the solid structure of xPbO-(1-x)P_2O_5 binary system. In order to confirm that the composition of 45 mol % PbO-55 mol % P_2O_5 is of amorphous nature. The XRD pattern is plotted separately in full scale in figure III-6:

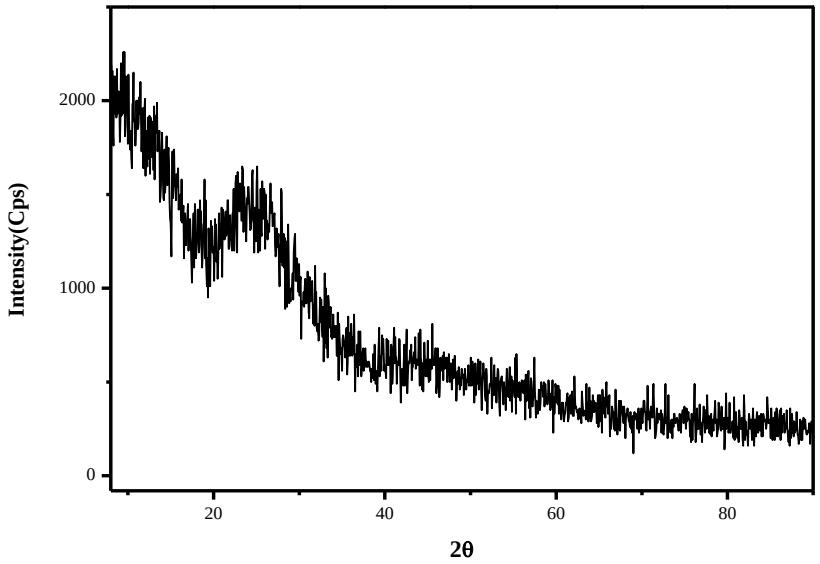

Figure III- 6 : XRD patterns showing the amorphous state of the host matrix of the composition mol % PbO-55 mol % P_2O_5.

As showed through Figure III- 6, only a broad peak appeared between 20 and 30° and very small peak around 45° confirming the amorphous state of (45 mol % PbO-55 mol % P_2O_5).

Hence, this glass composition will be used as matrix for further elaborated composites. Since the effect of heat treatment on the structure of these compounds seems to be influencing parameter; we proceed the checking of structural features through XRD patterns versus sintering temperature. The nature of these phases will be confirmed by SEM observations.

III.3.2.2 Effect of sintering temperature

In this study, we found that the effect of the sintering temperature is considered as an important parameter, further investigation must be performed to confirm this fact.

To do so, (45mol% PbO-55mol%P_2O_5) glass (PbP) was sintered at different temperatures, as given in figure III-7 :

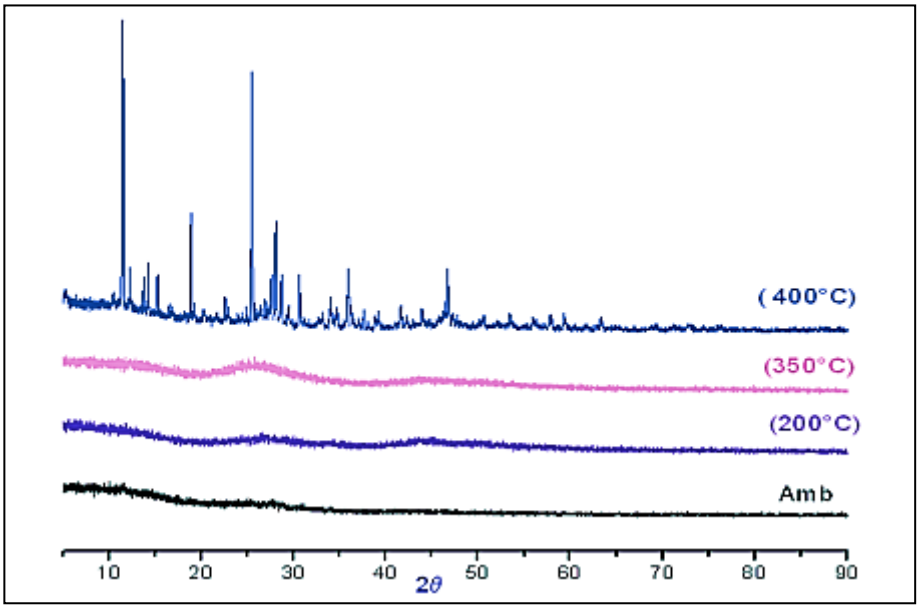

Figure III- 7 : Sintering temperature effect on 45mol% PbO –55 mol% P_2O_5 .

As shown in Figure III-7, at room temperature, the phase is amorphous, but as the temperature increases, we notice appearance of pseudo-peaks, and above 350°C, crystallization onset is visualized.Note that, increasing temperature allows progressively the formation of ordered network structure. This could be related to the fact that temperature elevation implies the increase of kinetic energy of different atoms, leading to long exchange, minimizing the global energy and disappearing the metastable states with crystallization process.

III.3.3 IR/ATR analysis

The infrared spectra were recorded using a Vertex 70 device, scanning the spectral range 4000-400 cm^{-1} with a resolution of 4 cm^{-1} at the laboratory of the Technical Support Units for Scientific Research (UATRS*) in the National Center for Scientific and Technical Research (CNRST*) in Rabat. All spectra were obtained for compounds in the solid state.

***The concerned are gratefully acknowledged**

The obtained spectra corresponding to $xPbO-(1-x)P_2O_5$ compounds, with x=20, 45, 60 and 85mol% of PbO, show two regions: a region between 4000 and 1400 cm^{-1} corresponding to the characteristic bands of water molecule, and another region more important within 1400-400 cm^{-1}. Our interest will therefore be exclusively focused on the latter region in order to see how the change could be observed as a function of the compositions and be in correlation with SEM (scanning electron microscopy) micrographs and XRD patterns observations.

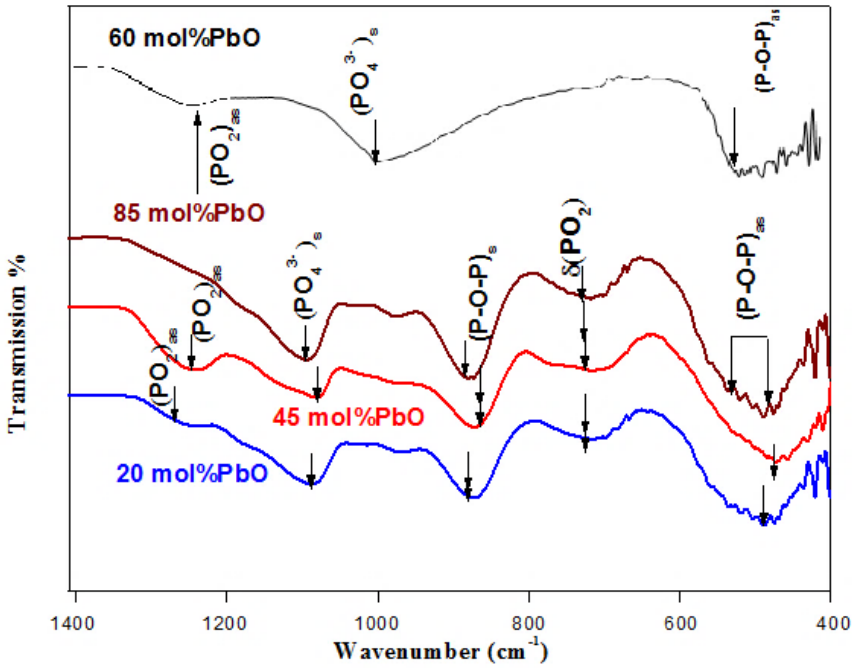

Figure III- 8 : IR spectra of xPbO-(1-x) P_2O_5 glasses (with x = 20, 45, 60, and 85 mol%PbO).

We note for both compositions (20mol%PbO-80mol%P_2O_5) and (45mol%PbO-55mol%P_2O_5), the appearing characteristic bands are almost at the same wavenumber, except a slight shift from 918 to 904cm^{-1} which was observed for symmetrical elongation of P-O-P. This displacement could be explained by thermal effect causing the crystallization onset of (20mol % PbO-80mol%P_2O_5).

Simple comparison between (45mol%PbO-55mol%P_2O_5) and (60mol%PbO-40mol%P_2O_5) enables to suppress symmetrical strips appearing around 900 cm^{-1} and the appearing of movement path around 750cm^{-1} for (60mol%PbO-40mol%P_2O_5) composition. This confirms the difference of amorphous nature of (45mol%PbO-55mol%P_2O_5) and crystalline structure of (60mol%PbO-40mol%P_2O_5) [181]:, confirmed by XRD and SEM observations.

Finally, the IR analysis confirms the difference in structure of crystalline phases of compositions (60mol%PbO-40mol%P_2O_5) and (85mol%PbO-15mol%P_2O_5) by the absence of the antisymmetric band (P = O) which appeared around 1200cm^{-1} within the binary system composition of (60mol%PbO-40mol%P_2O_5). The overall evolution of IR spectra is in good agreement with several studies [181-186] in where following classifications have been stated:

-Ultra phosphate (20 < x < 60 mol %), amorphous phases,

-Meta phosphate (x = 60 mol %), crystallized phase,

- Pyrophosphate (60 < x < 85%mol), crystallized phase.

Osaka et al. [187] have shown that PO_4 units have two bridging oxygens (P-O-P) and two non-bridging oxygens (P = O and P-O) and have shown that they are in resonance with each other.

For glasses containing 60mol% of PbO and higher, the intensity of the P=O band decreases rapidly. The sharp decrease in the intensity of P = O band of pyrophosphate glasses (x=60mol %) indicates that lead oxide is starting to become a forming oxide [197,198]. This is considered as an indication of pyrophosphate group formation.

The bands attributions are gathered in table III-2.

Table III- 2 : IR spectrum of $xPbO-(1-x)P_2O_5$ in the region of 1400-400 cm^{-1} .

Composition assignments	20mol %PbO	45 mol %PbO	60mol% PbO	85 mol %PbO
ν_aP = O	1259	1262	1236	----
$\nu_s PO_4^{3-}$	1100	1085	1014	1018
ν_sP-O-P	918	904	-----	889
δO = P-O	758	750	-----	746
Vibration band P-O-P	503	498	545	573-541

The obtained results provide a clear insight into structural changes when PbO concentration is varied. Indeed, these results show that the P=O band (1263cm^{-1}) is strongly affected by the concentration of PbO. This phenomenon has been observed in similar samples reported elsewhere [181-196].

The good chemical durability is tightly related to a large number of Pb-O-P bonds in binary system composition of 45mol%PbO-55mol%P_2O_5 [181,199]. It can be concluded that lead oxide acts as a modifier of the network beyond the ultra-phosphate and meta phosphate glasses .This means that P=O is significantly affected and transformed into a new connection mode namely the bridging PO-Pb and P-O-P beyond the meta phosphate [181-196], this has been thoroughly explained in chapter I.

III.3.4 Morphology study

In order to identify and characterize glass matrix. Morphology study was performed in laboratory of Technical Support Units for Scientific Research (UATRS*) of the National Center for Scientific and Technical Research (CNRST). These analyses are performed using a scanning electron microscope (SEM) coupled with chemical analysis (EDX) and working in ESEM mode. It is equipped with a complete X-ray microanalysis system (EDX-EDAX detector) and a backscattered electron detector.

Thus, the samples of $xPbO-(1-x)P_2O_5$ with increasing quantity of lead, x=20, 45, 60 and 85mol% are analyzed using different magnifications. The obtained images on (20mol%PbO-80mol%P_2O_5) are given figures III-9 (enlarged 500x) with EDX analysis and III-10 (2000x) :

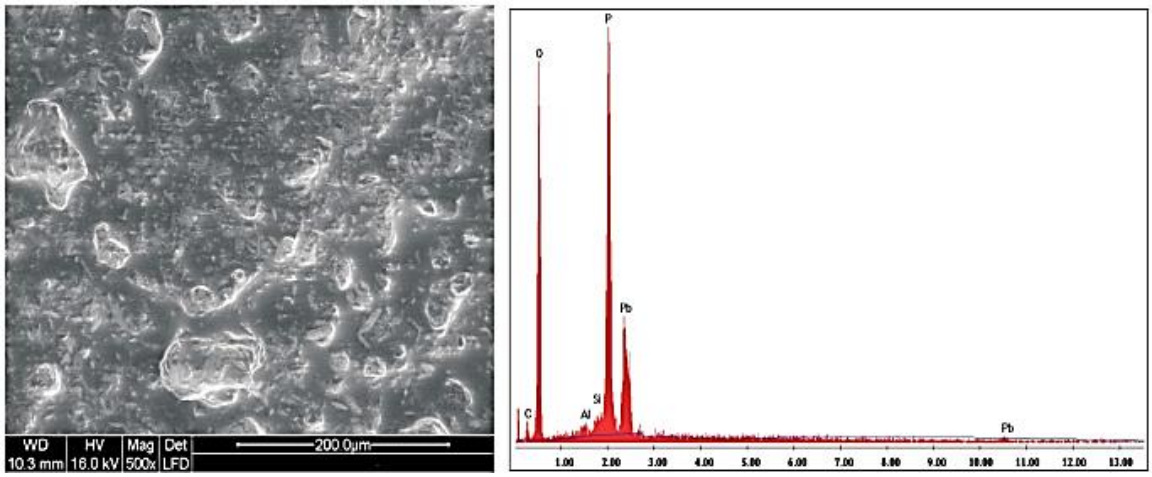

Figure III- 9 : SEM micrograph of 20 mol% PbO-80 mol% P_2O_5 (x 500) along with corresponding EDX spectrum.

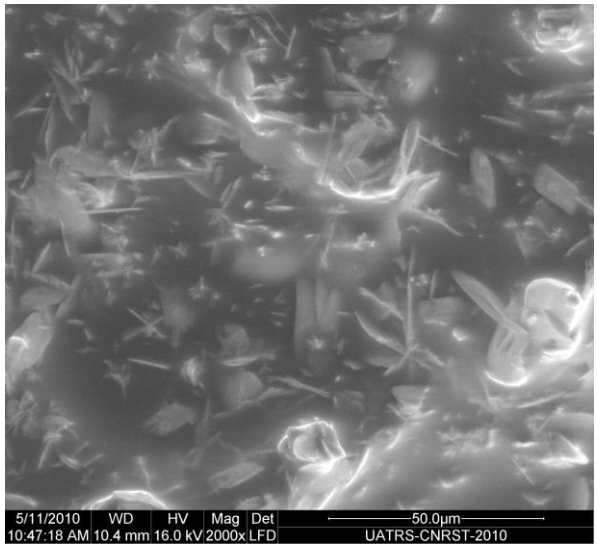

Figure III- 10 : SEM image Obtained with resolution of 16 KV and magnified(x2000) of (20mol% PbO-80mol% P_2O_5).

The figure III-8 shows almost homogeneous phase and the EDX analysis gives high intensities of phosphorus, oxygen and lead, mean constituents of (20mol%PbO-80mol% P_2O_5) compound. Quantities of carbon, aluminum and silicon are also observed. However, they are small and the sample can be considered valid for physical studies. When, the photo is taken at high magnification (2000x), some crystallites are observed, indicating that this phase is almost crystallized (see, figure III-9), confirming the XRD findings.

Then, SEM micrographs have been undertaken in the same conditions on (45mol% PbO - 55mol%P_2O_5) composition. The result is given in figures III-11 :

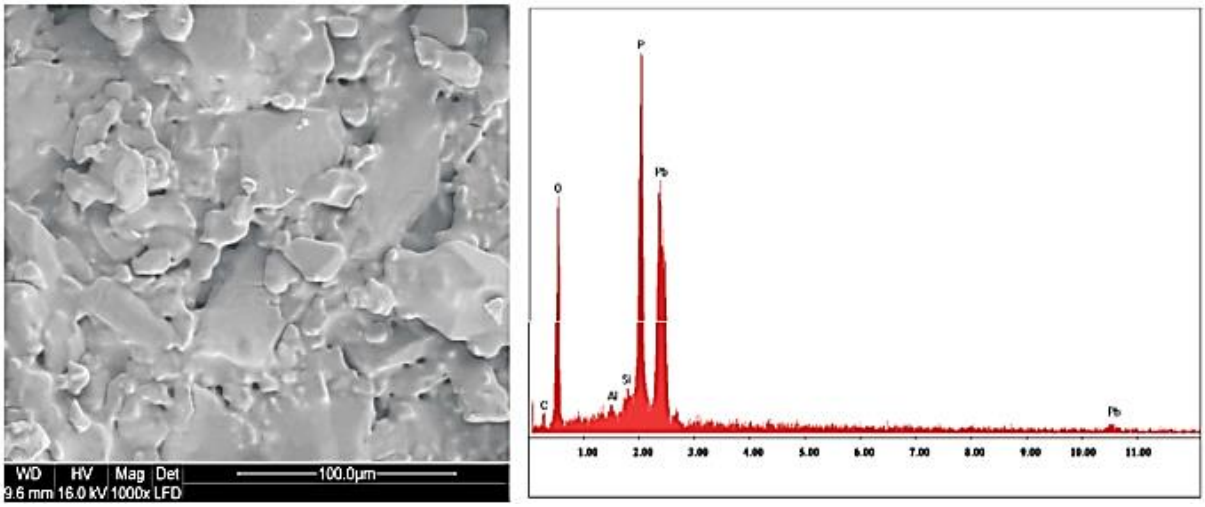

Figure III- 11 : SEM micrograph of (45mol%PbO-55mol%P_2O_5 (x 1000)) along with corresponding EDX spectrum.

SEM image of figure III-11 shows an isotropic and homogeneous morphology indicating amorphous state of the glass, in accordance with XRD pattern. The EDX analysis confirms the composition of the glass, with small impurities of carbon, aluminum and silicon.

The SEM images corresponding to compositions (60mol%PbO-40mol%P_2O_5) and (85mol%PbO-15mol%P_2O_5), respectively are showed in (Figures III-12 and III-13) :

***The concerned are gratefully acknowledged**

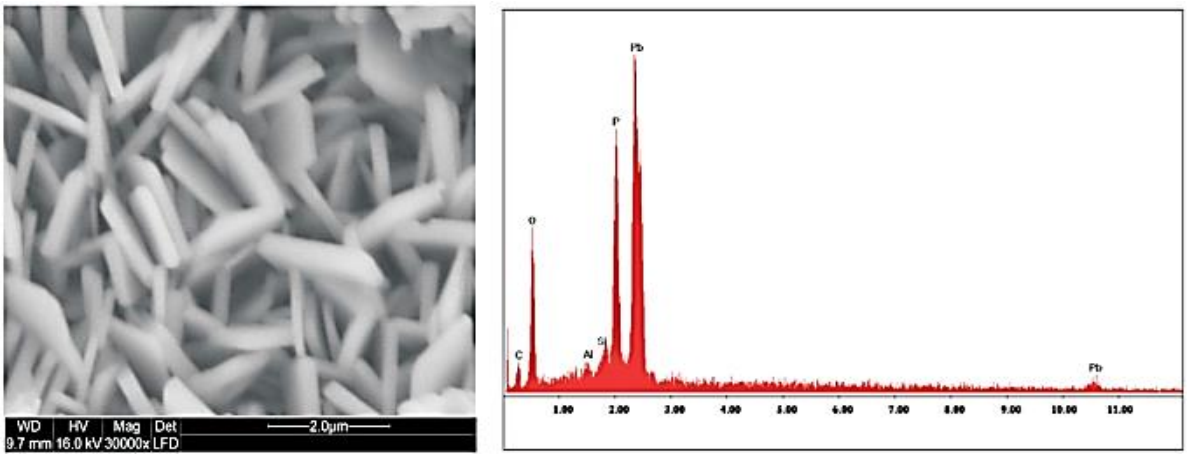

Figure III- 12 : SEM micrograph of (60 mol% PbO-40 mol% P_2O_5) (x3000)) along with corresponding EDX spectrum.

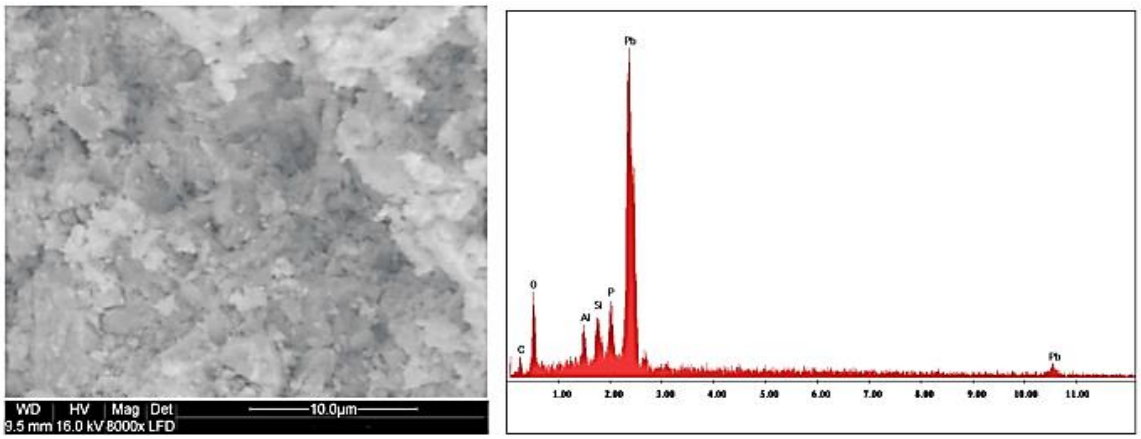

Figure III- 13 : SEM micrograph of (85 mol% PbO-15 mol% P_2O_5) (x8000)) along with corresponding EDX spectrum.

The figures III-12 and III-13show that the elaborated samples of (60 mol% PbO-40 mol% P_2O_5) and (85 mol% PbO-15 mol% P_2O_5) are homogeneous, with low porosity. The EDX analysis in surface gives high density of lead (Pb), phosphorus (P) and oxygen (O) mean constituents of the forming oxides. The impurities are low. Elsewhere, crystallites are observed, indicating order solid as showed with XRD measurements.

Finally, the density, XRD, IR analysis and SEM-EDX observations confirm that all the prepared phases are binary system, with low porosity and valid for more investigations.

Moreover, in order to find out more about the sample's surface topography, the considered glass matrix (45-mol%PbO-55mol%P_2O_5) was analyzed at higher magnification (x 2,000) using a scanning Electron Microscope of JEOL JED 2300 type equipped with 6380 LA EDX analyzer (available to Budapest Univeristy of Technology and Economics)[*](See the apparatus description

***The concerned are gratefully acknowledged.**

in the Appendix), after sputtering the sample with Au/Pd alloy. Digital X-ray maps were obtained on a matrix, which was set up at 512 x 384 points, with individual spectra acquired for up to 0.1 msec per point.

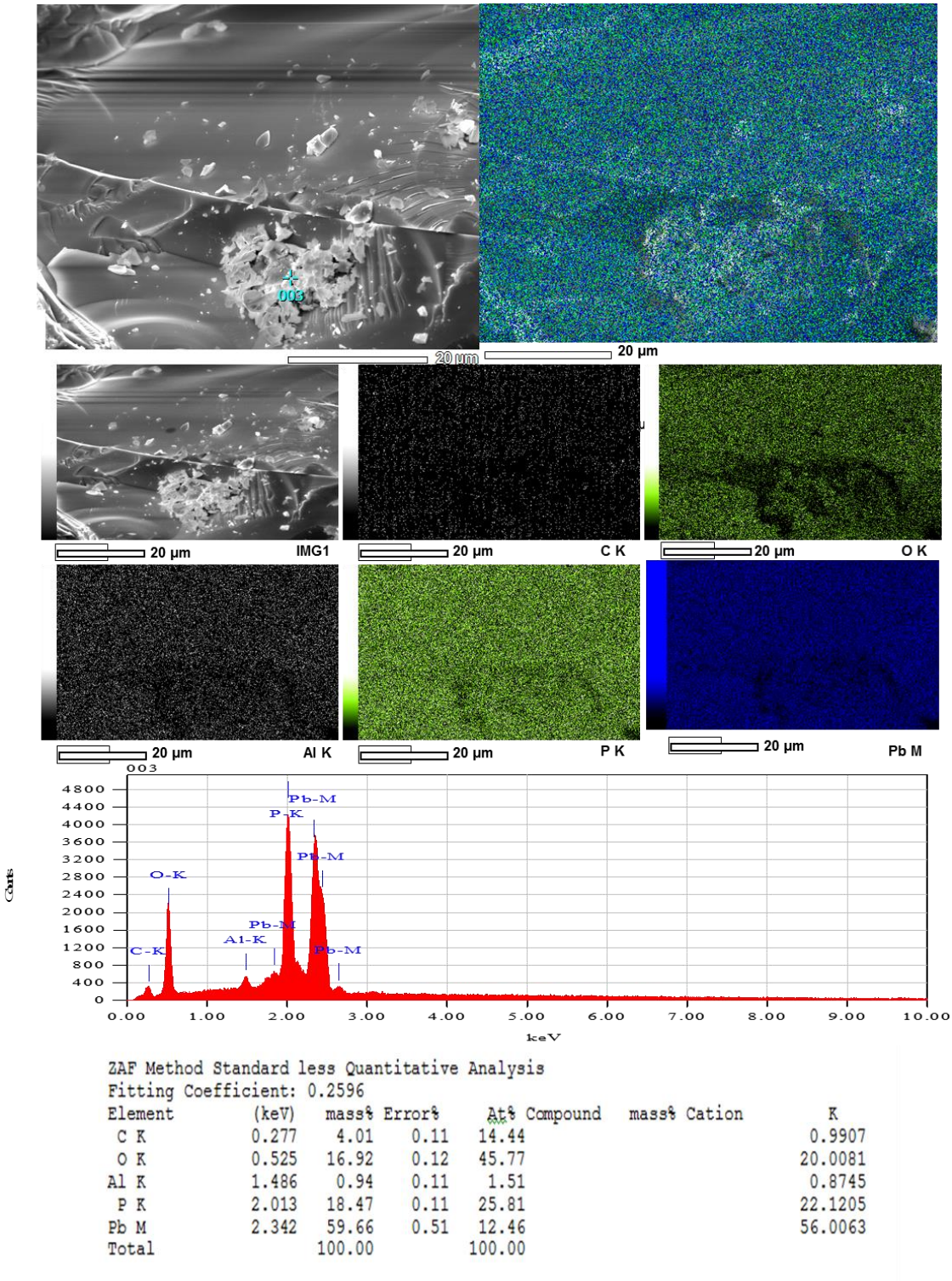

ZAF Method Standard less Quantitative Analysis
Fitting Coefficient: 0.2596

Element	(keV)	mass%	Error%	At%	Compound	mass% Cation	K
C K	0.277	4.01	0.11	14.44			0.9907
O K	0.525	16.92	0.12	45.77			20.0081
Al K	1.486	0.94	0.11	1.51			0.8745
P K	2.013	18.47	0.11	25.81			22.1205
Pb M	2.342	59.66	0.51	12.46			56.0063
Total		100.00		100.00			

Figure III- 14 : The element mapping images of the (45mol% PbO-55 mol% P_2O_5) glass along with Energy-dispersive X-ray spectroscopy elemental mapping.

Figure III-14 shows the SEM micrographs and EDX elemental maps of (45mol%PbO-55 mol% P_2O_5) glass. SEM maps suggest that the investigated glass composition is literally composed of P, Pb and O elements. This finding provides solid evidence again that (45 mol% PbO-55 mol% P_2O_5) glass was successfully prepared.

The map images reveal irregular shapes and size of clusters, also cracks and holes can be easily detected, which suggest the existing of some porosity. This glass matrix feature is of key importance, since it isis seeming able to allow the conducting particles to be imbedded within it after being milled. It is worth noting that milling process has also an important role on the resulting microstructure, it gives a rise to smaller particle size and broader distribution of conducting particles within the glassy matrix. Also, the milling process remarkably causes distance narrowing between the particles (see chapter IV). As consequence, particles interconnection would considerably contribute to strength of the obtained composites by inhibiting the dislocation movement. Also, it would be of crucial importance for further intriguing electrical and thermo-electrical properties. These later are going to be investigated within the coming chapters V and VI.

Now that we have highlighted the structural and morphological characteristics of the basic matrix which is useful candidate for our composites, and has a promising application in energy area, another window opens on how the chemical and thermal stability of this glass is satisfied.

III.3.5 Chemical and thermal stability of PbO-P_2O_5 binary system

III.3.5.1 Chemical stability of phosphate glass

It is well known that; the air weathering is considered as one of the important natural factors that can lead to deterioration of the studied glass. Thus, we are considering the influence of relative humidity as the main environmental parameter. This effect was evaluated on the lead phosphate glass by firstly weighing a newly prepared and dried glass then the moisture ratio was recorded with respect to time by continually weighing during 7 days using precision scale with four digits after decimal. The following relation [200]expresses the moisture content:

$$M\% = \frac{Wh - Wdry}{Wdry}.100 \qquad \textbf{(III-4)}$$

With,

Wh : The weight of the sample in humid state

$Wdry$: The weight of the sample in the anhydrous state.

The obtained results are gathered in Table III-3.

Table III- 3 : Weight variation record of lead phosphate glass in the air and calculation of moisture ratio.

Weight of dry glass (g) at t=0	Exposure time	Weight after exposure in humid air (g)	Moisture content (%)
2.5007	1h	2.5007	0
	24h	2.5007	0
	Day 1	2.5007	0
	Day 2	2.5010	0.03
	Day 3	2.5013	0.06
	Day 4	2.5014	0.07
	Day 5	2.5014	0.07
	Day 6	2.5016	0.09
	Day 7	2.5016	0.09

As can be seen, the studied glass matrix composition (45mol%PbO-55mol%P_2O_5) was found to be expressing moisture rate change not exceeding 1% .The minimal moisture content suggests that the chosen matrix composition is not indicating any serious hygroscopic behavior. This finding is in a good agreement with density data as obtained above and in a good correlation with thermogravimetric analysis which is carried out elsewhere [201].

Indeed, from chemical standpoint, pure vitreous phosphorus pentoxide (P_2O_5) is known to be unstable because of hydrolysis of the P–O–P bonding by atmospheric moisture, but in our case the addition of lead oxide may improve its stability towards atmospheric hydrolysis because of the possibility of P–O–Pb^+ bonds formation [181,182]. This cross-linking can increase the bond strength, which makes the phosphate glass more resistant to moisture attack. This has been clearly evidenced through some previous works [202,203].

III.3.5.2 Thermal studies

Differential scanning calorimetry was carried out in order to investigate the glass transition of the elaborated glass composition (45mol%PbO-55mol%P_2O_5) (Figure III-14). The procedure detail of DSC analysis is given in the Appendix [204].

A baseline deflection is observed over a temperature range. This deviation reflects a change in heat capacity corresponding to the "glass transition". The glass at the passage of this temperature (T_g), behaves like a soft material, with low viscosity, and beyond glass phase transition temperature (T_g), the glass can be shaped.

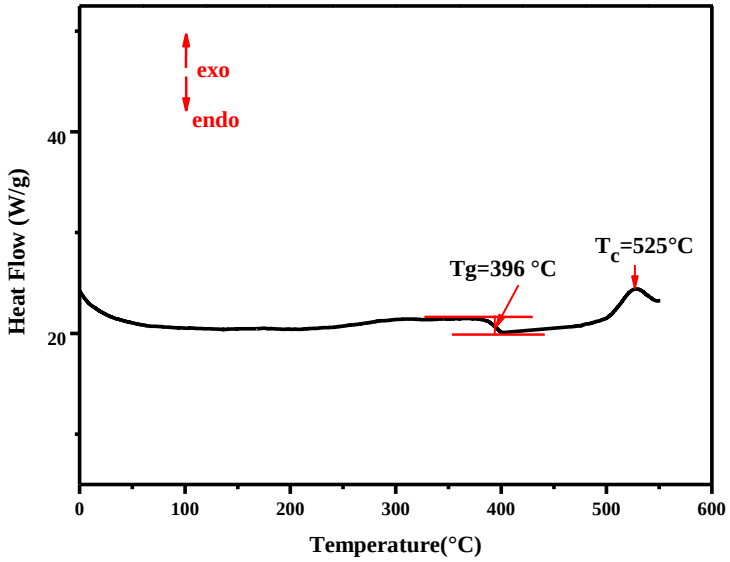

Figure III- 15 : DSC Curve of neat lead phosphate glass (45mol%PbO-55mol%P_2O_5).

According to above plotted DSC curve, we can see that the T_g of (45mol%PbO-55mol%P_2O_5) glass is about 396°C. This value is lower than found in the same composition of (45mol%ZnO-55mol%P_2O_5). It seems that this difference is related to the Zn and Pb sizes (atomic and Van Der Waals radius). Indeed, lead having high radius, this would favor less compact solid structure than zinc and leads more easily to the amorphous state. Therefore, lead phosphate glass (PbP) should have its vitreous transition lower than zinc-phosphate glass (ZP), when they have the same molar fraction in the two glasses (PbP) and (ZP) compositions. Elsewhere, the obtained values remain in the same order of magnitude as those found in similar systems; for close composition [205,206].

The figure III-15 shows also that the glass phase transition is followed by an exothermic behavior indicating onset of crystallization around Tx≈500°C and crystallization at Tc=525°C.

The melting point of the studied glass was determined by introducing the glass sample in the oven and heating slowly with rate of 5°C/10 min starting from 550°C and observing the temperature at which melting is occured. The melting temperature Tm was about 705°C.

On the basis of these results, it is possible to estimate the value of glass thermal stability.Note that T_g and the onset of crystallization temperature are frequently used to evaluate the stability of the glass. The stability of a given glass is defined as its resistance to devitrification, or to crystallization. It therefore takes into account the ability of a glass to be heated above its glass transition temperature without crystallizing.

Thermal stability (Ts) of such glass can be expressed using a simple criterion introduced by Dietzel [207].

$$\Delta T = T_X - T_g \quad \textbf{(III-5)}$$

The greater the difference between T_g and TC is, the more thermally stable the glass is.

The shape of the crystallization peaks also tells us about the stability of the glasses. Thus, a broad crystallization peak with low intensity means a low kinetics of crystallization and consequently a good thermal stability [208].

In addition to Tx and T_g, other characteristic temperatures, such as Tc (525°C) and Tm, have been used to assess this property. The glass stability factor (K_{gl}) suggested by Hruby [209] is given by the relation:

$$K_{gl} = \frac{T_x - T_g}{T_m - T_c} \quad \textbf{(III-6)}$$

It has been proved that for good glass forming system, the values of $K_{gl} \geq 0.1$ [210]. The thermal stability of the investigated glass composition (45mol%PbO-55mol%P_2O_5) was then calculated using Hruby criterion. The Kgl value obtained from DSC measurement, for the present composition is around $K_{gl} \approx 0.58$, this value is somewhat lower than found in the same composition of zinc-phosphate glass ($K_{gl} \approx 0.85$) [73]. As noted above this difference comes probably from the difference size of lead and zinc oxide respectively. However, the found value in present study remains upper than 0.1 and confirms that the lead phosphate glass matrix is characterized by good glass forming ability, in good agreement with moisture tests and previous studies [73, 205, 206,208,211].

III.4 Preparation of the lead phosphate glass-based composites

A composite is defined as a material composed of different heterogeneous elements. The composites are, in general, made up of a matrix, which ensures the rigidity, the material's texture, and another phase called charge which has specific properties (electrical, mechanical, thermal) that one wishes to find in the composite material [208].

Required amount of metallic powders (Chromium, Cobalt, Nickel and Zinc from Sigma-Aldrich) and phosphate glass were mixed together and pressed under 7 ton/cm^2 into compact disc having a diameter of 13 mm and thickness of 1–2 mm. Afterward, the sample discs were sintered at 300°C; below their glass transition temperature for 2 hours so as to ensure the composites cohesion. A series of composites were prepared with filler loading ranging from 7 to around 42 vol.% into the glass matrix. The characteristics of metallic powders are given in Table III-4.

Table III- 4 : Characteristics of filler particles : purity, mean size (φ) and density (d).

Samples	Purity (%)	ϕ (µm)	d (g/cm^3)
Zinc	99.9	15 ± 10	7.134
Chromium	≥99%	44	7.14
Cobalt	99.9	149µm	8.9
Nickel	99.9	149µm	8.9
Matrix (PbP)	-------	---------	4.13

III.4.1 Density and porosity measurements of the elaborated composites

Density is one of the most important characteristics for determining the properties of the composites. Density generally depends on the relative proportion of matrix and loaded fillers. In this section we have measured the density of PbP/(metals) composites by Archimedes method and using Eqt. (III-1). Theoretical density d_{th} of composite materials in terms of filler volume fractionsϕ can be easily obtained using the following equation for binary system [76]:

$$d_{th} = (1-\phi)d_m + \phi d_f \qquad \textbf{(III-7)}$$

Where ϕ: is the volume fraction of the charge, d_m and d_f stand for experimental densities of the matrix and the filler, respectively.

Porosity means the volume fraction of voids in the composites; it is estimated by using the equation (III-3). Density and porosity curves for the four studied composites series are reported in Figure III-16 and Figure III-17, respectively:

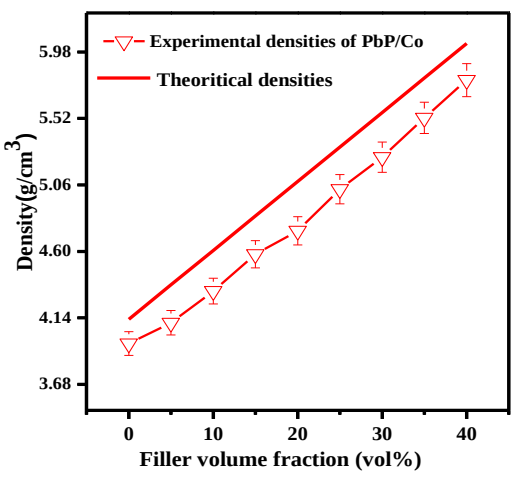

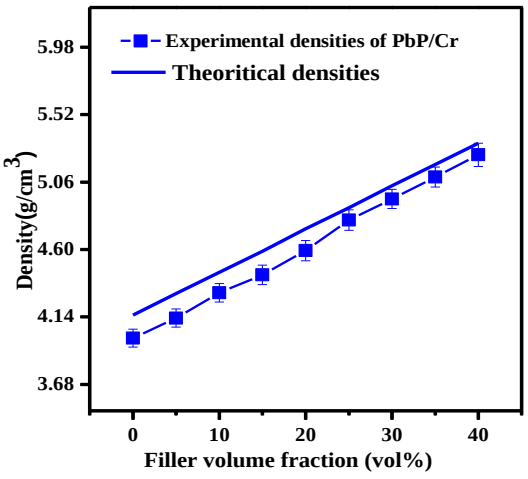

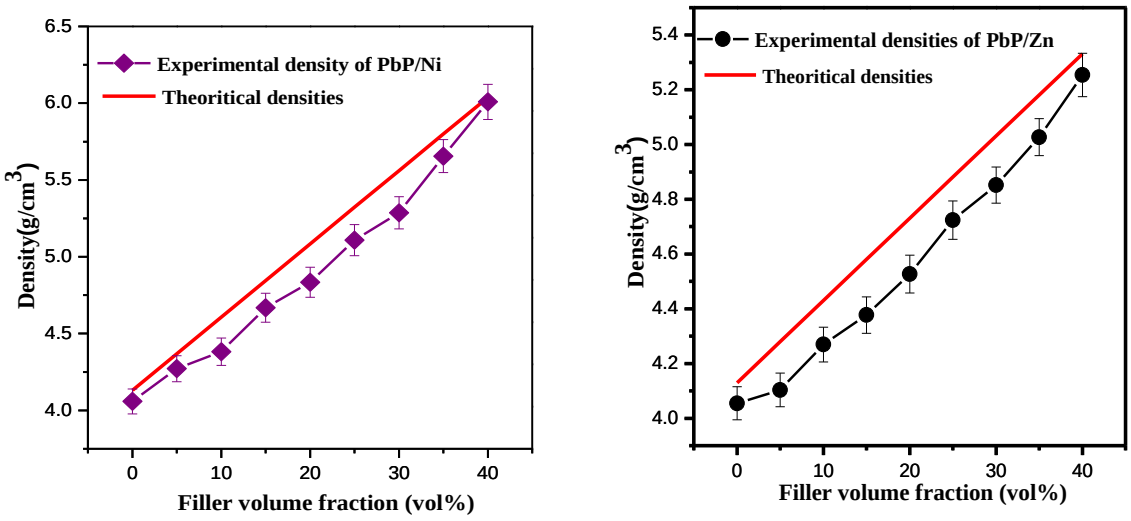

Figure III- 16 : Experimental density and calculated density (the upper solid line) of PbP/metal composites.

The figure III-16 indicates linear behavior with increasing filler amount for both densities, calculated one, considering two constituents of system (matrix and filler) and measured. The characteristic of binary system of composite (matrix +filler) is thus confirmed.

The theoretical density calculation involves the already measured density of matrix and the fillers densities, which are taken from Table III-4. The result is plotted as continuous lines in Figure III-16. The calculated values are always up the measured ones but they are almost parallel. The difference is related to the occurrence of voids, pores or porosity in the composites. The obtained results are given in Figure III-17:

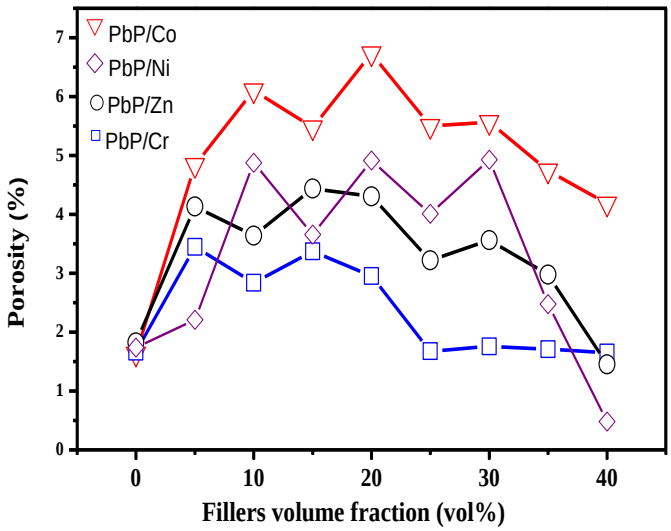

Figure III- 17 :Porosity rate in PbP/metal composites determined with equation (III-3).

The porosities of PbP/Co and PbP/Ni composites are around 5-7% and are high compared to the other obtained porosities. However, they remain lower than observed in the $ZnO\text{-}P_2O_5$ (τ~12-13%) [73,204]. This seems related, as noted above, to the size of fillers and the nature of filler and matrix (Table III-3). Elsewhere, the same overall behavior is showed for the whole composite series. Firstly, the porosity is substantially increasing with fillers loading, then stabilizes and decreases regularly above critical fillers concentration. This behavior seems to be connected with packing density coefficient effect, which increases to attain the limit value around 0.5 (to be seen in chapter V). In overall case, the porosity value is lower than 10% and the obtained composites can be considered good candidates to study their physical properties.

Note that numerous physical properties mainly depend on the porosity content. It was stated elsewhere that electrical conductivity decreases drastically with increasing of the porosity [207].

III.4.2 XRD analysis of PbP/(metals) composites

In this section, we give the preliminary results of structural approach of the glass/metallic powders composites. Note that X-ray diffraction (XRD) was carried out using a powder diffractometer in Bragg-Brentano geometry(available to Laboratoire de Chimie Appliquée des Matériaux)*. Scans were performed over a 2-theta ranging between 10 and 70◦ with a step size of 0.05◦ and a 5s count time at each step on disc of 13mm of diameter and 2-3mm of thickness.

The XRD scans of the unfilled glass matrix ($45mol\%PbO\text{-}55mol\%P_2O_5$) (PbP) indicate a typical amorphous band at $2\theta \approx 20\text{-}30°$. However, the matrix loaded with metallic fractions exhibit some crystallization peaks as depicted in Figure III-18. The intensities of crystalline phase peaks increase and the halo of amorphous phase disappeared with increasing of the incorporated amount of the metallic powders. These peaks have been indexed according to the International Center for Diffraction Data (ICDD), using the Bruker Diffrac plus EVA software. Cobalt and nickel are of hexagonal whereas zinc and chromium crystallizes in centered cubic structures. Note that at relatively high concentration of metal, XRD patterns indicate crystallized phase corresponding to the metal inside amorphous phase of the glass matrix. This has verified by obtained XRD spectra on compacted discs of the four used metallic powders, which are displayed in the corners of XRD patterns of each composites. Such phenomena are already observed in $ZnO\text{-}P_2O_5$/metal composites [73].

***The concerned are gratefully acknowledged.**

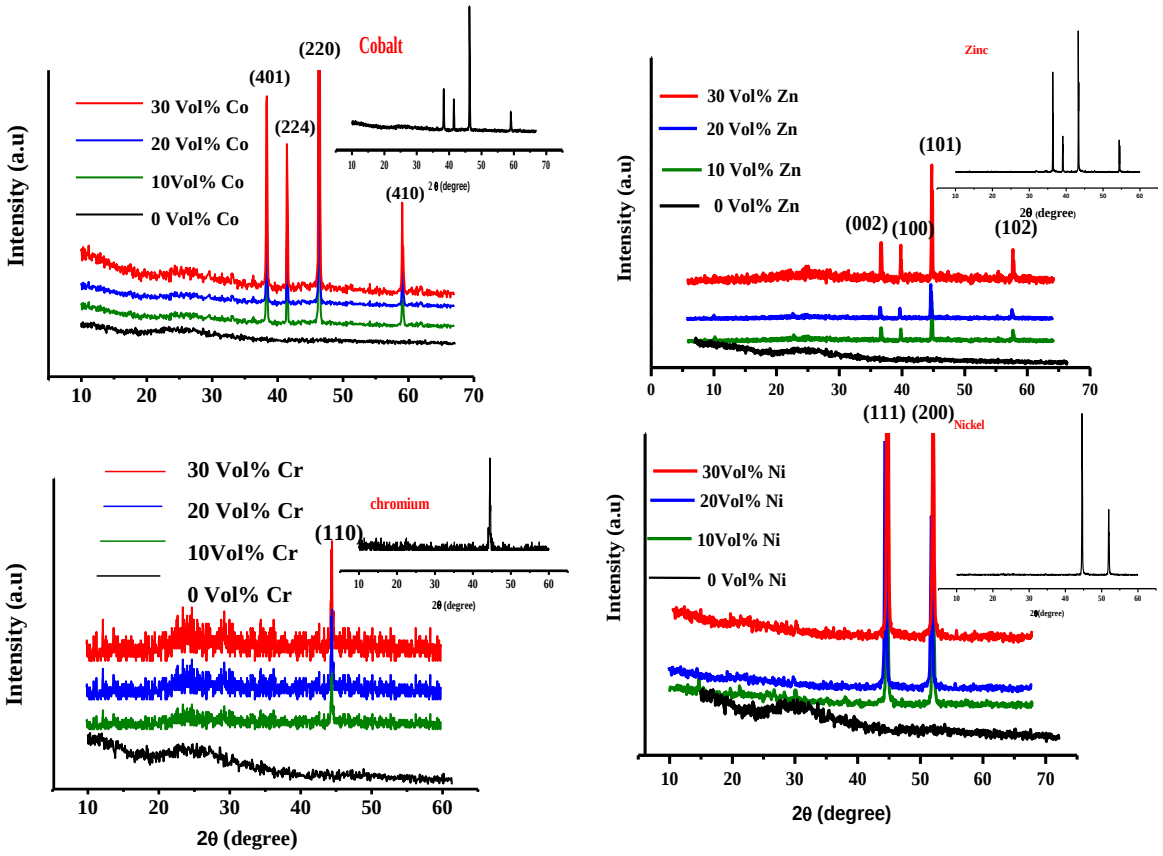

Figure III- 18 : X-ray diffractogram (XRD) of PbO- P_2O_5 glass filled with conducting particles.

Comparing these patterns to XRD results related to the composites, we concluded that the obvious sharp peaks displayed in the four cases of the figure III-18 are undoubtly attributed to the metallic inclusions.

III.4.3 -Thermal analysis of PbP/(metals) composites

This part is devoted to the determination of the glass phase transition temperatures T_g of elaborated composites. The purpose here is to investigate fillers loading effect on the evolution of this transition and therefore find out about the matrix-fillers interaction, Thus, a serial of composites (PbP/metals (Cr, Co, Ni, Zn), with filler contents below and above the percolation threshold was selected to determine their T_g using DSC analysis, with heating rate of 20 °/min. Note that the values of the glass transition are taken in the midpoint of DSC curves as shown in figure III-19:

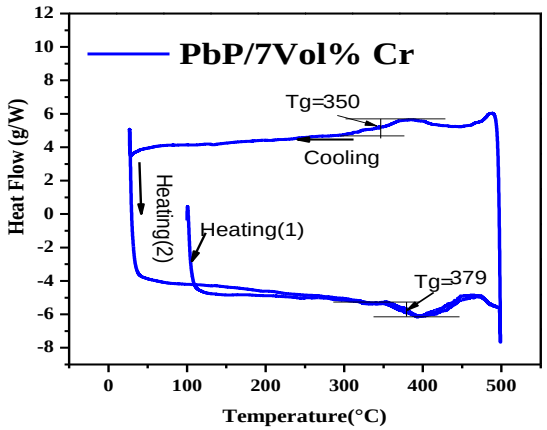
PbP/7Vol% Cr
Tg=350
Cooling
Heating(2)
Heating(1)
Tg=379
Heat Flow (g/W)
Temperature(°C)

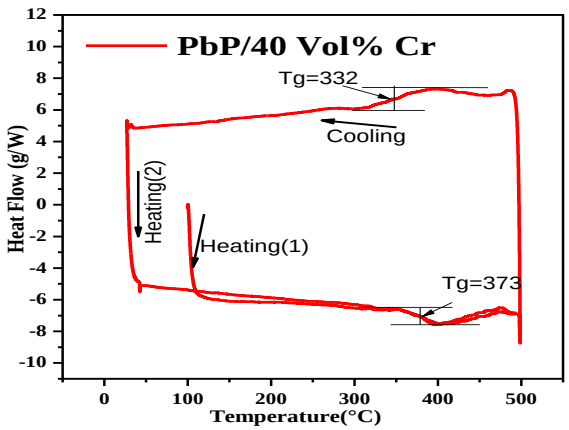
PbP/40 Vol% Cr
Tg=332
Cooling
Heating(2)
Heating(1)
Tg=373
Heat Flow (g/W)
Temperature(°C)

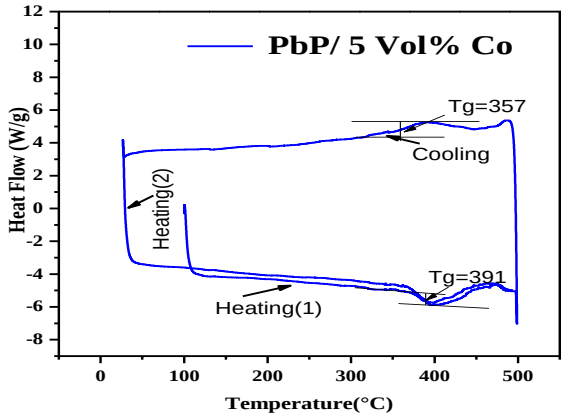
PbP/ 5 Vol% Co
Tg=357
Cooling
Heating(2)
Tg=391
Heating(1)
Heat Flow (W/g)
Temperature(°C)

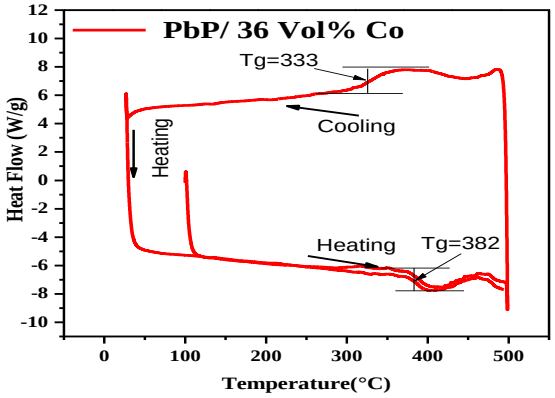
PbP/ 36 Vol% Co
Tg=333
Cooling
Heating
Heating
Tg=382
Heat Flow (W/g)
Temperature(°C)

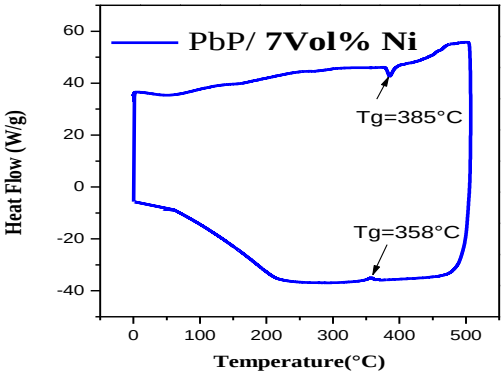
PbP/ 7Vol% Ni
Tg=385°C
Tg=358°C
Heat Flow (W/g)
Temperature(°C)

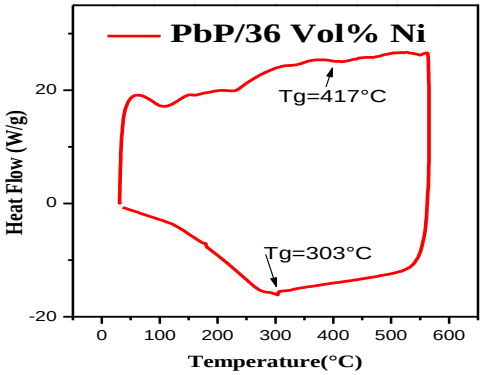
PbP/36 Vol% Ni
Tg=417°C
Tg=303°C
Heat Flow (W/g)
Temperature(°C)

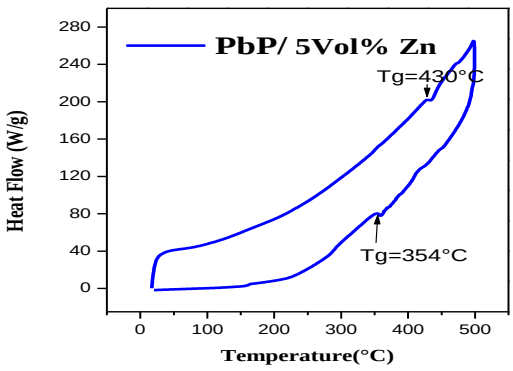
PbP/ 5Vol% Zn
Tg=430°C
Tg=354°C
Heat Flow (W/g)
Temperature(°C)

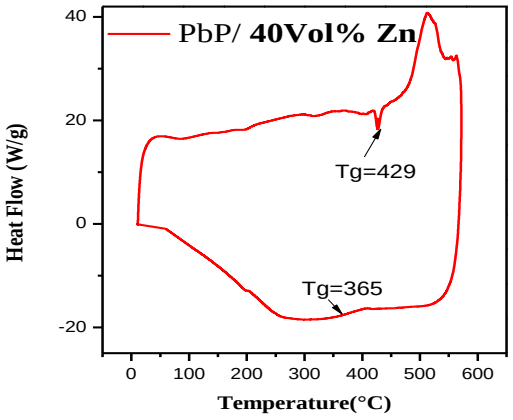
PbP/ 40Vol% Zn
Tg=429
Tg=365
Heat Flow (W/g)
Temperature(°C)

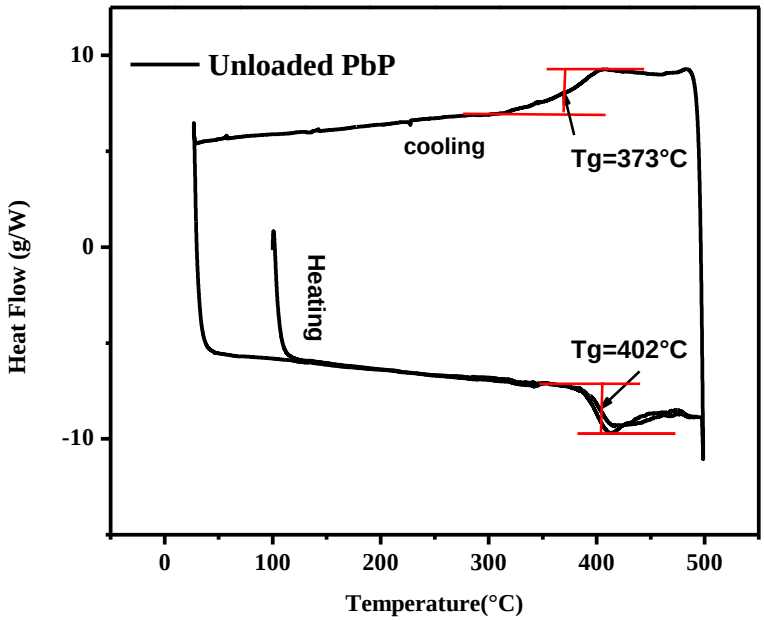

Figure III- 19 : DSC signal showing T_g transition of the unloaded lead phosphate PbP glass matrix and PbP/(Cr, Co,Ni,Zn) composites.

Concerning our matrix (45mol%PbO-55mol%P_2O_5) or (PbP), it is suitable to note that the characteristic shape of the endothermic effect in glass transformation region appears as a feature of all the vitreous states (figure III-19). The glass transition temperature (T_g) of our glassy composition is found to be about 402°C in increasing heating rate of 20 °/min, in good agreement with earlier studies on similar systems [213,214]. However, when the lead oxide PbO is replaced by ZnO for the same molar percent, T_g is shifted to the high temperature (430°C). This is probably associated to the nature of oxides (ZnO or PbO) or their size [215] and viscosity [216].

In the cooling process T_g is only about 373 °C, as depicted in figure III-19 and given in Table III-5. This significant decrease is probably related to the kinetic structural organization, which takes place with increasing temperature to attain true crystallization point at higher temperature. When the system is cooled this organization is relatively kept and consequently decreases T_g.

Concerning the PbP/metal composites, it's worthy to note that DSC analysis exhibits significant decrease in the T_g values, compared to the unfilled glass matrix, as given in Table III-5 :

Table III- 5 : Comparison of glass transition temperature T_g values of composites obtained by DSC measurement in heating and cooling rates.

Sample	**Glass transition temperature (°C) in heating rate**				**Glass transition temperature (°C) in cooling rate**			
Unloaded glass	402				373			
Composites	5Vol %	7vol%	36Vol %	40Vol%	5Vol %	7vol%	36Vol %	40Vol%
$PbO-P_2O_5$/Cr	-----	379	------	373	------	350	------	347
$PbO-P_2O_5$/Co	391	-----	382	------	357	------	333	------
$PbO-P_2O_5$/Ni		358	303			385	417	
$PbO-P_2O_5$/Zn	354			365	430			429

Indeed, the XRD analysis shows that the metallic fillers form crystallized network inside the amorphous matrix. The intensity of diffraction peaks increases with filler concentration. It seems obvious that the incorporation of the metallic fillers improves the thermal stability of the glass matrix, increases its mechanical properties, leading to more structural order and thus shifts its T_g to lower temperature. This stabilization of glass matrix by metal incorporation could be interpreted by the high heat capacity of metal, which allows absorbing significant heat, leading to preclude the thermal degradation and stabilizing the matrix [73,212,213, 218,219].

In fact, the samples had undergone reorganization during the heat run. The true properties of the material are only observed in the second heating run; this latter was found to be superposed to the first heating run. It seems that the same phenomenon has occurred in the unfilled matrix. A similar decrease of T_g as a function of the fillers has been observed in other glass composite materials [73].

III.4.4 Infrared spectroscopy of PbP/(metals) composites

The structural XRD study of PbP/metal composites was completed by the FTIR/ATR analysis. This technique must give additional informations of the studied composites and helping to understand the possible structural changes in the phosphate matrix due to the addition of conducting particles. For this aim, we have collected infrared spectra of the unfilled and filled (45mol%PbO-55mol%P_2O_5) glass matrix with metallic inclusions at different volume fractions.

The FTIR-ATR spectra of the composite samples were plotted at spectral range from 1600 to 400 cm^{-1} for better clarity (Figure III-20):

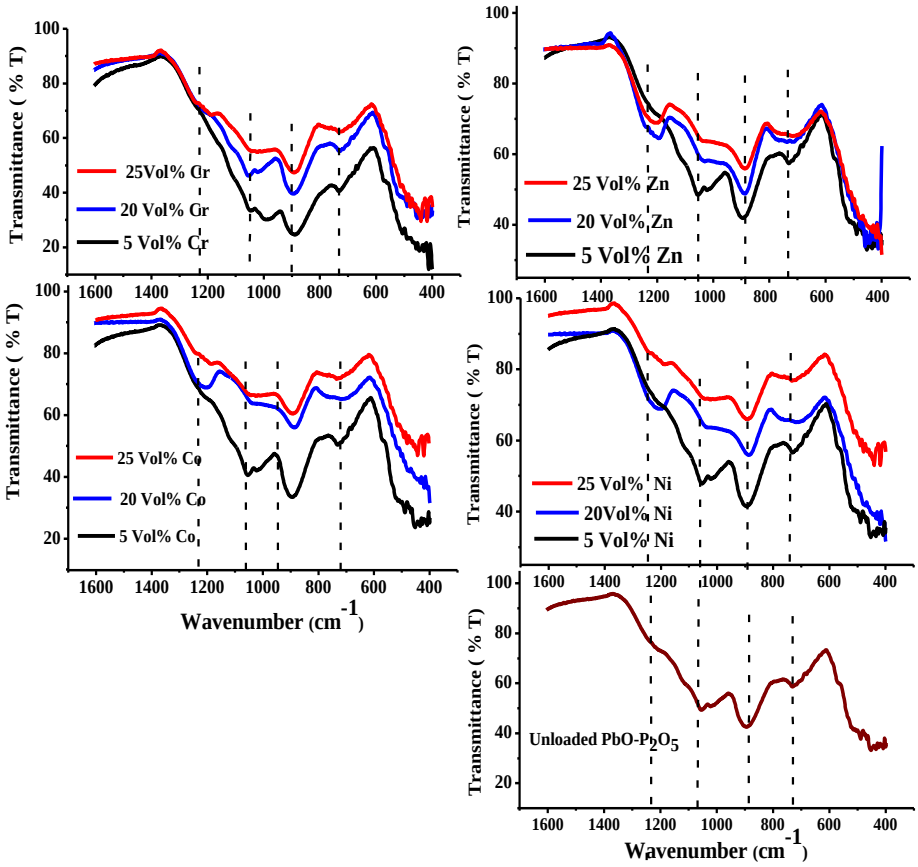

Figure III- 20 : FTIR/ATR plot of unloaded and loaded lead phosphate glass.

The results exhibit similar spectra shape, which suggest that the addition of metallic fillers did not cause any important changes in structural features of lead phosphate glass network.In a good concordance with X-ray data findings.Thus, the observed bands are mainly corresponding to the characteristic vibrations of the lead phosphate glass [181,182],.The appeared band at around 720cm^{-1} can be assigned to P-O-P symmetric stretching vibrations [9,10]. While the band observed at 900 cm^{-1} is attributed to the asymmetric stretching mode of P–O–P linkages [214,215,216,219,220,221]. According to the literature, it is also associated with the vibration of P-O bridging group as well as to the symmetric and asymmetric motions of the bridging oxygen in P–O–P linkages, indicating the presence of linear metaphosphate (P–O–P) chains in the phosphate glass [215,220]. This finding was further confirmed by the asymmetric vibrations of P–O–P groups ascribed to the spectral band around 1050 cm^{-1} which could be also assigned to P–O stretching modes [214,219].The appearance of P–O bond originates from the creation of additional non-bridging oxygen (NBOs) which are probably induced by PbO, leading to formation of P-O-Pb^{+} ionic bonding [216,221]. It should be mentioned that in the whole spectral

range we could find very weak characteristic band of the P=O linkage at around 1200cm^{-1}. According to Egili e al. [9] [181], this band can be considered as an indication for the formation of pyro-phosphate groups and this is more likely due to the conversion of NBOs to bridging oxygens upon the formation of P-O-Pb bonds [26,31]208,213. This finding confirms that PbO acts as network modifier in the studied glass composition, in good consistence with our previous work [186]. For the present samples, the FTIR-ATR band positions and their assignments are summarized in Table III-6. Finally, this analysis gives another confirmation that, the elaborated glass matrix is really a binary system, which is stable and suggesting that no chemical reactions have been occurred.

Table III- 6 : FTIR attribution bands of lead phosphate PbP glass matrix and PbP/(Co, Cr) composites.

Main characteristic groups	**Wave number (cm^{-1})** PbP glass matrix and PbP/ (Co, Cr, Zn, Ni) composites
***Assymmetric stretching vibration of P=Obond (ν_{as} (P=O))**	~1240cm^{-1}
***Symetric bending vibration mode of P-O-P group (ν_s P-O-P).** ***P–O stretching modes.**	1050 cm^{-1}
***Assymmetric stretching vibrations ν_{as} P-O-P.** ***Vibration of P-O bridging group**	900 cm^{-1}
***Symmetric stretching vibrations ν_s P-O-P.**	720 cm^{-1}

Conclusion

The goal of this chapter consists of developing electroconductive composites based on binary phosphate glass. Firstly, series of composition xPbO-(1-x)P_2O_5, with 20≤x≤85mol% have been synthesized and characterized using density measurements, scanning electron microscopy, x-ray diffraction and infrared vibrational spectroscopy. Thus, derived results from density data and SEM observations have been related to proper homogeneity of the obtained binary system. Infrared spectroscopy revealed that the addition of lead oxide causes changes in the structure of short-range order of the glass matrix; for x < 60 mol%, PbO acts as network modifier. While for x > 60 mol%, it was concluded that lead oxide plays both role of former and modifier. The x-ray diffraction has shown that the concentration of PbO and the temperature have an important effect on the nature of the crystallization of the glasses. We have then selected the most stable amorphous composition to prepare phosphate glass/conducting filler composites. The structural and thermal properties of the elaborated composites have been studied in the same conditions by

X-ray diffraction technique (XRD), and IR/ATR analysis, density measurements and DSC analysis. The structural results show two phases, amorphous for lead phosphate and growing crystallized filler network. The intensity peaks of crystallized phase increases with filler amount. The obtained glass temperatures phase transitiondecrease gradually with fillers loading, in good coherence with continuous apparition of order in composite system. The FTIR measurements do not show any glass-filler bonding, this seems that the composite mixture is purely physical; explaining the independent growing of filler network. The observed porosity inside composite is low and not exceed 7%.

Finally, these characterizations show a good quality of obtained composites materials, valid for further physical studies.

CHAPTER IV
Morphology investigations, wettability, surfaces and interfaces energies estimation of lead phosphate glass/(metals) composites

IV.1 Introduction

Recently, phosphate glass-based composites have attracted much attention as a simple and cost-effective material to enhance the glass properties by conductive particles loading [222-226]. According to several studies, the interface exchange between matrix and filler plays an important role in physical properties of materials (stability, mechanical, electrical properties,..). Thus, our aim of this chapter is to visualize the interface of elaborated composites PbP/metals using scanning electronic microscopy along with EDX analysis. Also, we attempt to estimate the surfaces and the matrix-filler interface energies of composites through contact angle measurements.

Another important parameter will be examined on this occasion, it is the wettability of the composite materials obtained. Indeed, in recent decades, the study of wettability has received a great interest. From fundamental point of view, it is important to understand the nature of the interactions that are established between the liquid and the wetted surface and why some liquids wet and spread on given solid surfaces and others no? This wettability phenomenon plays an important role in many industrial applications, such as adhesion in all painting processes of automotive, textiles, adhesives, printing, liquid coating, oil recovery, painting, lubrication, electrowetting, self-cleaning, nanofluidics, and more [227].

Concerning our studies, it is important to know how our elaborated materials behave in presence of liquids; water or others ? This parameter is of crucial importance in possible application, like solar or thermoelectric devices.

Usually the wettability is deduced from the measurement of contact angle of liquid droplet on surface of solid material. They are different methods to measure the contact angle (see, chapter II). Indeed, the measurements of contact angle allow the determination of the solid surface tension and solid/liquid interface tension. Then, the wetting characteristics of a solid material are highlighted.

IV.2 Morphology study of $PbO\text{-}P_2O_5$ /metals composites

It is well recognized that the morphology of the investigated composites has a major impact on further physical properties. Therefore, in order to get morphological insights of the elaborated composites, scanning electron microscope (SEM) and energy dispersive spectroscopy (EDS) analysis were undertaken. Indeed, SEM micrographs with high magnification permit us to observe the characteristic evolution of the particle's distribution. However, it should be noted firstly that, it is not obvious to obtain homogeneous dispersion of the fillers within the matrix. Indeed, many problems can be encountered. This is the case with the agglomeration of the fillers, which prevents

dispersion, the viscosity of the matrix, etc. This needs a lot of work and takes time in order to achieve a good result. Thus, the obtained results on (45mol%PbO-55mol%P_2O_5)/metals (Ni,Co,Cr,Zn) or PbP/metals composites, at low and high loading inside glass matrix are given in the figures IV-1 to IV-8, with EDX spectrum, mass and atomic percent's respectively :

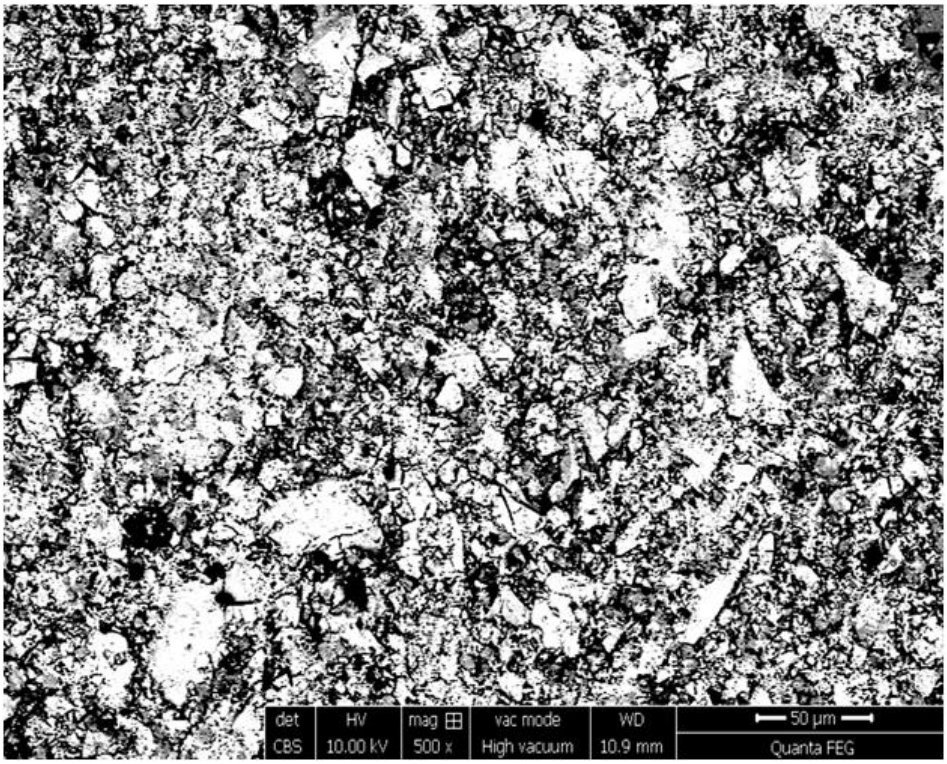

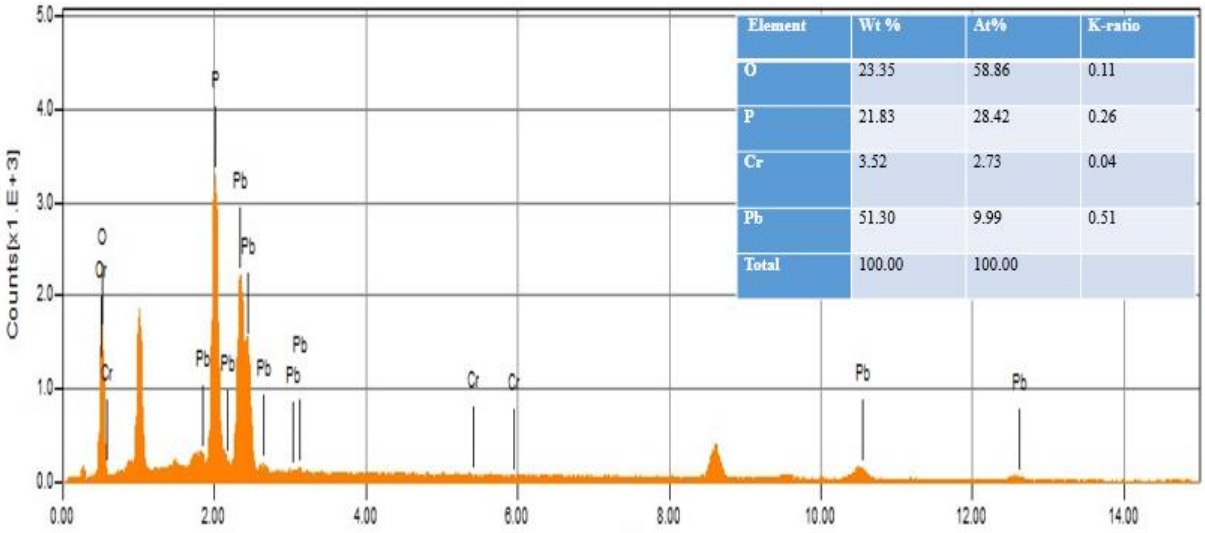

Figure IV- 1 : SEM micrograph along with EDS analysis of PbP/ Cr (5vol%).

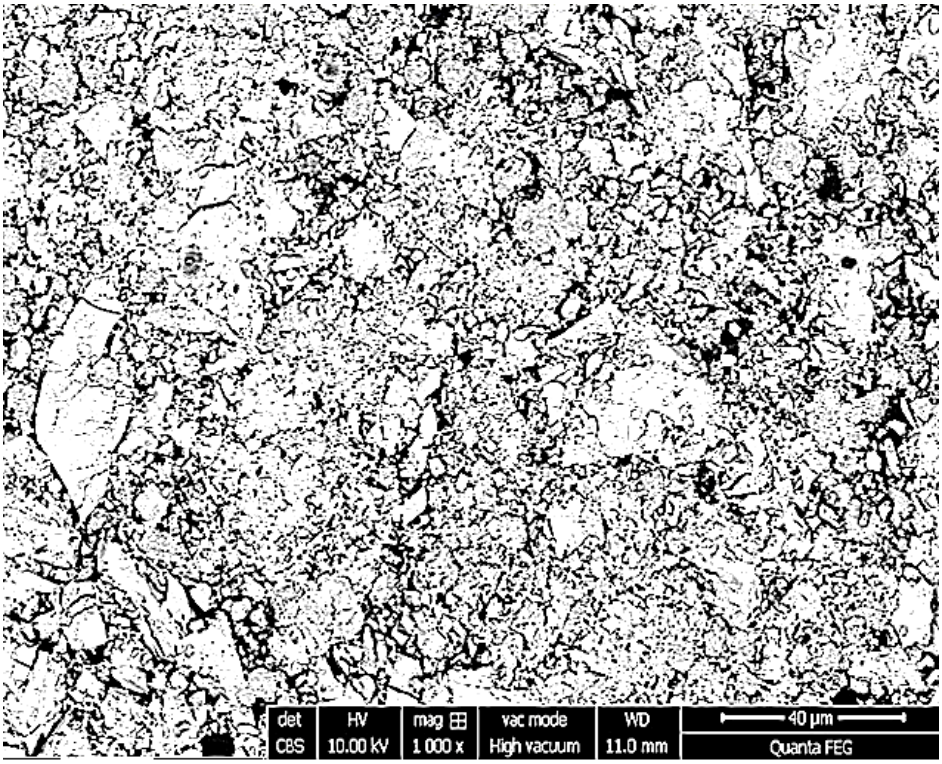

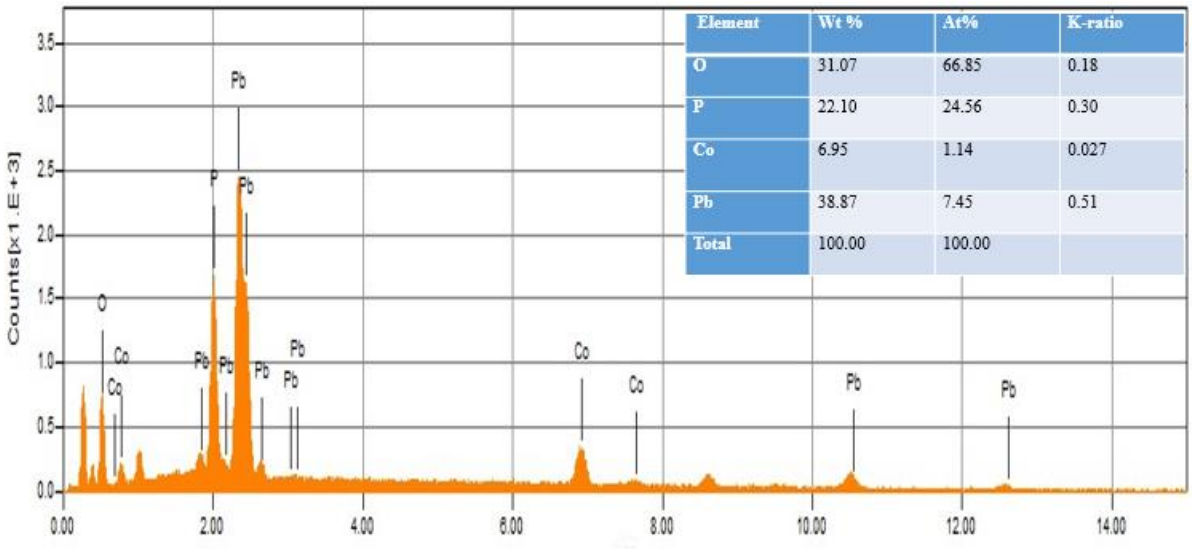

Element	Wt %	At%	K-ratio
O	31.07	66.85	0.18
P	22.10	24.56	0.30
Co	6.95	1.14	0.027
Pb	38.87	7.45	0.51
Total	100.00	100.00	

Figure IV- 2 : SEM micrograph along with EDS analysis of PbP/ Co (7vol%).

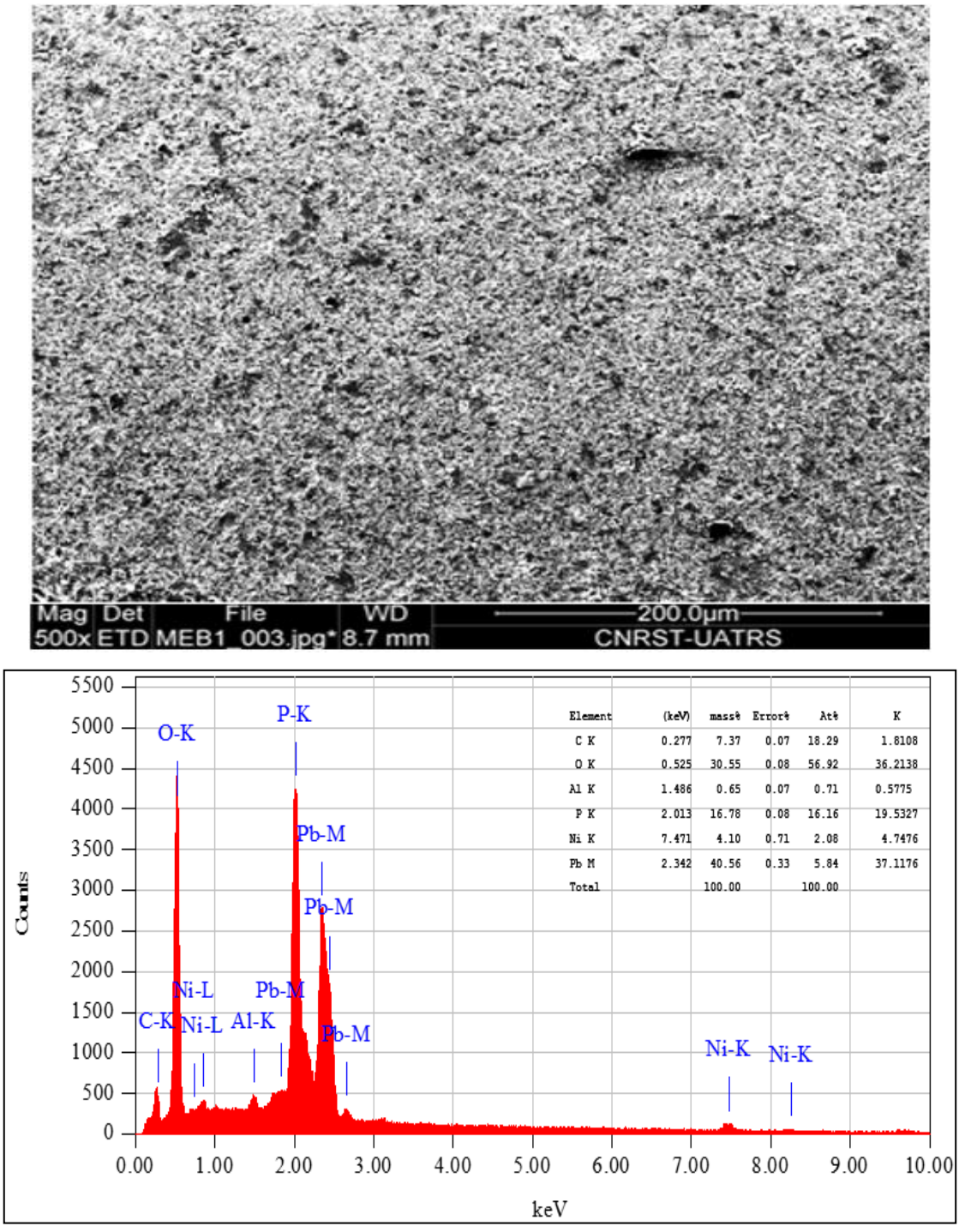

Figure IV- 3 : SEM micrograph along with EDS analysis of PbP/ Ni (4vol%) composite.

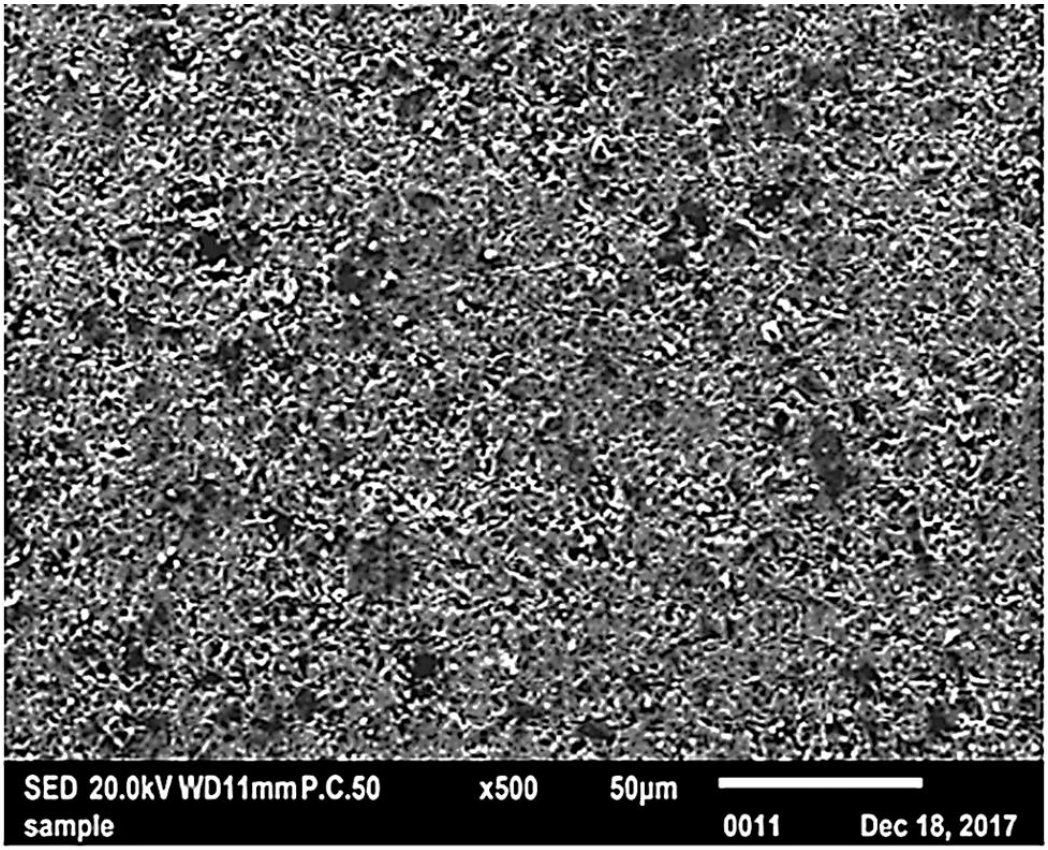

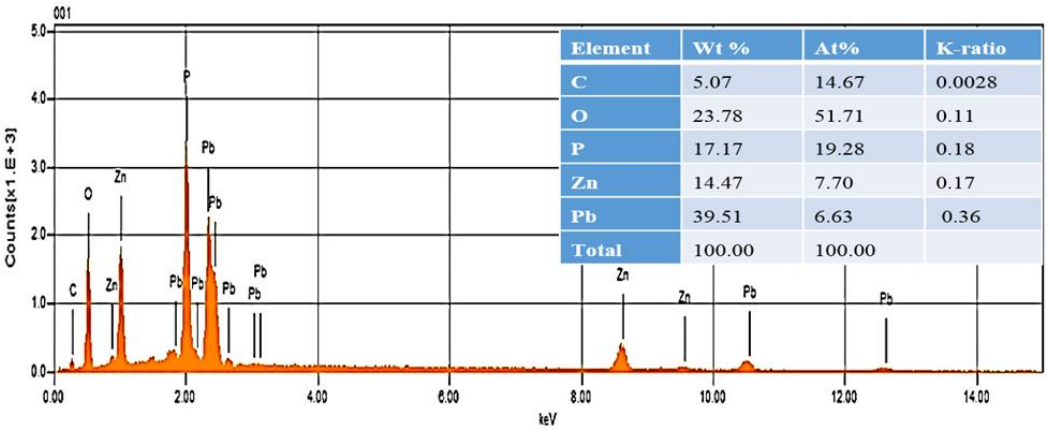

Element	Wt %	At%	K-ratio
C	5.07	14.67	0.0028
O	23.78	51.71	0.11
P	17.17	19.28	0.18
Zn	14.47	7.70	0.17
Pb	39.51	6.63	0.36
Total	100.00	100.00	

Figure IV- 4 : SEM micrograph along with EDS analysis of PbP/Zn(7vol%).

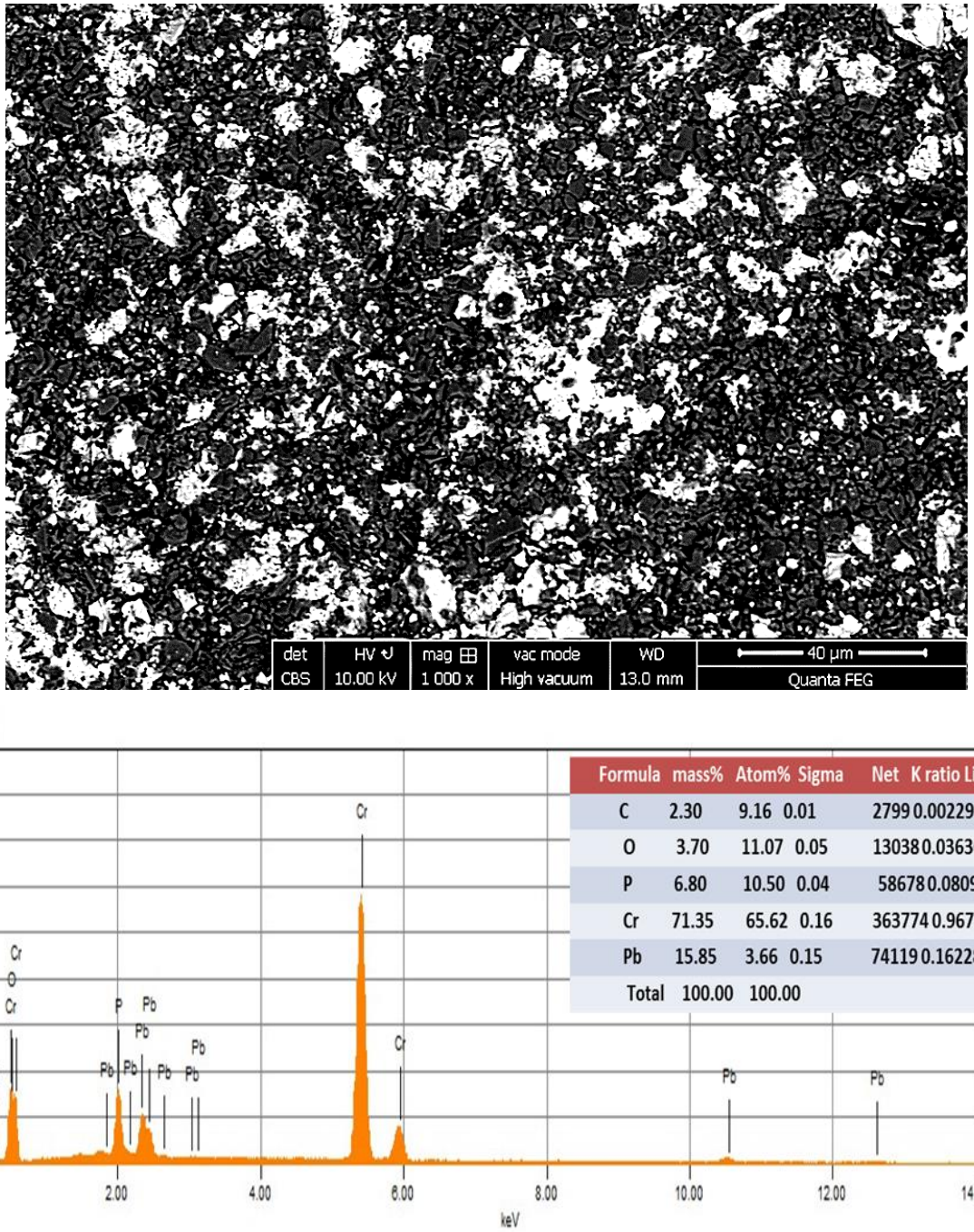

Figure IV- 5 : SEM micrograph along with EDS analysis of PbP/ Cr (40vol%).

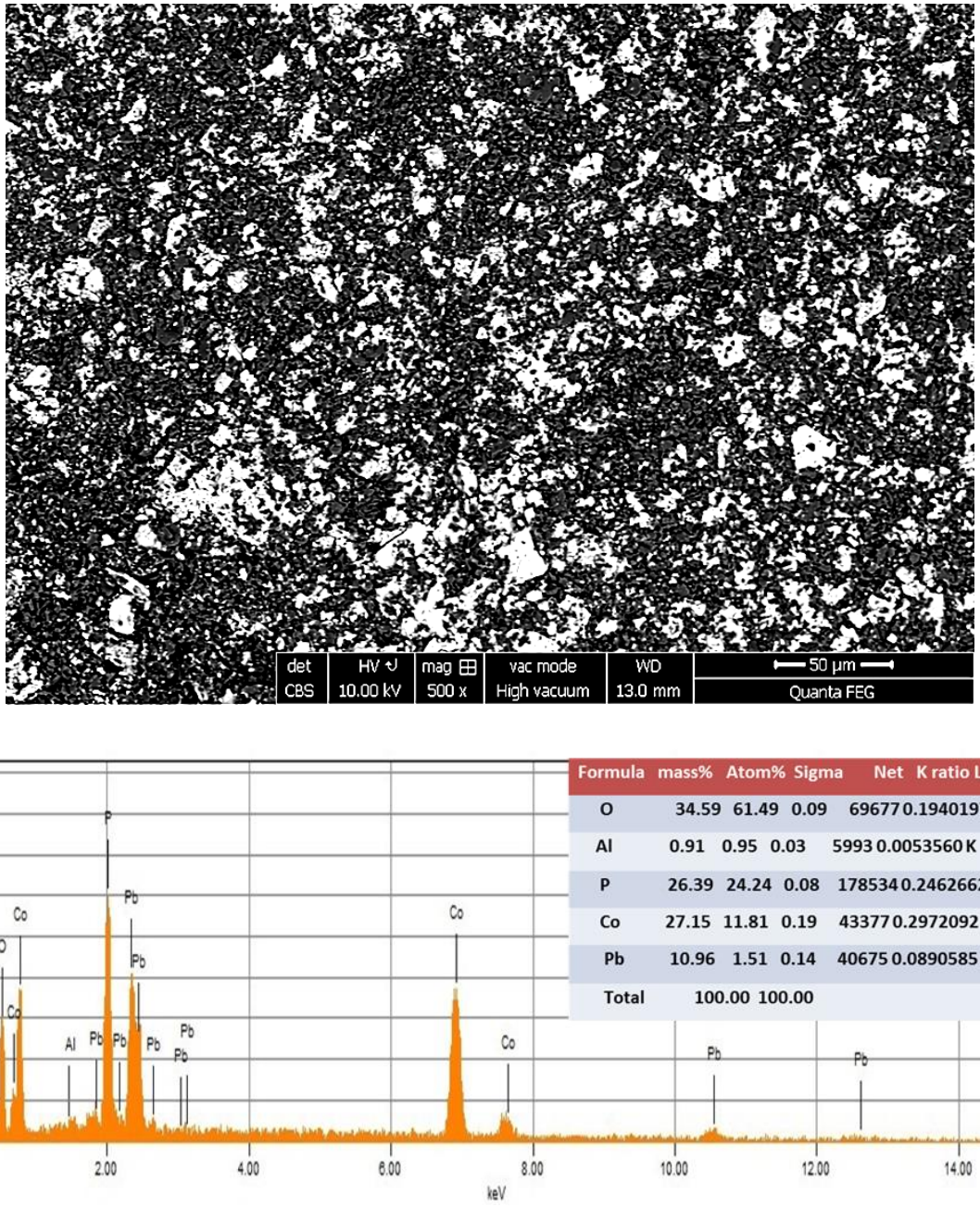

Figure IV- 6 : SEM micrograph along with EDS analysis of PbP / Co (40vol%).

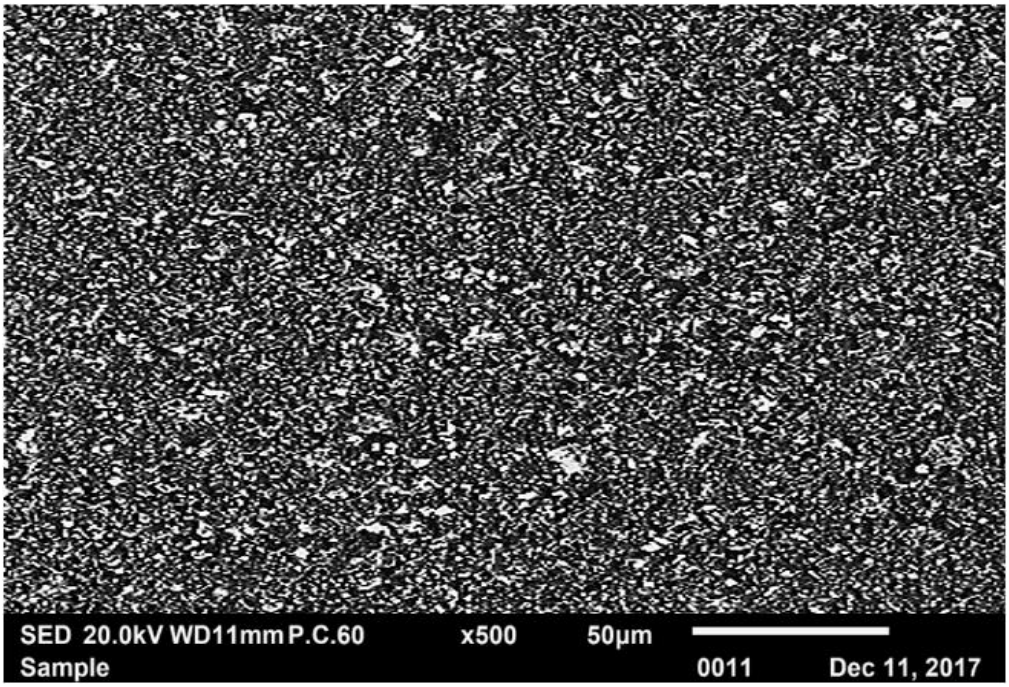

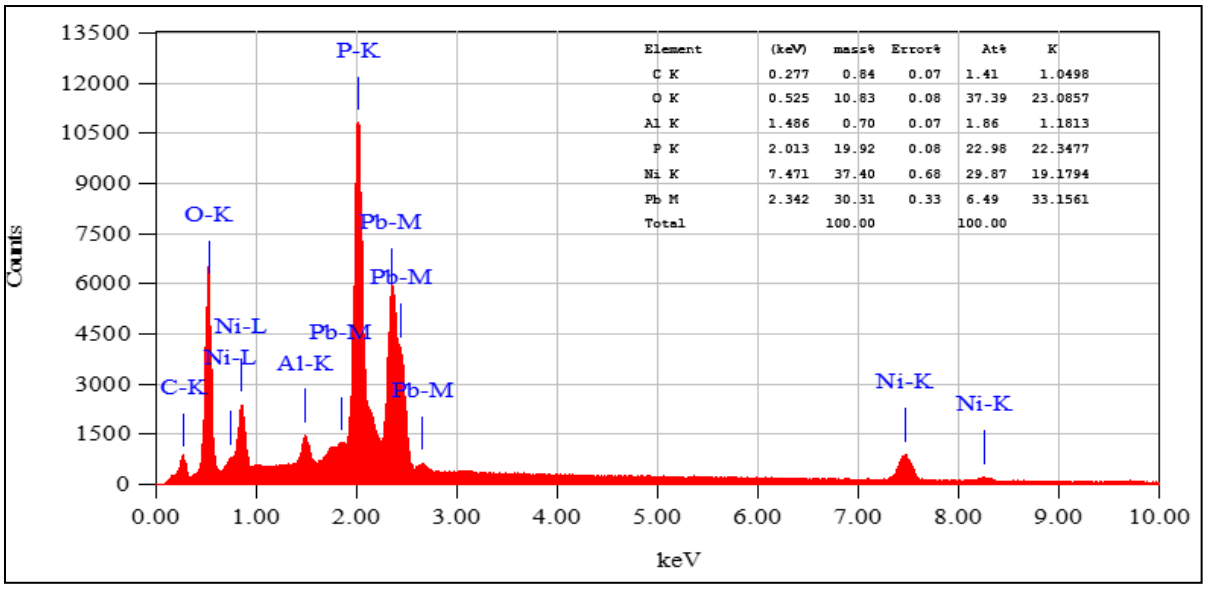

Figure IV- 7 : SEM micrograph along with EDS analysis of PbP / Ni (35vol%).

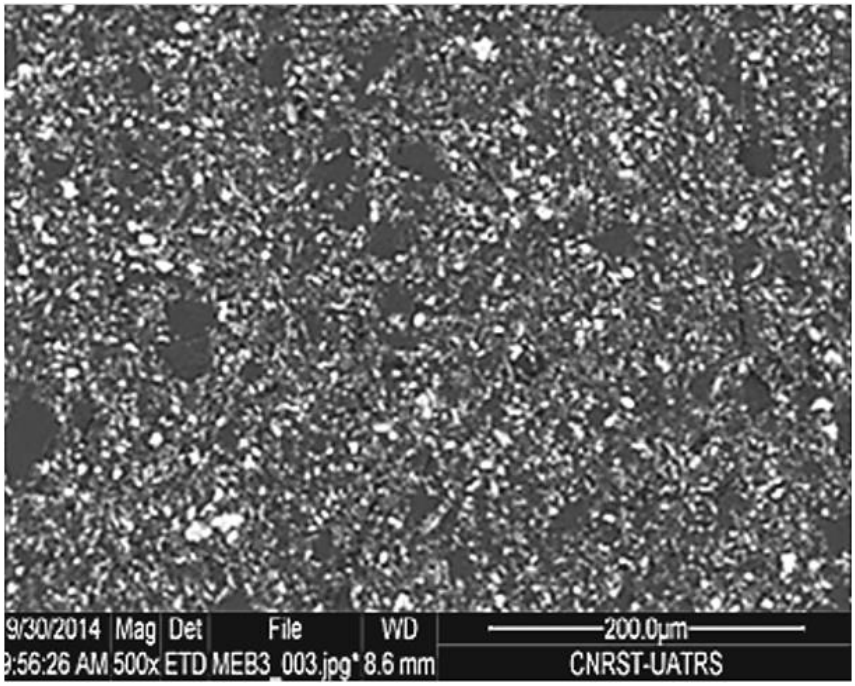

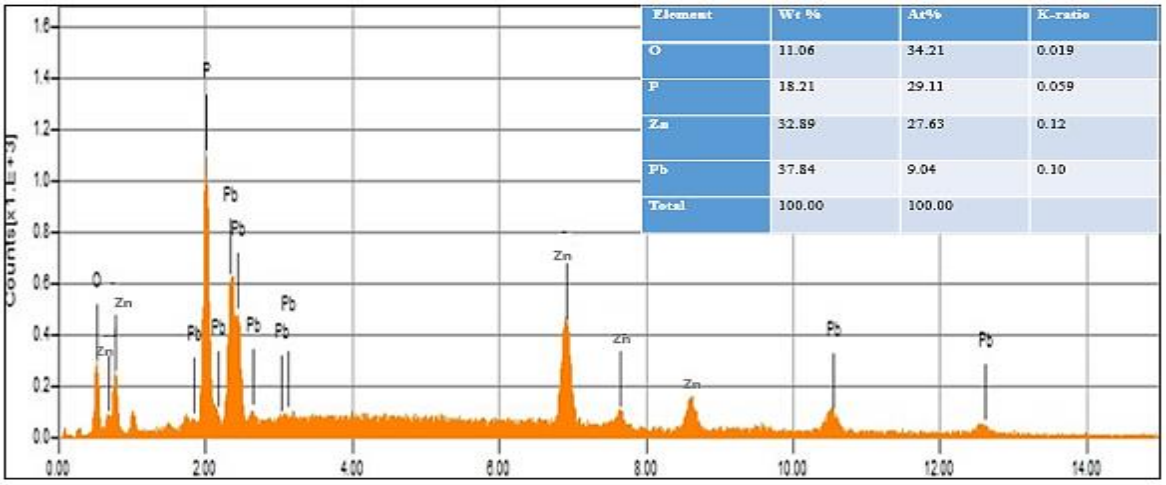

Figure IV- 8 : SEM micrograph along with EDS analysis of PbP / Zn (32vol%) composite.

The above figures exhibit micrographs of sintered composites samples. It should be noted that the EDS analysis depends on where the probe is pointed. Therefore, the percentages (weight, atomic) given do not represent an overall analysis of the sample area. Features or phases as small as 1 µm or less can be analyzed.

Note that at low inclusion rate, the particles are obviously farther apart, then at elevated fillers loading, the metallic particles are getting more and more in contact. We can see clusters of particles within the matrix. Also, continuous chains appeared inside the composite. At higher loading, the

incorporated fillers form the so-called infinite cluster, which enables conducting the electrical current.

Energy dispersive X-ray analysis (EDX) technique was employed in order to get additional information on loading concentration through EDAX signals and if there is any apparition of new phases or important impurities. Indeed, some minor intensity peaks related to impurities aredetected. The detected carbon is likely been generated from carbon tap used to fix samples on the substrate while performing SEM analysis.

Also, we note Al impurities with very small quantity. It is originated from the used alumina crucible during the glass synthesis.

Elsewhere, few porosities are also observed in some composites. Indeed, this phenomenon is inherent to heterogeneous composite materials and is in a good consistence with porosity results presented in chapter III where we have clearly explained that the decrease of porosity is achieved by filling the existing voids by fillers loading, evidenced by density measurement, which was found to be steadily increasing with loading increase.

Moreover, to test the surface roughness of our obtained composites, we have studied two samples: PbP/(Co, Cr) composites, using elemental mapping (EM) and energy dispersive X-ray spectroscopy (EDX). Thus, the result is showed in figures IV-9 an IV-10:

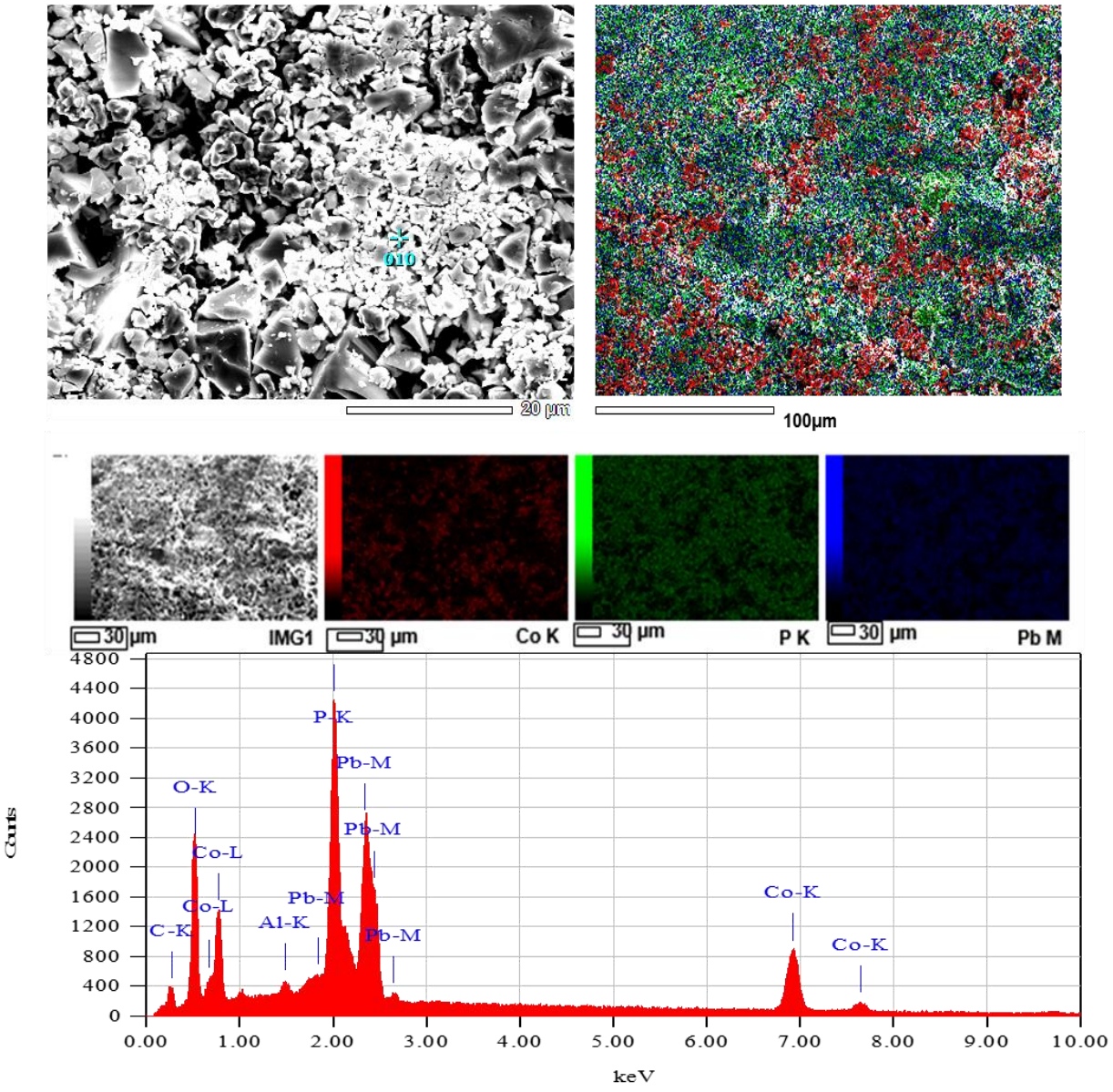

ZAF Method Standardless Quantitative Analysis

Fitting Coefficient: 0.2003

Element	(keV)	mass%	Error%	at%	Compound	mass% Cation	K
C K	0.277	4.67	0.06	15.56			1.1148
O K	0.525	14.67	0.06	36.66			17.7974
Al K	1.486	0.61	0.07	0.90			0.4871
P K	2.013	15.74	0.07	20.33			17.1264
Co K	6.924	29.13	0.48	19.77			32.4800
Pb M	2.342	35.18	0.30	6.79			30.9943
Total		100.00		100.00			

Figure IV- 9 : SEM image, corresponding elemental maps along with Energy-dispersive X-ray spectroscopy elemental mapping of PbP/ Co (20vol%) composite.

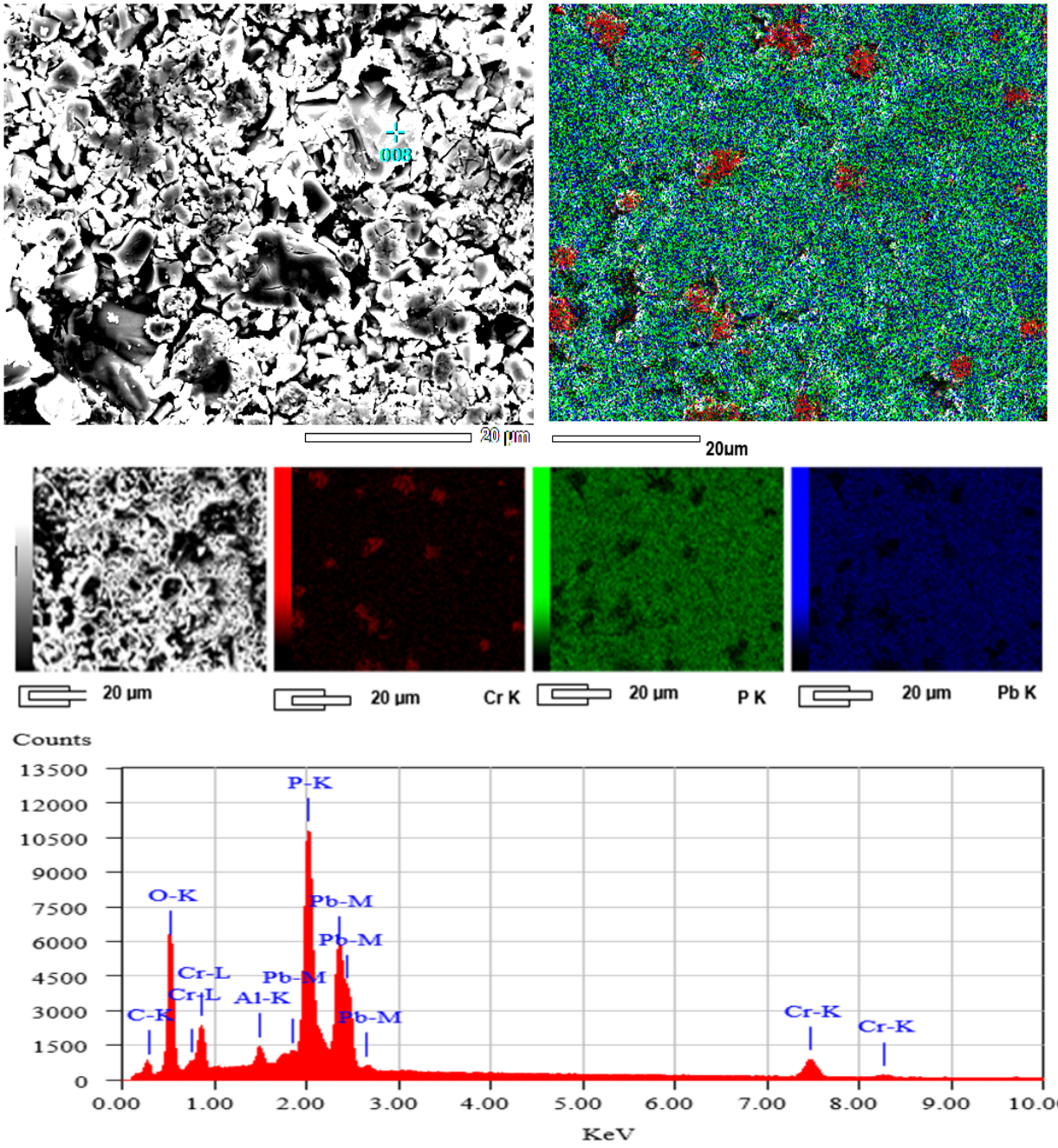

ZAF Method Standardless Quantitative Analysis
Fitting Coefficient: 0.1783

Element	(keV)	mass%	Error%	at%	Compound	mass% Cation	K
C K	0.277	4.84	0.07	14.41			1.0498
O K	0.525	19.83	0.08	44.29			23.0857
Al K	1.486	1.40	0.07	1.86			1.1813
P K	2.013	19.92	0.08	22.98			22.3477
Cr K	7.471	16.40	0.68	9.98			19.1794
Pb M	2.342	37.61	0.33	6.49			33.1561
Total		100.00		100.00			

Figure IV- 10 : SEM image, corresponding elemental maps along with Energy-dispersive X-ray spectroscopy elemental mapping of PbP/ Cr (15vol%) composite.

Elemental maps of samples indicate the presence of Cr or Co (red dots) inside PbP matrix.

Indeed, the element mapping by scanning electron microscopy and their corresponding EDX spectrum confirmed that the black areas in the studied composites are representing voids. The metallic fillers are imbedded inside the matrix by occupying partially the existing voids and their distribution is almost homogeneous. We have to recognize that the previously performed sintering process (chapter III) also contributes in closing the open porosity of the studied samples. Moreover, as displayed in both figures IV-9 and IV-10, EDS spectrum indicates traces of free-standing carbon and aluminum. They are standing for impurities; confirming the obtained results cited above.

Finally, the investigation of surface roughness by SEM mapping has clearly indicated fillers/ matrix interfaces. These latter might lead to certain fillers-matrix interactions; as showed above.

Metallic fillers play a role on reinforcement. Also, we have to extract more features about the fillers/ matrix interfaces which might influence many other intriguing physical properties of the elaborated composites. Therefore, we consider that surface energy calculations are of key importance, since they are going to open new window on the upcoming electrical and thermo-electrical properties modeling.

IV.3 Contact angles measurements, wettability and surface-interface energies determination

IV.3.1 Brief Theoretical Background

Consider a liquid droplet placed on flat, homogeneous and smooth surface of solid (Fig-IV-11):

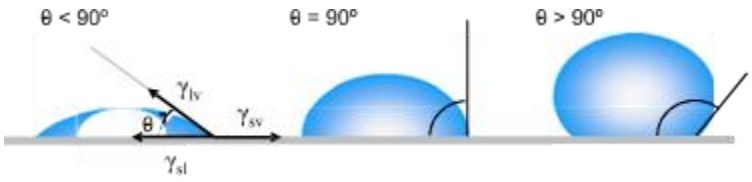

Figure IV- 11 : Contact angles formed by sessile liquid drops on a smooth homogeneous solid surface [6]226.

The angle θ formed by the intersection of the liquid-vapor interface and the liquid-solid interface is defined as contact angle. Thus, three phases, solid, liquid and vapor coexist to form "three- phase contact line" [6]226. As reviewed in chapter II, Thomas Young [227] was the first who described

the contact angle θ of a liquid drop on smooth, flat and homogeneous solid surface, defined by the mechanical equilibrium of the drop under the action of three interfacial tensions (Figure IV-11):

$$\cos(\theta) = (\gamma_{SV} - \gamma_{SL}) / \gamma_{LV} \quad \textbf{(IV-1)}$$

γ_{LV}, γ_{SV} and γ_{SL} are interfacial tensions which measure the free energy (per unit area) of liquid-vapor, solid-vapor, and solid-liquid, θ is the equilibrium contact angle.

If we consider that the measurements are taken at the saturation pressure, the Eq.(IV-1) becomes [228]:

$$\cos(\theta) = (\gamma_{S} - \gamma_{SL}) / \gamma_{L} \quad \textbf{(IV-1)'}$$

This relation clearly shows that the angle θ is determined by the ratio of the surface tensions. Thus, the shape of a liquid droplet is determined by the surface tension of the liquid.

Moreover, the Figure IV-11 shows that a small contact angle corresponds to the good wettability. If the liquid is water, the solid surface is called hydrophilic. At the limit, when this angle is zero i.e cosθ = 1, the complete wettability is obtained, showing a spread of flat liquid on solid surface. This condition gives :

$$\gamma_S = \gamma_L + \gamma_{SL} \quad \textbf{(IV-2)}$$

This relation indicates that to obtain a good wettability, the solid surface tension γ_S must be higher than that of the used liquid γ_L.

Thus, a contact angle less than 90° indicates that wetting of the surface is favorable, and the fluid will spread over a large area of the surface. However, when a large angle is measured, greater than 90°, the liquid stagnates on the solid surface forming a compact liquid droplet in order to minimize its energy and limit its contact with the solid. This means that the wetting of the surface is unfavorable. In this case, if the used fluid is water, the surface is called hydrophobic. Superhydrophobicity was obtained, with contact angle greater than 150° on lotus [229]. Almost no contact between the liquid droplet and the surface was observed. This phenomenon is known now as “lotus effect”. The term lyophilic is used for low contact angle in the case of non-water liquids, and the term lyophobic when higher contact angles are obtained.

On the other hand, after Young, Dupré [230] has established the general rule of the interaction energy between a liquid and a solid substrate, quantified by the work of adhesion W^a per unit area (A) of the liquid to the solid, which related to the characteristic surface energies γ_{ij} of the solid (S)–liquid (L)–vapour (V) system :

$$\mathbf{W^a} = \gamma_S + \gamma_L - \gamma_{SL} \quad \textbf{(IV-3)}$$

If we consider the free energy of adhesion ΔG^a , we obtain:

$$\Delta \mathbf{G^a_{SL}} = \gamma_{SL} - (\gamma_S + \gamma_L) = -\mathbf{W^a_{SL}} \quad \textbf{(IV-4)}$$

This relation means that, when two unlike phases are brought together reversibly, the free energy change per unit area is the free energy of adhesion, or the negative of the work of adhesion [231]. On the other hand, the adhesion appears as the formation of soli/liquid interface and conjointly to the disappearance of solid/vapor and liquid/vapor interfaces.Combining this expression with Young's equation leads to the following fundamental equation of wetting, known as the Young-Dupré equation [228,232]:

$$\Delta \mathbf{G^a_{sL}} = -\gamma_L(\mathbf{1} + \mathbf{cos}\theta) = -\mathbf{W^a_{sL}} \quad \textbf{(IV-5)}$$

Or :

$$\mathbf{Cos}\theta = \mathbf{W^a_{SL}} / \gamma_L - \mathbf{1} \quad \textbf{(IV-6)}$$

The relation (IV-5) allows the determination of the adhesion energy by the measurements of the contact angle. The same equation written as Eq.(IV-6) shows that the contact angle represents the balance competition between the adhesion energy (W^a_{sl}) and the cohesion energy of liquid ($W^c = 2\gamma_L$).

IV.3.2 Contact angle measurements

As noted above, the surface properties of solids are commonly investigated by the most widely used technique called a contact angle, this later is determined between a liquid and a solid surface. Contact angle often has been utilized to measure the hydrophobicity of the surface, since the wetting phenomenon is tightly related to the free energies of the liquids and solids [228,232].

Numerous techniques were carried out with the purpose to determine contact angle and liquid surface tension, such as the shape of a sessile drop, pendant drop, or captive bubble. However, several researchers studied the surface free energies using the mainly common method called sessile drop [226]. Thus, we are more interested to this method; we found it reliable and costless to investigate the wettability of the composites' surfaces and calculate the surface and interface energies.

The measurements of contact angle were undertaken at ambient temperature through placement of a liquid droplet with a syringe on the compacted composites discs of the four series containing metallic fillers with low, medium and high incorporation levels (in volume fraction). As to avoid

the gravity effect; the droplet size of the liquid was about 3 µL. The discs of samples were polished and cleaned in order to obtain a flat, homogeneous and smooth surface.

The wettability, surface energy and interface matrix-filler energy of our elaborated composites have been determined by the A. Maaroufi method [233], using the process of Owens–Wendt [234]. The image of droplet (Fig.IV-12) was taken with external CCD camera connected to the computer (see Appendix).

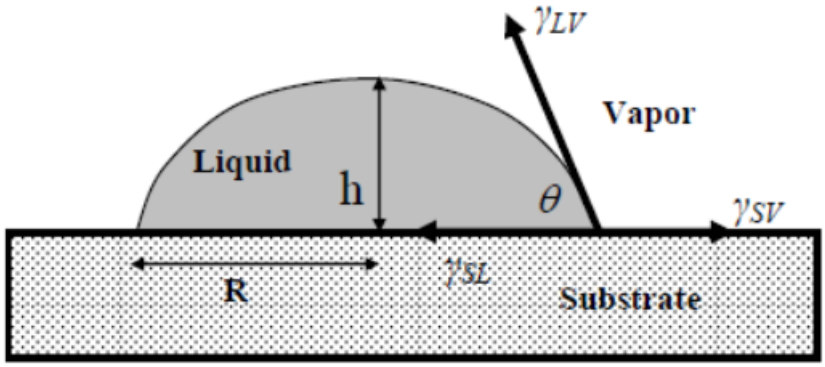

Figure IV- 12 : principle of contact angle calculation.

Then, the angle θ was calculated from the dimensions of the picture droplet, using the Analyzing Digital Images (software developed and freely distributed by STEM Education Institute, University of Massachusetts Amherst in USA) and the following relation [233]:

$$\theta = 2\,\mathrm{Arctg}(2h/d) \qquad \text{with : } \theta < 90 \qquad \textbf{(IV-7)}$$

Where h and d stand for the droplet's height and length, respectively.

For more precision, the angle θ was also directly measured through recorded image with high-resolution CCD camera of the liquid droplet profile sited on loaded lead glass matrix using screen protactor version 3.2 software of Iconico Inc., New York, NY, USA (see Appendix).

IV.3.3 Composites surface water Wettability

Firstly, it is important to signal that our investigation is limited to the static situation. The roughness, porosity and heterogeneity of the surface will be not taken in consideration [235-241]. Hence, the kinetic effects [242-244] are also not explored.

The SEM observations show that the surfaces of our samples are flat, homogeneous, smooth and non-reactive. Therefore, we suppose that is valid and we will take in account only the equilibrium state and applying the Young-Dupré equation.

Often the materials of the devices during operation are subjected to humidity due to the presence of water. For this reason, we have limited our study of wettability under the effect of water

(γL=72.8mJ/m2). Thus, micro droplets of water were placed on composite samples. The observed contact angle was determined with the methods described above. The results are given in Figure IV-13:

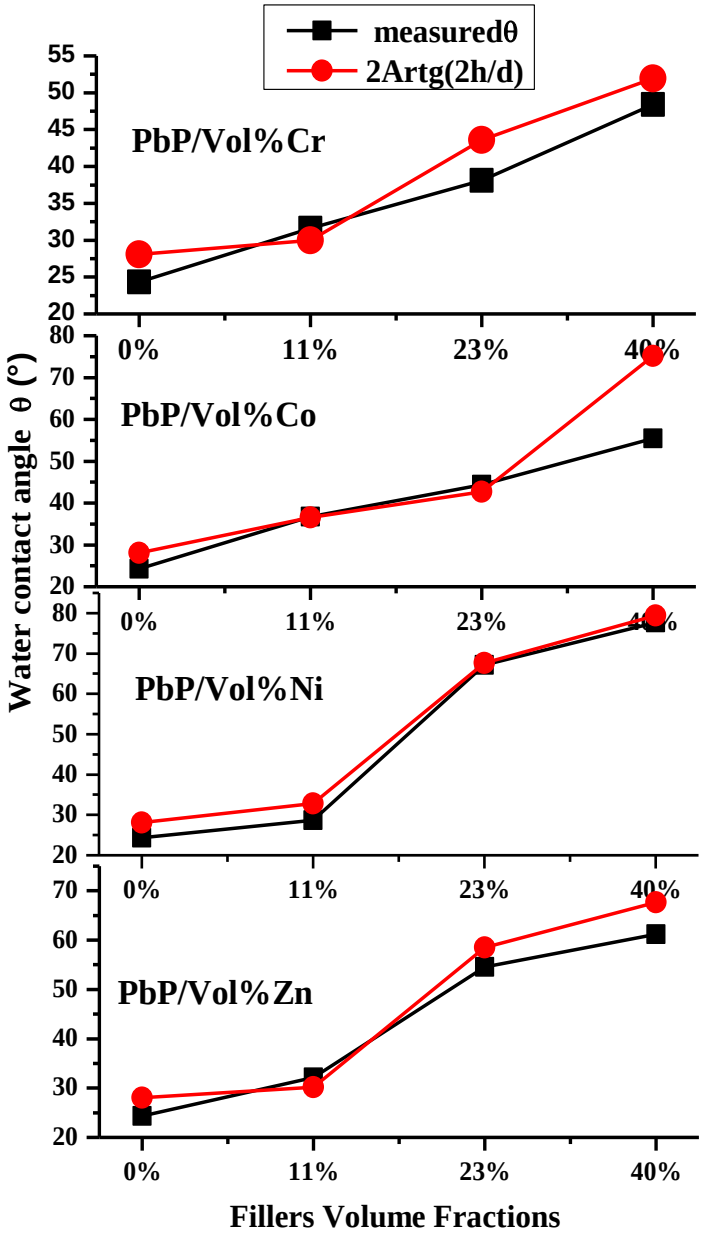

Figure IV- 13 : Evolution of Water contact angle as function of filler volume fractions (%).

The obtained water contact angle is lower than 90° for all samples. However, it exhibits an increase when the filler amount rises, showing some growth of the hydrophobicity nature. It is obvious that the moderate observed wettability decreases with filler content and the least values were observed at 40 vol%. This leads us to suggest that partial hydrophobicity is occurred at higher contact angle. Nevertheless, the measured contact angle is less than 90° for all samples, indicating that wetting

of the surface is almost favorable. The work adhesion W_{SL} was determined using the Eq.(IV-5) and given in table IV-1:

*Table IV- 1 : Contact angle and **work adhesion W_{SL}** of the studied composites.*

Sample	θ (°)	W_{SL} (mJ/m²)
Neat glass (Pb/P)	28.07	137.04
PbP/11vol%Cr	29.99	135.85
PbP/23vol%Cr	43.6	125.52
PbP/40vol%Cr	51.96	117.66
PbP/11vol%Co	36.53	131.29
PbP/27vol%Co	42.74	126.26
PbP/11vol %Co	75.19	91.41
PbP/11vol%Ni	32.87	133.95
PbP/23vol%Ni	67.64	100.46
PbP/40vol%Ni	79.38	85.90
PbP/11vol%Zn	30.21	135.71
PbP/23vol%Zn	58.49	110.84
PbP/40vol%Zn	67.64	100.49

It is clear that this energy decreases when the fillers content rises, favoring the growing of the hydrophobicity of lead phosphate/metals composites.

This phenomenon can be understood by using the Eq.(IV-6) given above, indicating that the contact angle which measures the wettability, is the balance between adhesive and cohesive energies. Indeed, the cohesive surface energy of liquid ($W^c = 2\gamma_L$) due to the van der Waals attractive intermolecular forces; dispersive (London), polar forces (Keesom, Debye), or hydrogen bonds [244] can be stronger than the force of adhesion attraction between the liquid molecules and the atoms in the solid ($W^c = 2\gamma_L > W_{SL}$) and hence the liquid will minimize contact with the solid surface and form a compact liquid droplet. Hence, the wetting of the surface is unfavorable. Elsewhere, the adhesion and cohesion energies balance expressed by the Eq.(IV-6) was also examined by De Gennes [245] in term of the surface polarizabilities (α_{ij}) ratio, originated in the attractive van der Waals interactions between the solid and liquid, as:

$$\cos\theta = \frac{2\alpha_S}{\alpha_L} - 1 \qquad \textbf{(IV-8)}$$

Where α_s and α_L are the polarizabilities of surface solid and liquid respectively.

In our case, the used fluid is water, with high surface tension of $\gamma_L = 72.8 mJ/m^2$ or cohesion energy of $W^c = 2\gamma_L = 145.6\ mJ/m^2$. The hydrogen bond of water may increase the interaction hydrogen of

water and oxygens vacancies of lead phosphate matrix favoring the wettability. Indeed, the role of oxygen vacancy on the hydrophobic behavior was observed on titanium oxide (TiO2) nanorods [26]246. Moreover, the lead phosphate glass is known as hygroscopic (likes water). This gives contact angle of $\theta \approx 28°$. The determination of the solid surface tension of the neat lead phosphate matrix (PbP) gives $\gamma_s = 53.42 mJ/m^2$. This value is somewhat high and according to the relation Eq.(IV-6) can lead to good wettability. However, when the surface of the matrix (PbP) is modified by loading with metallic fillers, the composites solid surface tension γ_s of all samples decreases continuously the (see, Table.IV-3). The forces attraction between the water molecules and the solid composite surfaces become lower than the cohesion forces of water ($\gamma_s << \gamma_L$). Hence, the surface develops hydrophobicity and the wettability decreases, as seen (Fig.IV-13). Similar results were obtained on the PMMA/ SiO2-MgO composites [247], on the polyurethane/clays nanocomposites [248] or the metallization of the polymethylpentene surface [249]. The hydrophobicity increases notably with varying the filler amount or type, modifying the surface nature.

Indeed, the modification of material surface to obtain desired wettability is actually an important industrial challenge. The wettability with water can be achieved by decreasing its tension surface (γ_L) by adding tension-active products or increasing the solid surface tension γ_s by modifying its surface with adsorption of organic polymers and surfactants [245]. On the other hand, the non-wettability or hydrophobicity can be also obtained by parallel process, controlling the chemical nature by adding various additives such as surfactants, sodium dodecyl sulphate (SDS), for example [245], coating process [250,251], or physically by controlling the roughness [252,255] of the solid surface ($\gamma_s << \gamma_L$). Such processes are very used to hydrophobic or superhydrophobic surfaces in high-tech applications, as photovoltaics requiring self-cleaning surfaces [252,255].

In conclusion of this part, the study of the wettability by water of lead phosphate/metals composites showed that the loading of metallic fillers modifies the surface of materials. This effect has lowered their solid surface tension (γ_s), and consequently favoring the apparition of the hydrophobicity. This result is important because not only the insulator phosphate products are transformed in conducting materials but also, they become hydrophobic by loading it with metallic particles. Finally, the obtained results show a coherent behavior of the wettability by nature modification of the elaborated composite surfaces, in good agreement with SEM observations, which revelated smooth and homogeneous surfaces.

IV.3.4 Investigation of fillers-glass interaction by surface energy calculations

Fowkes [256,257] was the first to propose that the surface energy due to the van der Walls forces, in condensed macroscopic media, can be expressed into its different components, as :

$$\gamma = \gamma^{d} + \gamma^{p} + \gamma^{ind} + \gamma^{H} + \ldots \quad \textbf{(IV-9)}$$

where, the subscripts d, p, ind and H refer to dispersion (London forces), polar forces (Keesom, Debye), induction or hydrogen bonds respectively.

After, Owens and Wendt [256] have proposed to group all components of surface tensions of the right member of the Eq.(IV-9), except γd, in only polar interaction γp , as:

$$\gamma = \gamma^{d} + \gamma^{p} \quad \textbf{(IV-10)}$$

Using the equation of Girifalco and Good [38] giving the interfacial solid- liquid interaction as:

$$\gamma_{SL} = \gamma_S + \gamma_L - 2\Phi\left(\gamma_S\gamma_L\right)^{1/2} \quad \textbf{(IV-11)}$$

Where Φ takes often the value: Φ = 1

Combining the Eqs.(IV-10 and 11), Owens-Wendt[14] and Kaelble [39] obtained:

$$\gamma_{SL} = \gamma_S + \gamma_L - 2\left(\gamma_S^d\gamma_L^d\right)^{1/2} - 2\left(\gamma_S^p\gamma_L^p\right)^{1/2} \quad \textbf{(IV-12)}$$

Using the Dupré Eq.(IV-3), we obtain the work of adhesion as:

$$W_{SL}^a = 2\left(\gamma_S^d\gamma_L^d\right)^{1/2} + 2\left(\gamma_S^p\gamma_L^p\right)^{1/2} \quad \textbf{(IV-13)}$$

Combining the Eqs.(IV-4 and 13) gives :

$$W_{SL}^a = \gamma_L\left(1+\cos\theta\right) = 2\left(\gamma_S^d\gamma_L^d\right)^{1/2} + 2\left(\gamma_S^p\gamma_L^p\right)^{1/2} \quad \textbf{(IV-14)}$$

Owens-Wendt [256], Kaelble [39] and Rabel [40] have written the Eq.(IV-14) in a linear form of the type y = ax+b, as :

$$\frac{\left(1+\cos\theta\right).\gamma_L}{2\sqrt{\gamma_L^d}} = \sqrt{\gamma_S^p}.\sqrt{\frac{\gamma_L^p}{\gamma_L^d}} + \sqrt{\gamma_S^d} \quad \textbf{(IV-15)}$$

Where:

$$y = \frac{\left(1+\cos\theta\right).\gamma_L}{2\sqrt{\gamma_L^d}} \quad \textbf{(IV-16)}$$

$$x = \sqrt{\frac{\gamma_L^p}{\gamma_L^d}} \;;\; a = \sqrt{\gamma_S^p} \;;\; b = \sqrt{\gamma_S^d} \quad \textbf{(IV-17)}$$

The Eq.(IV-15) was used to determine the dispersive and polar components of γ_s by measuring the contact angle θ and plotting y=f(x). This method is well known as Owens-Wendt- Rabel -Kaelble

(WORK) method. Also, as can be seen, these measurements will allow the determination of the interfacial energies (γ_{SL}), using Eq.(IV-12) and verifying the values of adhesion work (W_{SL}) by Eq.(IV-13) of our phosphate glass/filler composites materials.

In order to determine the surface energy of composites, three liquids were used (distilled water, ethylene glycol and glycerol) whose surface tensions, polar and dispersion components are known (see Table IV-2):

Table IV- 2 : Values of the polar and dispersive surface energy of each solution.

γL	Glycol ethylen[261]	Glycerol[261]	Distilled water[234,262,263]
γ_L^p (mJ/m²)	19	26.4	51
γ_L^d (mJ/m²)	29.3	37	21.8
γ_L(mJ/m²)	48.3	63.4	72.8

The obtained results are plotted in figure (IV-14), with linear regression using Eq.(IV-15) :

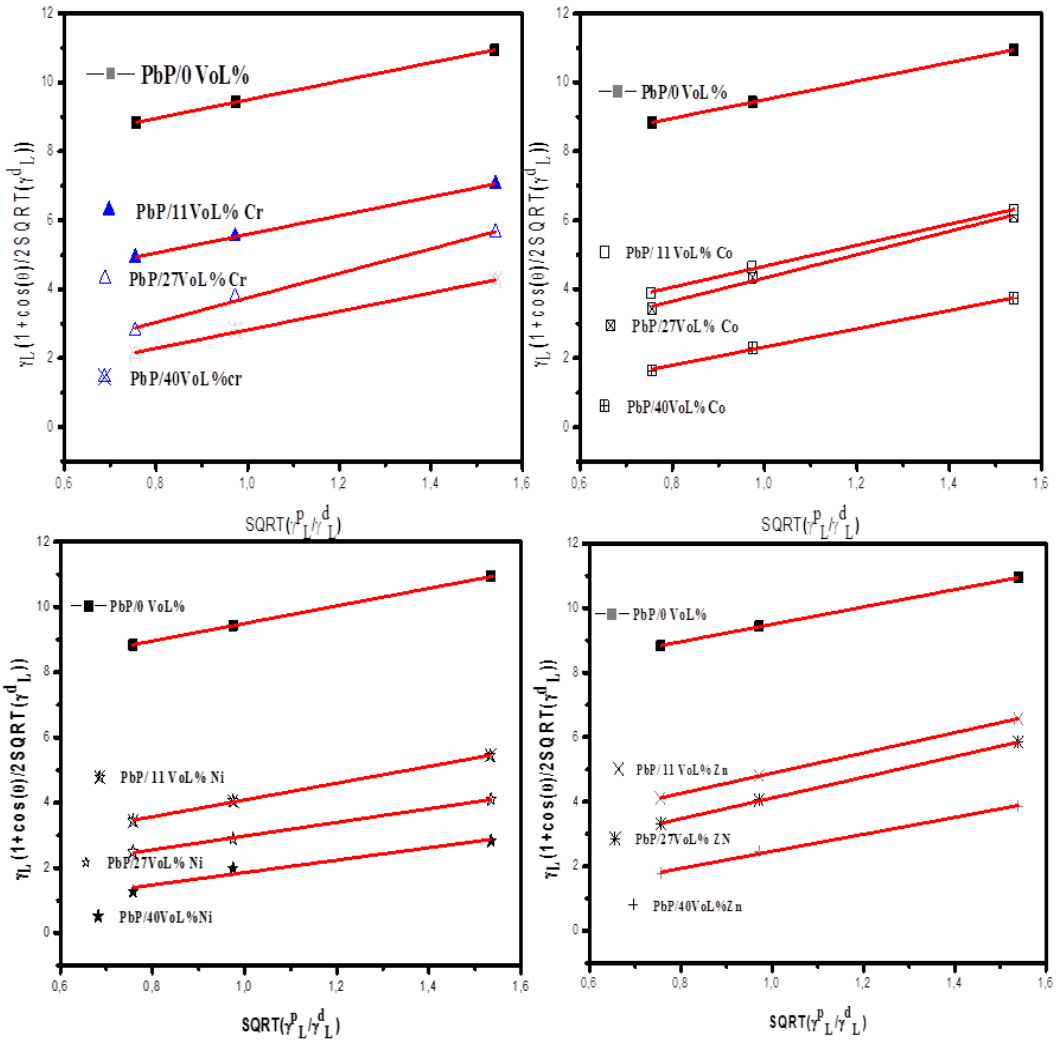

Figure IV- 14 : Regression curves of (WORK) method.

The surface energies of the PbP/(metals) composites and their components were determined versus fillers volume fraction. The extracted data are compiled in Table IV-3 :

Table IV- 3 : Values of total surface energy of different composition along with their polar and dispersive components.

Sample	γ_s^p (mJ/m²)	γ_s^d (mJ/m²)	γ_s(mJ/m²)
Neat glass ($PbO-P_2O_5$)	7.18	46.24	53.42
PbP/11vol%Co	17.81	6.92	24.7
PbP/27vol%Co	11.42	0.88	12.3
PbP/40vol%Co	7.02	0.10	7.12
PbP/11vol%Cr	19.18	13.98	33.16
PbP/27vol%Cr	24.30	0.42	24.72
PbP/40vol%Cr	13.76	0.33	14.09
PbP/11vol % Ni	18.83	7.84	26.67
PbP/27vol%Ni	10.31	0.80	11.11
PbP/40vol%Ni	6.96	0.03	6.99
PbP/11vol%Zn	12.67	6.10	18.77
PbP/27vol%Zn	4.36	0.75	5.11
PbP/40Vol%Zn	3.61	0.00	3.61

Table IV-3 gives polar and dispersive components of the surface energies, the total surface energies of the phosphate glass matrix (PbP) and its composites. The results show that the solid surface energy of the matrix (γ_s =53.42mJ/m^2) is somewhat high and the dispersive component is dominant ($\gamma_s^d >> \gamma_s^p$). This should be attributed to the cohesive energy ($W^c=2\gamma_s$) of covalent (-P-O-) and ionic (-O-Pb-) bonds inside the matrix. The polar interaction due to the ($Pb^{2+}\ldots O^-$) bond should be weak. However, the solid surface energy γ_s values evidenced a significant decrease when the glass matrix is filled with metallic powders (Fig.IV-15):

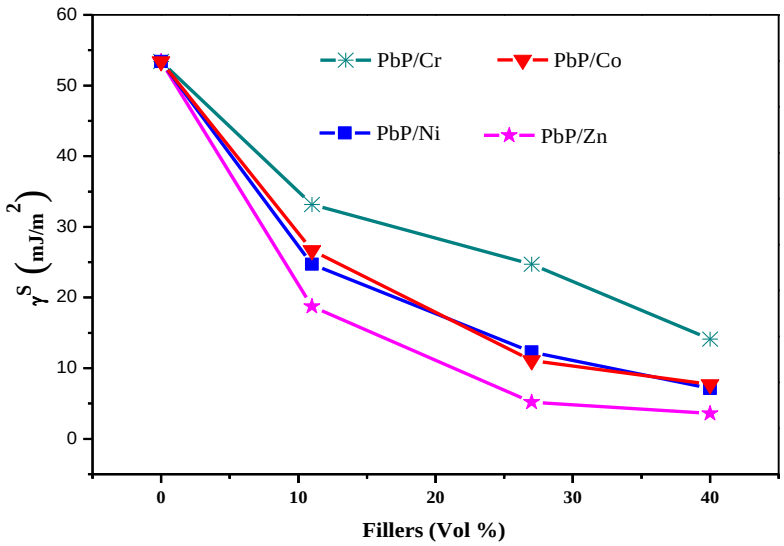

Figure IV- 15 : Evolution behavior of solid surface energy of PbP/metals composites versus fillers content.

As can be seen, the minimal solid surface tension γ_s is ascribed to 40 vol.% in each of the four type composites. Moreover, the polar contribution becomes important ($\gamma_s^p >> \gamma_s^d$) and inverse situation is observed. It seems that this phenomenon is linked to the attractive Van der Waals polar interactions between metals and the oxygen of the matrix. In order to confirm this assumption, we have undertaken the measurements on the polished filler discs. The results are given in table (IV-4). Indeed, the polar contribution is dominant in surface tension of the metallic fillers.

This effect may modify the surface composites chemical nature and increase the hydrophobicity, confirming the lowering of the wettability as found above with water. Indeed, the hydrophobicity increases continuously when the filler content loaded in glass matrix rises, indicating a lowering of γ_s. This effect can be attributed to the surface modification by fillers. Such surface change can be explained by enhanced interfacial interaction (γ_{mf}) between matrix and fillers when the fillers loading increase, in good agreement with observed behavior on SiO2-MgO/PMMA composite films [247] and polyurethane/clays nanocomposites [248].

This study shows that the inclusion of metallic fillers inside insulator phosphate glass matrix plays an important role in the chemical structure of the obtained composites. This phenomenon seems related to the attractive interfacial filler-matrix interaction which is remarkably increasing with filler contents, leading to decrease of the surface energy γ_s as indicated in curves of Figure IV- 15. As known γ_s is related to the cohesion energy ($\gamma_s = W^c /2$). Thus, the surface energy γ_s can be high for the named hard solid, formed with covalent, ionic, or metallic bonds, or low for weak crystals, like some polymers or liquids, bound by van der Waals intermolecular forces dispersive (London) or polar forces (Keesom, Debye), or by hydrogen bonds. Therefore, in our case, the metallic

loading inside lead phosphate glass matrix seems alter the structure of chemical bonds, probably more at the surface. Therefore, the study of the moisture uptake behavior of fillers/glass composites and the effect of moisture on the surface properties is very important. Indeed, Moisture is one of the important characteristic parameters of our studied composites surfaces and enable to explain the tendency of interfacial adhesion.

To verify this assumption, a single sample was taken from each set glass/ metal composites. The four selected samples were then used to determine the water uptake. They were weighed directly after the sintering process. Then they were placed in the same environmental moisture conditions. They were also weighed after different periods in a high precision balance (accuracy of 0.1 mg). The water content of the samples can be calculated by the weight difference between samples before and after water uptake, which is expressed by the equation as follows [264]:

$$M\% = \frac{Wt - Wdry}{Wdry}.100 \qquad \textbf{(IV-18)}$$

Where W_{dry} and W_t stand for the weight of the sample in anhydrous state and the weight of the sample after exposure time. The obtained results are given in table IV-4:

Table IV- 4 : Weight variation record of PbP/metal composites in the air and calculation of moisture ratio.

Samples	Weight of dry sample (g) at t=0	Exposure time	Weight after exposure in humid air (g)	Moisture content (%)
PbP/27vol%Co	1.9391	24h	1.9391	0
		Day 7	1.9401	0.001
		Day 15	1.9732	1.75
		Day 30	2.074	6.95
		Day 45	2.1191	9.28
PbP/21vol%Ni	1.9340	24h	1.9340	0
		Day 7	1.9386	0.237
		Day 15	2.002	3.5
		Day 30	2.0522	6.11
		Day 45	2.0977	8.46
PbP/23vol%Zn	0.7932	24h	0.7932	0
		Day7	0.7932	0
		Day 15	0.8350	5.26
		Day 30	0.8470	6.78
		Day 45	0.9001	13.47
PbP/19vol%Cr	2.2468	24h	2.2468	0
		Day 7	2 .2569	0.44
		Day 15	2.3144	3.008
		Day 30	2.3790	5.88
		Day 45	2.4992	11.23

The summarized results of table IV-4 show that the moisture absorption content was related to fillers percentage for a duration of up to 45 days. From the data summarized in table we presume that the water uptake increases over time. For a long period of time, changes in surface properties occurred presumably as a result of the degradation of the interface. Therefore, the composites contact angles express higher values than that of the reference sample, confirming the obtained behavior of figure IV-15. The loading of glass matrix with metallic particles decreases its surface energy γ_s and hence increases its alteration.

IV.3.5 -Interfacial interactions of (PbP) matrix –filler particles

The filler –matrix interface interaction energy γ_{mf} can be estimated by writing the Eq.(IV-12) as:

$$\gamma_{mf} = \gamma_m + \gamma_f - 2(\gamma_m^d.\gamma_f^d)^{0.5} - 2(\gamma_m^p.\gamma_f^p)^{0.5} \quad \textbf{(IV-19)}$$

Where γ_m stands for the surface energy of the host matrix and γf presents the surface energy of the filler, the superscript d and p refers to the dispersive and polar components of the surface energy. In order to calculate the interface energy between fillers and host matrix, we have measured the contact angle on polished filler discs using the same experiment and calculation methods described above to determine their surface energies, polar and dispersive components respectively. The obtained results are depicted in figure (IV-16):

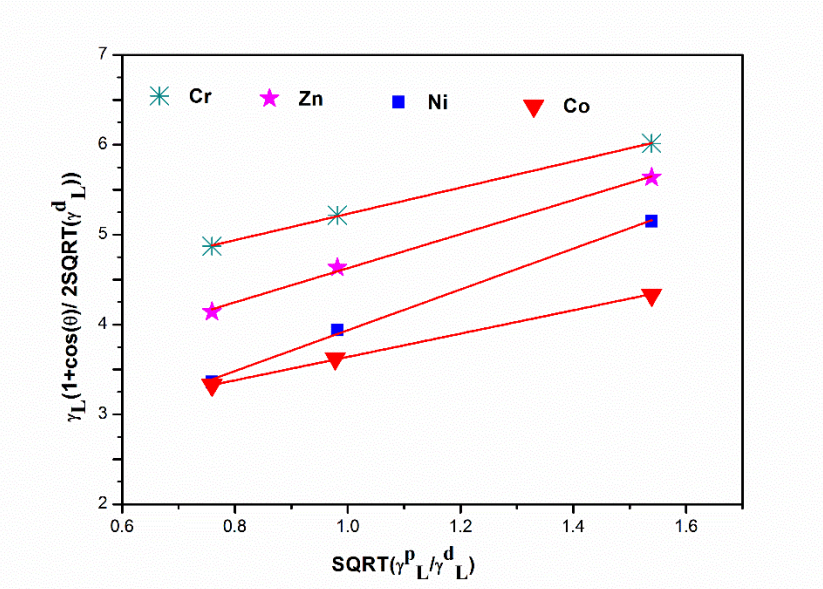

Figure IV- 16 : Owens-Wendt- Rabel -Kaelble (OWRK) method regression determining filler surfaces.

The linear fit and the calculations lead to the parameter values gathered in following table IV-5:

Table IV- 5 : The dispersive and polar components along with γ_{mf} values.

fillers	γ_s^p (mJ/m²)	γ_s^d (mJ/m²)	R^2	γ_f (mJ/m²)	γ_{mf} (mJ/m²)
Co	7	5.5	0.99	12.5	19.84
Cr	12.04	4.245	0.99	16.285	23.08
Ni	8.122	2	0.99	10.122	29.03
Zn	7.25	5	0.99	12.25	20.82

Then, the interface energy γ_{mf} between matrix and fillers was calculated through equation (IV-19) by taking into account the already calculated value of γ_m =53.42mJ/m^2 ascribed to the unloaded glass matrix (see, table IV-3). The results are given in table IV-5. It can be seen that the interface exchange energy between matrix and fillers depends on the nature of filler. It drops below the host matrix (PbP) value at room temperature, 53.42 mJ/m^2 and greater than that of the filler. This is could be probably due to the coating process of filler by the matrix. Hence, the interface is dominated by matrix contribution to the surface exchange. Conducted studies on some composites have shown quite similar findings [258,259].

Conclusion

In order to investigate the glass-fillers interactions within the elaborated composites and evaluate the quality of their surfaces, it was necessary to conduct contact angle measurements.

A good correlation between contact angle measurement and surface morphology was made since the contact angle is highly influenced by surface quality. Indeed, contact angle measurements on our composite's materials are coherent. It is costless and reliable tool of determining the surface energy. Since, surface and interface energy play an important role in the possible industrial applications. Moreover, the determined interfacial surface energy γ_{mf} will be used in the electrical conduction modeling (see, chapter V).

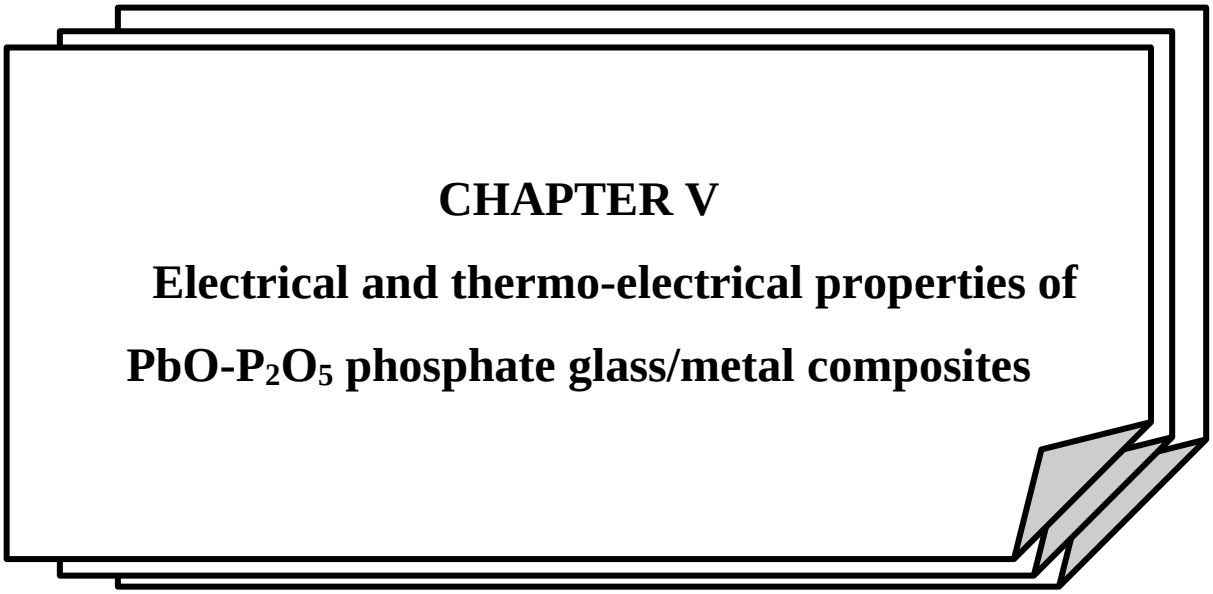

CHAPTER V

Electrical and thermo-electrical properties of $PbO-P_2O_5$ phosphate glass/metal composites

V.1 Introduction

The electrical conductivity of lead phosphate glass can be enhanced by the incorporation of metallic fillers; the resulting composites are useful in several applications. Electrical conductivity models are often established to explain and predict the conduction process within the composites. The electrical conductivity depends on the different factors. It is function of the nature of matrix and filler, the fraction content included in matrix and the temperature.

The aim of this chapter is to explore the effects of filler inside the matrix and the temperature on the electrical conductivity of the elaborated composites. Different theoretical approaches reviewed in chapter II will be applied to understand the several conducting behaviors.

V.2 Electrical conductivity as function of filler content and modeling analysis

V.2.1 Method of measurement

The electrical measurements were performed using sandwich method as described elsewhere [1]265. In order to decrease the contact resistance, the sample surface was coated with silver paint and dried during 24h. Then, the electrical resistance lower than 103 ohms was measured with a digital multimeter Leader model 856. However, the higher resistance was measured using a programmable megohmeter Quadtech model 1865. A constant voltage of 100 V was applied to the sample during one minute and after its resistance was measured, using a test cycle of 20s charge, 20s dwell, 20s measure, and 20s discharge. To start a new measurement, the electrodes were short-circuited for 5 min in order to remove any effect of the previous electrification (see photo of the used system in the appendix).

V.2.2 Modeling analysis of conductivity as function of filler content

Materials are generally classified as insulators, semiconductors, conductors and superconductors based on their electrical properties. A material with conductivity less than 10^{-7} S/cm is regarded as an insulator. Metals have conductivity larger than 10^{3} S/cm whereas the conductivity of a semiconductor varies from 10^{-4} to 10 S/cm depending upon the degree of fillers incorporation. Within composites, fillers describe conducting pathway where metallic particles agglomerate as clusters. The size and number of the clusters increase with increasing filler content. At some critical content, called percolation threshold or conducting threshold, the cluster becomes infinite and contributes to the composite conductivity. Several factors can influence the percolation threshold, such as the nature of the loads, its form and size, the nature of the matrix, and the

arrangement of inclusions within the matrix or the energy of interaction at the interfaces between the fillers and the matrix [2].The composites containing metal particles are developed with the aim to obtain the highest level of conductivity and low conduction threshold. Four sets of composites (PbP/Cr, Co, Ni and Zn) are elaborated and structurally characterized as described in chapter III.Their electrical conductivity results as function of filler volume fraction ϕ are plotted in Figures V-1, V-2, V-3 and V-4, respectively.

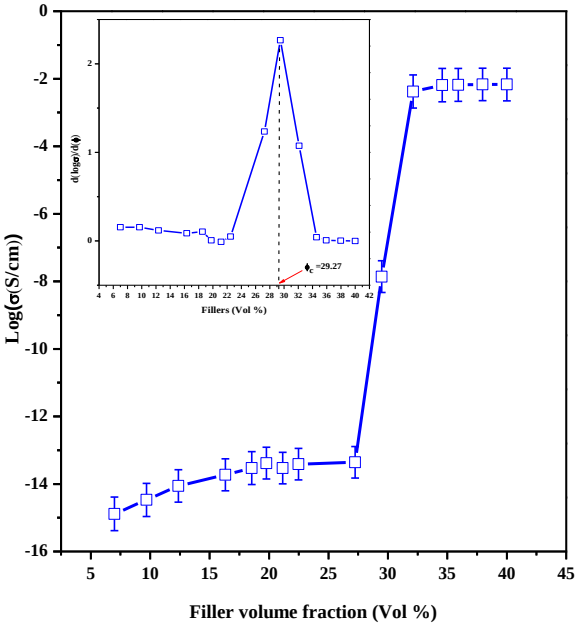

Figure V- 1 : Plot of the non linear evolution of electrical conductivity versus fillervolume fractions percent of chromium and the first derivative of log (σ) versus (Φ) of PbP/Cr composites.

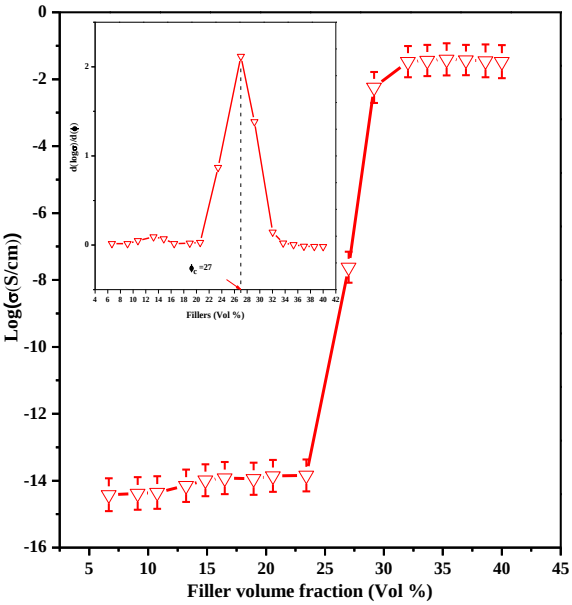

Figure V- 2 : Plot of the non linear evolution of electrical conductivity versus filler volume fractions percent of cobalt and lot of the first derivative of log (σ) versus (Φ) of PbP/Co composites.

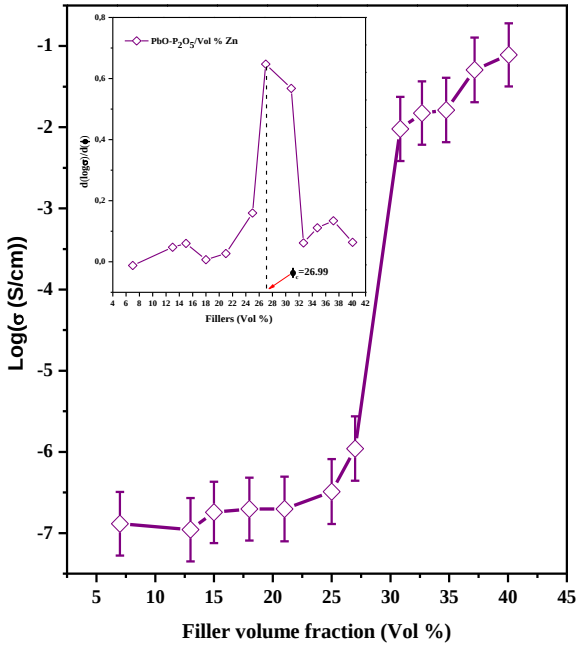

Figure V- 3 : Plot of the non linear evolution of electrical conductivity versus filler volume fractions percent of nickel and plot of the first derivative of log (σ) versus (Φ) of PbP/Ni composites.

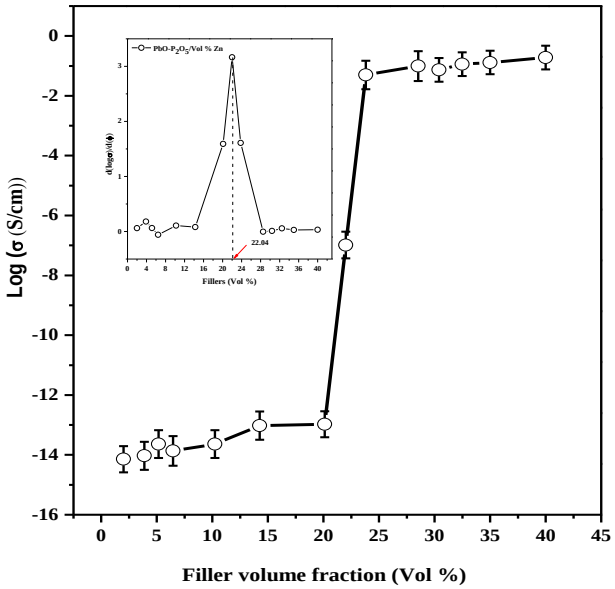

Figure V- 4 : Plot of the electrical conductivity of PbP/Zn composites versus filler volume fractions percent of zinc and plot of the first derivative of log (σ) versus (Φ) of PbP/Zn composites.

As far as one can notice, a typical behavior of the obtained composites, namely an insulating state which is assigned to the lowest concentrations for which the composite behaves as dielectric materials. Then, a very significant increase in electrical conductivity from a particular

concentration ϕ_c, called percolation threshold is observed. Above this threshold, an electrically conductive state is obtained.

It's worthy to be noted that the experimental percolation threshold was determined using the first log deriving method versus the fillers volume fraction ϕ. This method was proposed elsewhere [3]267. The maximum of this derivative as a function of ϕ gives the values of the conduction thresholds corresponding to each composite series as depicted in the same figures (from V-1to V-4). Obviously, in the case of PbP/Cr composites, percolation threshold is around 29vol %, whereas in the case of the same matrix loaded by cobalt or nickel fillers, the percolation threshold of is around 27Vol % and in the case of Zinc inclusions, the percolation threshold reached 22% only. This is in a good agreement with the above discussion, saying that the percolation threshold depends on the several specific characteristics of composite constituents such as filler's nature, size, geometry and nature of matrix, matrix-filler interface interaction and composite elaboration process [268,269].

Note that, in the present case, the composites processing was uniform for all samples and all used fillers have the same nature, considered as transition metals. Hence, it seems that the observed difference in the threshold's values could be due to the small difference in their size (chapter III). Elsewhere, it was proved that the threshold value decreases with lowering filler size [270].

In order to adjust these experimental data, the various models reviewed in chapter II will be used. Indeed, the use of accurate models aid in the understanding of the mechanisms that control the conduction in these composites. It helps us to reduce costly experiment and the risk of wasting big amount of chemical products through the ability to target a desired conductivity level for the composites based on a set of fitting percolation models. However, in this study, as noted in chapter II, we took into consideration two relevant models which in our opinion, are most significant namely, that of Kirkpatrick [271] and Mamunya [272].

Kirkpatrick model is selected because it proved the possibility to predict the percolation threshold by considering a finite regular array of points. This model is used to check if that cluster spanned the boundaries of the system. This proposed model is given by the power law equation [271] :

$$\sigma = \boldsymbol{\sigma}_0 (\phi - \phi_c)^t \qquad \textbf{(V-1)}$$

In this equation, σ is the composite conductivity, σ_0 is the filler conductivity, ϕ is the volume fraction of filler, $\phi_c$is the conducting percolation threshold and t is the critical exponent, which is mainly depending on the lattice dimension. Thus, the percolation threshold and the critical exponent are extracted from the fitting curves as illustrated in figure V-5. Their critical fitted parameter values are given in table V-1. The fit is obtained with a good correlation factor of 0.99.

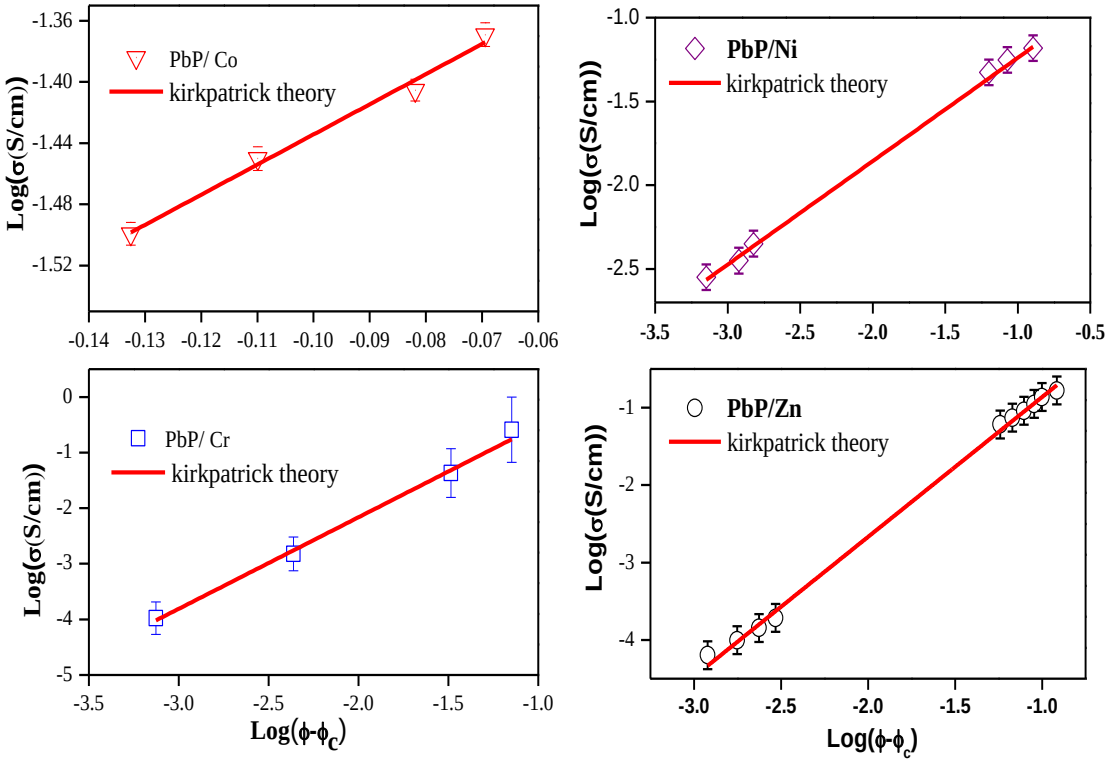

Figure V- 5 : DC experimental conductivity results and the fit obtained using Eq.(V-1), plotted as the log of the conductivity against Log (ϕ-ϕ_c).

The statistical scaling theory of Kirkpatrick is simple and do not take into account any interactions or particular nature of matrix or filler. However, some experimental data showed important discrepancies with this theory. These discrepancies are mainly ascribed to the fact that the obtained critical exponents t values are sometimes upper than the universal mean field value of 1.7-2 [269,272-277]. Therefore, several models have been proposed to clarify this situation. These models take in consideration the experimental literature data, which show the important role of matrix nature, fillers characteristics and possible mutual interface interactions. Among these models, we have chosen the one proposed by Mamunya et al. [269,272], which introduce the matrix-filler interface interactions in the Kirkpatrick basic equation. Thus, the normalized percolative model allows to the critical exponent taking values upper than 2. The mathematical expression of this model given in chapter II, is:

$$\sigma = \sigma_o + (\sigma_m - \sigma_o).\left(\frac{\phi - \phi_c}{F - \phi_c}\right)^{t_{eff}} \qquad \textbf{(V-2)}$$

Where σ is the conductivity of the composite and σ_m is its maximal value, σ_o is the filler conductivity, F is the filler packing density coefficient (equivalent to the maximal value of the filler volume fraction which can be loaded) and t_{eff} is effective critical exponent. The following relation gives it:

$$t_{eff} = t_1 + t_2 \qquad \text{(V-3)}$$

The component t_1 is equivalent to the t parameter in the basic Kirkpatrick Eq.(V-1). It is corresponding to the universal conductivity critical exponent for three –dimensional lattices in the mean field theory [276,277]. It takes a value near 2. The component t_2 is supposed to take into account the constituent characteristics of composites, matrix/ filler interface interactions and possible interparticles tunneling exchange [276,277] or anisotropy effect [281]. Thus, these effects allow to teff taking higher values and even breaking the universality of the critical exponent.

As forementioned, Kirkpatrick model ignores the characteristics of the matrices and the fillers, the composites preparation mode and any interaction between the host and the particles loaded. However, the Mamunya's approach takes in consideration the interface interaction between matrix and filler. Hence, the experimental data are also fitted with Eq.((V-2)) using a damped least-squares (DLS) method. This method is based on the Levenberg-Marquardt (LM) algorithm and is the most widely used algorithm in nonlinear least squares fitting [282]. The results are obtained with high correlation factor R^2, showing good agreement between experiment and theory. They are presented in Figure V-6:

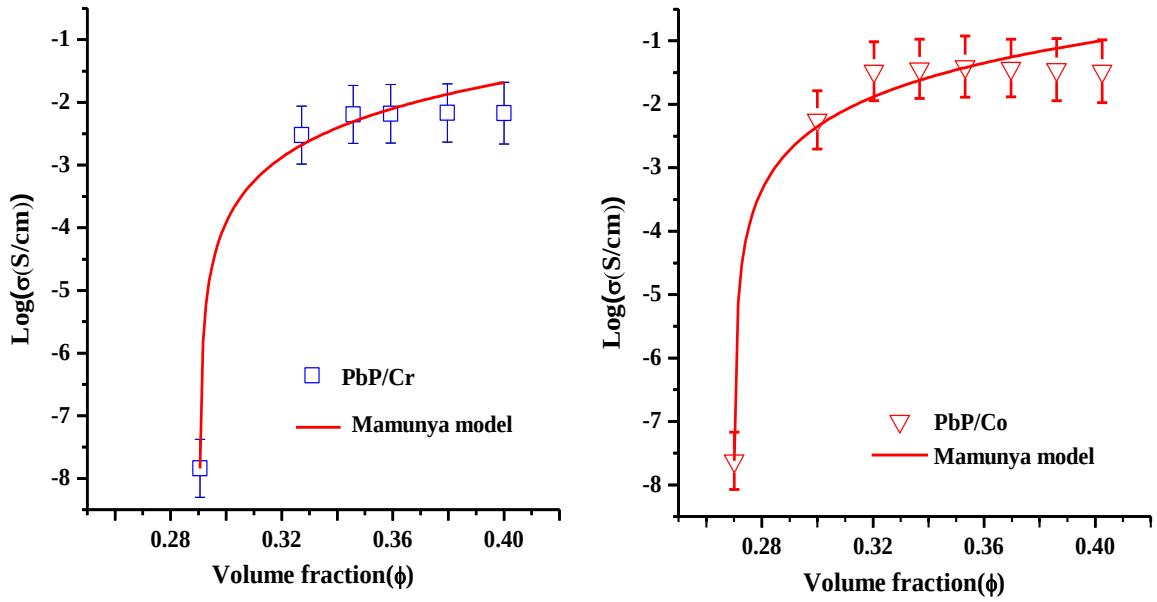

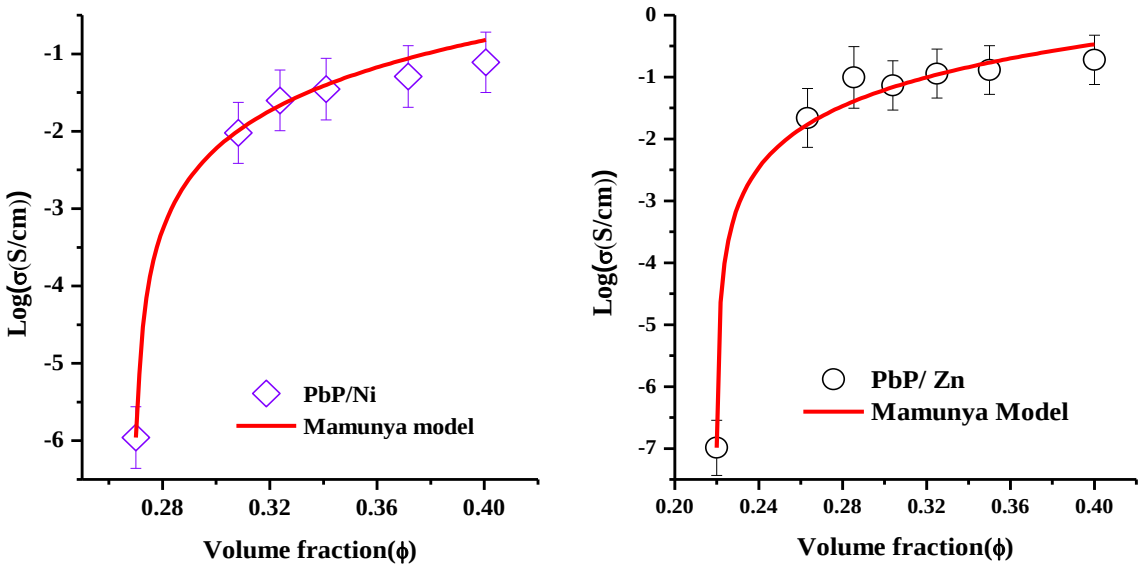

Figure V- 6 : Experimental data compared to curves generated using the conductivity model by mamunya (Eq. (V-2)).

The fit parameters such as, ϕ_c, F and t_{eff} are summarized in Table V-1:

Table V- 1 : Critical conduction threshold from experimental data and percolation models, critical exponents and curve- fitting parameters for the four series of composites extracted from equations ((V-2)) and ((V-3).

Composites	Φ_c (vol%)$_{exp}$ (±0.05)	Φ_c (vol%) Eq. (V-1) (±0.08)	Φ_c (vol%) Eq. (V-2) (±0.06)	t Eq. (V-1)	t_{eff} Eq. (V-2)	F
PbP/Cr	29.05	30	29.05	1.64	2.1	0.42
PbP/CO	27.01	27	27	1.98	2.1	0.35
PbP/Ni	27.04	27	27	1.87	2.2	0.38
PbP/Zn	22.12	21.9	22	1.92	2.09	0.36

It seems that the Mamunya model leads to some improvements, showing by obtained t_{eff} values that interfacial interaction between matrix and filler exist., However, the obtained critical parameters are almost the same. This may mean that the interactions between matrix (PbP) and fillers (Cr, Co,Ni, Zn) are weak, in good agreement with XRD, SEM morphology and FTIR analysis (chapter III) and earlier study on similar composites[278]. Moreover, the adjusted critical volume fraction values obtained with the fits in frame of the two models, Kirkpatrick and Mamunya, are in good consistence with these obtained experimentally.

The determined packing density parameter F (F≈35-42%) seems in good coherence with the prediction of Eq.(V-2) [283]. Indeed, the composites elaborated with filler rates higher than the values of F showed decays and defects. Concerning the critical exponents t and t_{eff}, the obtained values are around 2, except for PbP / Cr composite for which t = 1.6 obtained by the fit using Kirkpatrick's theory. They are slightly different from those obtained for similar composites of (ZnO-P2O5)/(Ni, Co) [265], but overall values are well compatible with the accepted value of mean field theory for three dimensional lattice. It can be also noted that almost same values of critical exponents are obtained for all composites of PbP/(Cr, Co, Ni, Zn) composites. This means that their values are independent of chemical composition of the composites, in good agreement with theoretical consideration [284,285]. Moreover, the values of t_{eff} are slightly upper than those of t, which seems to be indicating a weak interaction between matrix and fillers, in good agreement with XRD and FTIR results (see chapter 3).

Elsewhere, the electrical conductivity measurements have been revealed to be depending on several parameters [284,285], as the shape, the size, the matrix and fillers nature, their surface tension, the filler dispersion procedure inside the matrix, the anisotropy, the porosity of obtained composite, etc. In the present study, the matrix for all obtained composites is the same (PbP), all used fillers are metal transition nature and the dispersion procedure of fillers inside the matrix was maintained uniform. However, the filler's size can play an important role in disparity observed in threshold values of PbP/(Cr,Co,Ni, Zn) composites.

Indeed, cobalt and nickel powders have the same size of 149μm and their composites show the same percolation threshold of 27vol.%, but the zinc powder size is only 10-15μm, giving a small percolation threshold of 22vol.%. These results are in good agreement with earlier study showing that the percolation threshold decreases with lowering filler's powder size [281].

Elsewhere, the conductivity seems not affected by the observed porosity between 1.5 and 7% (chapter 3). Basically, it is well known that this parameter plays an important role on the conductivity behavior. It showed that this porosity has certain critical value called tap porosity, which is very dependent on particle shape, size and distribution. When this limit is reached, the effective conductivity tends to zero [286,287]. It seems that in our present investigation this limit was not reached.

The best fit is obtained by Mamunya model; this was caused by occurrence of weak fillers –matrix interaction. This interaction is worthy to be evidenced using contact angle measurements (carried out in chapter IV) which is considered as suitable tool to investigate filler-matrix interaction within the studied composites. Similar investigations have been undertaken elsewhere [287]. Indeed,

Mamunya et al. have predicted elsewhere, the conductivity by updated equation taking into account the matrix-fillers interactions, and have shown that conductivity is related to surface energies of the matrix and fillers. Thus, in this case, the electrical conductivity is given by the following equation [288,289,290] (see, chapter II):

$$\log \sigma = \log \boldsymbol{\sigma}_0 + (\log \boldsymbol{\sigma}_{\mathbf{m}} - \log \boldsymbol{\sigma}_0).\left(\frac{\phi - \phi_c}{\mathbf{F} - \phi_c}\right)^k \qquad \textbf{(V-4)}$$

$$\text{where} \quad k = \frac{\mathbf{K}\phi_c}{(\phi - \phi_c)^{\mathbf{n}}} \qquad \text{(V-5)}$$

and

$$\mathbf{K} = \mathbf{A} - \mathbf{B}\boldsymbol{\gamma}_{\mathbf{mf}} \qquad \text{(V-6)}$$

k is related to filler fractions, the percolation threshold and to the fillers /matrix interfacial tension γ_{mf} , A and B are constants.

The updated version of Mamunya model, called thermodynamic model, is expressed using Eq. (V-4) in order to predict electrical conductivity of a composite material beyond percolation threshold [27]. The parameter K in Eq. (V-6) is a function of interfacial tension between filler and matrix (γ_{mf}) which is determined in chapter IV (Table IV-5) and used here as adjustable parameter.

As indicated above, the fit with Mamunya model shows that the effective exponent t_{eff} is slightly upper than Kirkpatrick exponent t. This means that the interface fillers- matrix interaction is weak. In order to confirm this assumption, we have fitted the experimental through Eq.(V-4) using exponent *k* as given by Eq.(V-5), with γ_{mf} as adjustable parameter. We attempt to verify how the exponent *k* is corroborated to t_{eff}. The fittings of electrical conductivity are displayed in figureV-7 and the parameters derived from updated version of Mamunya model are gathered in Table V- 2.

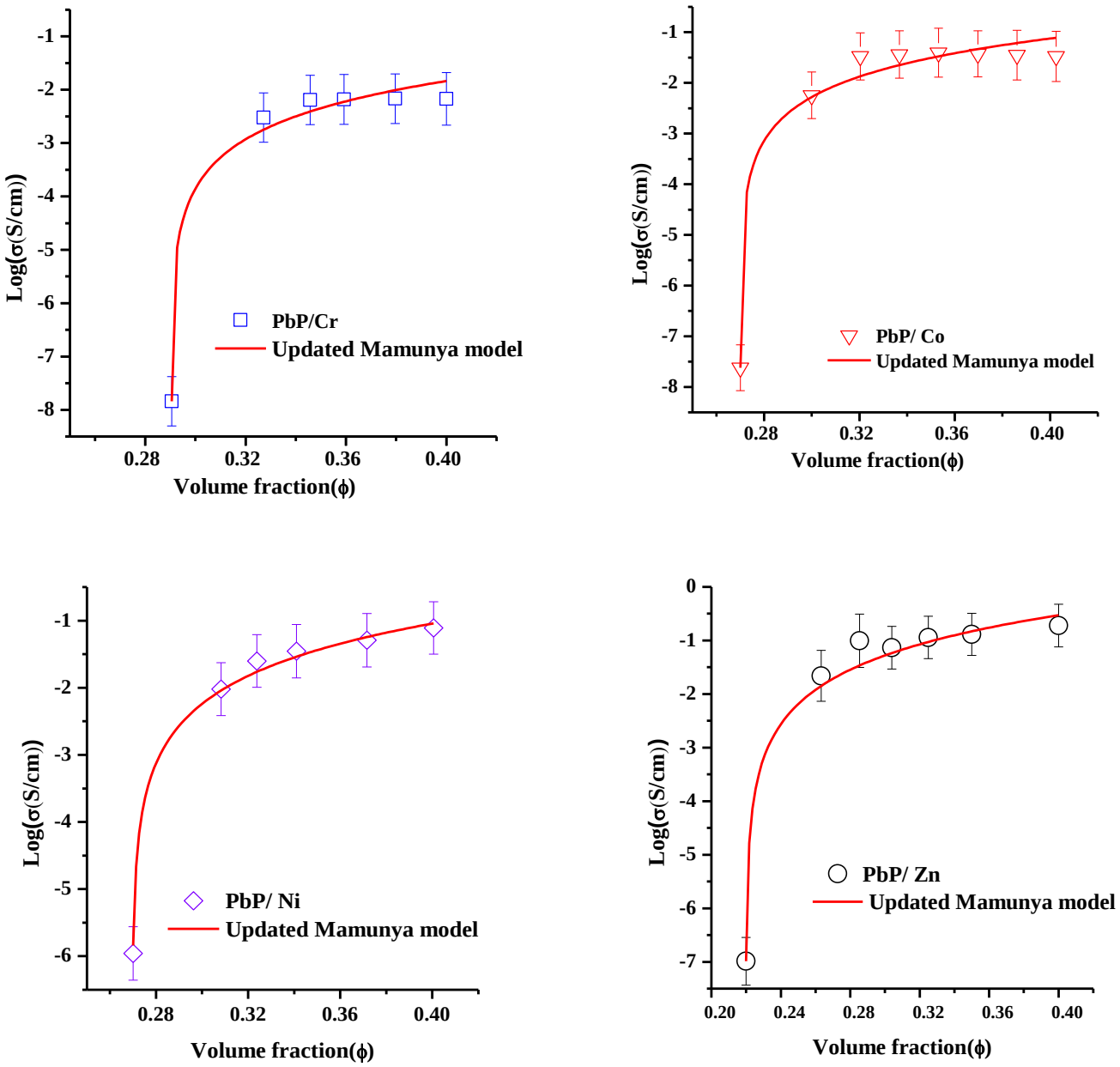

Figure V- 7 : Fit with Eq.(V-4) of the experimental data of the electrical conductivity of PbP/metals composites above the percolation threshold.

Table V- 2 : Critical exponents and curve- fitting parameters for the four series of composites extracted from udapted Mamunya equation.

Composites	K (calculated from (Eq. (V-6))	*k* (calculated from Eq. (V-5)	γ_{mf} (mJ/m²)	A	B	F	Φ_c	Correlation factor (R^2)
PbP/Cr	2.11	2.63	17	2.51	0.024	0.50	29	0.99
PbP/Co	1.97	2.45	24.36	2.48	0.02	0.46	27	0.98
PbP/Ni	1.87	2.27	26.29	2.66	0.03	0.44	27	0.99
PbP/Zn	2.07	2.19	22.28	2.55	0.02	0.35	22	0.98

The values obtained for γ_{mf}, taken as fitting parameter, are somewhat different from these found in chapter IV (Table IV-5). This difference is probably related to the used methods. The values given in chapter IV are more accurate because they are obtained from direct contact angle measurements. However, the fitting of Eq. (V-4) used 7 adjustable parameters, which can be give less accurate values (Table V-2). Moreover, comparing the parameters *k* and t_{eff} they are almost close. This means that the use of Eq. (V-2) or Eq. (V-4) is valid as approach to explain the electrical conductivity as filler content function behavior.

In order to find out how far these obtained parameters are authentic, we have plotted the curve of variation of K versus γ_{mf} and we checked if the obtained parameters A and B are close to the values obtained from the updated Mamunya fitting or no. The obtained fitting curve is illustrated in figure V-8.

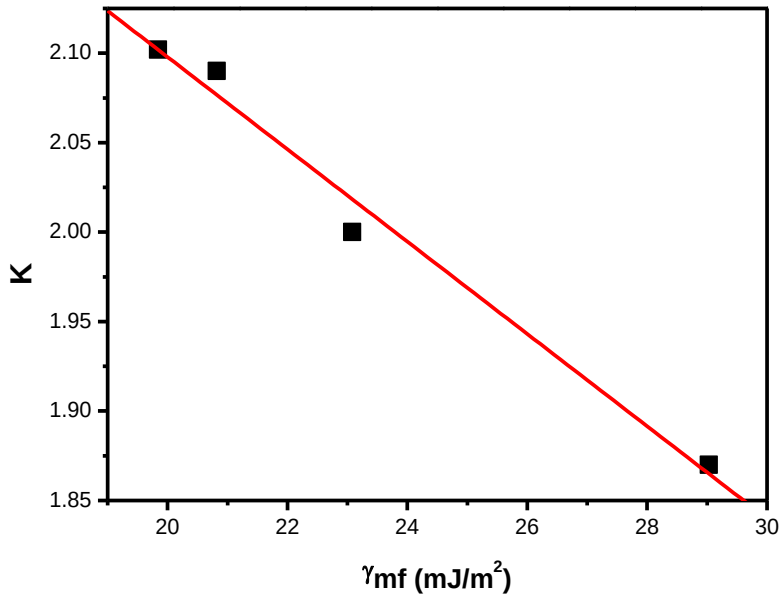

Figure V- 8: Fitting of plot of K versus γ_{mf}.

In the fitted equation $\mathbf{K = A - B\gamma_{mf}}$

B has been extracted as the slope with value of 0.026 and A is the intercept, it took the value of 2.61. We note that A and B parameters are very close to those extracted above from updated Mamunya model. Also, similar values of A and B were found by Clingerman [293,294] while studying polymers based bulk composites.

The calculated K from the new parameters (A and B), leaded to values close to the extracted values from updated Mamunya fit. This means that our fit procedure is correct and the obtained parameters are consistent.

Updated Mamunya model is able to capture the effect of surface energy on the percolation behavior [292]. It was found to be more accurate because it involves more vital factors affecting the percolation.

Note that the fitted parameters are adjustable and a good agreement was obtained for filler loadings above the percolation threshold. However, factor F, which is expressing the maximum filler concentrations, is greater than that obtained with Mamunya model for the whole experimental data.

As indicated above, the electrical conductivity of the composites depends on several parameters. Among these, the temperature plays an important role. It is important then to conduct studies in this regard by exploring the conduction behavior of composites at fixed fillers concentration and variated temperature.

V.3 Thermo-electrical conductivity

V.3.1 Conductive mechanism of glass/metallic fillers composites below the percolation threshold ($\phi \leq \phi c$)

The measurements of electrical resistance vs. filler volume fraction have been showed the occurrence of insulating or semiconducting to conducting phase transition at percolation threshold of ϕc. Indeed, the measurements of the conductivity of composites versus the temperature in the range of $300 \leq T \leq 715K$ have been revealed that its behavior in insulating phase ($\phi \leq \phi c$) and conducting state ($\phi > \phi c$) is different.The obtained data below the percolation ($\phi \leq \phi c$) of PbP/metals (Cr, Co, Ni, Zn) composites as a function of the inverse of the temperature are given on Figure V-9 . As can be seen, at least two behaviors are occurred.

The conductivity increases linearly from 300K to around 510K, then the slope changes above this temperature. Such behavior suggests several conduction mechanisms.

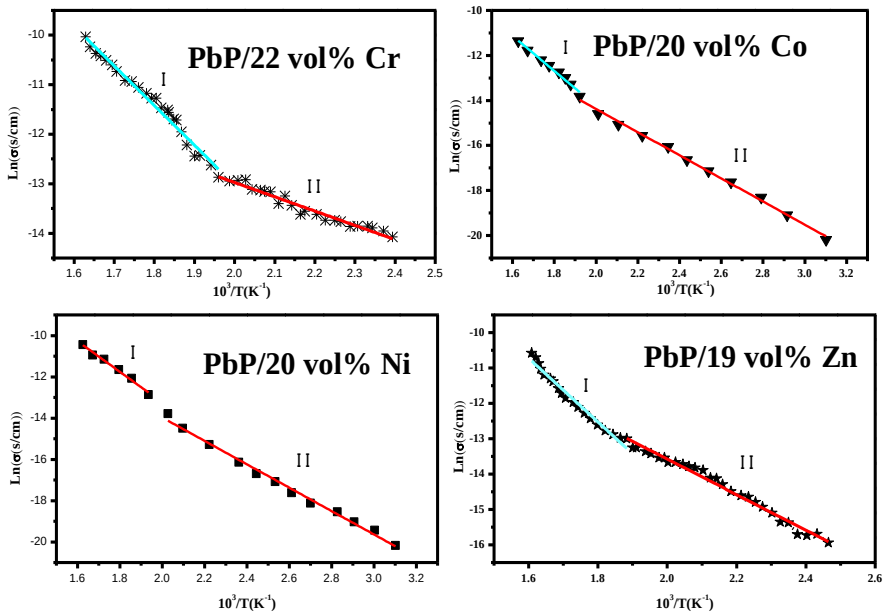

Figure V- 9 : Experimental thermal conductivity plot below the threshold with fitting by eq.(V-8) for PbO-P_2O_5 glass filled with metals.

So, to clarify if the thermo-electrical conduction behavior of lead phosphate glass filled with transition metal powders is thermally activated hopping mechanisms in localized states and in the extended states of the conduction band (see, chapter II), the data were fitted with Arrhenius law:

$$\sigma = \sigma_0 e^{\left(-\Delta E / KT\right)} \qquad \textbf{(V-8)}$$

Here ΔE is the activation energy, $\boldsymbol{\sigma_0}$is a pre-exponential factor depending on mobility of charge carriers,T is the absolute temperature, and K is the Boltzmann constant.

The shape of curves depicted in the above figure, revealed that the composite conductivity is influenced by activation energy effect, this suggests that the hopping mechanism is thermally activated, and the nearest neighborhopping mechanism is more likely governed by Arrhenius law. Then, it is possible to determine the energy gap just by determining the slope of the linear variation of ln (σ) as a function of 1/T. Slope changing temperatures exhibits at least two energy gaps. Thus, the figure V-9 shows that the linear fit of the conductivity data versus (1/T) gives two different values of activation energies (see, Table V-4).

The fits were obtained with high correlation coefficients, showing a good agreement with Arrhenius law. This confirms the thermally activated hopping mechanism of carriers between localized and delocalized states near the Fermi level in the tails of valence and conduction bands. Such results are in good coherence with values obtained in similar phosphate materials [297]. Moreover, the activation energy values corresponding to high temperature are higher than obtained

at low temperature. Indeed, the mechanism of activation is complex and depends on different parameters; like the composition of glass materials [32,33]294,295. Thus, the slight difference observed in the activated energy's values (Table V-4) seems related to different mechanisms of conduction, one at high temperature (ΔE<<KT) and one at low temperature (ΔE>>KT), depending of the contribution of localized states in tail of bands or near the Fermi-level [296]. Elsewhere, the obtained activated energy values are in the same orders of similar phosphate materials [297].

Table V- 3: Activation energies obtained by the fit with the Arrhenius ΔE_I and ΔE_{II} attributed to high and low temperature range respectively.

Composites	Slope change temperature Tc(K)	ΔE_I(eV)	ΔE_{II}(eV)	θ_D
PbP/Co	520	0.66(R^2=0.98)	0.44(R^2=0.99)	1040
PbP/Cr	510	068(R^2=0.95)	0.24(R^2=0.97)	1020
PbP/Ni	515	0.63(R^2=0.99)	0.48(R^2=0.98)	1030
PbP/Zn	526	0.77(R^2=0.98)	0.43(R^2=0.97)	1052

Moreover, the change in slope occured around 510K seems to suggest that the behavior of conductivity with temperature is more appropriate to be described by Mott's Variable Range Hopping (VRH) theory [298] at low temperature(see, chapter II).Such a mechanism very often proposed to explain the dc conductivity in disordered and amorphous materials [298] . The mechanism is based upon the idea that carriers tend to hop larger distant sites, which lie energetically closer rather than to their nearest neighbors.

Indeed, in 1968 Mott demonstrated that at low temperature, electrons perform electronic jumps between sites that are increasingly spaced but close in energetical point of view. Hence, at low temperature range, Mott's treatments of variable range hopping [298,299], leads to temperature dependence for the conductivity of the form:

$$\sigma T^{1/2} = A\exp\left(-B/T^{1/4}\right) \quad \textbf{(V-9)}$$

Whence,

$$A = \left[e^2/2(8\pi)^{1/2}\right]\nu_{ph}\left[N(E_F)/\alpha kT\right]^{1/2} \quad \text{(V-10)}$$

$$B = 2.1\left[\alpha^3/kN(E_F)\right]^{1/4} \quad \text{(V-11)}$$

'A' denotes the conductivity at infinite temperature, 'T' is absolute temperature and 'B' is the characteristic temperature of system. One can see by equation (V-11) that larger 'B' implies a stronger localization of the charge carriers, which is showed by decrease of the conductivity at low temperatures.Whereas a low 'B' implies a weak localization. 'k' is the Boltzmann constant, 'α' is the decay of the localized state wave functions (i.e. the inverse localization length of the localized wave functions), 'e' is the electron charge, 'N(EF)' is the state density at the Fermi level 'EF', and 'ν_{ph}' is optical phonon frequency.

The experimental data are fitted with Eq.(V-9) at low temperature range (300 to 520K). The results are given in Figure V-10. Thus, the linear fit of $Ln(\sigma T^{1/2})$ versus $T^{-1/4}$ obtained with high correlation factor, indicates a three-dimensional conduction process occuring in the PbP/(Cr, Co, Ni, Zn) composites below the percolation threshold and at low temperature, in good agreement with the variable range hopping mechanism [299].

The slope change temperature is revealed as a signature of conduction transition mechanisms from high temperature non-adiabatic Small Polaron Hopping (SPH) to VRH [24,40-45]. SPH-VRH shifting mechanism predicts slope change at critical temperature Tc ($Tc=\theta_D/2$; θ is Debye temperature) from the linear conductivity behavior versus inverse temperature. It's worthy to mention that the transition temperature Tc at which the SPH to VRH crossover occurs, was found from intersection of the linear fits to the low temperature and high temperature data. The solid lines in the plots refer to least-squares fits. The parameters α and N(EF) were calculated using the relations (V-10) and (V-11).The extracted parameters from fit with the Mott theory at low-temperature conductivity are gathered in Table V-5.

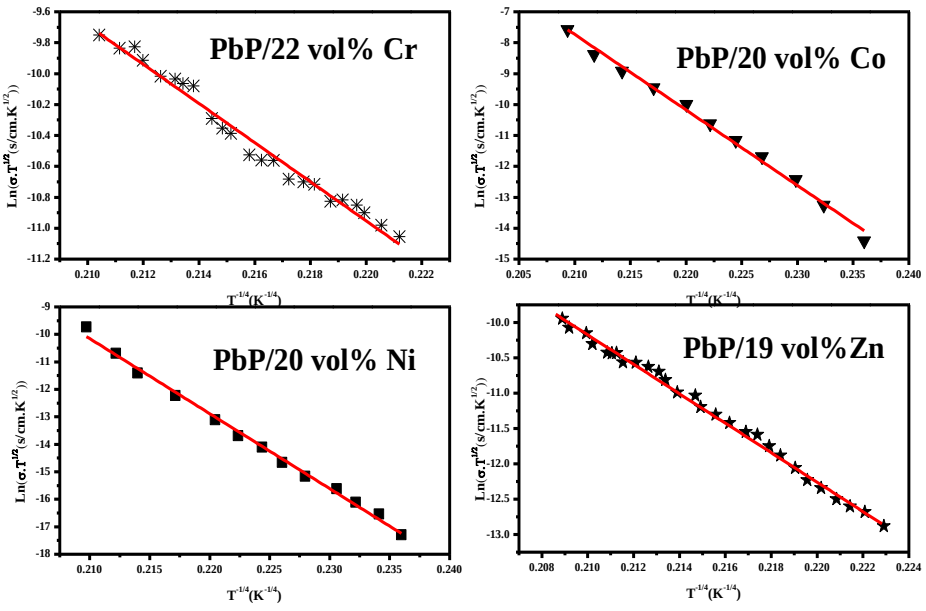

Figure V- 10 : Experimental thermal conductivity plot below the threshold with the fitting by Eq.(V-9) (continuous lines) for PbO-P_2O_5 glass filled with metals.

As reviewed in chapter II, the mean hopping distance R and hopping energy ΔE_H can be calculated from the relations [32] :

$$R = \left[\frac{9}{8\pi\alpha N(E_F)kT} \right]^{1/4} \quad \textbf{(V-12)}$$

$$\Delta E_H = 3 \Big/ \left[4\pi R^3 N(E_F) \right] \quad \textbf{(V-13)}$$

The physical parameters $\alpha, N_{(EF)}$, R and ΔE_H are calculated from the fitted parameters A and B, from the equations V-10 to V-13. They are compiled in Table V-5.

The optical phonon frequency ν_{ph} is determined by the Debye temperature 'θ_D' (Table V-4) as:

$$k\theta_D = h\nu_{ph} \quad \textbf{(V-14)}$$

Where, 'h' is the Plank's constant and $\theta_D = 2Tc$.

Taking in consideration the slope change at Tc (Table V-4). Debye temperatures may be of order $\theta_D \approx 2Tc$. Hence, from equation (V-14), the values of 'ν_{ph}' can be estimated (Table V-5), which are in good agreement with the optical phonon frequency (10^{12} -10^{13}Hz). The parameters R, ΔE_H can be determined from equations (V-12) and (V-13) , respectively (Table V-5).

Table V- 4 : Parameters of fit with the Mott theory of low-temperature conductivity of PbO-P_2O_5/(Cr, Co,Ni or Zn) composites.

Composites	A ($S.cm^{-1}K^{1/2}$)	B ($K^{1/4}$)	α (cm^{-1})	N(EF) ($eV^{-1}.cm^{-1}$)	R (cm)	ΔE_H (eV)	ν_{ph} (Hz)
PbP/22 vol%Cr	16.88	126.54	$4.49*10^9$	$7.9*10^{22}$	$1.52*10^{-8}$	0.86	$1.06*10^{13}$
PbP/20vol%Co	43.57	244.34	$4.05*10^9$	$4.28*10^{21}$	$4.63*10^{-8}$	0.56	$1.08*10^{13}$
PbP/20vol%Ni	47.16	272.93	$5.71*10^8$	$7.6*10^{19}$	$1.86*10^{-7}$	0.48	$1.07*10^{13}$
PbP/19vol%Zn	33.61	208.51	$1.68*10^8$	$5.66*10^{17}$	$8.33*10^{-7}$	0.73	$1.09*10^{13}$

Through examining the table V-5, we can deduce that globally, the obtained parameters values are close to that found in glass Zinc-phosphate/metals (ZnO-P_2O_5)/(Ni, Co) composites [36,37]297,298 and in other phosphate glass material [36]. However, they are slightly higher than values related to amorphous semiconductors (B $\approx 100K^{1/4}$) which have indicated a weak value of

'N(EF)' and relatively strong localization states [30,39]. However, the obtained state density values remain in the same order of magnitude, just like the values of semiconducting glasses (10^{21} eV-1.cm^{-3}) [32, 33, 46].

Moreover, according to Mott's theory [34], at low temperatures, the hopping energy of the Polarons becomes smaller than the energy of the 'W_D' disorder; which can at least be approximately equal to ΔE_H ($W_D \approx \Delta E_H$) [299]. For instance, in the case of studied composites the gap energies are between 0.48 and 0.86eV (Table V-5). These disorder energy values are obviously greater thank T ($W_D >> kT$(=0.0255eV) at T=300K , which leads to $\alpha R >> 1$.This confirms that VRH conduction process is valid at low temperatures range. However, When we increase the temperature, the thermal energy exceed the gap of the composites, because the electron in valence band get enough energy to be promoted to the closest conduction band by jumping this gap and crossing the Fermi level. Thus, VRH is not valid any more in this case. The phenomenon is rather explained by small polaron hopping theory framework [294,298].

V.3.2 Conductive behavior above the percolation threshold ($\phi > \phi c$) or Positive temperature coefficient effect

V.3.2.1 Experimental results

In the literature, several conductive composite materials have found to be indicating a sharp decrease in conductivity as a function of temperature. This phenomenon is known as a semiconducting-insulating phase transition, it is called Positive Temperature Coefficient (CTP). Frydman [299] was the first to observe this phenomenon (PTC) in 1945 in the low density polyethylene composite filled with carbon black. After this invention, numerous studies have been performed on different types of composites. Similar conducting-insulator transition has also been observed in ceramic materials such as BaTiO3 or V_2O_3 [294,298].It is observed for the first time on phosphate glasses by our group [294,298].

In this section we have shown that PTC phenomenon is expressed also by metallic fillers-glass matrix composites. The PTCphasetransition is characterized by a sharp decrease in conductivity at a certain critical temperature. Unlike the most common thermally activated behavior in which conductivity increases with temperature [300], this effect is particularly observed for higher filler content($\phi > \phi_c$).The obtained Temperature dependence of electrical conductivity behaviors of the studied composites are depicted in figureV-11:

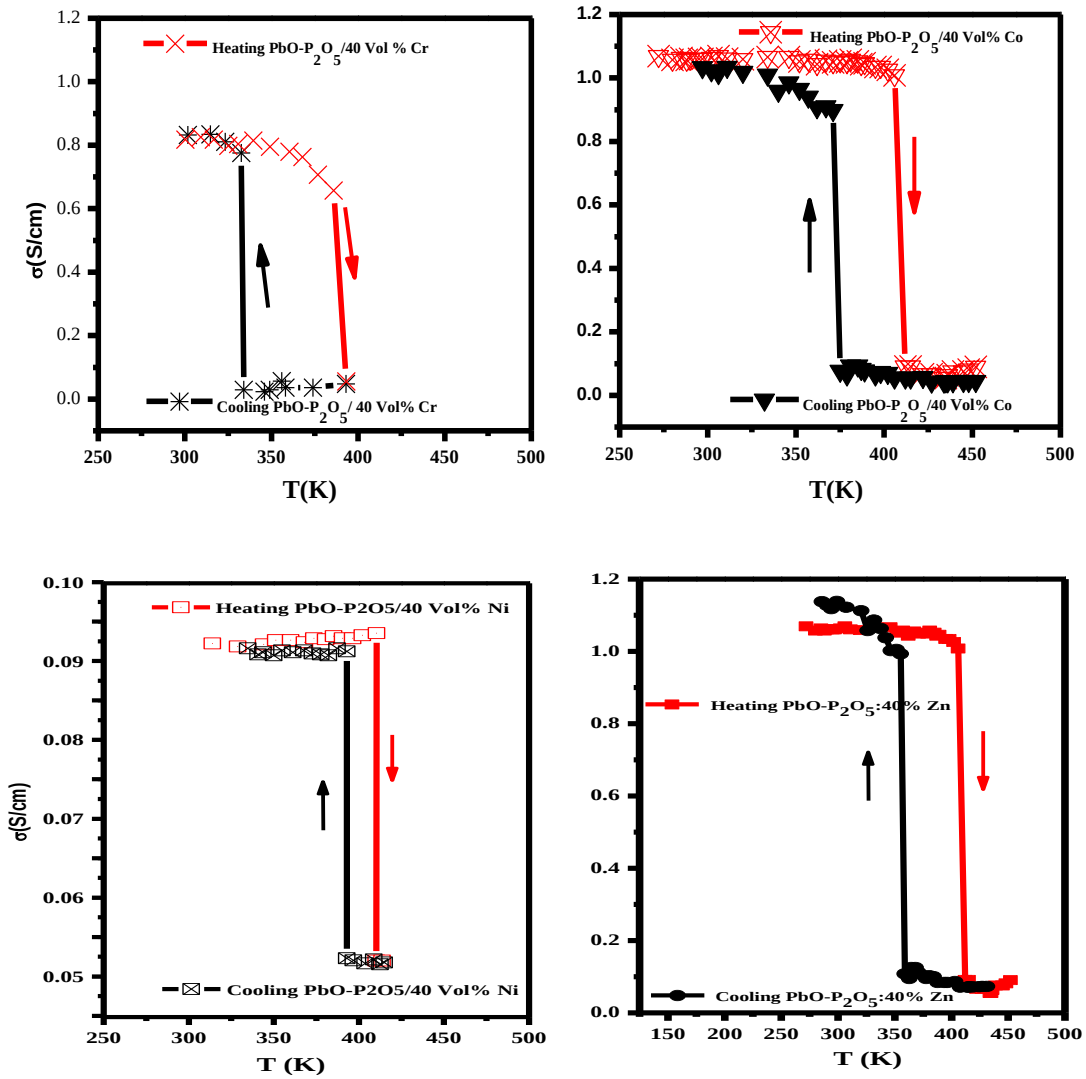

Figure V- 11 : Temperature dependence of electrical conductivity of PbO-P_2O_5/ conducting fillers composites above percolation threshold in heating and cooling rates.

Figure V-11 shows that the conduction process of the studied composite is decreasing slowly within the low temperature range area but at higher and some accurate temperature T_{PTC}, the electrical conductivity has drastically dropped off. This behavior originated from the 'positive temperature coefficient' (PTC) effect.It is defined by the amplitude of the conductivity jump called intensity or I_{PTC}[37]. The PTC intensity is given by the following equation:

$$I_{CTP} = \log\left(\sigma_{low} / \sigma_{RT}\right) \qquad \textbf{(V-15)}$$

Where σ_{RT} is the conductivity at room temperature and $\boldsymbol{\sigma_{low}}$ is the lowest conductivity after the PTC transition. This intensity is given in Table V-6 along with the corresponding transition temperatures of the studied composites.

Table V- 5 : PTC transition temperatures and I_{CTP} intensities of the studied composites.

Composites	$T_{PTC(K)}$	I_{PTC}
PbP/40%Cr	394	1.14
PbP/40%Co	412	1. 27
PbP/40%Ni	410	1.22
PbP/40%Zn	412	1.2
ZnO-P_2O_5/Ni (40Vol.%) [36]300	412	2
ZnO-P_2O_5/Co(40Vol.%)[301]	420	1.5

After the examination of the gathered intensities of PbP/(metals) composites, we note that they are smaller than those obtained by our lab team (I_{PTC}=1.5-2) on similar phosphate glasses (ZnO-P_2O_5) filled with metals (Ni, Co) composites [300,301]. This difference is probably related to the size and nature of ZnO and PbO modifier oxides. Concerning the found I_{PTC} are in good agreement our group earlier studies [300,301]. Moreover, the intensity ascribed to relatively small fillers size such as Zinc, Chromium are slightly smaller than that of grater size. The obtained experimental data suggested that the composite loaded with the larger average filler size exhibit a larger PTC intensity [299].Note that the responsible mechanisms for the PTC effect are rather complicated. The PTC effect arise from a sudden drop of conductivity, leading to the break-up of the conducting chains, this behavior is probably due to expansion of the host matrix [301].

V.3.2.2 Explanation of PTC effect by glass matrix volume expansion

The PTC effect is observed for the first time, in this kind of phosphate –glass materials. Its origin is related to different parameters and complex mechanisms, among them we state:

Electronic conduction mechanisms based on the Heywang model [292], which allows a good explanation of the PTC effect observed in the $BaTiO_3$ material families [293]. This theory supposes a two-dimensional layer of electron traps or acceptor states, along the grain boundaries. This interface attracts the electrons of clusters, creating a potential barrier. This potential increases above the ferroelectric transition by the traps of electron along the grain boundaries. The electrical resistivity is an exponential function of this potential and consequently becomes very high, implying the PTC transition.

The thermal volume expansion, which characterizes Mott type transition, observed in vanadium compounds [294]. The volume expansion is also at the origin phase transition that was discovered in semi-crystalline or amorphous matrix of the polymer/conducting filler composites [300,302]. Indeed, above the percolation threshold, the conducting particles are connected by path-way.

Consequently, the electrical conductivity becomes high. The possible PTC transition is induced by a large volume expansion near the melting point of the semi-crystalline polymer matrix, or at glass phase transition for the amorphous polymers. The path–way is broken and the conducting particles are disconnected. Hence, the conductivity drops very quickly, showing a PTC transition. Similar phenomenon was observed on cristobalite/graphite ceramic composite [296] as well as in similar phosphate glass/metal composites (ZnO-P_2O_5/(Ni,Co)) [295,296].

It is important to note that usually the behavior of PTC transition is complex. Indeed, such transition was observed above or below the glass phase transitions (T_g) in some thermosetting polymer composites [295,296]. In this case, the PTC phase transition seems associated to the volume expansion of the matrix, inducing the decrease of internal constraints and the disconnection of conductive particles. It is well-known that the phosphate glasses are generally characterized by low glass transition temperature (T_g) and optimizing coefficient of thermal expansion (CTE) based on the change of composition. Such a phenomenon was observed in case of binary zinc phosphate glasses [303]. Therefore, in order to confirm the origin of the observed PTC transition observed in our glass matrix, we have used the data of Zerzouf et al.[304], measuring the dilatometry or relative length ($\Delta L/L_o$) of PbO-P_2O_5 binary glass. The linear expansion curve of PbO-P_2O_5 is given in figure V-12:

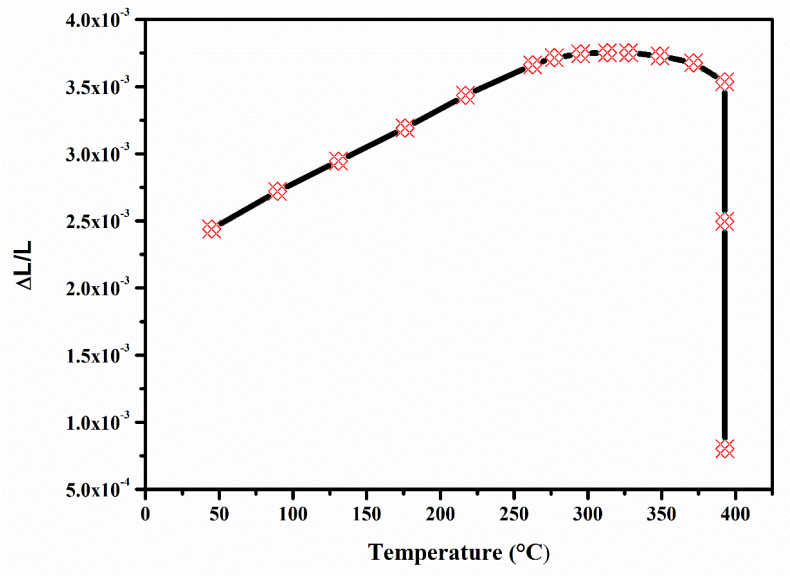

Figure V- 12 : Linear expansion curve of lead phosphate glass [304].

As can be seen on the figure V-12, the relative length ($\Delta L/L_o$) increases almost linearly with the increasing of temperature and beyond 300°C ,the curve exhibits slow increase followed by quick drop at 400°C.It is clearly showed that the PTC transition is due toexpansion of the matrix PbO-

P_2O_5, in good agreement with similar phosphate glasses/metals (ZnO-P_2O_5 and CaO-P_2O_5)/ (Co,Ni) composites investigated by our group [300,301]. Indeed, the volume expansion of the composite under the temperature effect, significantly increases the interparticle distances and decreases the conductive cluster connectivity. Hence, when the infinite conductive path is broken, the material becomes insulator. Note that, since the studied composites are amorphous. Hence, they can be considered as isotropic system and the volume expansion coefficient αv can be written as αv =3αL or simply α. The linear expansion coefficient αL can be written as :

$$\alpha_L = \frac{\Delta L}{L_0} \cdot \frac{1}{\Delta T} \qquad \textbf{(V-16)}$$

With, α_L is the length expansion coefficient or linear expansion coefficient, $\Delta L = L - L_0$, is the change of the length of the sample caused by the temperature change ΔT, $\Delta T = T - T_0$, T_0 and L_0 are the initial temperature and length respectively. L is the length measured under temperature T.

Indeed, the volume expansion coefficient seems to play an important role on the PTC phase transition bydisconnecting the conducting chainsand increasing the interparticle distances. This effect has been noted, by Gul et al.[305], using equation which indicates the effect of the volume expansion coefficient of the composites on the electrical conductivity:

$$\sigma = \sigma_0 \exp\left(-\alpha T\right) \qquad \textbf{(V-17)}$$

Where σ_o is the electrical conductivity of the composite at room temperature and α is the thermal volume expansion coefficient.

As can be seen, the coefficient α has an important effect on the electrical conductivity behavior. The electrical conductivity can drop down when α takes important values, giving arise to PTC phase transition.Such behavior seems to happen in (PbO-P_2O_5)/metals composites . As already observed on the ZnO-P_2O_5 and CaO-P_2O_5/metals composites by our group [298,300,302].

Conclusion

Through this chapter, we aimed to improve the electrical conduction behavior of binary lead phosphate glass by metal powders loading .Also, we contribute to the development of theoretical models to describe the change in the electrical conductivity of lead phosphate glass-transition metal composites depending on the fillers volume fraction. Afterward, we have investigated the effect of temperature on the variation of electrical conductivity. In the light of all the obtained results, we have drawn the following concluding remarks:

- The percolative models enable to improve the estimation of the conductivity parameters within the studied composites at room temperature.

-The thermodynamic model of Mamunya seems to provide the best fit of the experimental data since it took into consideration the fillers-matrix interface interaction and surface energy.

-The temperature dependence of the electrical conductivity of the studied samples below percolation threshold have been reported in the temperature range 300-715K.It has been observed at least two different conduction mechanisms occurred.Also, the conduction mode changed from small polaron hopping(high T) to variable range hopping with the decrease in temperatures.

- The effect of temperature above the percolation threshold ($\phi > \phi c$) shows an important phase transition called Positive Temperature Coefficient (PTC). This transition was successively explained by volume expansion coefficient.

- Finally, this study shows that, this kind of materials can be used in thermoelectrically industrial applications related to energy field.

CHAPTER VI

Synthesis and Structural Characterizations of unloaded and loaded phosphate glass thin films

VI.1 Introduction

Recently, nanomaterials have received enormous attention because of their applications in several scientific fields [301, 302, 303,30 4]. The current requirements provide a general tendancy towards the miniaturization of new materials whose properties are the same as in bulk forms [5]. Thus, in the current context, extensive research has been developed for the use of nanoscale semiconductors in thin film form [306, 307]. Note that nanostructured materials, have allowed the integration of thousands of components leading to the miniaturization of devices used in numerous high tech applications such as light-emitting diodes, laser devices and photovoltaic cells [308,309,310, 311,312].

Glass thin films represent an important class of materials. They have been extensively used in fields as varied as optics, mechanics, electronics, etc [313]. They served as reflective layers in the manufacture of mirrors, anti-reflective layers, in glassware, as abrasive or protective layers or as conductive layers in electrical devices.

In the middle of the 20th century, the development of electronics unveiled new horizons and brought a major interest to the thin film technology [314]. Nowadays, semiconducting thin films have revolutionized microelectronics; they have spurred much interest to this field [315, 316]. That is to say that, miniaturized semiconductor is currently a key material in many fields like electronics, photonics and optoelectronics.

The renewable energies and their exploitation have given privileged place, not only in the research but also in the industry by the appearance of the first solar cells in amorphous silicon thin films .It was evidenced that these films enable the conversion of solar energy to electricity. Hence, it is challenging to develop next generation materials [317-323].

In the same study framework, many amorphous glasses were elaborated, such as chalcogenide glasses, which are considered good semiconductors [322, 323, 324-339]. Generally, the glassy materials are meant to be used as semiconducting thin films because they are isotropic [337, 340-45] and they keep simultamously good conductivity and transparency properties [346].

In this perspective, we are interested to lead phosphate glass based composites. In the best of our knowledge, no phosphate glass based thin film has been yet developed except $ZnO\text{-}P_2O_5$ glass thin films that we have prepared ourselves and characterized on structural and optical point of view[347]. Also, in our previous work, lead phosphate glass/transition metal composites in the bulk form were subjected to electrical and thermoelectrical studies [348]. They revealed exclusive properties that make them promising materials for photovoltaics as thermoelectric devices.

Furthermore, some physical properties of bulk lead phosphate glass are already studied and reported elsewhere [349].

Hence, the present chapter is focused on synthesis of lead phosphate glass by sol gel route and deals with extended structural investigations of in situ loaded lead phosphate glass thin films with metal particles forming binary systems. Also, this chapter is devoted to the corroboration of structural features with morphological studies of the studied thin films.

VI.2 Elaboration process of unloaded and loaded $PbO-P_2O_5$ glass with Ni, Cr, Co and Zn metal particles

VI.2.1 Synthesis procedure of unloaded lead phosphate glass

VI.2.1.1 Starting materials

In order to synthesize binary phosphate glass $PbO-P_2O_5$ in thin film form by sol-gel process, the following chemical products have been used as starting materials : lead nitrate ($Pb(NO_3)_2$) as a source precursor of lead oxide (PbO), $NH_4H_2PO_4$ as reagent which allows obtaining peroxide (P_2O_5) and diethanolamine (DEA) which is generally used for synthesis as a stabilizer. This later has an important role on maintaining the particles within the solution and avoid precipitation. The ethanol is largely utilized as a solvent because it provides many advantages such as the facility of drying and it enables the integrity of the final material. The above-mentioned chemicals are mixed in weight proportions and adequate volumes. Thus, precursors are weighed using a very sensitive balance and the preparation of solutions was considered with care to avoid the presence of undesired dust particles.

VI.2.1.2 Experimental procedure

To develop thin films of lead phosphate glass we first started with the colloidal method, a bibliographic research guided our choice of optimal conditions of sol gel based thin films development. Therefore, in the early first step we proceeded the variation of weight ratios of precursors namely $NH_4H_2PO_4$ and $Pb(NO_3)_2$ to check the forming ability of unloaded lead phosphate glass. After ageing process, the very stable composition of the gel was found to be 44wt%$NH_4H_2PO_4$-56wt%PbO.Thin films of the selected composition were prepared by sol-gel method which is considered as the most widely used technique [350,351,352]. The obtained gel was aged then deposited onto silica glass substrates.

Since, sol-gel films contain an important amount of solvent and precursor species, solvent traces are removed by drying process. In addition, subsequent thermal treatment was carried out in order to ensure densification of thin films and remove the remaining precursor traces. The last annealing step takes place at higher temperature, by trying several temperatures. Finally, we could set our choice on optimal annealing temperature, which can allow further investigations such as structural morphological, optical and dc conductivity measurements.

In the view of preparing the mixture having the composition 56 wt%PbO-44wt%P_2O_5, we have determined the weight proportion as follows:

$W(Pb(NO_3)_2)$=56%(PbO) * Wt*$M(Pb(NO_3)_2)$ /M(PbO) and

$W(NH_4H_2PO_4)$= 44%(P_2O_5) *Wt *$M((NH_4H_2PO_4))$/ $M(P_2O_5)$

Where Wt denotes the glass mixture weight we need to prepare.

The synthesis procedure for glass consists in adding to 4 g of $NH_4H_2PO_4$,50 ml of distilled water. The mixture was kept under vigorous magnetic stirring for 30 min at room temperature. Then, In another flask, 5 ml of DEA was mixed with 20 ml of 2-Propanol.Afterward, we have added $Pb(NO_3)_2$ and the obtained solution was stirred until getting a complete dissolution. Both solutions were mixed and vigorously stirred. The sol was kept in closed flask to avoid the contact with humidity of the environment and the ageing process was performed at ambient temperature during 48 hours.

VI.2.2 Synthesis procedure of metal particles loaded thin films

In this section, we focus our attention on composites of insulating glass matrix with the metal nanoparticles. The metal nanoparticles can be generated from suitable precursors. In situ generation of the nanoparticles is done through dissolution of the appropriate precursors and elimination of acid traces during the thermal annealing. The starting precursors for metal particles are described in Table VI-1.

Table VI- 1 : Description of the used metal particles precursors and their purity.

Source product	Purity	Derived element
Cobalt nitrate hexahydrate [$Co(NO_3)_2$,$6H_2O$]	99.99%	cobalt(II)
Zinc nitrate hexahydrate [$Zn(NO_3)_2$,$6H_2O$]	≥98%	Zinc(II)
Nickel nitrate hexahydrate [$Ni(NO_3)_2$,$6H_2O$]	99.99%	Nickel(II)
Chromium nitrate nanohydrate [CrN_3O_9,$9H_2O$]	99%	Chromium(III or II)

It is worthy to mention that such route is especially useful to achieve homogeneous distribution of metal nanoparticles within a solid film. Therefore, this in situ method has become very popular, because it is easy to implement and mainly give arise to homogeneous thin films.

VI.2.3 Experimental procedure

The experimental procedure for the synthesis of metal-glass composites was performed using metal precursors mentioned in Table VI-1, diethanolamine as stabilizer and ethanol as solvent.
Firstly, we fix the quantity of DEA to be used, forming molar ratio of 1 with nitrates precursors. DEA was diluted in 10ml pure ethanol under vigorous magnetic stirring for 15 min.Then appropriate amounts of metal nitrates with concentration of 0.3M were added to the solution and vigorously stirred at 70°C until a clear solution was formed.
To obtain glass/ metal composites, the corresponding glass matrix in sol state was mixed with metal related sol. The mixture was sonicated for 30 min , followed by magnetic stirring under 100°C and ageing for 24hours.
After obtaining consistent gel, we have proceeded with deposition on well-cleaned and preheated silica glass substrates. We have obtained uniform films. It is worthy to mention that all the synthesized thin films were obtained under the same conditions. They were divided into 4 batches, each one is containing appropriate precursors of metal nanoparticles in weight percent ranging from 0 to 16wt% which undergo chemical and physical treatments such as dissolution and annealing processes with the aim to generate well densified glass/metal nanocomposites.

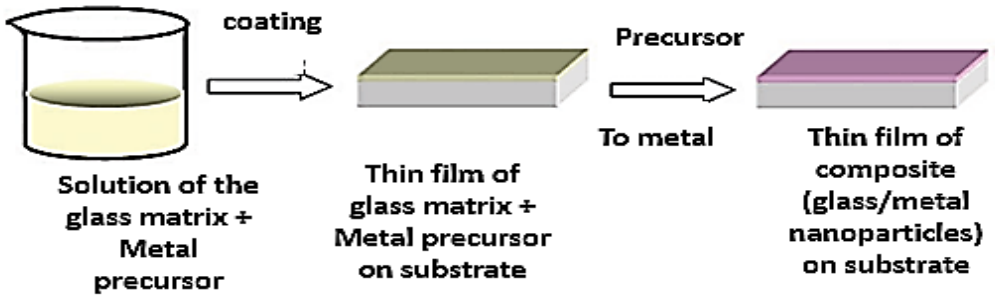

Figure VI- 1 : Schematic diagram of the employed procedures for the in situ synthesis of metal nanoparticles inside a glass matrix.

The elaboration route of glass/ metal nanoparticle composites is outlined above, it is of a good convenient. This process leads to unique application of thin films with the in situ generated metal nanoparticles in areas such as nonlinear optics. The final step consist of the annealing of the film

from [353].Thus, once the different layers are deposited, we operated the heat treatment on the air at 100°C for 60 min in order to eliminate the residues of the precursors. Then the annealing was carried out at subsequent temperatures of 180, 250 and 350°C.

VI.3 Structural and morphological characterization

Unloaded and loaded glass thin films require means of characterization. In this section, we have used X-ray diffraction, IR-ATR and Raman spectroscopy to characterize the neat and loaded thin films. Through the above-mentioned methods, we can determine structural features of the elaborated thin films and follow their evolution versus temperature and fillers concentration. Also, scanning electron microscopy (SEM) along with EDS analysis were carried out with the aim to visualize the influence of annealing temperature and the metallic particles loading effect on the solid thin films morphology. All measurements took place at ambient temperature.

VI.3.1 Structural characterization by X-ray diffraction

VI.3.1.1 Influence of Heat treatment on structural properties of thin films

The heat treatment is a critical step to be optimized for obtaining appropriate microstructure of the thin films. In our work, we performed the heat treatment after the deposition of the films by heating the backside of the substrate and the crystallization were monitored by XRD analysis.

X-ray diffraction patterns were recorded over an angular range of 10 to 60 degrees in (2θ); with a step of 0.04 ° (2θ) and a counting time of 4s per step. Once the XRD patterns are recorded, the positions and intensities of the different diffraction lines are compared with those available in the database grouping the PDF2-2010 files of the ICDD (International Center for Diffraction Data), using Bruker DIFFRAC plus EVA software.

In the figure VI-2, we have superimposed XRD spectra of the neat thin films of annealed PbO-P_2O_5(PbP) phosphate glass at subsequent temperatures ranging from 180°C to 350°C.

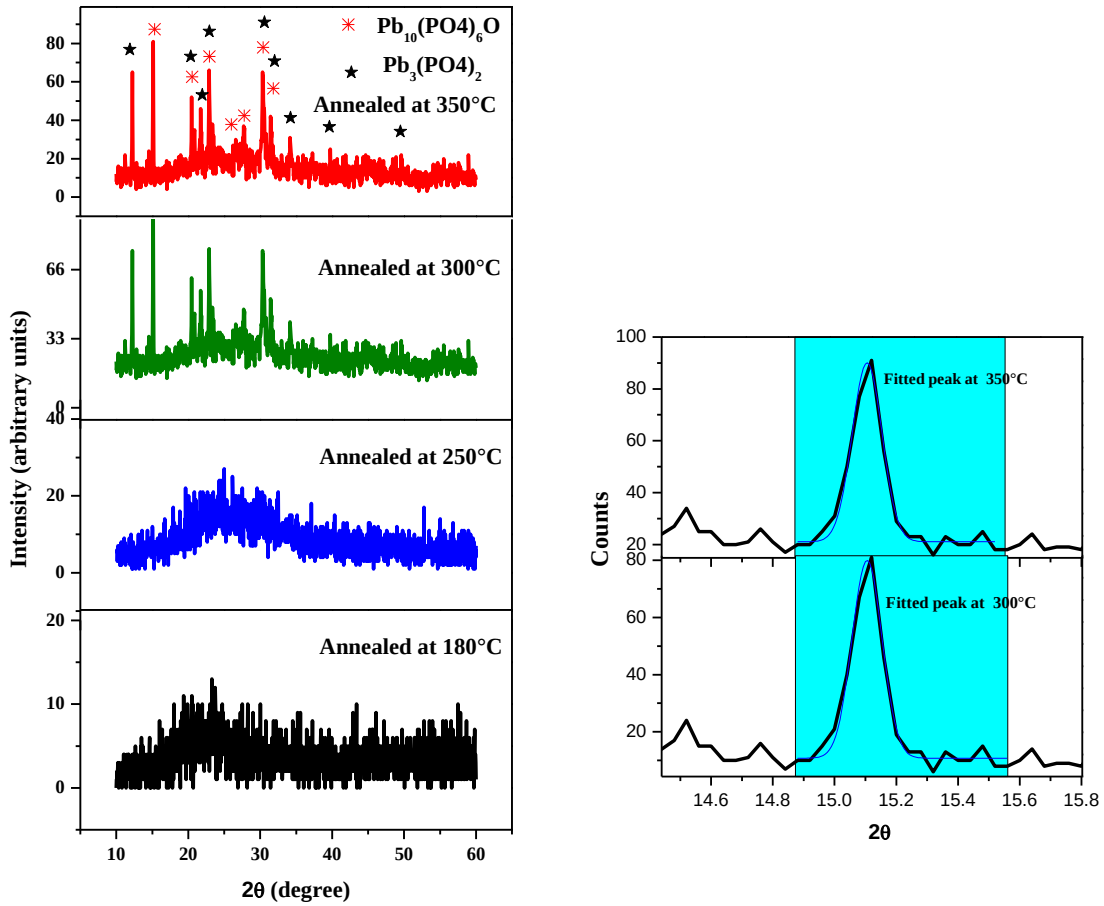

Figure VI- 2 : XRD patterns of PbP thin film and Peak fit profile of the deposited samples as function of the annealing temperature.

For annealed samples at 180 and 250°C, the X-ray patterns reveal amorphous nature since no sharp peak is observed. Such results were detected elsewhere for many other glasses [354, 355, 356]. For heat treated thin films at 300°C, we observe initial appearance of low intensity peaks towards 2θ≈15°, 20° and 30°.They are assigned to $Pb_{10}(PO_4)_6O$ and $Pb_3(PO_4)_2$.These crystalline phases were attributed using XPowder software to hexagonale and monoclinic lattices, respectively. Moreover, at elevated annealing temperature of 350°C, we observe the same peaks located at the same positions with enhanced intensities showing the same structures. We notice that the intensity of these peaks increases with annealing temperature augmentation.

This is more likely due to the increase in the size of the clusters; similar results are obtained within reported previous work [357]. Also the figure VI-2 shows the relationship between the full width at half maximum (FWHM) of diffraction peaks and clusters size with temperature increase. Indeed FWHM decreases with the annealing temperature. The crystallite size D was calculated using Scherrer's formula:

$$D = \frac{K\lambda}{\beta(2\theta).cos\theta} \qquad \textbf{(VI-1)}$$

where k is the shape factor (0.89), λ is the wavelength of $Cu_{K\alpha}$ radiation, θ is the Bragg diffraction angle and the β is the full width at half maximum (FWHM), respectively.

Scherrer equation is used for determination of crystallite size from XRD via originlab 8.5 software.We proceed by magnification of the major peak from Xray diffraction patterns , then we have extracted FHWM values using Guaussian peak which is fiting better. We have chosen the FWHM and 2θ corresponding to the main intense peak for the calculations. The crystallite size depends on the broadening of the diffracted peak and Williamson-Hall approach [358]. The average crystallite size of lead phosphate glass thin films is obtained as 13.84nm and 15.38nm for annealing temperatures of 300 and 350°C respectively. It is worth mentioning that a crystallization level tends to increase with increasing temperature. Thus, in order to avoid the problem of anisotropy while performing further investigations, we have kept the best-optimized heat treatment temperature at 250°C. It should be mentioned that, heat treatment duration is typically 10 min for different thin films.

VI.3.1.2 Metal particles loading effect on the structural properties of glass thin films

The X-ray diffraction spectra of the composite thin films along with fit profiles of the main crystalline peaks are reported in the figures VI-3, VI-4, VI-5 and VI-6, for different fillers loading ranging from 3wt% to 16wt%. It can be seen for whole recorded patterns at low loading level, the composites keep their amorphous state, but at significantly high metal particles concentration, we observe the emergence of small peaks matching to metal particles elements that are gradually embedded in the glass network structure, namely chromium, cobalt, Nickel and zinc metal particles.

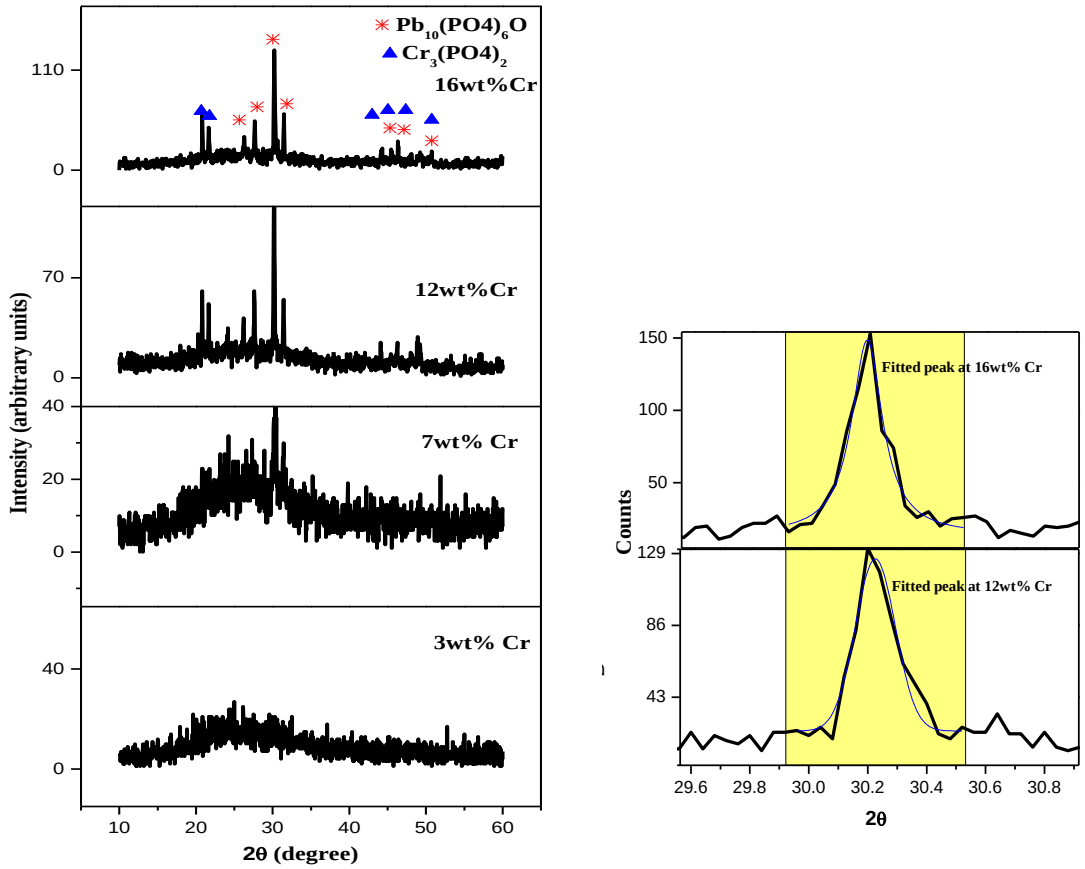

Figure VI- 3 : XRD patterns of (PbO-P_2O_5/(14 and 16wt%Cr) composite thin films and fit profile of the main crystalline peaks.

When the fillers loading is enhanced, defined peaks appeared around 20° and 30° with sustained halo indicating that there is substantial amorphous phase. The intensity of these peaks increases more and the halo disappears with increasing the fillers concentration. According to the X-Powder identifications, these peaks are attributed to at least two phases $Cr_3(PO_4)_2$ and $Pb_{10}(PO_4)_6O$ which crystallize in monoclinic and hexagonal geometries, respectively.

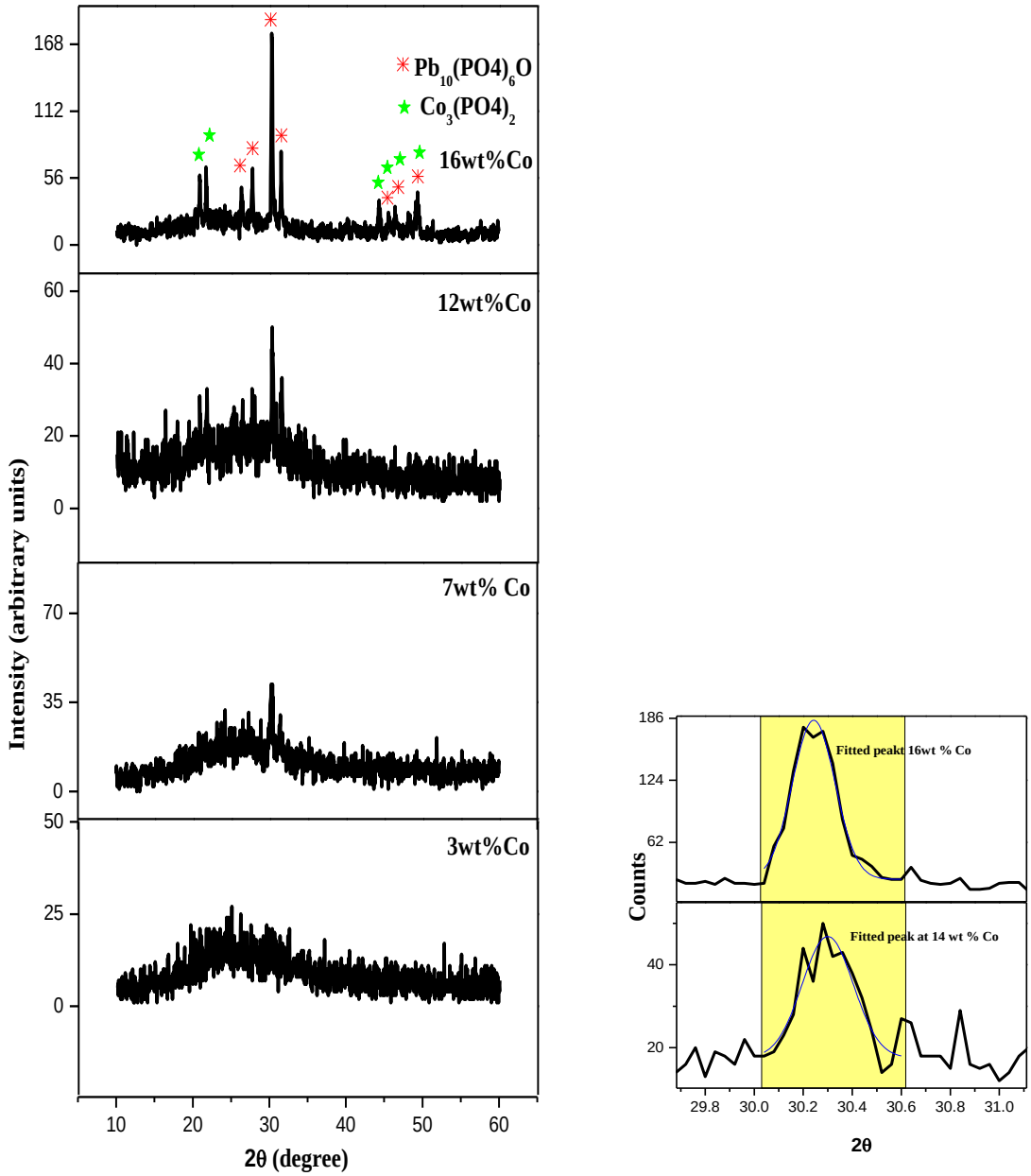

Figure VI- 4 : XRD patterns of (PbO-P_2O_5/(14 and 16 wt% Co)) composite thin films and fit profile of the main crystalline peak.

XRD patterns indicated well identified peaks at higher fillers loading. These peaks are attributed to hexagonal and monoclinic crystallized networks of $Pb_{10}(PO_4)_6O$ and $Co_3(PO_4)_2$,respectively.

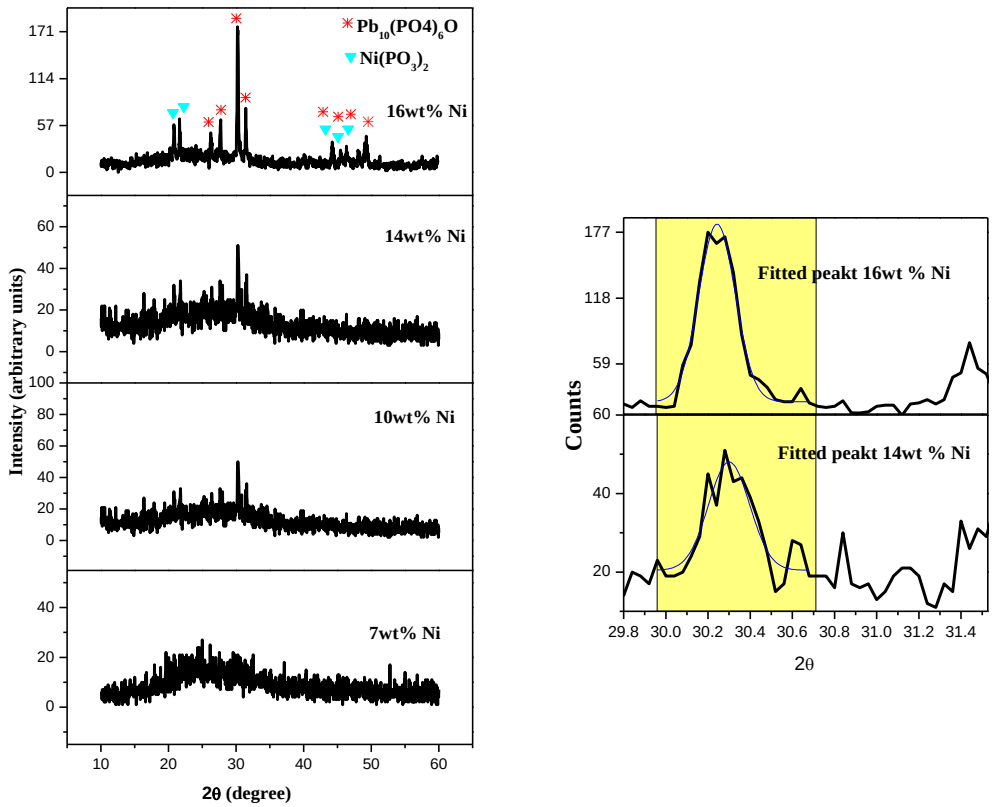

Figure VI- 5 : XRD patterns of (PbO-P_2O_5 /14wt% and 16wt% Ni) composite thin films and fit profile of the main crystalline peak.

XRD of glass thin film loaded with Nickel particles exhibits polycrystalline structures at higher loading level ,revealing two well crystallized phases ,namely $Pb_{10}(PO_4)_6O$ and $Ni(PO_3)_2$ which crystallize in hexagonal and monoclinic geometries.

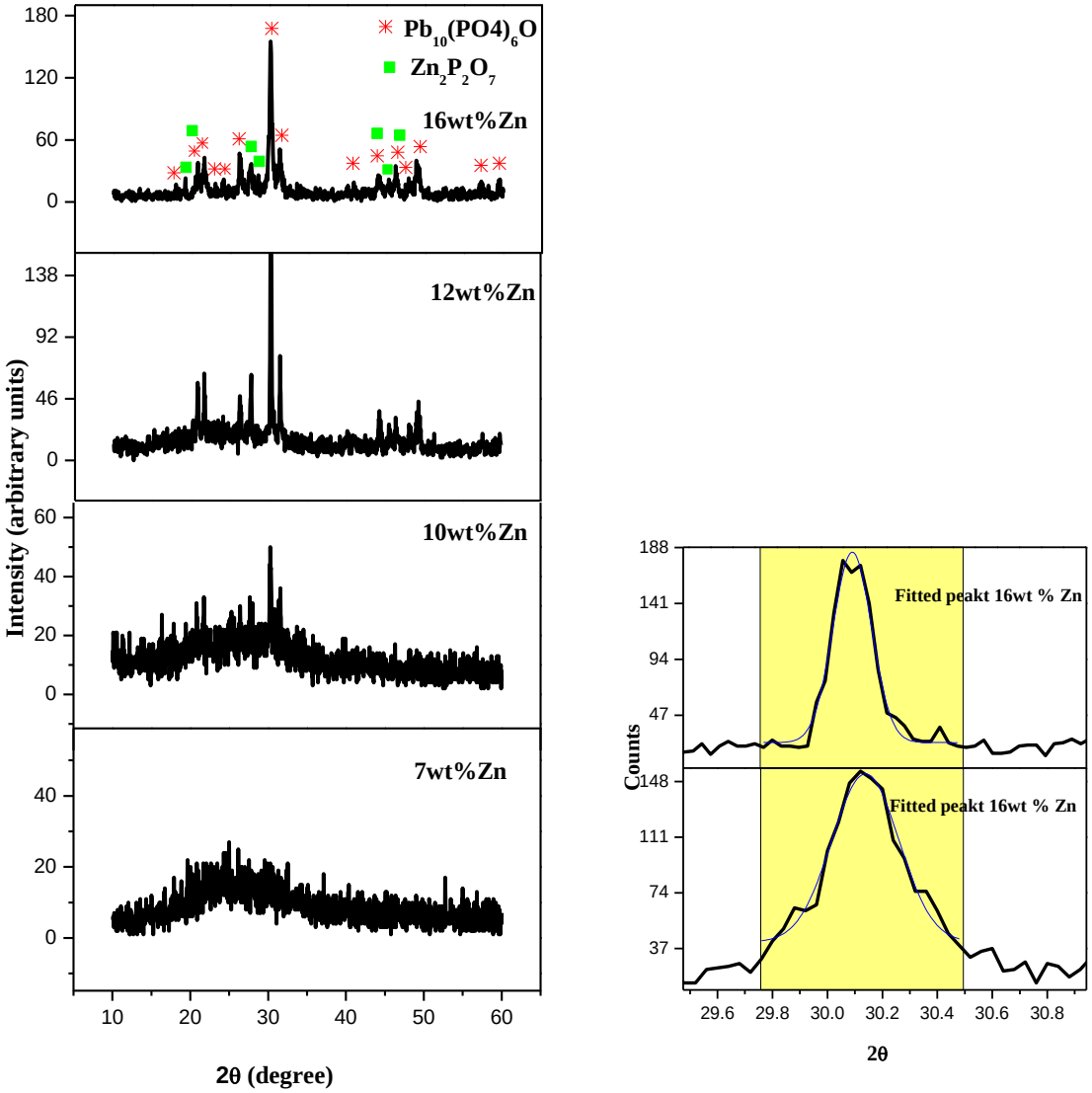

Figure VI- 6 : XRD patterns of lead phosphate (PbO-P_2O_5 /12wt% and 16wt% Zn) composite thin films and fit profile of the main crystalline peak.

Unlike the above investigated thin films, in the case of zinc filled lead phosphate glass (PbP/Zn) thin films, we can see the crystallization at a bit earlier filler's concentration. Indeed, XRD patterns are indicating the onset of crystallization peaks at 12wt %. This is probably related to the high known catalytic effect of zinc, as pointed out [59].

The above depicted figures show typical XRD spectra, The spectrum of glass thin films loaded at low filler's concentration show a broad peak at $2\theta \approx 18.6$ ° indicating that the amorphous phase of

the matrix is still sustaining. However, at enhanced loading level, the peaks are more intense which explains growing crystallinity.

Moreover, it important to note that these results show for all loaded metals, the crystallized phases corresponding to $Cr_3(PO_4)_2$, $Co_3(PO_4)_2$, $Ni(PO_3)_2$, $Zn_2P_2O_7$ seem less important and the major part of crystallization at high loading is due to the lead-phosphate glass matrix, probably by metal catalytic effect.

Therefore, it could be pointed out that XRD patterns revealed that nanocomposite thin films are obtained through mixture of amorphous and crystalline phases, like in the case the bulk composites samples. According to XRD findings, it seems that metal induced crystallization has occurred. This can be evidenced if we compare the crystallization temperature of the neat matrix and the temperature of appearance of identified peaks in amorphous glass matrix/ metal composites. It seems that under temperature effect, when the incorporated metal comes into contact with the glass matrix, the films show crystallization peaks at much lower temperature (250°C, Table VI-2). Nevertheless, unloaded thin films are annealed at the same temperature but did not show any crystallization peak. This simple comparison suggests that, effectively fillers loading induce the observed crystallizations. This phenomenon has been studied elsewhere in the case of Nickel-induced crystallization of amorphous silicon **[360].**

The determined cluster sizes, using the relation (VI- 1) are given table VI-2:

Table VI- 2 : FWHM (β) and Crystallite Size of annealed composite thin films.

Sample	Annealing Temperature °C	Bragg diffraction angle (2θ)/(degree)	FWHM (β) (degree)	Crystallite Size D (nm)
Neat matrix	300	15.10	0.10	13.84
	350		0.09	15.38
PbP/14wt%Cr	250	30.20	0.13	10.98
PbP /16wt%Cr			0.12	11.89
PbP /14wt%Co	250	30.28	0.21	6.79
PbP /16wt%Co			0.17	8.39
PbP /14wt% Ni	250	30.24	0.20	7.21
PbP /16wt% Ni			0.17	8.48
PbP /12wt% Zn	250	30.12	0.22	6.49
PbP /16wt% Zn			0.17	8.39

Figure VI-5 reveals a pronounced size growth of clusters forming Ni loaded thin films, at 16wt%, at enhanced loading level, FWHM has remarkably decreased showing minimal value. Clusters growth is probably due to higher loading concentrations.The same evolution is observed for glass

thin films filled with chromium and cobalt as depicted in figures VI-3 and VI-4, respectively, but the evolution of cluster 's sizes are less.

It is clear that the obtained results reveal a pronounced size growth of clusters forming for all metals at enhanced loading level. While, FWHM has remarkably decreased showing minimal value.

Similar phenomenon was observed elsewhere [361]. It was revealed that at lower metal particles content, the cluster size is about 4.89nm and with higher fillers loading, it becomes 6.52nm.

VI.4 Structural characterization by IR-ATR and Raman spectroscopy

VI.4.1 IR/ATR

The studied films were characterized by Fourier transform infrared attenuated total reflection (FT-IR/ATR) absorption spectroscopy. The IR/ATR method has several advantages over other available IR spectroscopy. It is very sensitive to thin films matrix [362] because the beam interacts with the sample upon each reflection and it's not distorted by heterogeneous or light particulate scattering processes.

In this section, we describe the FT-IR/ATR absorption properties of lead phosphate glass thin films as a function of fillers loading concentrations. According to FT-IR/ATR spectra of Figure VI-7, a band at 920 cm^{-1} is assigned to a symmetric stretching vibration of P–O–P linkages (ν_S (P–O–P)) [363-368]. This band is slightly shifted to a lower wave number (920–890 cm^{-1}) and its relative area decreases until it becomes a small band.The band at 1300 cm^{-1} is attributed to asymmetric stretching vibration (ν_{as} (P=O)) [369, 370].The band at 1036 cm^{-1} is attributed to symmetric stretching vibration of PO34- tetrahedra (P–O ionic group) [371].The spectra exhibit a very weak band in the region 1600–1660 cm^{-1}. The absorption band at 480–508 cm^{-1} is assigned to harmonics of bending vibration of P–O linkages [365,368]. The weak absorption band at 809–776 cm^{-1} is attributed to the bending vibration of P–O–P linkage .The band at 687 cm^{-1} is due to the asymmetric vibration of these linkages (ν_{as} (P–O–P) [372, 373].The whole obtained spectra do not express any metallic environment band at high fillers loading, even though they are existing inside the glass matrix and cause ordered networks as revealed through XRD patterns.

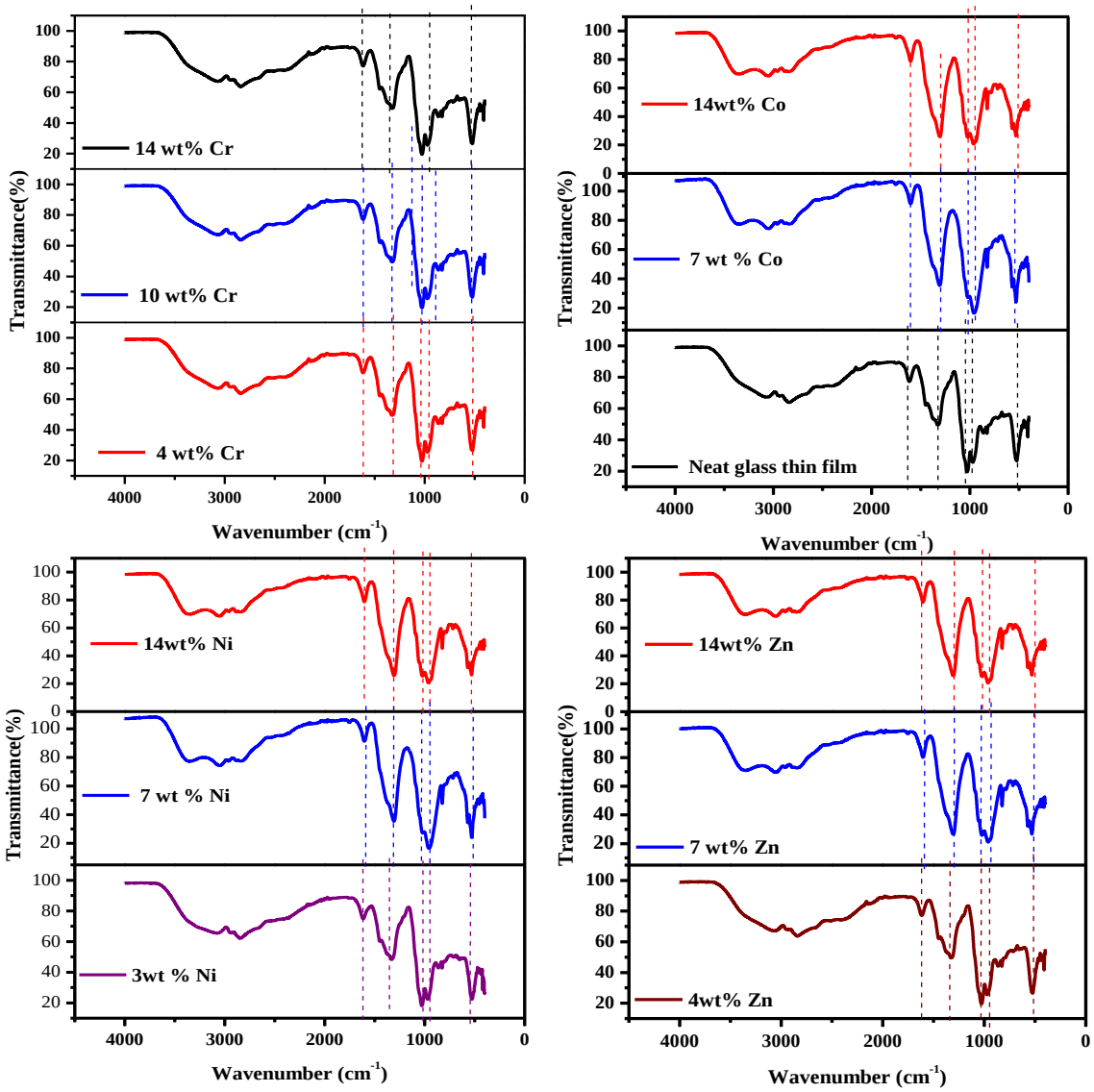

Figure VI- 7 : FT-IR /ATR spectra of the as prepared sol gel thin films recorded at room temperature in the range of 500-4000cm^{-1} and vertically offset for better clarity.

VI.4.2 Raman Spectroscopy

Vibrational properties of the elaborated composite films are studied by Raman scattering at room temperature. This technique is based on inelastic light diffusion phenomenon. In other words, when a sample is irradiated by an electromagnetic wave of frequency υ_o, one part of the light is absorbed and the other part is diffused either with the same frequency, it is the elastic scattering (Rayleigh), or with a different frequency, it is Raman scattering [374]. Indeed, the diffusion of a monochromatic radiation by sample causes the appearance of radiation of low intensities whose frequencies are different from that of the incident radiation and they tend to change in accordance

with the vibratory and rotational energies. These are specific to each entity. Therefore, the intensity of scattered radiation is characteristic of the examined material [375].

Raman spectroscopy is considered as an experimental technique appropriate for revealing information about the structure of local arrangements of the atoms in glasses. Raman spectra of thin films were collected in the range of 3000-500 cm^{-1}, in order to investigate the local structure of phosphate glass loaded with transition metal particles, namely Cr ,Co ,Ni and Zn.

It is noteworthy that, Raman spectra of crystalline samples are connected to narrow peaks, while broad lines are due to disordered structure [376]. Indeed, this technique has confirmed the formation of lead phosphate glass by the appearance of broad peak at ~1344 cm^{-1} which is attributed to symmetrical vibration of P-O bonds, ν_s(P-O) [377]. The Raman spectra of loaded phosphate glass thin films with different concentrations of transition metal particles are exhibited in Figure VI-8

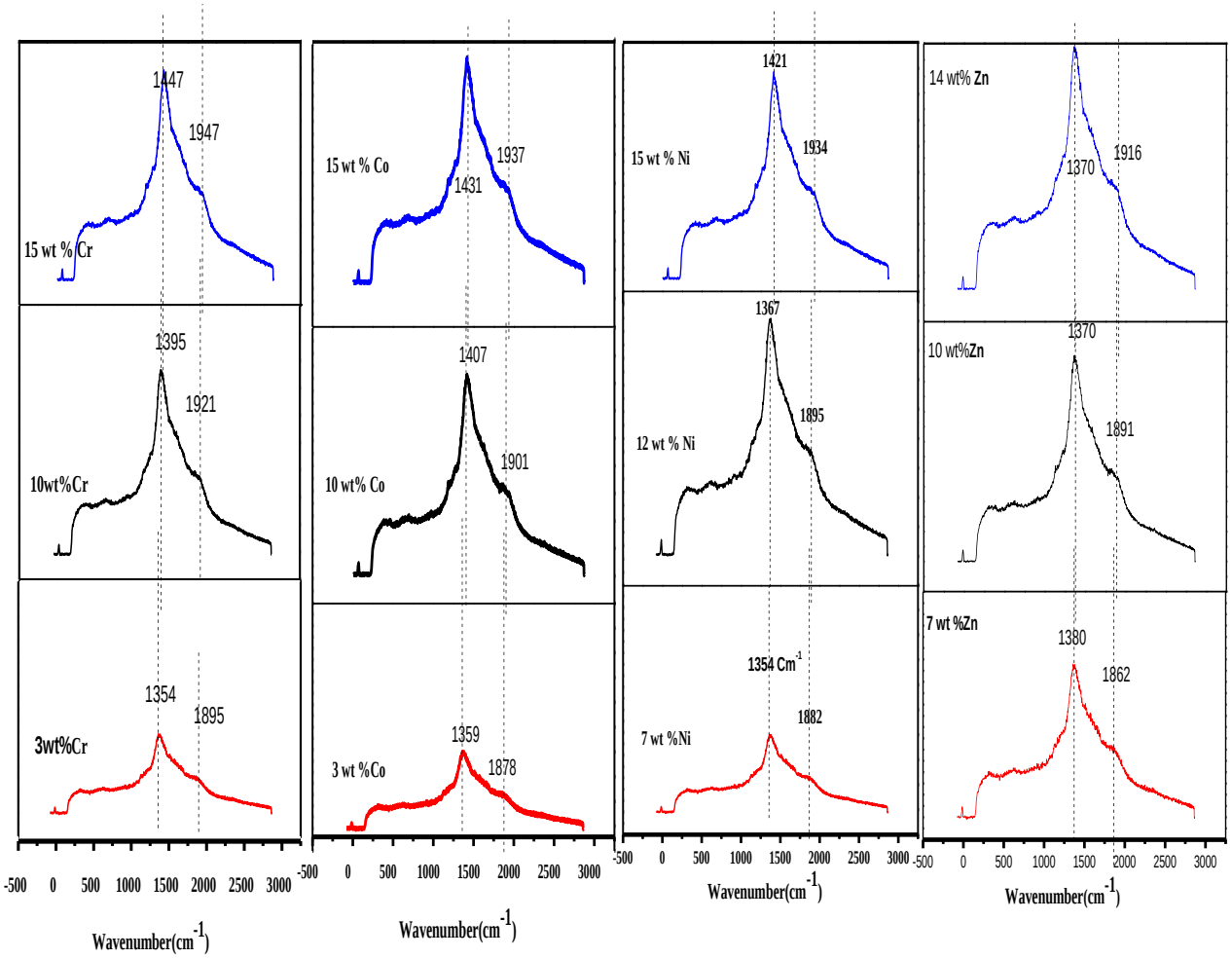

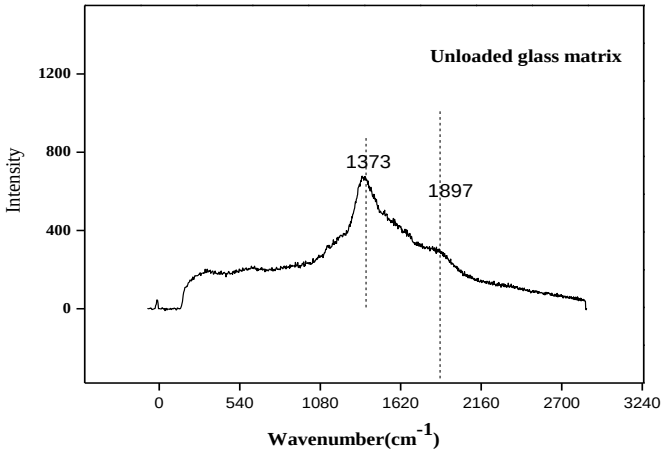

Figure VI- 8 : Raman spectra of the as prepared sol gel thin films recorded at room temperature in the range of 500-3000 cm^{-1} and vertically offset for better clarity.

The quantity of loaded metal transition elements is represented by weight percent. The loading of small amounts of fillers, around 3wt%, does not influence the corresponding Raman profiles, which suggests that the short-range order structure of the glass matrix was not altered by the nature of loaded metal particles. Nevertheless, with higher loading, we have observed slight shift of bands situated at 1500cm^{-1} towards the low frequencies. This is probably due to the small crystallite sizes formation. The high loading level has caused the appearance of new and small vibration band located at around 2000cm^{-1}. Also, we observed narrowing and increase of peak intensity, especially at highly loaded films with Zn and Ni. This new feature is probably attributed to the appearance of partially ordered structure, in a good consistence with XRD patterns.

VI.5 Morphological studies of unloaded and loaded glass thin films

VI.5.1 SEM analysis

In order to assess the structural data and get better insights on the obtained thin films, the prepared samples undergone further investigations by examining their surface morphology using scanning electron microscope (SEM), since it's the only technique which also allows us visualizing some surface properties such as homogeneity, roughness and grain texture of the deposited film. Microstructural studies of thin films were carried out also in order to highlight some effects due to the annealing temperature. The micrographs of thin films are obtained by electron scanning microscopy (SEM) using apparatus of FEI FEG 450 type (see Appendix).

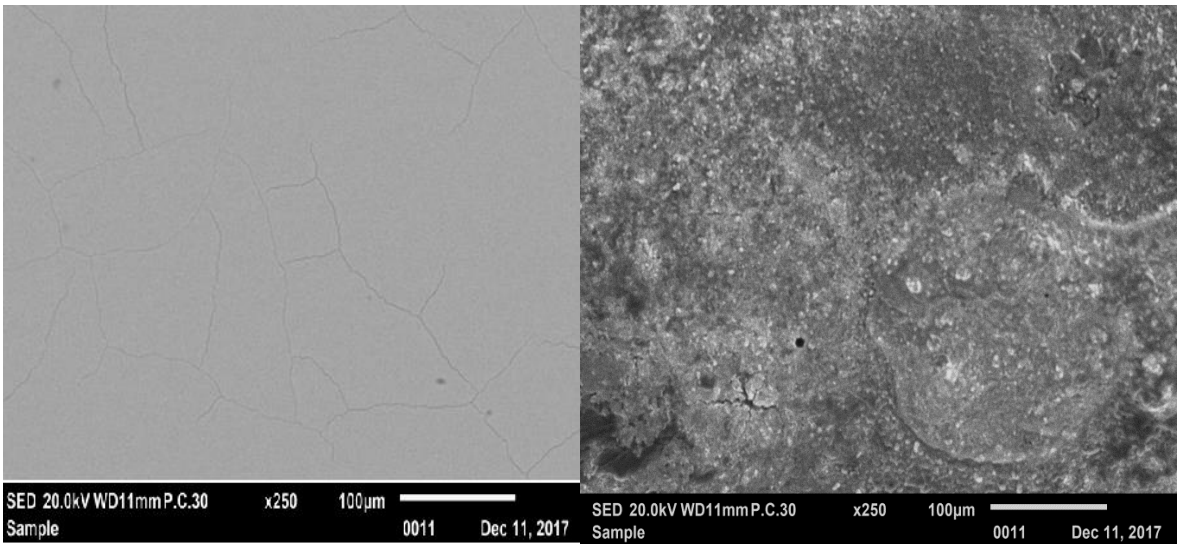

(a) (b)

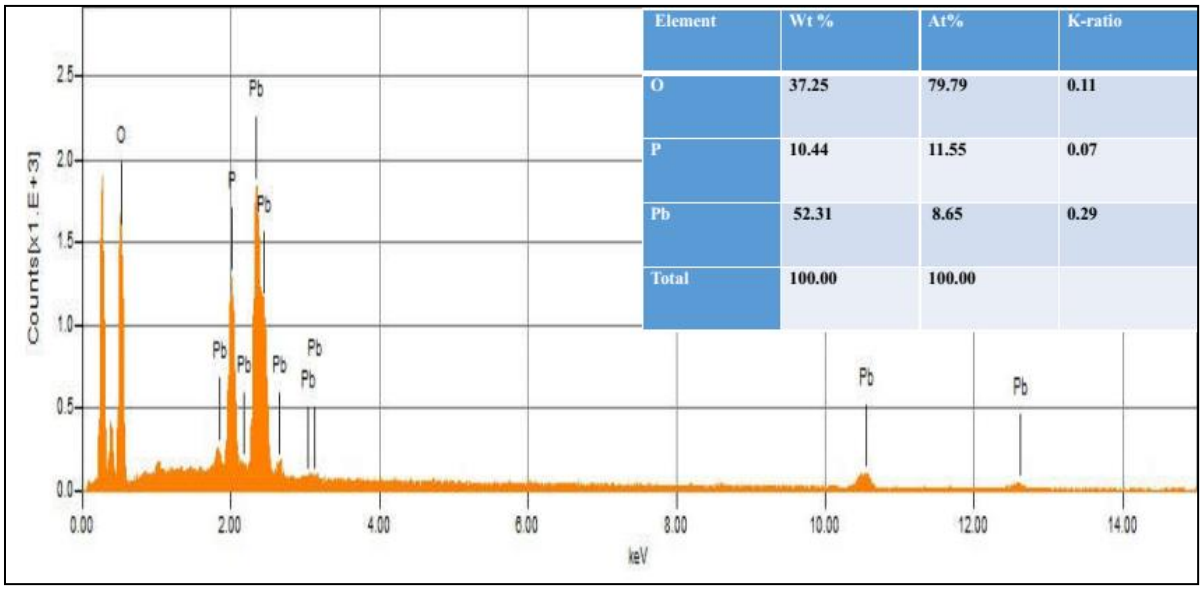

Element	Wt %	At%	K-ratio
O	37.25	79.79	0.11
P	10.44	11.55	0.07
Pb	52.31	8.65	0.29
Total	100.00	100.00	

(c)

Figure VI- 9 : (a) : PbO-P_2O_5 thin films at 250°C, (b): PbO-P_2O_5 thin films at 350°C, (c): EDX spectrum of PbP thin films.

The scanning micrographs of unloaded lead phosphate glass films which were annealed at 250°C and 350°C are shown in the inset of figures VI-9-(a) and VI-9-(b), respectively. At relatively low temperature, it is obvious that thin film exhibits amorphous smooth surface. The smoothening of the grainy character of thin film surface morphology has presumably took place after film thermal stabilization at 250°C.However, with enhanced temperature, especially at 350°C, there is an appearance of surface roughness, some porosity and breaks.We consider that the grainy character of surface morphology of as-deposited thin films is related to the agglomeration of clusters during elevated heat treatment. This suggests that the increase of treatment temperature leads to a

progressively increasing concentration of the glass material and hence, increase of cluster size. In a good agreement with XRD findings. The existing roughness at this stage is troublesome, it is probably related to starting of some degradation of the film under the thermal treatment.

Thus, 250 °C has been chosen as an optimal annealing temperature for the investigated thin films. Figures VI-10, VI-11, VI-12 and VI-13 illustrate the surface topography obtained by Scanning Electron Microscopy (SEM) of glass thin films loaded with different concentrations of chromium, cobalt, nickel and zinc fillers with annealing temperature of 250°C.

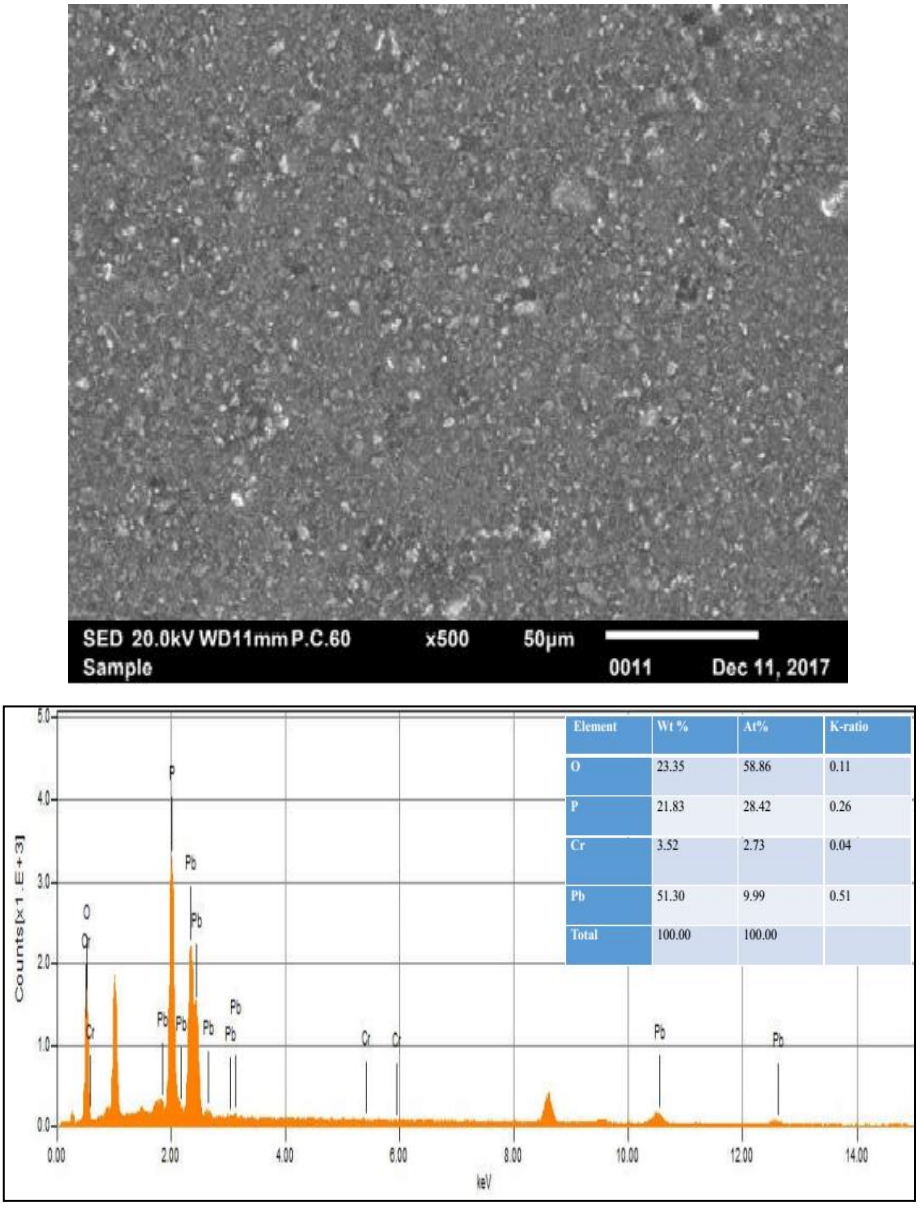

Figure VI- 10 : SEM/EDX of PbP/7wt%Cr thin films annealed at 250°C.

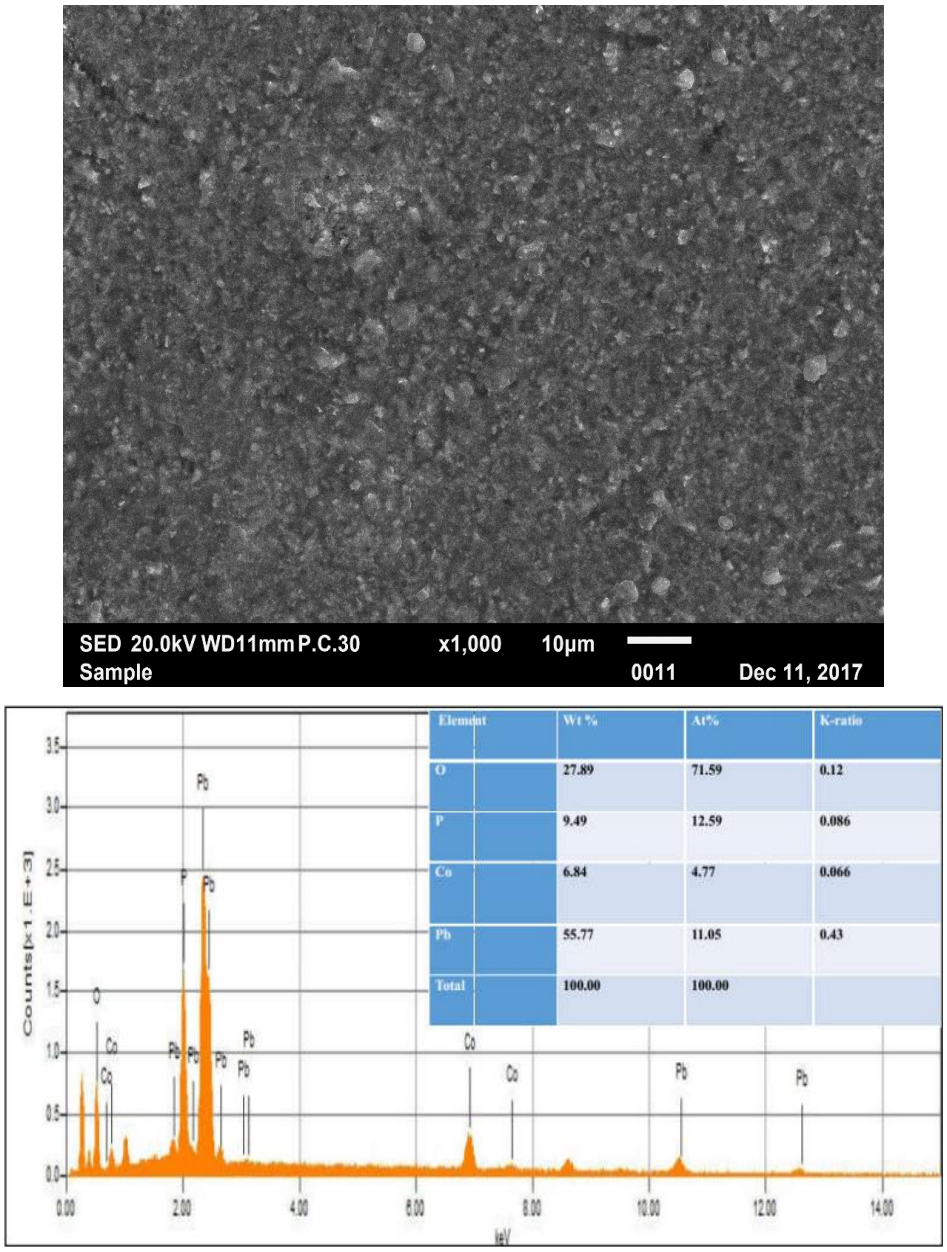

Figure VI- 11 : SEM/EDX of PbP/7wt%Co thin film annealed at 250°C.

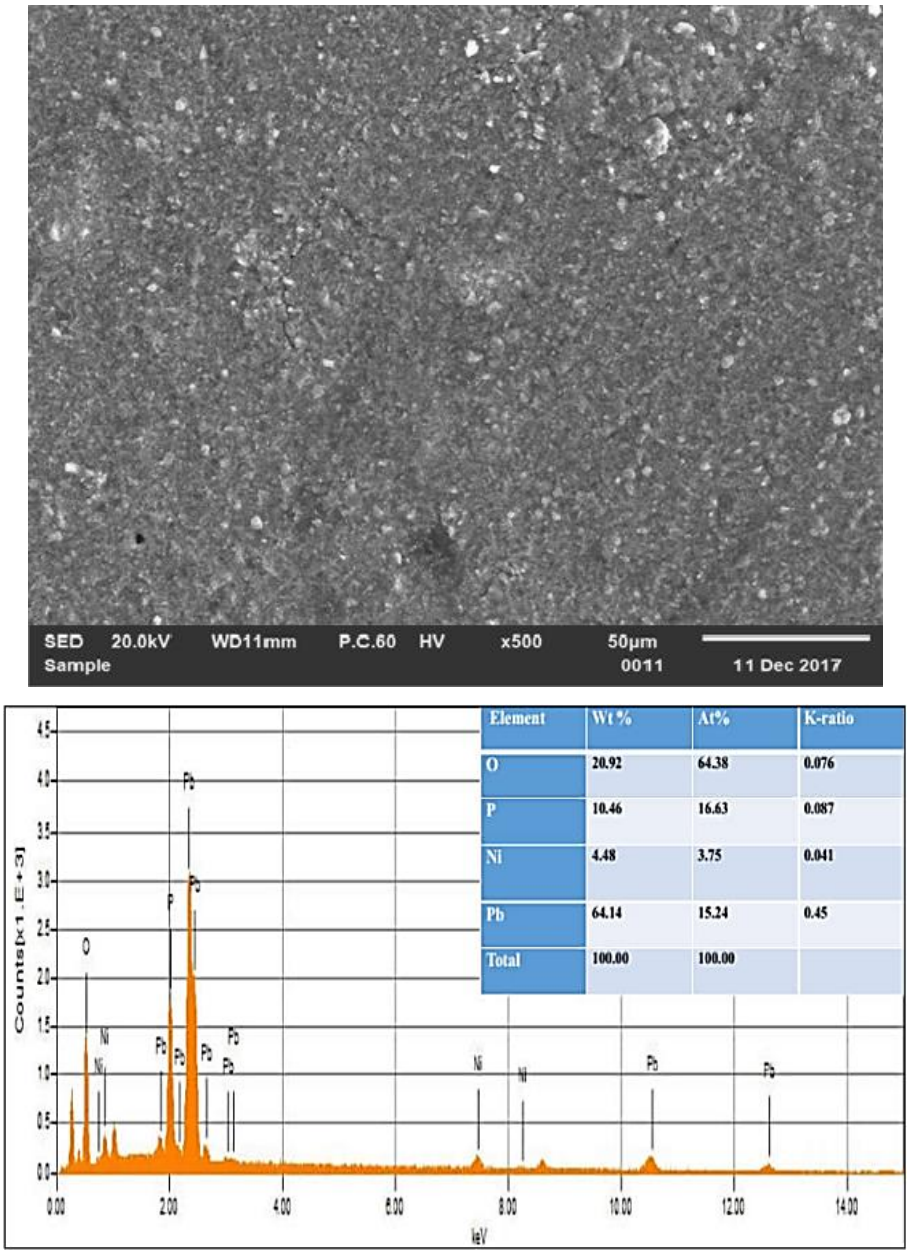

Figure VI- 12 : SEM/EDX of PbP/5wt%Ni thin film annealed at 250°C.

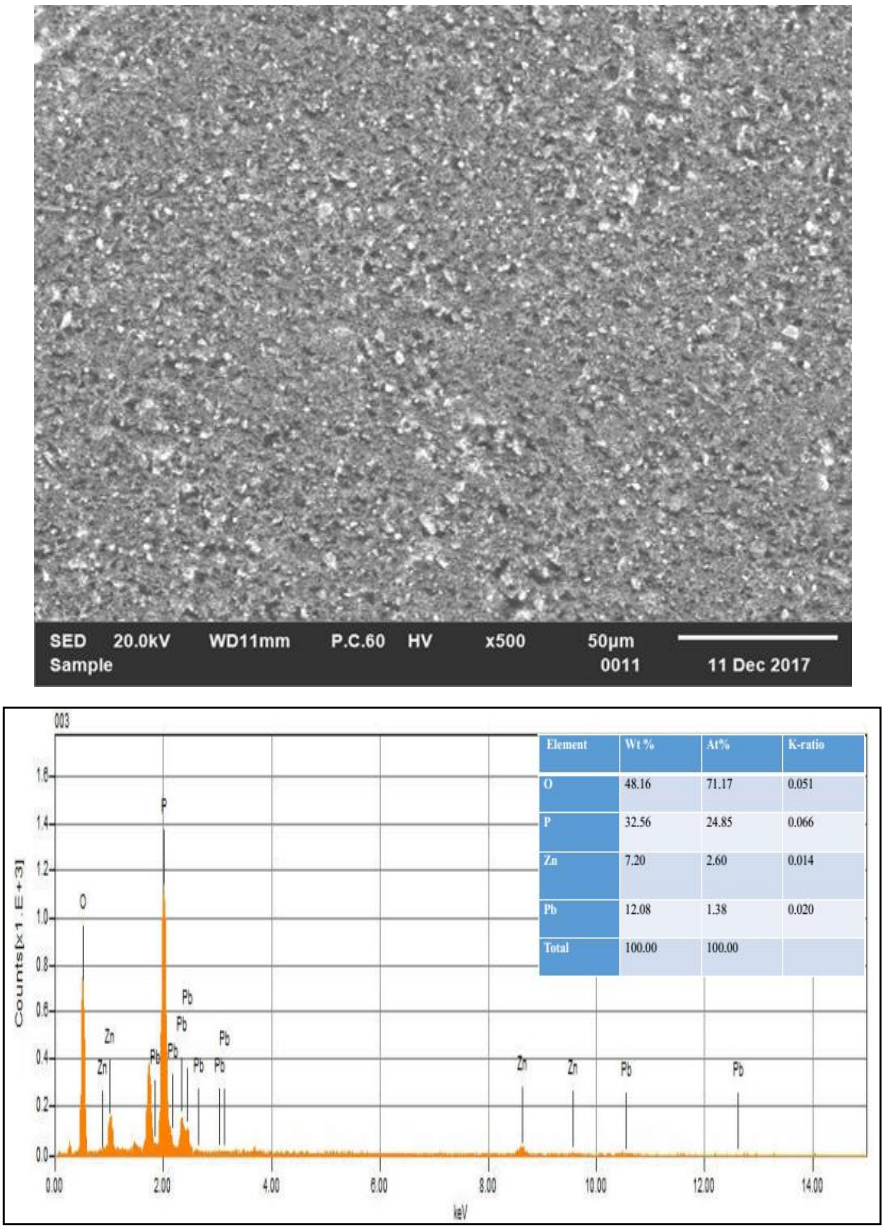

Figure VI- 13 : SEM/EDX of PbP/7 wt% Zn thin films annealed at 250°C.

SEM micrographs at low loading levels reveal a dense and uniform granular structure whose clusters are very small. The distribution of clusters heights is tight which means that the majority of clusters present somewhat similar dimensions.

At higher fillers loading, we note formation of a larger cluster's size. The films morphology is dominated by a majority of randomly big crystallized clusters in the case of chromium and cobalt loading at 16wt% (Figures VI-14 and VI-15).However,in the case of Zinc and nickel loading, the high loading levels leads to well ordered surface morphology containing crystalline phase(s) (see figures VI-17 and VI-18).

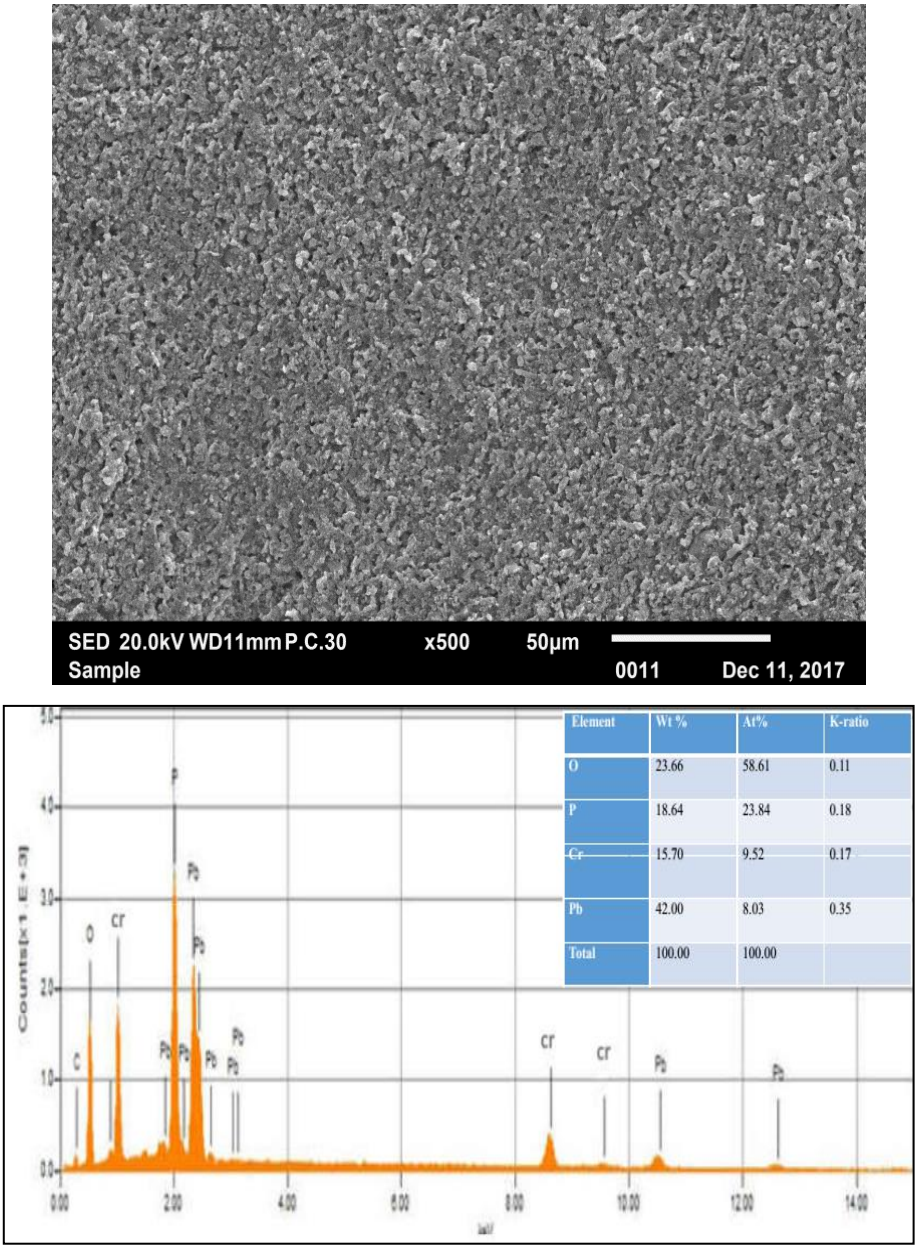

Figure VI- 14 : SEM/EDX of PbP/15wt% Cr thin films annealed at 250°C.

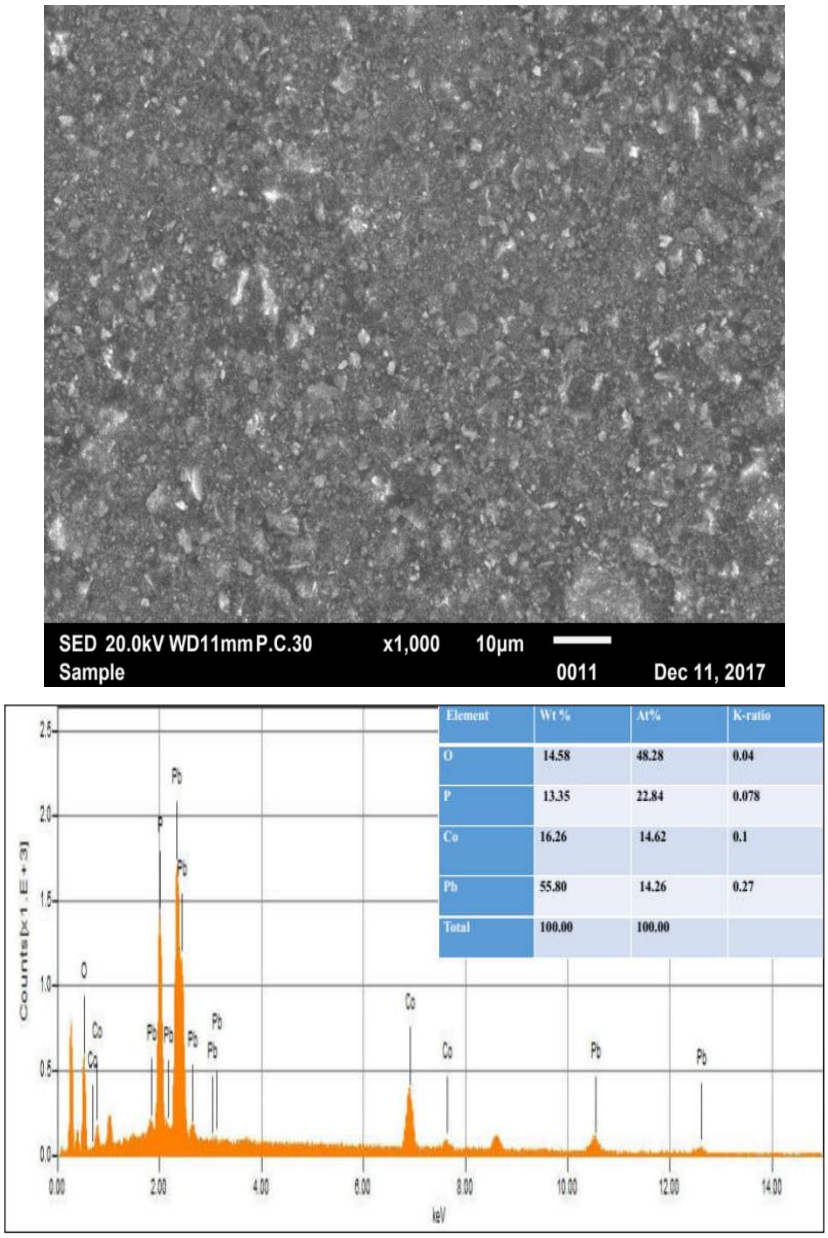

Figure VI- 15 : SEM/EDX of PbP/16wt%Co thin films annealed at 250°C.

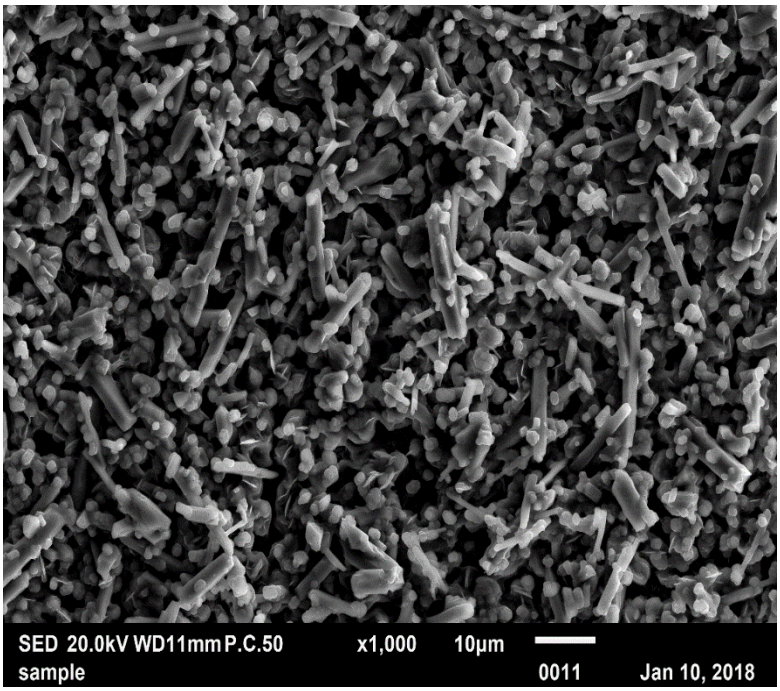

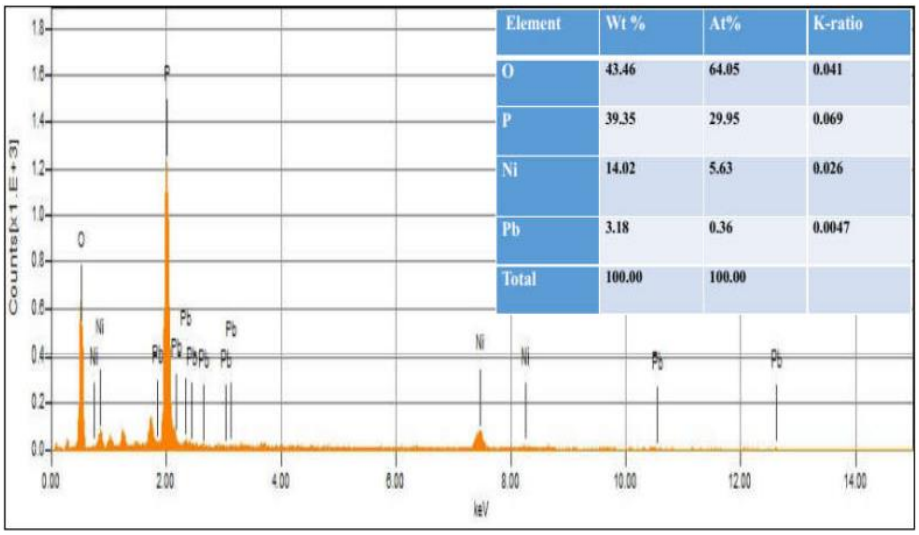

Element	Wt %	At%	K-ratio
O	43.46	64.05	0.041
P	39.35	29.95	0.069
Ni	14.02	5.63	0.026
Pb	3.18	0.36	0.0047
Total	100.00	100.00	

Figure VI- 16 : SEM/EDX of PbP/16wt% Ni thin films annealed at 250°C.

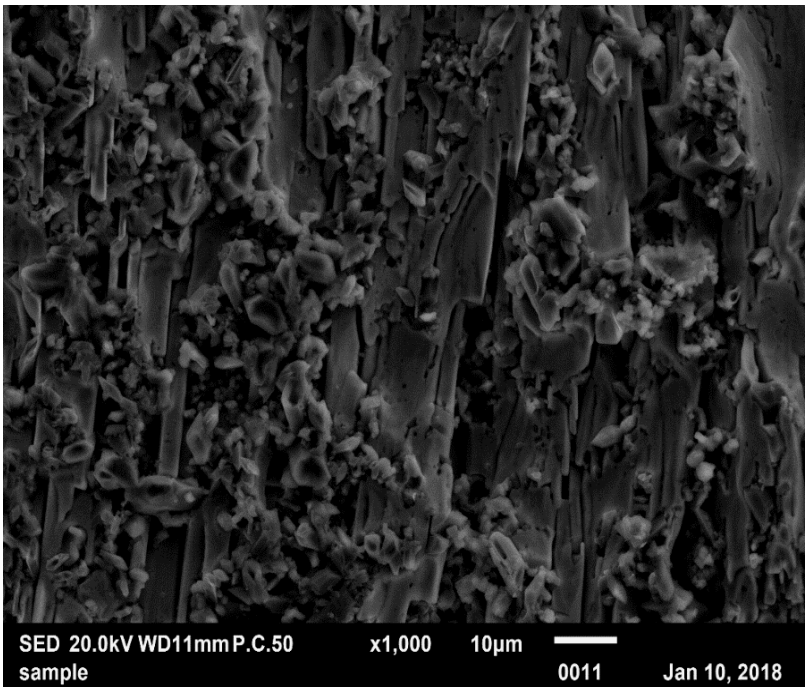

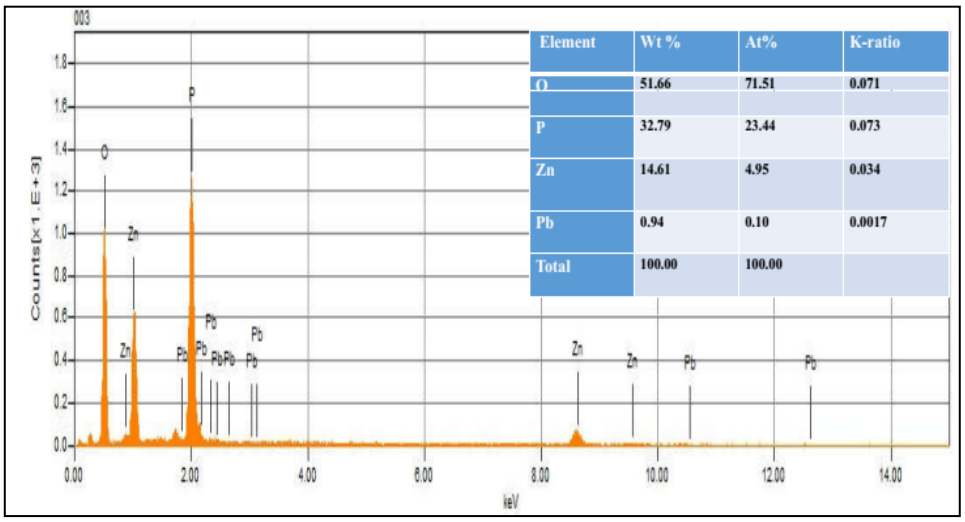

Figure VI- 17 : SEM/EDX of PbP/16wt%Zn thin films annealed at 250°C.

These figures illustrate the morphological details of the surface of as-deposited glass-based films revealing the apparent grainy morphology created most likely by evaporation of the solvent during film deposition process.

Indeed, SEM micrographs of glass films with different nickel concentrations suggest that the loading concentration has big influence on crystallization process.

Elsewhere, the films surface is smooth and the grains are uniform. However, as the loading concentration further increases, the grains begin to grow loosely. Typically, the surface of the 16

wt% Ni loaded glass thin films is rough. Hence, the existing roughness at this stage will not allow a good contact between the layers for further processing such as performing P-N Junction [378].
Concerning, the effect of increase of Zn content in glass thin films might be clearly understood from the surface morphology. The micrograph of Zn loaded glass thin films shows spherical granules irregularly distributed over the substrate. SEM confirms that high level Zn content has effectively changed the microstructure of glass thin films, in good agreement with XRD patterns.
Through these significant findings, we can conclude that the annealing temperature of loaded thin films must be fixed at 250°C, and the loading level should be at around 14wt %. In a good agreement with X-ray patterns results.
The effect of increase of Zn content in glass thin films might be clearly understood from the surface morphology. The micrograph of Zn loaded glass thin films shows spherical granules irregularly distributed over the substrate. SEM confirms that high level Zn content has effectively changed the microstructure of glass thin films, in good agreement with XRD patterns.
Through these significant findings, it was concluded that the annealing temperature of loaded thin films must be fixed at 250°C, and the loading level should be at around 14wt %. In a good agreement with X-ray patterns results.

VI.5.2 Elemental analysis

The elemental analysis of the as prepared thin films was performed by a technique known as Energy Dispersive X-ray (EDX).The emitted X-ray spectrum was recorded in order to determine qualitatively and quantitatively the surface composition of each sample and to ensure the sample homogeneity. The electron beam energy 20kev was selected for two reasons; the first is because, the maximum X-ray energy collected by the device is 20kev on the X-ray scale. The second reason is to prevent high penetration of the film. The chemical composition allows us the determination of the accurate composition of thin film samples and checking their homogeneity, by collecting X-ray from sample at random areas and comparing their results.
EDX spectrum presented in Figure VI-9 represents the composition of the unloaded glass thin film. The whole marked peaks are assigned to the binary glass composition. The EDX spectra of glass thin films loaded with chromium, cobalt, nickel and Zinc are shown along with SEM micrographs of composites thin films. The spectra reveal the presence of metal particles in the films. The atomic percentage composition of Cr, Co, Ni and Zn are displayed in the inserted tables along with the EDX spectra. It is noticed that the amount the fillers shows an increasing trend with increase in the loading concentration.

Conclusion

Unloaded and loaded glass thin films have been successfully prepared by sol gel technique and deposited on glass substrate. The effect of annealing process of the unloaded glass was evaluated by XRD analysis, allowing the calculation of the cluster size at elevated annealing temperature. The most suitable temperature for annealing process was selected in order to obtain high quality thin films, with good structure and morphological properties.

Also, the structural and morphological properties of loaded glass was studied using XRD, IR/ATR, Raman and SEM/EDX characterizations. According to the obtained XRD results, it was revealed that the deposited thin films exhibit the co-existence of amorphous and crystallized phases at elevated fillers inclusion, as in the previously studied bulk glass/metal composites. The emerging diffraction peaks at defined high loading level are indicative of induced crystallization of the loaded films. Moreover, at high loading concentrations, small FWHM values or large cluster size indicates that he grainy surface pattern is related to the cluster size. These findings were corroborated with morphological results, suggesting that Cluster agglomeration is apparent at elevated metal particles concentrations.

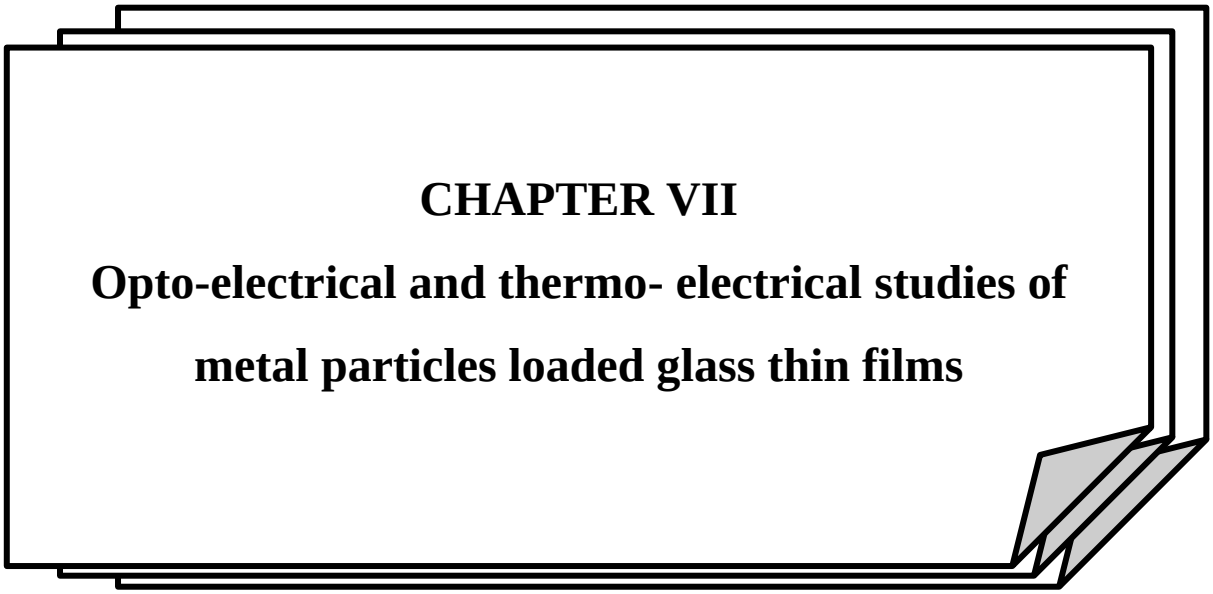

CHAPTER VII

Opto-electrical and thermo- electrical studies of metal particles loaded glass thin films

VII.1 Introduction

Lead phosphate glasses containing metal particles are considered as amorphous semiconductors. These latter have attracted much attention in the field of electronics as well as photovoltaics. The studied composites are like chalcogenide glasses which are known as typical semiconductors, they are applicable to optical, electrical and opto-electrical devices such as image sensors, electrical switches, non-volatile memories and optical data storage etc [401,402,403]. Thus, optical and electrical properties have been extensively studied for the last two decades [402, 403]. It is well known that electrical and optical properties of amorphous semiconductors depend mainly on fillers loading [404].

Therefore, amorphous thin films based on lead phosphate glass have been prepared by cost effective sol gel route. Optical, electrical and thermo-electrical properties such as optical constants, optical gap energy, Urbach energy and electrical conductivity at room temperature and versus temperature have been investigated, and the findings were analyzed within this chapter.

VII.2 Optical and electrical properties

VII.2.1 Light-mater interaction

Spectroscopy uses the absorption, emission, or scattering phenomena of light. The interaction of radiation with matter can cause redirection of the radiation and/or transitions between their energy levels. Hence, the study of the interaction of light with matter can be done in terms of transmission T, reflection R and absorption A. The interaction of light and matter is defined then as exhibited in Figure VII-1.

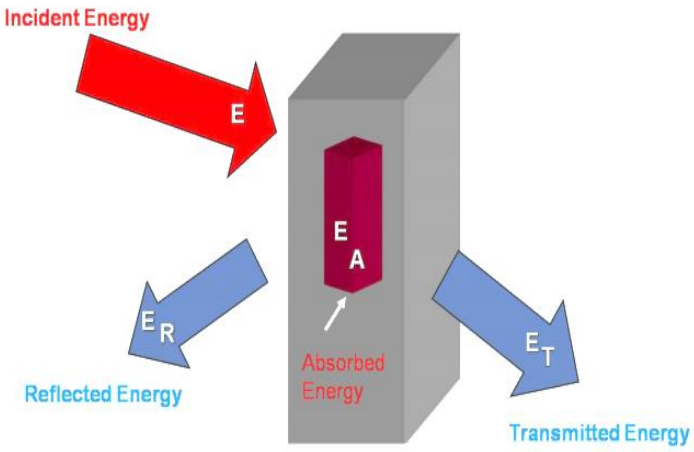

Figure VII- 1 : Absorbed, transmitted and reflected Light by sample.

The observed phenomena depend on the wavelength and polarization. Generally, the diffusion is neglected and we can write:

$$T+R+A=1 \quad \textbf{(VII-1)}$$

with

$$T=\frac{I_t}{I_0} \quad \textbf{(VII-2)}$$

$$R=\frac{I_r}{I_0} \quad \textbf{(VII-3)}$$

$$A=1-R-T \quad \textbf{(VII-4)}$$

Where I_0, I_t and I_r are respectively the intensity of the incident, transmitted and reflected wave. Reverse engineering is used in thin films to go back from R, T or A, to the characteristics defining the optical parameters such as the refractive index, absorption coefficient, extinction coefficient… Note that interactions of visible light with matter can be described by refraction index, which is a complex number:

$$n^*=n+ik \quad \textbf{(VII-5)}$$

Real component is related to phase velocity and the imaginary component refers to the extinction coefficient. At visible wavelengths, the reflected light fraction mainly depends on the real component of the refraction index (more details are discussed in chapter II).

VII.2.2 Transmittance data

UV-Visible Spectrophotometry is a nondestructive optical characterization technique. It allows working on small amounts of substances. It provides information on the optical properties of the sample to be analyzed, such as light transmission and absorption, optical gap as well as layer thickness estimation. The absorption coefficient (α) and the optical energy gap (Eg) have been determined through transmission measurements. Transmittance spectra of based phosphate glass thin films were measured in the spectral wavelength range 300-800 nm using Shimadzu double beam spectrophotometer of model UV310PC.

Optical properties are the most significant aspect of thin films. Hence, we used a dual-beam UV-Vis spectrometer. One for the reference (glass substrate) and the other for the investigated sample (thin film + glass substrate). The obtained spectra show a variation of transmittance T (%) as a function of the wavelength (nm) for different samples. In Figure VII-2, we have presented the transmission spectra, in the range of 300 to 800 nm. Note that the prepared films are loaded with

different concentrations of metal particles precursors (Cr, Co, Ni and Zn) as forementioned in chapter VI. Figure VII- 2 indicates that spectra shapes are almost identical and consist essentially of two regions:

-A region of strong absorption which corresponds to fundamental absorption (λ<380nm). This absorption is resulting from band-band electronic transitions. The variation of transmission in this region is exploited for the determination of optical gap.

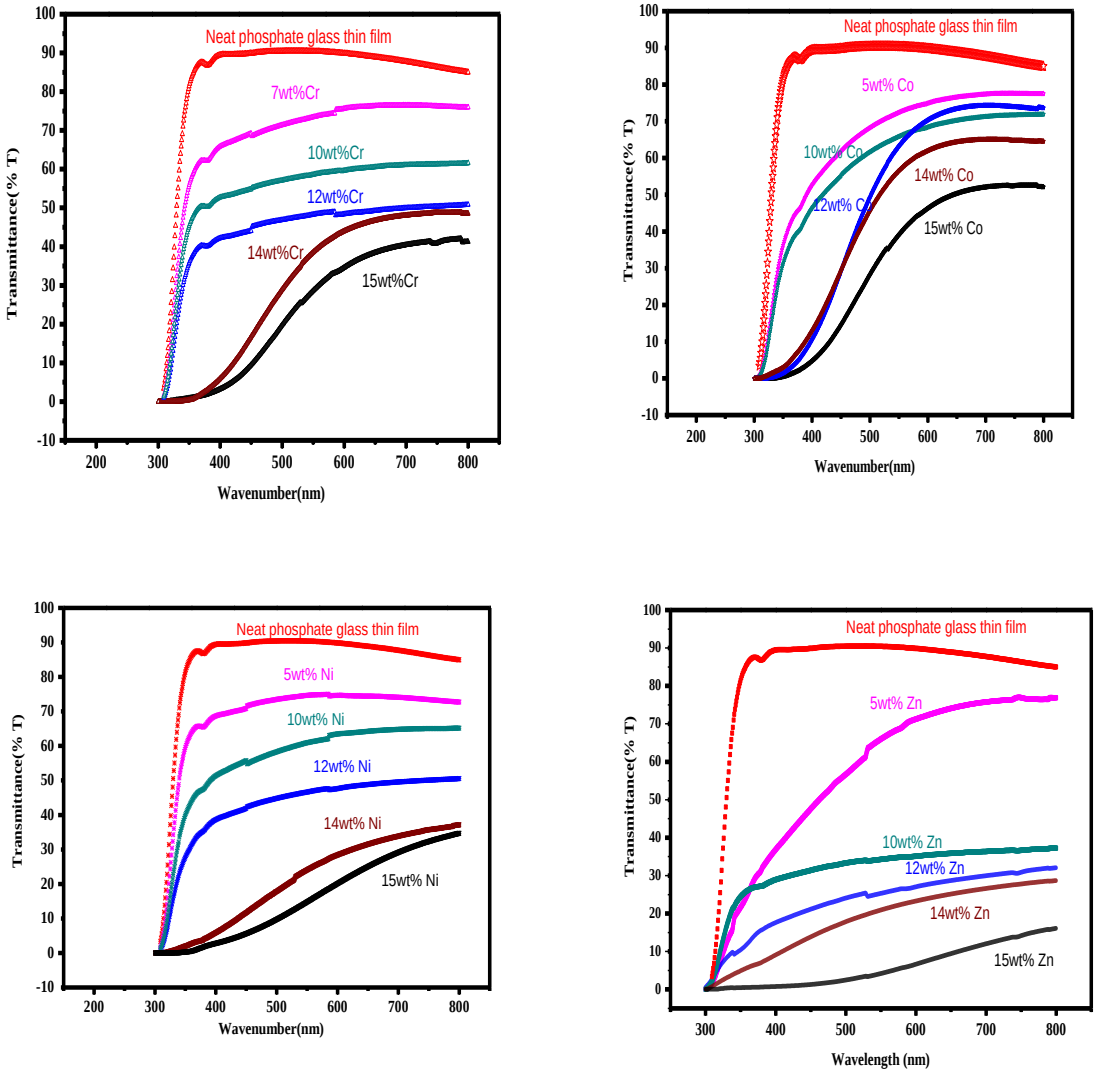

Figure VII- 2 : Plot of transmittance (T) versus wavelength of unloaded and loaded glass thin films.

-A region of high transparency located between 380 and 800 nm.

From the above depicted transmittance data, it can be seen that glass based thin films are almost transparent in the visible range. However, there is a decrease in the transmittance of lead phosphate

glass thin films with the rise of metal particles concentration. This is more likely due to the increase of absorption phenomenon induced by increasing charge carriers concentration.

By exploiting these curves. It is possible to calculate optical characteristics (thickness and refractive index), optical absorption threshold (gap energy), absorption coefficient and the width of the band tails (Urbach parameter).

In the spectral range where the light is absorbed, and knowing the thickness of the thin film, we can determine the absorption coefficient [4] :

$$\alpha = \left(\frac{1}{d}\right)\ln\left(\frac{100}{T\%}\right) \qquad \textbf{(VII-6)}$$

Where d is film thickness and T denotes the measured transmittance. Note that this calculation implies that (1-T) is the absorption of the layer. Whereas, in fact, a part of the incident light is neither absorbed, nor transmitted but is reflected, that is to say: A+T+R=1. This approximation is less valid as the thickness of the layer is relatively low [405, 40 6].

VII.2.3 loading effect on optical transmission

Figure VII-2 shows transmittance spectra of loaded glass thin films ranging from 0 to 15wt%. The spectra display the same shape for all the films. Moreover, it is observed for the whole studied films, that fillers loading increase leads to transmittance decrease. However, we notice that transmittance ascribed to nickel (at 10wt.%) and Zn (10 and 12 wt.%) decreases more remarkably. This behavior seems to be related to the number of charge carriers increase with higher fillers loading. The system gradually tends towards a semiconducting behavior. Hence, more states are present for the photon energy to be absorbed thereby increasing the absorption [407, 408].

VII.2.4 Optical gap and Urbach energy

VII.2.4.1 Optical gap

In semiconductor physics, the bandgap is always one of two types, a direct band gap or an indirect band gap. The minimal-energy state in the conduction band, and the maximal-energy state in the valence band, are each characterized by a certain k-vector in the Brillouin zone. If the k-vectors are the same, it is called a "direct gap". If they are different, it is called an "indirect gap".

Direct semiconductors are characterized by having the minimum transition energy to promote an electron from the valence band to the conduction band without a change in the electron momentum

(this energy separation is known as the band-gap). However, for indirect semiconductors, excitation at the band gap energy is accompanied by a change in the electron's momentum.

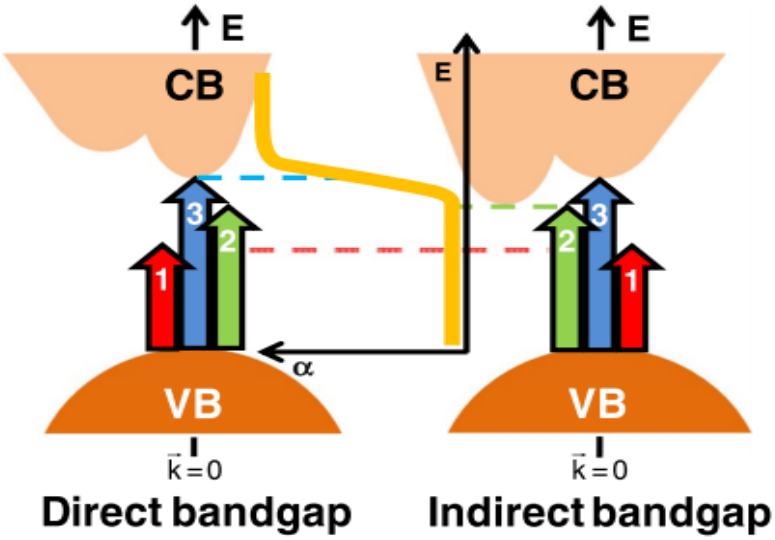

Figure VII- 3 : Simplified energy diagram illustrating the valence (VB) and conduction (CB) bands of direct and indirect bandgap of semiconductors. Also, some optical transitions (denoted by 1, 2, and 3) are represented. According to the figure, as the photon energy E increases, the following optical phenomena take place: 1– below bandgap (no absorption); 2– absorption onset and 3– high absorption edge (maximum of the optical absorption).

The absorption coefficient is related to the photon energy and the gap Eg wich is determined in the case of a semiconductor by Tauc's relationship [409]

$$\alpha h\nu = B\left(h\nu - E_g\right)^n \qquad \textbf{(VII-7)}$$

This relation can be also rewritten in logarithmic scale as:

$$\ln\left(\alpha h\nu\right) = \ln B + n\ln\left(h\nu - E_g\right) \qquad \textbf{(VII-8)}$$

Where, h is Planck's constant, α is the absorption coefficient, ν is the frequency of absorption, B is a constant and sometimes called the band tailing parameter, and Eg is the optical energy gap, which is situated between the localized states near the mobility edges according to the density of states model proposed by Mott and Davis [410]. The exponent n is a constant which takes values for direct allowed or indirect allowed transitions as ½ and 2, respectively. Note that, the energy gap or the electron transition is tightly dependent upon the composition itself, its constituents and its electronic band structure as revealed by khashan et al. [411].

In order to determine if the occurred electronic transition in the studied samples is direct or indirect, the obtained experimental curves (αhν) versus photon energy hν (Figures VII-4,VII-5,VII-6 , VII-7and VII-8) were fitted with Eq. (VII-8) in the almost end straight region, using the mean square

method, with n, B and Eg as adjustable parameters [408]. The results are obtained with good correlation factors. They are shown by solid lines in the inset of Figures VII-4, VII-5, VII-6 , VII-7and VII-8 and extracted parameters (n, B, Eg) are given in Table VII-1. Moreover, in order to check the validity of the used method, the obtained parameters were introduced in Eq. (VII-7).

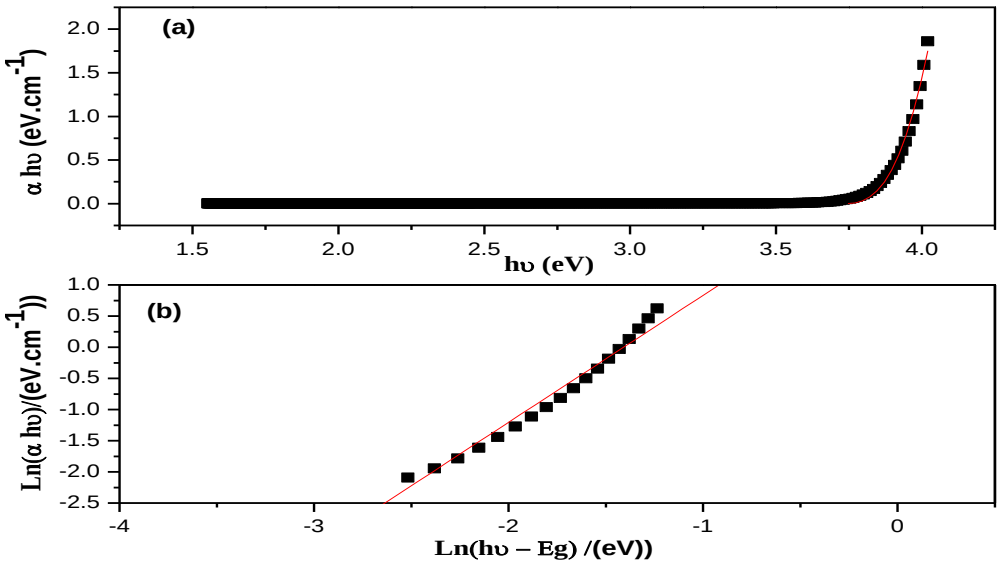

Figure VII- 4 : (a) Determination of type of optical transition by plotting (αhν) versus photon energy (hν) using mean square fit of Eq.(VII-7) –(b)Representation of ln(αhν) against ln(hν-Eg) for PbP film.

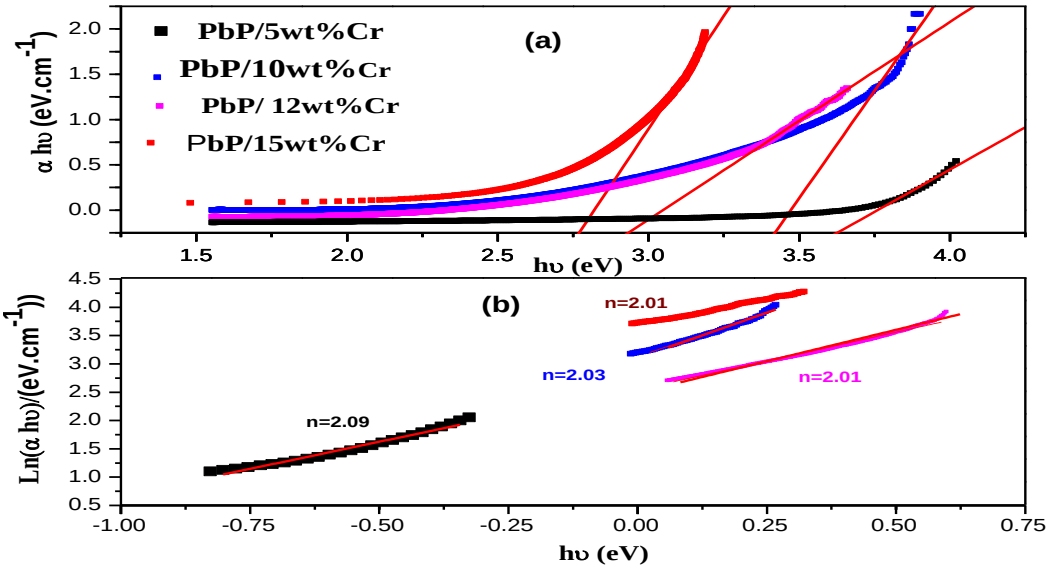

Figure VII- 5 : (a) Determination of type of optical transition by plotting (αhν) versus photon energy (hν) using mean square fit of Eq.((VII-7) –(b)Representation of ln(αhν) against ln(hν-Eg) for different PbP /Cr composite films.

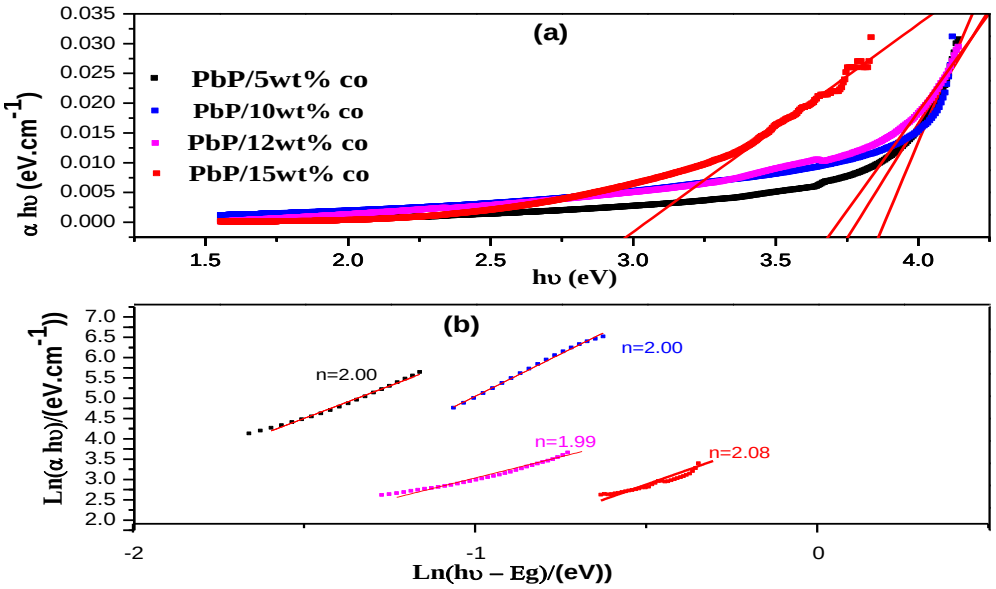

Figure VII- 6 : Determination of type of optical transition by plotting (αhν) versus photon energy (hν) using mean square fit of Eq. (VII-7) –(b) Representation of ln(αhν) against ln(hν-Eg) for different PbP /Co composite films.

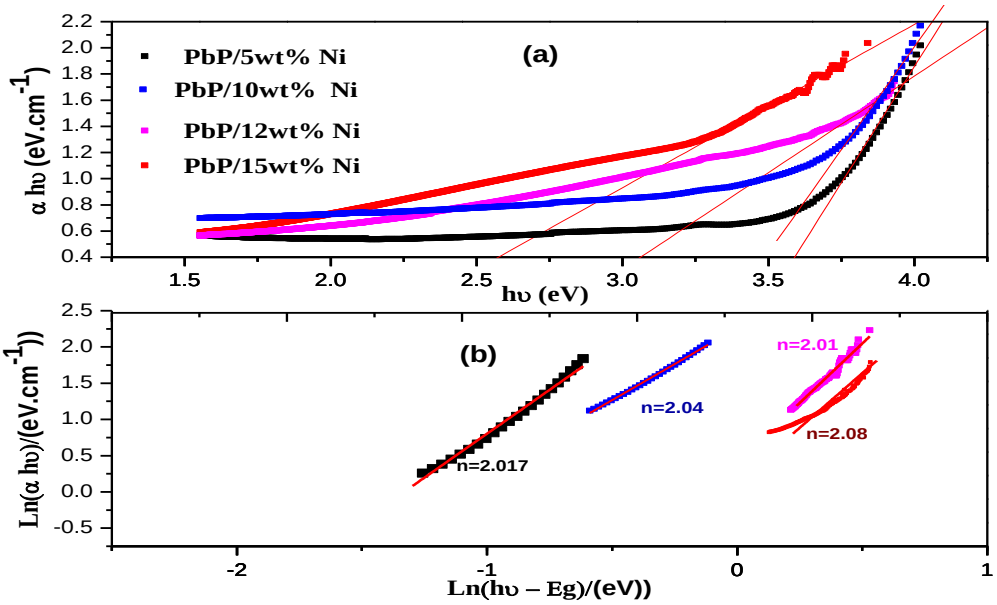

Figure VII- 7 : Determination of type of optical transition by plotting (αhν) versus photon energy (hν) using mean square fit of Eq. (VII-7) –(b)Representation of ln(αhν) against ln(hν-Eg) for different PbP/Ni composite films.

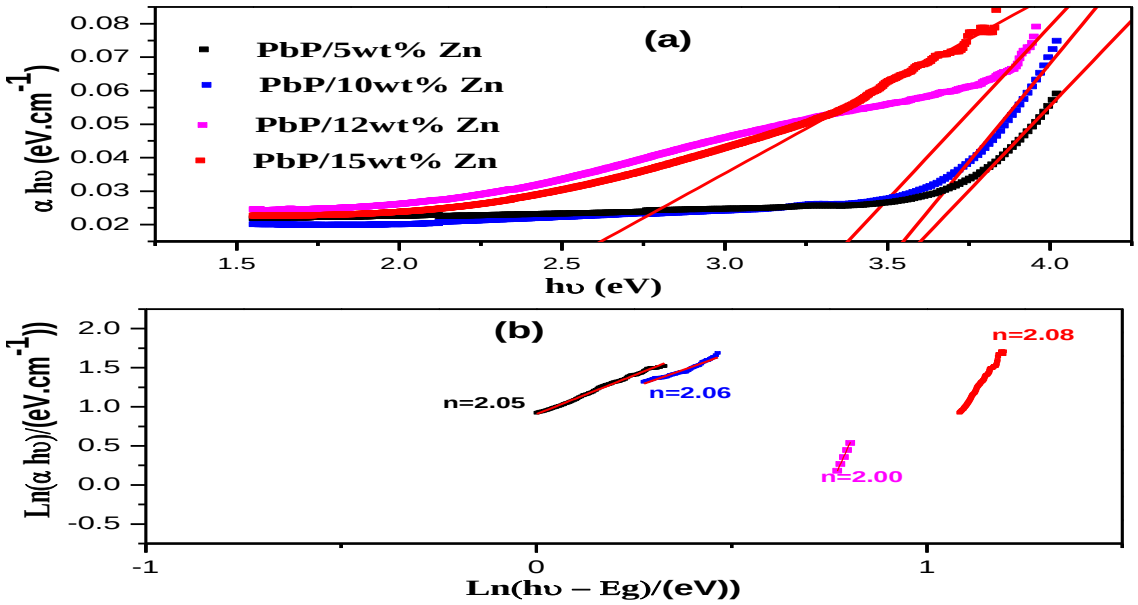

Figure VII- 8 : Determination of type of optical transition by plotting (αhν) versus photon energy (hν) using mean square fit of Eq. (VII-7) –(b)Representation of ln(αhν) against ln(hν-Eg) for different PbP/Zn composite films.

As can be seen the correlation between experiment and theory is good. This treatment may show that, the kind of the optical transition of the elaborated unloaded and loaded thin films is indirect with n≈2. The plot $(\alpha h\nu)^{1/2}$ versus hν, using the power factor n obtained by forementioned fit, gives good agreement of band gaps and Tauc's slopes (Table VII-1).

Figures VII-9, VII-10, VII-11, VII-12 and VII-13 exhibit the evolution of optical band gap with the variation of loading concentration corresponding to every metal particles (Cr, Co, Ni and Zn) .The whole curves reveal that the obtained plots give a straight line in a certain region. In order to obtain the value of the indirect allowed optical energy gap (Eg) of thin films, we can extend this straight line to intercept with x-axis.The intersection of the tangent with the x-axis represents the gap Eg.

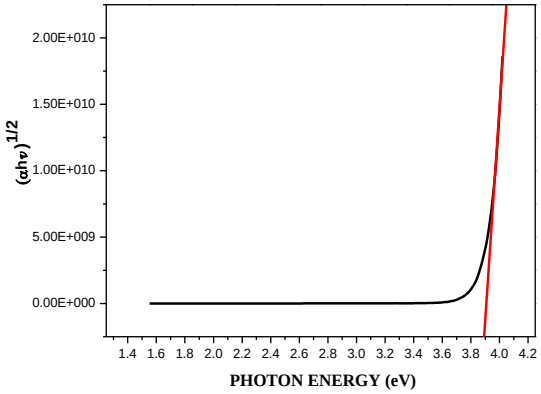

Figure VII- 9 : $(\alpha h\nu)^{1/2}$ versus energy plot for Tauc gap extraction for unloaded glass thin films.

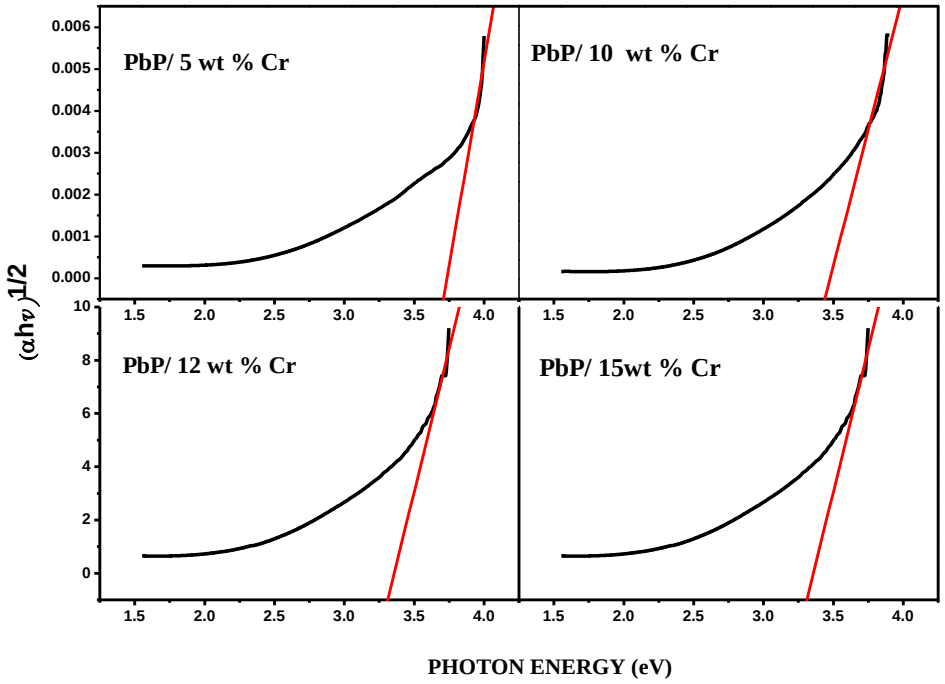

Figure VII- 10 : $(\alpha h\nu)^{1/2}$ versus energy plot for Tauc gap extraction for PbP/Cr nanocomposite films.

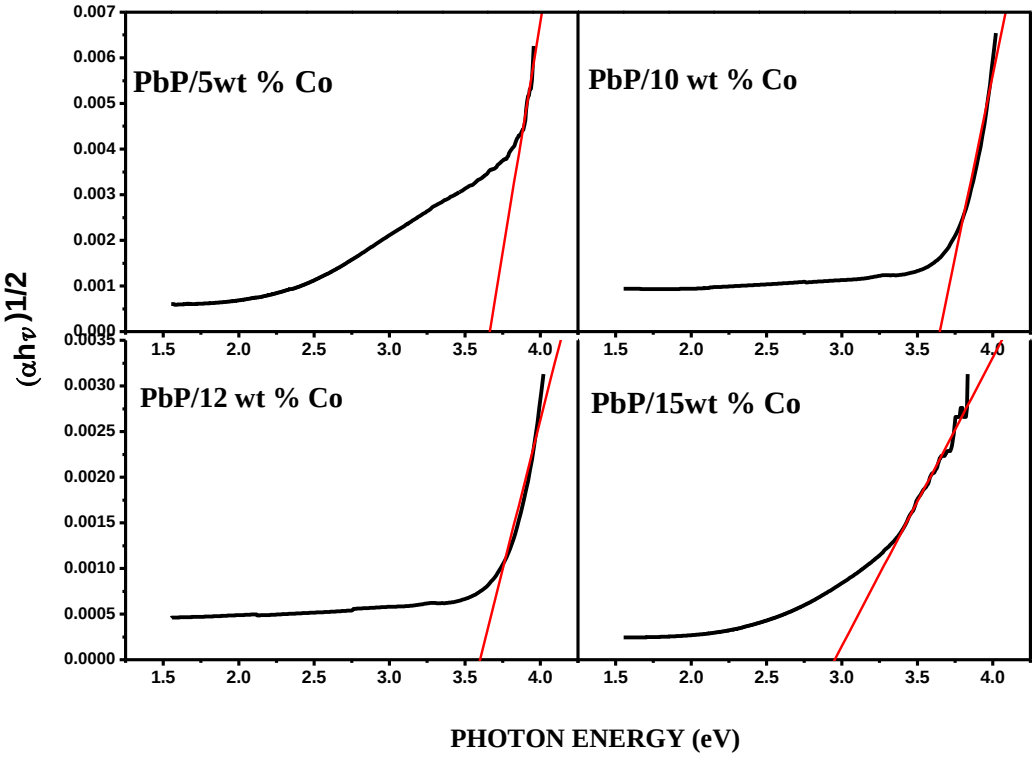

Figure VII- 11 : $(\alpha h\nu)^{1/2}$ versus energy plot for Tauc gap extraction for PbP/Co nanocomposite films.

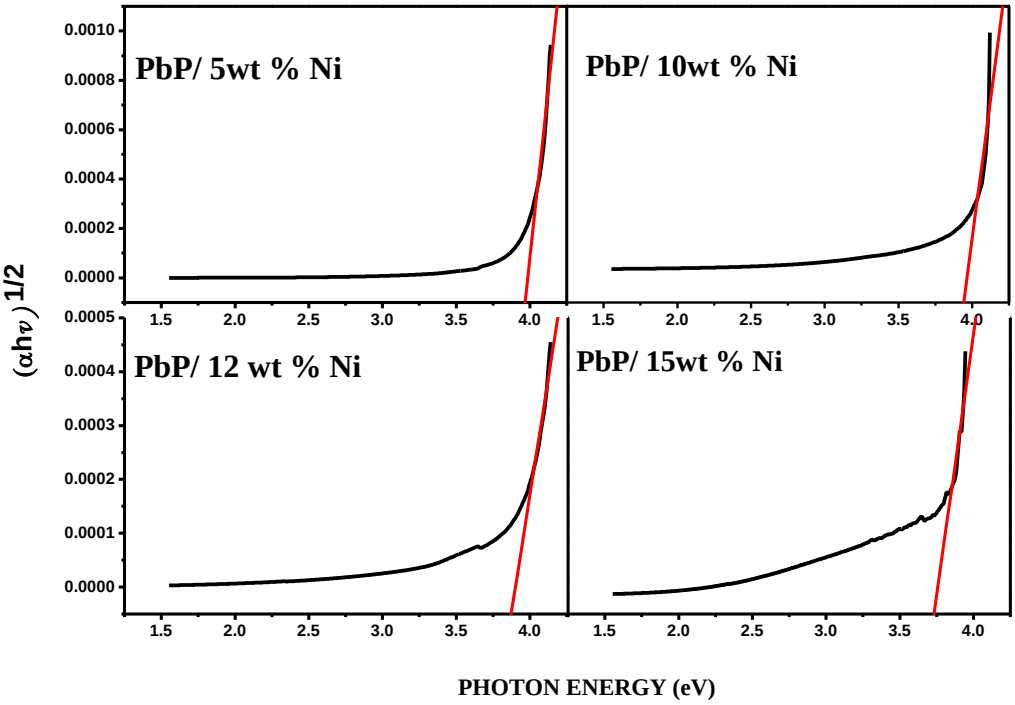

Figure VII- 12 : $(\alpha h\nu)^{1/2}$ versus energy plot for Tauc gap extraction for PbP/Ni nanocomposite films.

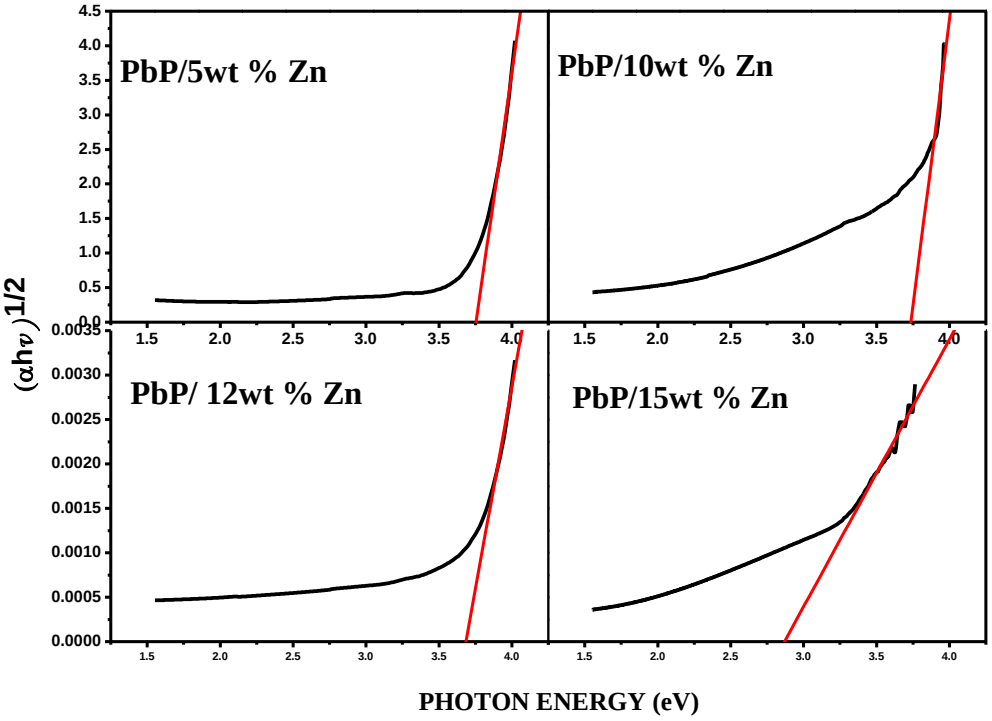

Figure VII- 13 : $(\alpha h\nu)^{1/2}$ versus energy plot for Tauc gap extraction for PbP/Zn nanocomposite films.

Table VII- 1: The optical parameters like thickness, band gaps, correlation coefficients, Tauc slopes and Urbach energy of PbP/metals nanocomposite films.

PbP/(metallic fillers thin Film (wt.%)	Thickness (nm)	band gap (eV)	Power factor (n)	Tauc slope $(eV.cm^1)^{1/n}$	Correlation coefficient R^2	Band gap (eV)	Tauc slope $(eV.cm^1)^{1/n}$	Correlation coefficient R^2	Urbach energy (eV)
		Parameters obtained by Eq. (VII-8)				Verified parameters Eq. (VII-7)			
PbP unloaded	534	3.73	2.68	$48.87.E^7$	0.99	3.75	$20.3 .E^7$	0.96	0.2
PbP/Cr(II)									
5	691	3.26	2.19	526	0.99	3.28	209	0.99	0.098
10	759	3.22	2.035	136	0.91	3.12	201	0.98	0.13
12	899	3.20	2.035	136.68	0.91	2.98	201	O.99	0.25
15	911	2.28	2.00	23.61	0.99	2.32	203	0.99	0.34
PbP/Co(II)									
5	750	3.06	1.25	0.087	0.91	3.17	208	0.99	0.12
10	771	2.94	2.00	0.078	0.99	2.92	206	0.98	0.4
12	835	2.83	1.16	0.036	0.98	2.65	205	0.97	0.43
15	895	2.71	2.36	0.025	0.98	2.38	200	0.92	0.46
PbP/Ni(II)									
5	659	3.28	2	0.03	0.99	3.15	208	0.94	0.065
10	796	2.99	1.86	0.0187	0.98	2.86	200	0.98	0.07
12	810	2.98	1.93	0.0136	0.98	2.19	202	0.99	0.15
15	921	2.13	2.08	0.181	0.98	2.09	199	0.98	0.31
PbP/Zn(II)									
5	600	3.41	2.08	27.52	0.98	3.39	208	0.96	0.035
10	787	3.17	2.06	0.052	0.96	3.11	200	0.98	0.073
12	874	2.69	2.02	0.783	0.99	2.74	24	0.98	0.26
15	921	2.28	1.98	0.0974	0.96	2.22	21	0.98	0.51

The optical energy gap was estimated from the absorption coefficient values using Tauc's procedure. It was found that the obtained optical gap is high for neat phosphate glass thin film, it exhibits a band gap value of 3.73ev (table VI-1). It is optically transparent and this means that no absorption of charge carriers was done, because they cannot be excited across such wide band gap. However, the bad gap Eg shifts towards lower values with the rise of metal concentrations, attaining a minimal value of 2.13eV for the glass thin film loaded with 15wt % Ni . These obtained results of indirect optical energy gap (Eg) are consistent with those found in some literature works [412,413, 414]. Also, the optical band gap values are close to the band gap obtained with spin coated on chalcogenide glass, as reported in previous studies [415], which evidenced that the investigated chalcogenide glasses can be regarded as amorphous semiconductors since their band –gap can range between 1eV and 3eV. Thus in our case this shift is an expected behavior [416]. The obtained results are in good agreement with other previous works [417,418].

The Tauc's slope B of energy band gap decreases steadily from $48.87*10^9$ $(eV.cm^{-1})^{1/2}$ for pure lead phosphate glass matrix to much more lower values for the four sets of composites (Table

VII-1). This behavior seems to be related to the number of the free carriers increase with metallic concentration. Indeed, the addition of metallic nanoparticles leads to a formation of crystallized clusters inside the amorphous matrix as shown by XRD patterns in chapter VI. This seems to have prominent effect on electronic conduction of the composite's thin films. It seems that the effect of growing crystal structure by addition of metallic filler even at ambient temperature, increases lattice quantized vibrations, growing the life and density of the phonons. The phonons are always present in solid at high or low density, depending on its lattice-quantized vibrations. In amorphous solid phonon's effect is vanished by diffusion. However, in the metal particles - periodic structure to a long distance, such the present case, their energy becomes not negligible and they can be absorbed and contribute to the transition. Their exchange with electrons becomes therefore pertinent, allowing indirect interband transitions. Moreover, for such behavior can take place, the electrons must exchange their energy with photons and their momentum with phonons [408]. Elsewhere, it was evidenced that there is no selection rule for electronic transitions in an indirect gap, unlike the direct gap where the selected rule is the conservation of the momentum. Thus, when the energy of the photon reaches the energy of the direct gap, the absorption will rather be dominated by the direct transitions more than the indirect transitions, since the latter involves a three-particle process: electron, photon and phonon for the conservation of lattice momentum. Therefore, the indirect transitions process can be occurred in two-steps: absorption of energy by the absorption of a photon, followed by the conservation of momentum by emission or absorption of a phonon [408]. Therefore, it seems that the contribution of phonon is important in lead phosphate glass/ fillers nanocomposites with favorited indirect transition of the studied nanocomposites thin films. Similar behavior was observed elsewhere [419].

VII.2.4.2 Urbach energy

VII.2.4.2.1 Reminders about energy bands in amorphous materials

Many authors have focused on describing the distribution functions of energy states (Eg) in energy bands. We mention works done by Mott et al [420] as well as those of Spear et al. [421]. The energy separating the valence band and the conduction band is respectively, denoted by Ev and Ec. The difference (Ec – Ev) corresponds to the energy of the forbidden band. The appearance of the distribution functions of energy states is represented in Figure VII-14.

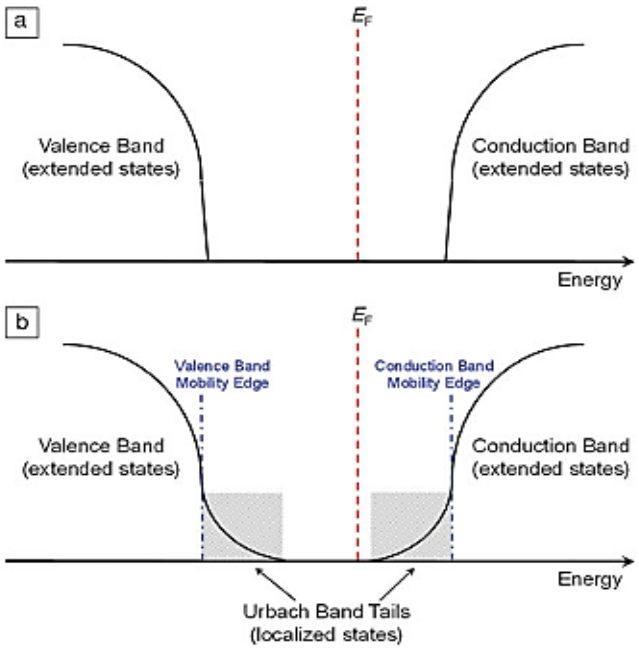

Figure VII- 14 : Schematic illustration of bands allowed electron energy levels and their occupancy in (a) a crystalline semiconductor, and (b) an amorphous semiconductor, illustrating urbach band tails and the mobility edge [422].

When variations of interatomic distances lengths or angles of connection occur in a material, it appears what is called a "disorder". In this case, the band edges described in the case of crystalline solids and delimited by Ev and Ec may disappear. We observe localized states formed at boundaries of the forbidden band in the valence and conduction band.

VII.2.4.2.2 Determination of urbach energy

An important parameter, which characterizes the disorder in the material, is called the Urbach energy. It characterizes the disorder or defects in poor crystalline or predominantly amorphous solid. It is measured as width of exponential band tail energy of localized states, near band edges [23].

These exponential tails are mainly formed by structural disorder or defects, which produce localized states extended in the band gap. It is possible to deduce Urbach energy from the variation of the absorption coefficients.

In fact, the absorption coefficient is linked to the disorder by the law [424]:

$$\alpha = \alpha_o exp\ (h\nu / E_U) \qquad \textbf{(VII-9)}$$

Where α_o is a constant, h is the Planck's constant, ν is the frequency of absorption and E_u denotes the width of band tail or Urbach energy, which is weakly dependent upon temperature and is often interpreted as the width of the band tail due to localized states. This is associated with disordered or low crystalline materials.

Taking the logarithm of the two sides of the last equation, one can get a straight-line equation. It is given as follows:

$$ln\alpha = ln\ \alpha_o + (h\nu / E_U) \qquad \textbf{(VII-10)}$$

Therefore, the band tail energy or Urbach energy (E_U) can be obtained from the slope of the straight line of ln (α) against the incident photon energy (hν).

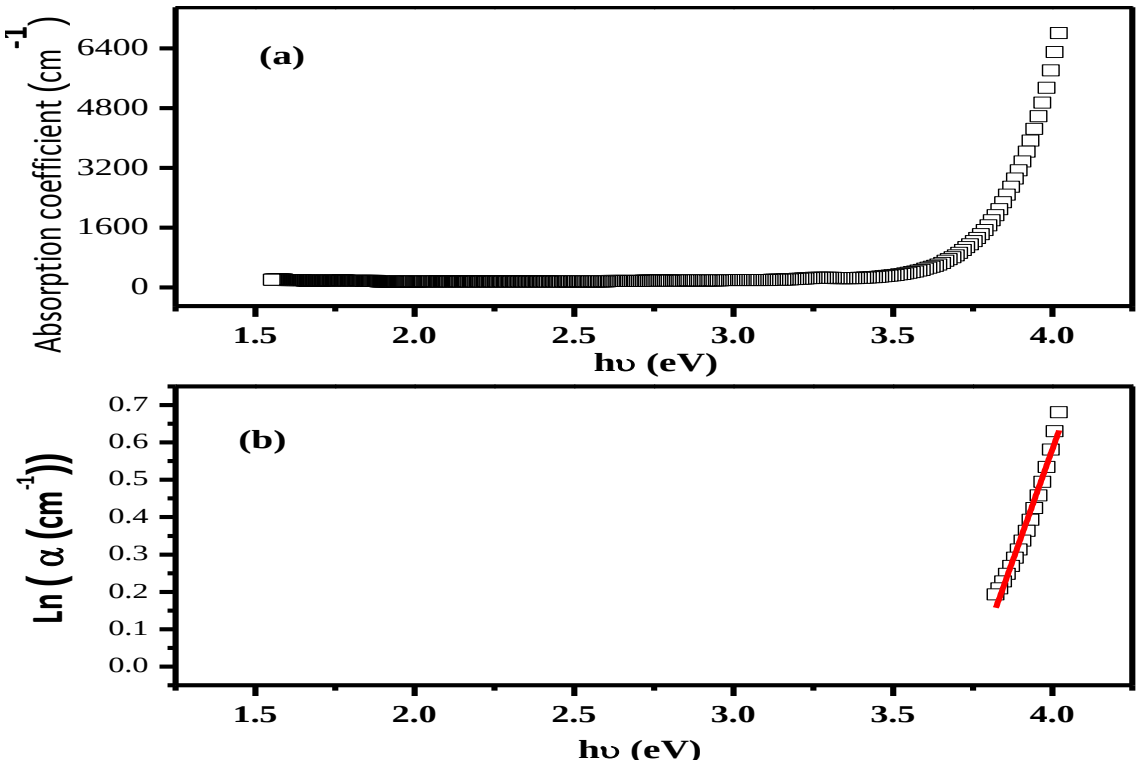

Figure VII- 15 : (a) Absorption coefficient (α) versus photon energy (hν) of unloaded PbP film. (b) Determination of Urbach energy using ln(α) as function of photon energy (hν) for unloaded PbP film.

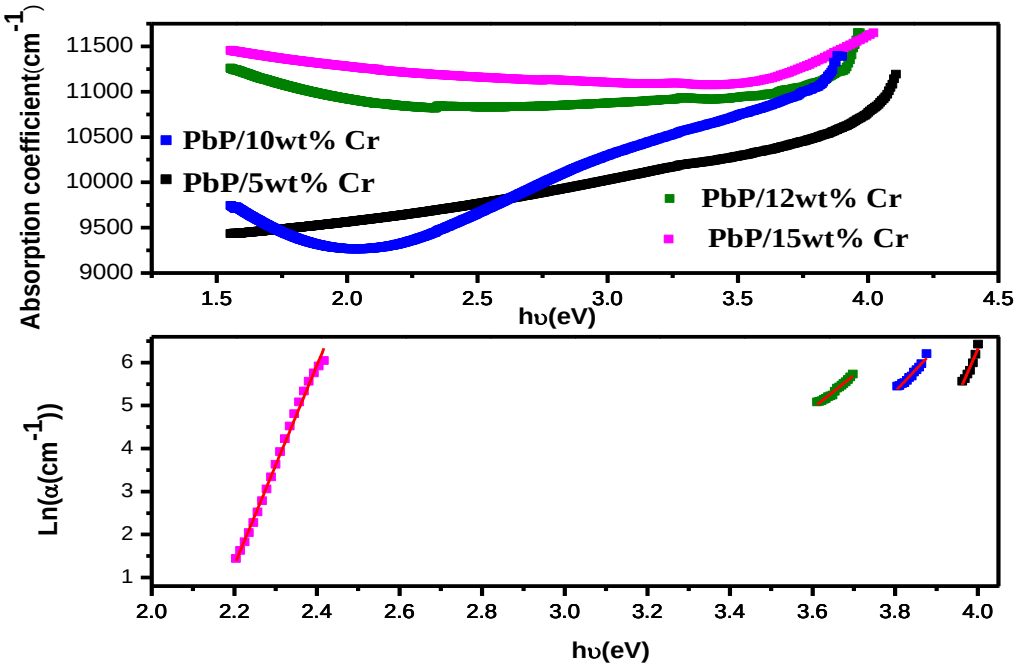

Figure VII- 16 : (a) Absorption coefficient (α) versus photon energy (hν) of PbP/Cr composite films. (b) Determination of Urbach energy using ln(α) as function of photon energy (hν) for PbP/Cr composite films.

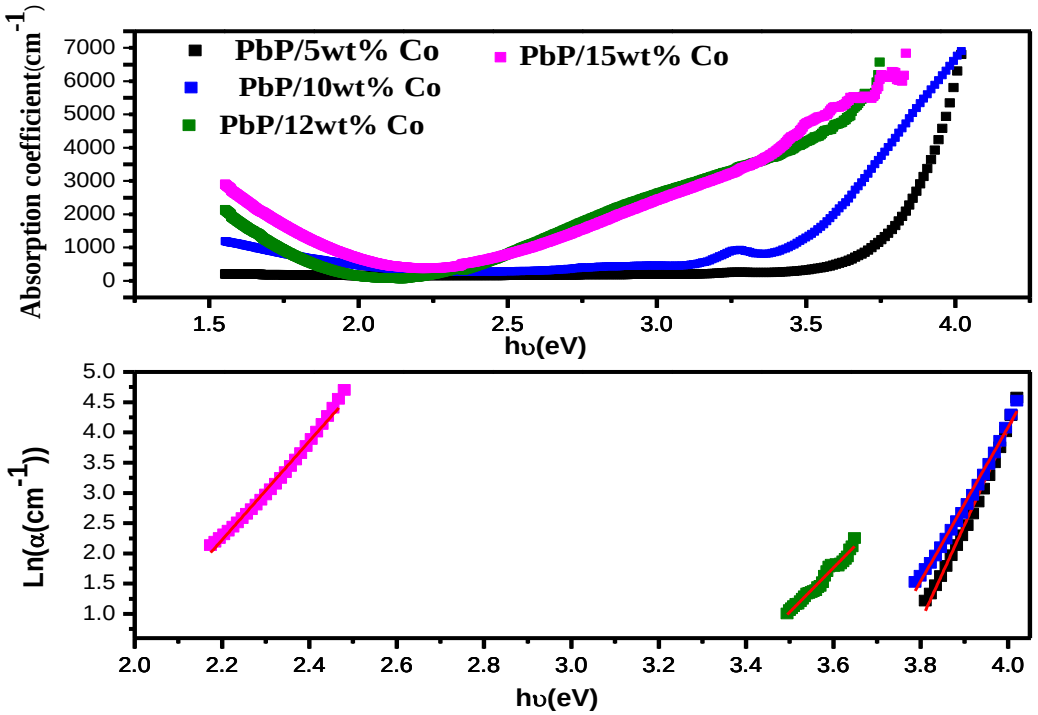

Figure VII- 17 : (a) Absorption coefficient (α) versus photon energy (hν) of PbP/Co composite films. (b) Determination of Urbach energy using ln (α) as function of photon energy (hν) for PbP/Co composite films.

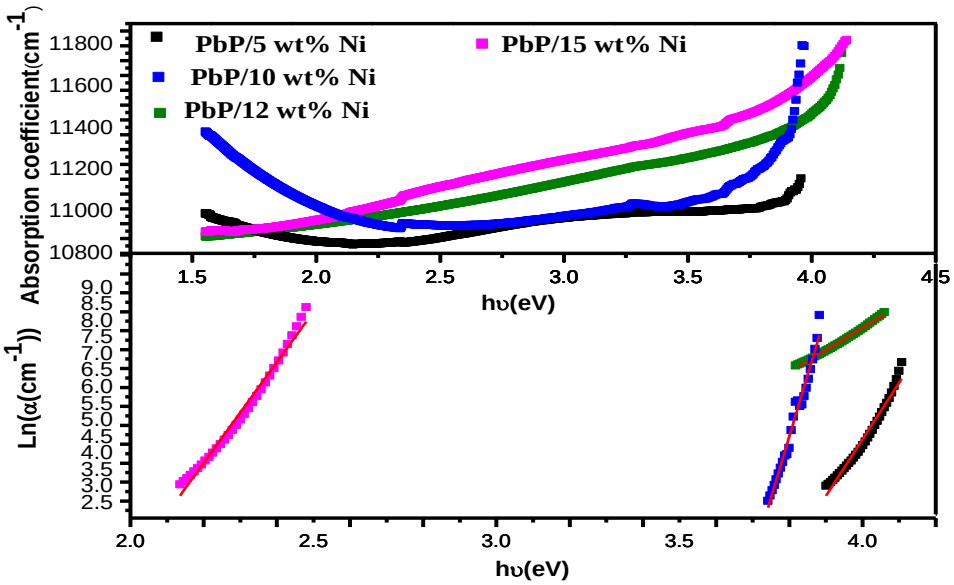

Figure VII- 18 : (a) Absorption coefficient (α) versus photon energy (hν) of PbP/Nicomposite films. (b) Determination of Urbach energy using ln (α) as function of photon energy (hν) for PbP/Ni composite films.

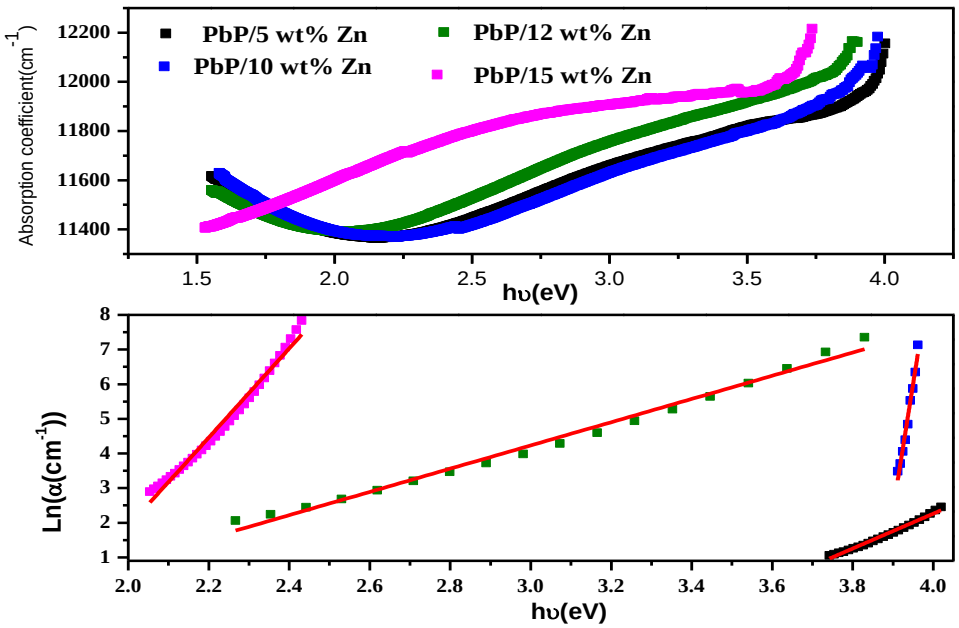

Figure VII- 19 : (a)) Absorption coefficient (α) versus photon energy (hν) of PbP/Zn composite films. (b) Determination of Urbach energy using ln (α) as function of photon energy (hν) for PbP/Zn composite films.

One can note that, the value of absorption coefficient depends on the filler fraction. This behavior is attributed to the absorbing nature of metallic particles. Thus, Urbach energy is tightly related on the absorption coefficient (Eq. (VII-9)).

The value of Urbach energy varies in the range [0.065 to 0.51ev]. The obtained values in our study are comparable to those found by Fayek et al. [425]. They have interpreted Urbach energy as being the width of the bands of located states inside the width of the forbidden band.

The Urbach energy E_u manifests increase, while E_g decreases from 3.68 (almost without tailing) to 1.32 eV when the conducting particles amount rises (see Table VII-1). The observed variation in E_u indicates that the addition of metallic fillers creates some local structural order inside the phosphate glass matrix. This finding is presumably in good agreement with X-ray analysis, showing some crystallizations. Indeed, the PbP/metal nanocomposites consist of a heterogeneous binary system formed of an amorphous lead phosphate glass and a crystallized phase. The disorder is characterized by the tail width of valence or conduction band, the optical gap is the energy gap between the tails of bands. Thus, an increase in disorder with the rise in weight fraction of metal, is accompanied by a decrease in the optical gap. The increase of Urbach energy comes opposite to the narrowing of the optical band gaps with the rise in weight fraction of metal particles as shown in Figure VII-20:(a), Figure VII-21:(a), Figure VII-22:(a), Figure VII-23:(a) and Figure VII-24:(a). It is clear that the Urbach energy is coherent with the determined values of band gap energy (Figure VII-20:(b),) Figure VII-20:(b),) Figure VII-20:(b) and Figure VII-20:(b)). Such behavior was firstly observed by our equip on epoxy/Ag nanocomposites [408].

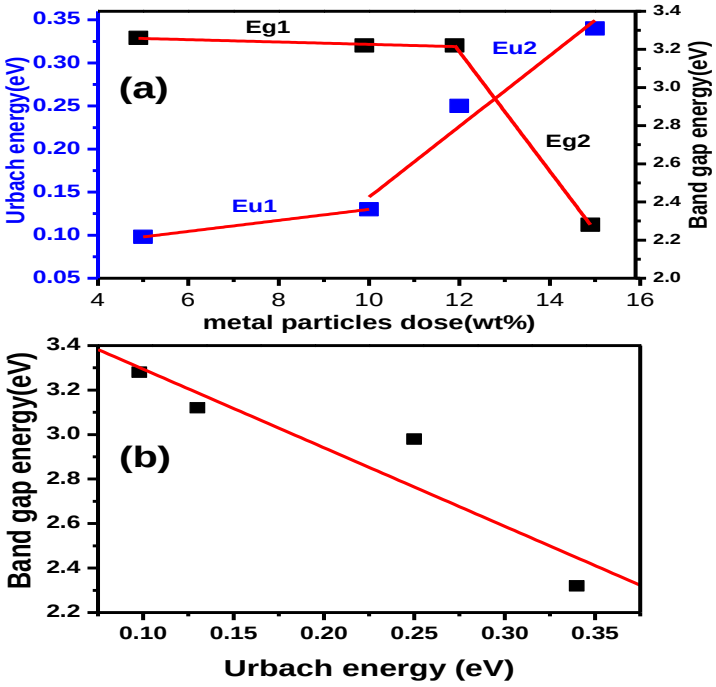

Figure VII- 20 : (a) Variation of band gap and Urbach energy of glass/Cr nanocomposite films versus fillers content (b) Band gap energy versus Urbach energy of PbP/Cr nanocomposite films. The solid line serves as a guide to the eyes.

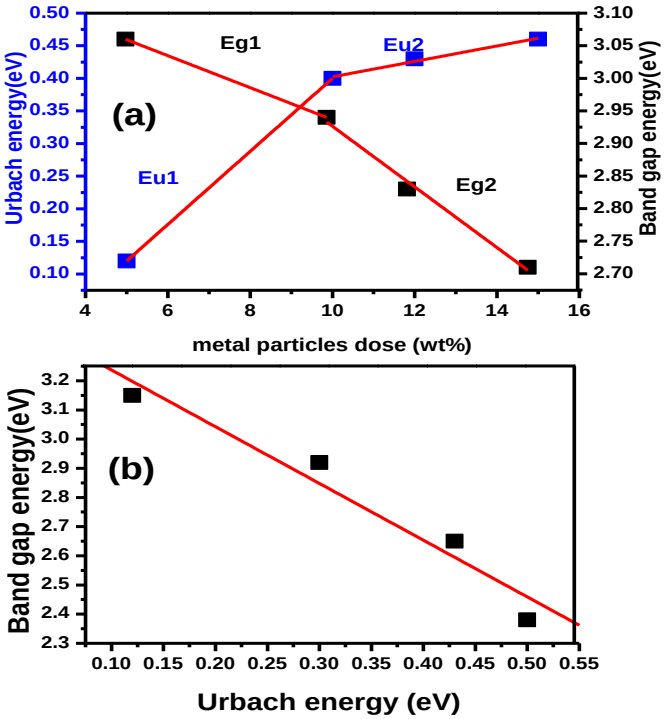

Figure VII- 21 : (a) Variation of band gap and Urbach energy of glass/Co nanocomposite films versus fillers content (b) Band gap energy versus Urbach energy of PbP /Co nanocomposite films. The solid line serves as a guide to the eyes.

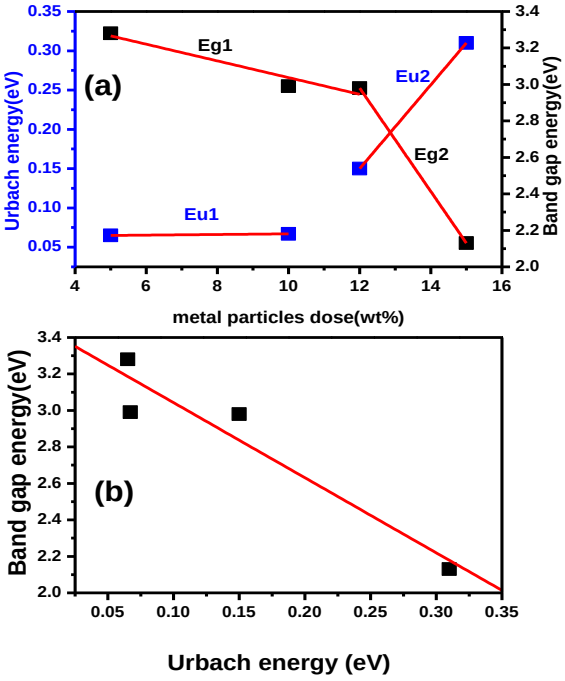

Figure VII- 22 : (a) Variation of band gap and Urbach energy of glass/Ni nanocomposite films versus fillers content (b) Band gap energy versus Urbach energy of PbP/Ni nanocomposite films. The solid line serves as a guide to the eyes.

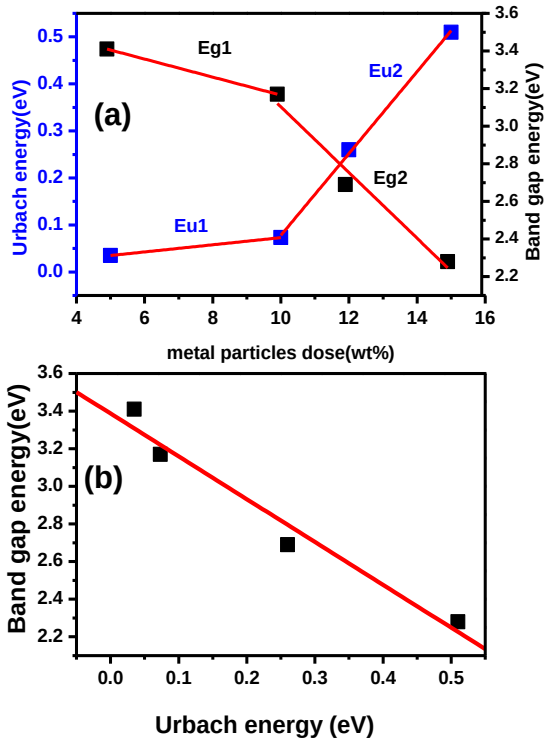

Figure VII- 23 : (a) Variation of band gap and Urbach energy of glass/Zn nanocomposite films versus fillers content (b) Band gap energy versus Urbach energy of PbP/Zn nanocomposite films. The solid line serves as a guide to the eyes.

VII.3 Thickness determination from optical transmittance

Thickness of the obtained films has been measured by optical interference methods, these later were used elsewhere [426, 427]:

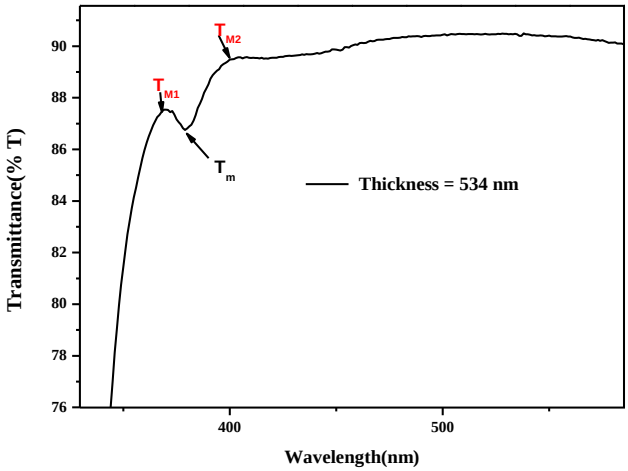

Figure VII- 24 : Optical transmittance spectrum of thin film illustrating parameters to be considered for the calculation of thickness of thin films.

In fact, in the case of a relatively thick and smooth layer, multiple reflections of the light take place between the lower surface in contact with the substrate and the free surface of the layer. This leads to the transmission spectrum containing interference fringes with minima and maxima as a function of the wavelength. Let us consider wavelengths (λ_1 and λ_2) related to two consecutive transmission maxima (T_{M1} and T_{M2}) and Tm the transmission of the minima between the two maxima (see figure VII-24). The thickness of the obtained layers is determined from the following relation [428]:

$$d = \lambda_1\lambda_2 \Big/ 2\left(\lambda_1 n_2 - \lambda_2 n_1\right) \qquad \textbf{(VII-11)}$$

n_1 and n_2 are the refractive index of the layer for the wavelengths λ_1 and λ_2 respectively. The index n_1 and n_2 are derived from the relationship [429]:

$$n_{12} = [N + (N^2 - S^2)^{(1/2)}]^{(1/2)} \qquad \textbf{(VII-12)}$$

Where, S is the refractive index of the glass substrate and $N_{1,2}$ can be calculated using the relation:

$$N_{1,2} = 2S.[(T_M - T_m)/(T_M.T_m)] + (S^2 + 1)/2 \qquad \textbf{(VII-13)}$$

The obtained results are given in Table VII-1. As can be seen that the fillers loading might be influencing the growth rates of thin films. Also, this may result in a slight increase in film thickness as the metallic fillers content increased.

VII.4 Refractive index

It is important to remind that, in given relation VII-5, the real part index n is given by $n = c/v$, it is a measure of the propagation speed of light in medium by defining the ration of velocity c of light in free medium to the velocity v. Its dependence on wavelength is at the origin of dispersion phenomena and usually given by Cauchy's law. The imaginary part κ; extinction coefficient, characterizes the absorption. It is important to note that the anisotropic effects are not considered in this work. Thus, we used the mean values.

The optical constants can be determined from the UV-Visible transmittance spectra, using the approximate method ($n >> \kappa$) of Manifacier and Swanepo [426, 427]. Thus, the refractive index n of the film is determined by equation (VII-12). The refractive index values are compiled in Table VII- 2, it is slightly increasing with increasing fillers content. Indeed, it was shown in chapter III

that the density of the composite increases linearly with filler enhancement. This densification slows down the propagation of light by lowering its speed and therefore increases the refractive index.

Table VII- 2 : Refractive index of different loaded thin films.

Sample	Refractive index			
$PbO-P_2O_5$(unloaded)	2.17			
loaded thin films	5wt %	10wt%	12wt %	15wt %
PbP/Cr	2.23	2.28	2.31	2.32
PbP/Co	2.23	2.24	2.25	2.40
PbP/Ni	2.17	2.18	2.19	2.22
PbP/Zn	2.21	2.22	2.23	2.43

However, refractive index remains relatively low, ranging from 2.17 to 2.43.

Elsewhere, the porosity of thin films is estimated from the following equation [430]:

$$Porosity = \left(1 - \frac{n^2 - 1}{n^2{}_D - 1}\right).100(\%) \qquad \textbf{(VII-15)}$$

Where n_D is the refractive index of pore-free lead phosphate glass and n is the refractive index of the porous thin films.

From this equation, we can assume the relationship between the refractive index and the porosity. Mathematically, low porosity led to the increase of n. Thus, in order to have remarkably higher refractive indexes, our films must be highly densified.

Note that the high absorption coefficient and the relatively low refractive index are two main criteria that make these materials good candidates for the realization of solar cells [30].

VII.5 Electrical properties of loaded phosphate glass thin films

In forementioned figures (from Figure VII-20 to Figure VII-23) the whole curves exhibit a prominent change in the slope at a specific threshold related to glass/ metal composite film for both Urbach energy and optical band gap. The decrease of Eg and increase of Eu becomes faster above this threshold. It seems that this behavior is related to the percolation transition. In order to assess this behavior, it will be more convenient to measure the DC conductivity at ambient temperature versus fillers loading variation.

VII.5.1 DC conductivity measurements at ambient temperature

The DC conductivity is based on resistivity measurements. Studies of the electrical resistivity measurement by two-point probe method [431] were carried out within room temperature. Note that the resistivity represents its ability to oppose the flow of electric current. It is expressed in [Ω.cm]. The electrical Resistivity measurements at ambient temperature are performed through plotting current-voltage characteristics (I=f (V)), as showed in figure VII-25:

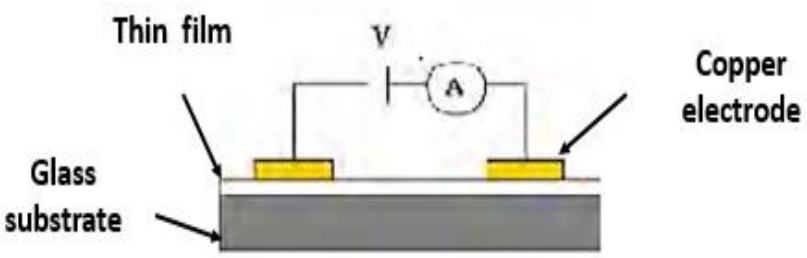

Figure VII- 25: Experimental device for measuring current-voltage characteristics.

Current-voltage characteristics curves are exploited to extract the resistance from the slope of the linear curve. Note that the two-point measurement method was used to measure the electrical conductivity, as well as the variation of the electrical conductivity and the activation energy as a function of the annealing temperature (See next section).

The loading process of thin films may play a role in decreasing the electrical resistivity values; thus, it was suitable to measure the sheet resistance. Firstly, we have measured the electrical resistance of the deposited material. Then knowing its dimensions, the calculation of sheet resistance can be easily performed using the following formula [432]

$$R_{sh} = R.W/L \qquad \textbf{(VII-16)}$$

$\mathbf{R = \rho.\frac{L}{A} = \rho.\frac{L}{d.W} = \frac{\rho}{d}.\frac{L}{W} = Rs.\frac{L}{W}}$ Where ρ : resistivity (Ω.cm), Rs=ρ/d: electrical sheet resistance (Ω.cm), w: width (cm), d: thickness (cm) which can be determined with optical measurements, L: length (cm).

And the conductivity is given by $\sigma=1/\rho$ $(\Omega.cm)^{-1}$.

The curves of DC conductivity behavior versus metallic fillers concentrations are represented in figure VII-26:

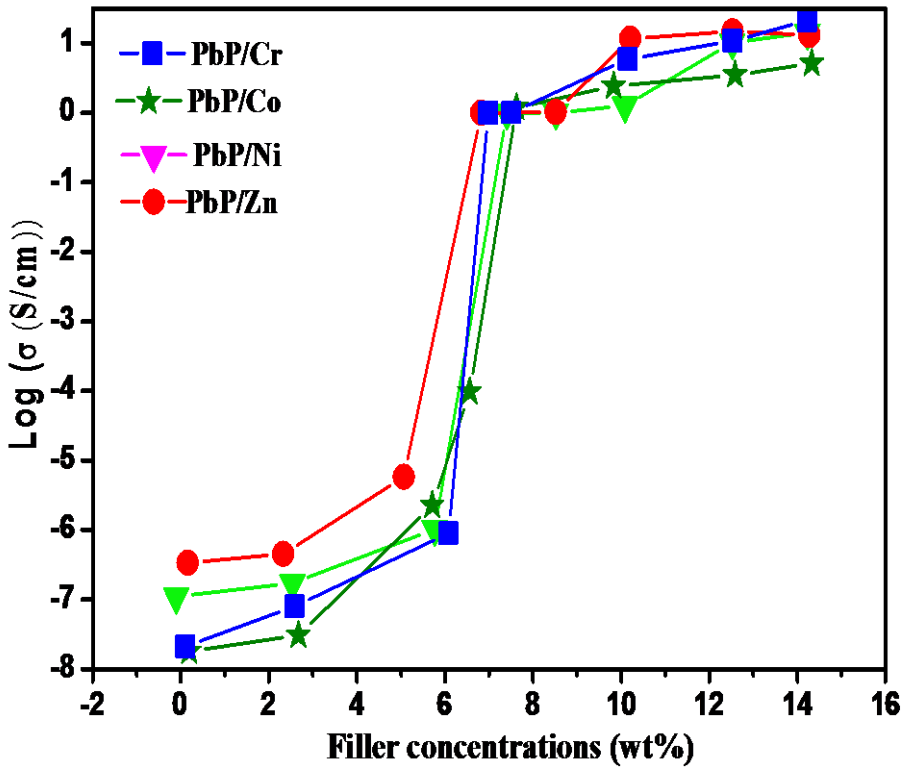

Figure VII- 26: Electronic conductivity of loaded lead phosphate glass thin films versus conducting particles concentrations.

According to figureVII-26, it is worthy to note that electrical conductivity of unloaded thin film is of the order of 10^{-7} $(\Omega.cm)^{-1}$. It is nonlinearly enhanced when the concentration of metal transition particles is elevated. Typical curve shapes are obtained for thin films loaded with chromium, cobalt, nickel and Zinc particles. The studied thin films exhibit a sharp electrical conductivity transition at critical concentration (around 6wt%). Thus, the conductivity is found to be expressing percolating behavior; this is quite similar to the previously examined conductivity behavior of bulk composites (chapter V).

Like in the case of bulk composites, this behavior is more likely attributed to percolative phenomenon. Indeed, above the percolation threshold, the composites become semiconductor and their number of carriers increases significantly. Therefore, the gap must drop significantly, in good agreement with Burstein -Moss theory [433,434].

VII.5.2 Correlation of electrical findings with optical, structural and morphological properties

Optical transmission spectra of thin films were plotted in the spectral range of 300-800nm. It was found that the determined optical gap decreases with increasing fillers concentration.

The minimal band gap value is achieved at the highest loading level for all the elaborated thin films.However, even at elevated fillers concentrations,the films are still retaining relatively transparent quality (T% ≈ 40%).

These results are in good agreement with the electrical conductivity curves, which are increasing progressively as a function of the fillers concentration,they express sharp and sudden increase of 7 orders of magnitudes at critical fillers concentrations . The enhanced electrical conductivity is probably due to the increase in free carriers within the insulator glass films. In this case, the free charge carriers contribute to the increase of the mobility and thus give arise to electrical conductivity of nanocomposite thin films. After examining the structural, morphological (in chapter VI), optical and electrical properties of the elaborated nanocomposites thin films, it should be concluded that all the fndings are perfectly corroborating.

VII.5.3 Evaluation of Thin films performance through the calculation of Figure of merit

The optical and electrical properties of thin films are very important features for all known transparent conducting oxides (TCO) applications. Ideally, a good TCO is recognized by optical transmission factors as well as high electrical conductivity.This later is directly related to one of the most characteristic of transparent conductor thin films, which is the charge carrier mobility. Thus, the material is considered as performant when both, the optical transmission and electrical conductivity are important. These two parameters are inversely dependent and linked by a single factor called figure of merit (FOM).Figure of merit allows reasonable comparison of thin films properties and permits to estimate their opto-electrical performance [435].

Researchers have developed several methods for determining the figures of merit of the elaborated thin films. Fraser and Cook have set earliest equations [436].In order to measure the thin films performance the following equation is expressed :

$$F_{FC} = \frac{T}{R_S} \qquad \textbf{(VII-17)}$$

Where T is the transmission and Rs is the sheet resistance of the thin film.

Haacke has developed another equation defining strategy of the figure of merit calculation. It is noted FH [437]. It is also linked to the above-mentioned relation. However, FH puts more emphasis on the optical transparency because FFC was too much in favor of sheet resistance, resulting in a maximum figure of merit at relatively large film thicknesses. The figure of merit was redefined as:

$$F_H = \frac{T_a^x}{R_s} \qquad \textbf{(VII-18)}$$

Where x > 1 , Haacke's definition is also thickness dependent.

Iles and Soclof established the third definition for figure of merit. It is independent of film thickness and is given by [438].

$$F_{Is} = R_S\left[1-T\right] = \frac{\alpha}{\sigma} \qquad \textbf{(VII-19)}$$

The inverse of the sheet resistance and the visible absorption coefficient allow the identification of the figure of merit.

By this definition, a low value of figure of merit indicates films of better quality.

The studied thin films represent a compromise between electrical conductivity and optical transmission. Reduction of resistivity involves either increase in the carrier concentration or in their mobility. Increasing the number of carriers leads to an increase in the absorption, while increasing the mobility has no negative effects on the figure of merit.

In our case, the quality of the elaborated thin films can be compared by calculating the figure of merit, using following equation [438]:

$$\frac{\sigma}{\alpha} = \frac{1}{\rho\alpha} = \left(\frac{1}{R_{Sh}\ln\left(T+R\right)}\right) \qquad \textbf{(VII-19')}$$

Where

σ [Ω^{-1}]: electric conductivity

α [cm^{-1}]: absorption coefficient

R_{Sh} [Ω] = $\frac{\rho}{d}$: sheet resistance

T [%] : Total transmission

R [%] : totale reflexion

Here, the best figure of merit is related to good optical transmission and electrical conductivity.

The above relationship expressing the figure of merit is practically the inverse of relation (VII-19) and both are approximate because they assume very low absorption and high conductivity. That spurred us to find a compromise. It has been shown that, useful thin films must have FOM greater than or equal to 7 [39, 40].

Thus, taking into account relationship (VII-19'), the variation of determined FOM values of the studied thin films as a function of fillers concentration is plotted in the inset of Figure VII-27. We noted an enhancement of figure of merit values by increasing loading concentration.

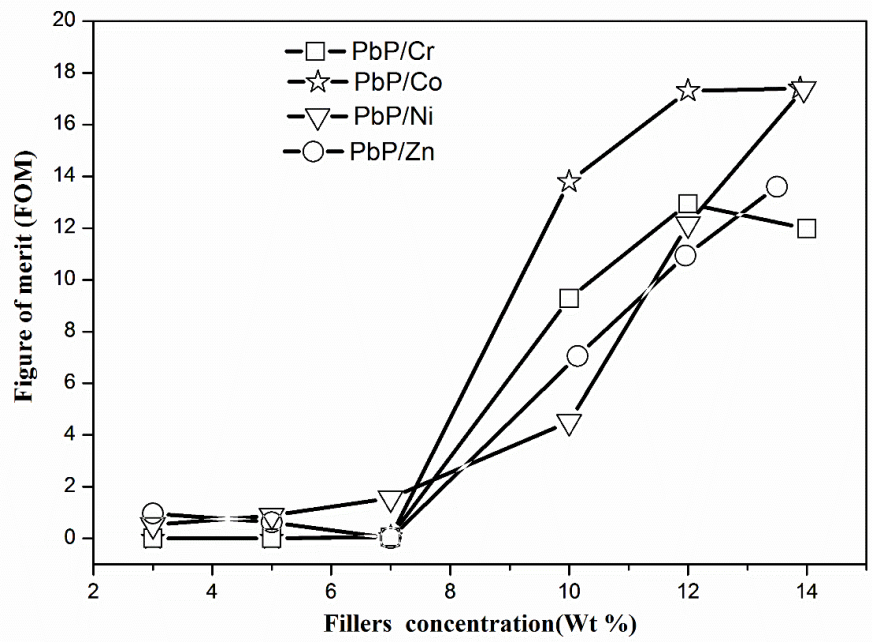

Figure VII- 27 : *Variation of optical figure of merit versus metal particles concentration.*

Electrical conductivity presents a particular interest of semiconductor materials. Measuring the electrical conductivity of semiconducting thin films is a rather difficult problem, since it depends upon a series of factors whose actions cannot be separated, especially the temperature.

VII.6 Temperature dependent conductivity of glass composites thin films

The goal of this section is to present some experimental results related to the electrical conductivity dependence of loaded phosphate glass in thin film shape versus temperature.

The characterizations of the studied thin films were performed by determining temperature dependent dc conductivities through measuring electrical resistance of thin films with fixed concentration (we have chosen 6wt %)versus varying temperatures from 300 to 500K. Note that the current–voltage (I–V) measurements were performed on samples placed in the dark.

Schematically, The plots of Lnσ as a function of reciprocal absolute temperature (1000/T) take linear behaviors with slope changes at specific point as shown in FigureVII-28.

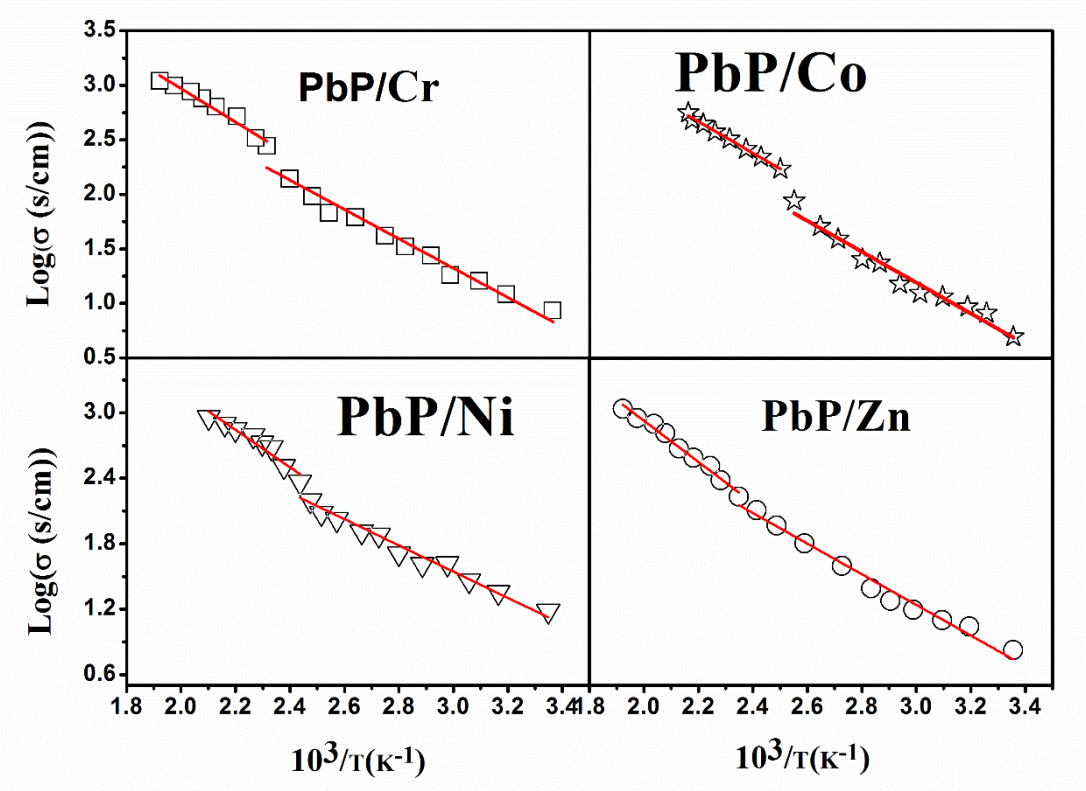

Figure VII- 28 : Plot of Lnσ versus 1000/T of loaded glass thin films.

The variation of Lnσ with reciprocal temperature exhibits two main linear parts. It is noteworthy that the slop changes did not occur at the same temperature for all samples. Thus, the slope change cannot be assigned to any change of structure, in a good consistence with the early XRD patterns, it is rather due to two different mechanisms of conduction.

The mechanism of amorphous semiconductor films is complex and depends on several parameters; such as the contribution of localized states in tail of bands or near the Fermi-level [441, 442] and the glass composition [443, 444].

Thus, at high temperature, the conduction is thermally stimulated following Arrhenius behavior and at lower temperature, it seems that, the process of this conduction is ensured by hopping of charge carriers in localized states near the Fermi level EF and in the tails of conduction and valence bands, this is corresponding to a transport type of variable range hopping (VRH) mechanism [441, 442]. This process is usually predominant at low temperatures [439]. Elsewhere, activation energy values in the same orders were obtained in similar phosphate materials [443, 444, 445, 446]. It should be mentioned that, DC conductivity behavior versus temperature of the studied thin films is similar to bulk phosphate Pb/metals composites (see, chapter V).

Generally, such variation in electrical conductivity as a function of temperature obeys to arrhenus law which unquestionably characterizes a semiconductor. The conductivity of a semiconductor

increases with temperature increasing. It was shown that increase in conductivity is also explained by the increase of the clusters size with the temperature of the substrate such behavior was revealed in chapter VI. Indeed, we have highlighted the variation in cluster's size as a function of temperature of the substrate.

From these findings, it is possible to express the conductivity of nanocomposites thin films using the following expression:

$$\boldsymbol{\sigma} = \boldsymbol{\sigma}_0 \exp\left(\Delta \mathbf{E} \big/ \mathbf{KT}\right) \qquad \textbf{(VII-20)}$$

σ_0 the pre exponential factor, σ is the DC conductivity, ΔE is activation energy which is expressed as follows :

$$\Delta E = \left(\mathbf{E_C} - \mathbf{E_F}\right) \qquad \textbf{(VII-21)}$$

Where EC defines the mobility edge in the conduction band of the films and EF is the energy of the fermi level.

The modeling of DC conductivity versus the reciprocal of temperature is performed by introducing the logarithm in equation (VII-20) as follow:

$$Ln\sigma = Ln\sigma_0 - \Delta \mathbf{E} \big/ KT \qquad \textbf{(VII-22)}$$

We can see that the activation energy is deduced from the slope of ln σ variation versus the inverse of the measurement temperature.

According to FigureVII-28, electrical conductivity increases with increasing temperature, this behavior indicates that the conductivity is thermally activated.The variation of the activation energy of the electrical conductivity is reported in tableVII-3.

Table VII- 3 : Activation energies obtained by the fit with the Arrhenius ΔE_I and ΔE_{II} attributed to high and low temperature range respectively.

Composites	Slope change temperature Tc(K)	ΔE_I (eV)	ΔE_{II} (eV)
PP/Cr	416	1.53(R^2=0.95)	1.34(R^2=0.96)
PbP/Co	380	1.44(R^2=0.99)	1.41(R^2=0.98)
PbP/Ni	404	1.71(R^2=0.92)	1.20(R^2=0.96)
PbP/Zn	436	1.88(R^2=0.98)	1.40(R^2=0.97)

According to TableVII-3, it is noteworthy that the activation energy provides information on the position of the Fermi level, which is relative to the bottom of the conduction band. The nature of the states involved in transport essentially depends on the position of the Fermi level, which is typically halfway located between the last occupied state and the first empty level as reported

byAdler &Yoffa [447]. In chapter II, we have clearly stated that band structure of amorphous or polycrystalline semiconductors and band structure of crystalline semiconductors are similar. It was noted that,the existing short range in amorphous semiconductors give rise to band-like structure of electron energy states similar to that of crystalline semiconductors.

The maximum value of the activation energies of PP/Cr and PbP/Co samples took values which are less than the half of the optical gap [448,449,450,451].This is indicating that films are of n-type. Whereas the activation energies related to PbP/Ni and PbP/Zn express values greater than the half of the mobility gap assigned to each sample respectively[451].Consequently, they can be useful as p-type thin films[452]. Therefore, these sets of nanostructured thin films are potentially useful in industrial devices, as P-N junctions, etc. Thus, their practical application in materials development for energy sector needs to be carefully considered.

Conclusion

Lead phosphate glass based nanocomposites thin films were investigated on optical and electrical point of view. Thin films showed high transmission property (up to 70%) in the visible wavelength region. The optical band gap was found to be narrowing by higher fillers loading. The best-estimated optical and electrical characterizations are achieved in lead phosphate glass film loaded with metallic fillers around 10 wt %. At this loading rate (10 wt %), the films provide a good figure of merit (FOM). Measurement results of electrical conductivity thin films as function of temperature evidenced semiconducting nature of two conduction mechanisms showing two different sets of activation energy values; thermally activated behavior at high temperature and Variable Range Hoping (VRH) at low temperature. The optical transparency, electrical and thermo-electrical conductivities are intriguing assets that give the investigated thin films optimal opportunities to satisfy the increasing demands on materials applicable in optoelectronics, thermoelectricity and solar cells.

CHAPTER VIII

Potential application of PbP/metals nanocomposites films in energy field

This chapter is divided into three main sections. The first section is devoted to the presentation of solar cells terminologies, the concept of energy conversion and the principle of photovoltaic effect. The second section shows the steps of the realization of photovoltaic cells and their most important parameters. Final section is devoted to the fabrication of P-N junction using the investigated PbP/metals nanocomposites thin films, which are regarded as semiconductor materials, were deposited on glass substrates by low cost chemical bath deposition and used as an absorber layers for solar cell fabrication. Post deposition annealing treatment has been carried out to improve the quality of the thin films, since it is required to form the heterojunction solar cell structure. The configuration of the P-N junction solar cells has been tested in illuminated condition.

VIII.1 Objective

The aim of this section consists of simulating solar cell and determine light intensities that make solar cell work using light emitting diodes [451]. Thus, we have chosen three different colors namely Red, Blue and Green. They are used in order to change the wavelength of the emitted light on the fabricated junction.

VIII.2 Introduction to photovoltaics

One of the major drawbacks of the existing solar cells is that they have limited resources. Thus, there is always necessity to find new solar cell conceptions with lower manufacturing costs. This situation has urged us to fabricate a P-N junction based on our elaborated nanocomposites thin films, which are still in development stage but with promising prospect for the near future. Before any experimental attempt, it is more convenient to define the conversion of solar energy. It is an operation that consists of transforming the photon energy coming from the sun into electrical energy. Thus, it was necessary to implement optoelectronic devices called solar cell in order to execute the mentioned conversion. Therefore, in this section, we will first show the main characteristics of the solar spectrum. Then, we present the main idea on the photovoltaic conversion and the principle of photovoltaic conversion is reminded.

VIII.2.1 Solar spectrum

VIII.2.1.1 What is light?

A light beam is a displacement of small energy-carrying bodies called photons, as described by Einstein in 1905.Afterward, Louis de Broglie highlighted corpuscle-wave in 1924. Light is also described as an electromagnetic wave, like X-rays or radio-frequency waves.

Everything is a matter of wavelength, or frequency, for these oscillations that cross-space and sometimes the material. Each photon carries a quantity of energy directly related to its wavelength [1]451. The Sun emits radiation of electromagnetic type. The white light reaches us in a very short time (it takes on average about 8 minutes and 19 seconds to reach us) because it moves at the speed of light, 299 792 458 m / s.

This radiation constitutes a continuous spectrum ranging from ultraviolet to infrared passing through the visible, which emit the maximum intensity. The observable spectrum from the surface of the Earth is therefore a spectrum of absorption rays. Thus, solar radiation on the Earth's surface includes 5% ultraviolet, 40% of visible light and 55% of infrared.

Solar radiation can be considered as a set of photons, particles which are able to carry a quantity of energy called "quantum of energy" and denoted "ΔE" .The energy of a photon with frequency υ (in Hz) is expressed by the relation:

$$\Delta E = h.\nu = {}^{(h.c)}\!/_{\lambda} \qquad \textbf{(VIII-1)}$$

h denotes the Planck constant, (6.63 * 10^{-34}J/s).

VIII.2.1.2 Solar cell terminologies

VIII.2.1.2.1 Irradiance and Spectral Irradiance

Irradiance is the power of electromagnetic incident radiation per unit area (radiative flux) on a surface and its SI unit is W/m^2. It is also common to consider each frequency in the spectrum discretely. When this is worked out for energy incident on a surface, it is called spectral irradiance, and has SI units W/m^3, or commonly W. m^{-2} nm^{-1}. Spectral irradiance as a function of wavelength is shown in Figure VIII-1.

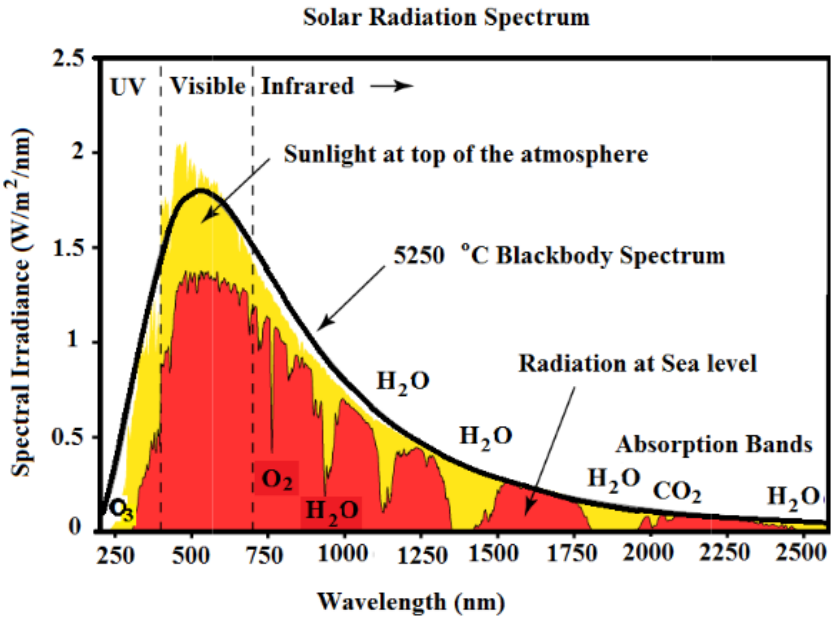

Figure VIII- 1 : Spectral irradiance as a function of wavelength [452].

VIII.2.1.2.2 Solar Constant

The solar constant is nothing but measure of flux density i.e. the amount of incoming solar electromagnetic radiation per unit area which is incident on a perpendicular plane to the rays, at a distance of one astronomical unit (AU). The "solar constant" includes whole solar spectra, not just the visible light. Its recent recalibrated average value is 1.361 kW/m² [452].

VIII.2.1.2.3 Air Mass Coefficient

The air mass coefficient is the ratio of direct optical path length through the earth's atmosphere to the path length perpendicularly upward,i.e at the zenith. The air masse coefficient is commonly used to characterize the performance of solar cells under standardized conditions, and is shown by the syntax "AM" followed by a number and "AM1.5" is collectively worldwide accepted for the testing of solar cells.

$$AM = \left(\frac{L}{L_0}\right) = \frac{1}{\mathrm{Cos}\, Z} \qquad \textbf{(VIII-2)}$$

Where AM is the air mass coefficient, L is the path length through the atmosphere, L_0 is the zenith path length i.e. normal to the earth's atmosphere and Z is the zenith angle.

VIII.2.1.2.4 AM0 (Air Mass index 0)

AM0 means no atmosphere. Mainly solar cells used for space applications are characterized by AM0 and solar intensity is about 1361W/m^2

VIII.2.1.2.5 AM1 (Air Mass Index 1)

The spectrum after travelling through the atmosphere to sea level with the sun directly overhead is referred as "AM1" meaning "one atmosphere AM1 (Z=0°) to AM1.1 (Z=25°) is a useful range for estimating performance of solar cells in equatorial and tropical regions. Its solar intensity varies 1040 to 1020 W/m^2 respectively.

VIII.2.1.2.6 M1.5 (Air Mass Index 1.5)

Solar panels do not generally operate under exactly one atmosphere's thickness i.e. ideal condition. If the sun is at some angle to the Earth's surface, the effective atmospheric thickness changes and is always greater than one atmosphere.1.5 atmosphere thickness is referred as "AM1.5" and corresponding zenith angle and intensity is Z = 48.20, 1000 W/m^2 respectively.

VIII.3 Wavelength and light

VIII.3.1 Principle of Photoelectric conversion

The term "photovoltaics" stands for the physical process of transforming light energy into electrical energy. The prefix Photo comes from the Greek "phos" which means light. "Volt" comes from the surname of Alessandro Volta (1745-1827), physicist who contributed to research on electricity. Photovoltaic (PV) literally means light electricity [453]. Nowadays widely used photovoltaic conversion can be simply defined like transforming photon energy into electrical energy through the absorption process of light by a material.

When a photon is absorbed by the material, it loses a part of its energy by collision with an electron literally tearing it from the material. The electron gains a higher energy level, creating an electrical disequilibrium within the material, which is expressed by an electron-hole pair. Generally, the electron-hole pair returns quickly to equilibrium by transforming its electrical energy into thermal energy [455].

Indeed Most photovoltaic cells use semiconductors to harvest the electron-hole pairs created by the collision of photons in the material. However, according to the used material, the number of

absorbed photons differs. Indeed, each material has its own energy gap (forbidden energy band). Any photon with an energy below this gap and arriving at the surface of the material would be unable to tear an electron off the material even if the collision has occurred. The current produced by a PV cell is therefore much lower than the amount of photons. There are several specific conditions which must be met for the photo-electrical conversion occurs(compatibility of the material with the wavelengths of the solar spectrum, energy of the photons upon their emission on the material, probability of encountering a photon with an electron, incidence of radiation, thickness of material, ...). In addition, the designer of PV cell must be fulfilling another compromise. If the gap of the material is large, few photons will have enough energy to create current but at the terminals of the cell, the open circuit voltage will be large and will further facilitate the exploitation of electrical energy. Conversely, a material with a weak gap absorbs more photons but has a lower voltage at its terminals. Shockley and Quessier [456] quantified this compromise. For instance, with a single material, the yield of theoretical maximum conversion is 31% for an energy gap of about 1.4eV. By comparison, the silicon gap, which is up to date the most used material for cells in terrestrial PV sensors is not very far from this optimum with 1.12eV.Thus, the theoretical maximum for a single Si junction is about 29%. The potential difference occurring at the terminals of a PN junction subjected to an illumination is also measurable between the terminals of the PV cell. Typically, the maximum voltage of a cell (PN) is about 0.5 to 0.8V. It can be directly measured at its terminals without load (open circuit). This voltage is called open circuit voltage (V_{oc}). When the terminals of cells are short-circuited, the maximum current produced by the PV cell can be measured and commonly called short-circuit current (Icc) [457].

VIII.3.2 Basic Physics of Solar cell device

Solar cell is a new and clean way to produce energy. We are therefore interested in the functioning of the cells as well as their performance in order to discover the efficiency of this system. Photocells are semiconductor electronic components, which can develop an electromotive force capable of delivering a current in an external circuit when they are illuminated by solar radiation.

VIII.3.3 Principle of solar cell's function

Cell is the basic building block of a photovoltaic panel. It converts the light energy of photons into electrical energy by photoelectric effect. The general principle of photovoltaic cell operation is described by the diagram in Figure VIII- 2.

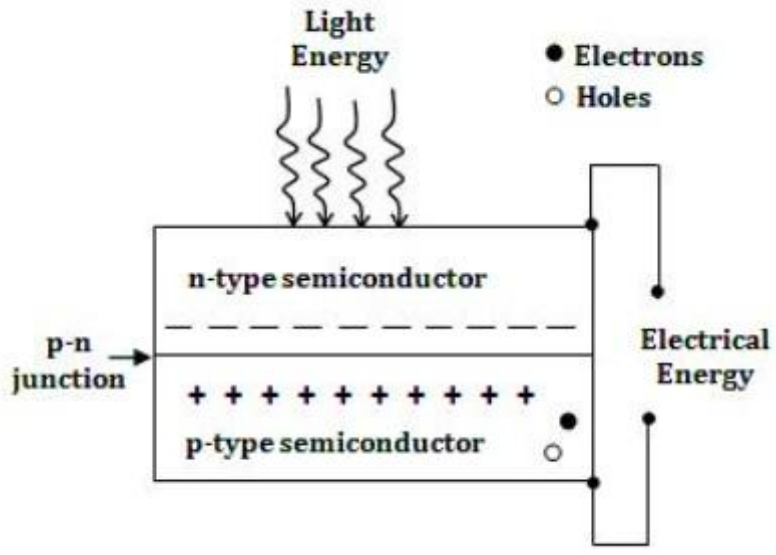

Figure VIII- 2 : Explanatory diagram of the operation of a photovoltaic cell [457].

Conventional devices are generally made of a semiconductor material, which absorbs photons from incident light. A semiconductor consists of a valence band and a conduction band, in which charge carriers, positive (the holes) and negative (the electrons) circulate, respectively. The forbidden band Eg (or gap) is then defined by the energy difference between the top of the valence band Ev and the bottom of the conduction band E_c. When the energy of the incident photons hν is greater than the forbidden band Eg of the semiconductor, an electron of the valence band is excited in the conduction band, which creates a hole: we say that there is photo generation electron-hole pairs.

As a result, the concentration of carriers in the energy bands increases. The energy, which is absorbed in excess with respect to Eg, is lost in the form of heat by de-excitation of the carriers: this is the thermalization process. These photogenesis carriers must then move towards the contacts to be collected in order to generate a current in the connected electrical circuit.

One can create for example such an electric field through P-N homojunction or heterojunction by combining two materials of different natures and types [458,459].

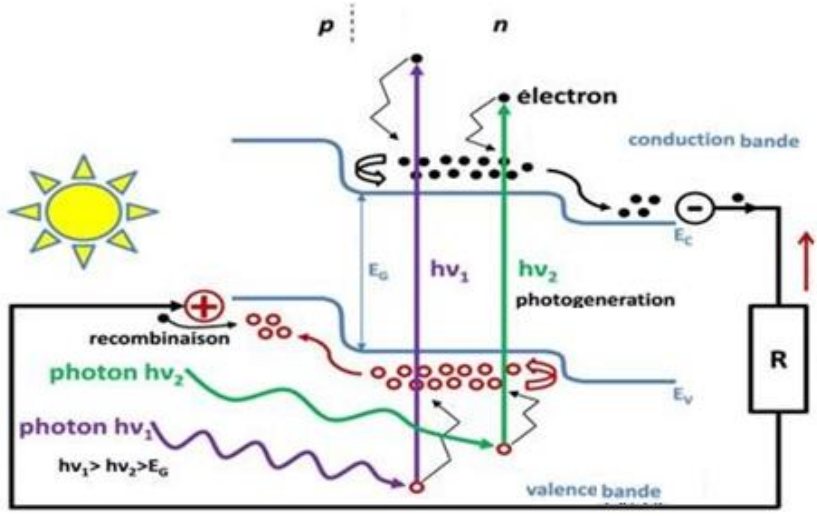

Figure VIII- 3 : Explanatory diagram of a solar cell function [459].

Today, laboratories and industries are working together to develop new concepts or new processes that can improve electrical performance and reduce the costs of solar cells. This is how modern photovoltaic modules, composed of interconnected cells, have largely proven their efficiency and high reliability. In addition, their field of application continues to expand, from pumping to lighting, including all pocket electronic applications. Investigation of numerous materials for solar cell applications led to the development of new and innovative classes of semiconductor devices.

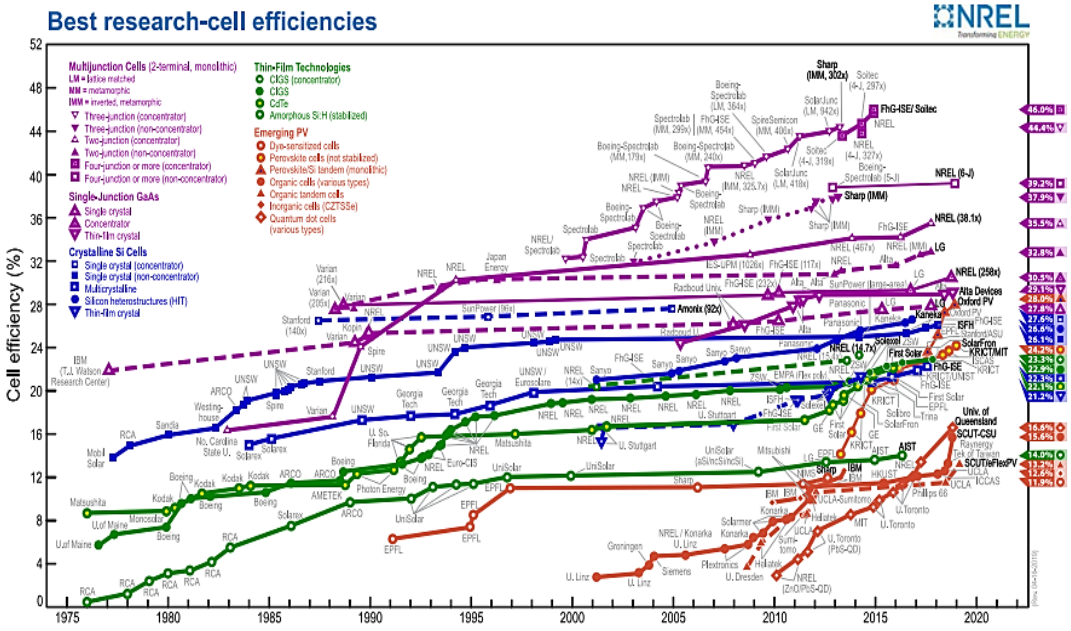

Figure VIII- 4 : Best research-cell efficiencies published by NREL.

FigureVIII- 4 shows the structure of classic cells, which represent almost the entire market today. The first cells are based on crystalline or polycrystalline silicon wafers; they cover approximately 84% of the market. The second is based on thin films structures, firstly based on amorphous silicon (around 5% of the market), then on cadmium telluride (CdTe) whose market share increased from 1% in 2005 to almost 10% in 2009, and finally cells based on copper, indium and gallium diselenide (CIGS), which represent around 1% of the market.

VIII.3.4 Important parameters

The most important technique for characterizing a photovoltaic solar cell is its current-voltage characteristic under illumination I (V). The latter makes it possible to calculate the power supplied by the cell and its conversion yield.

Figure VIII- 5 shows the current-voltage characteristic of a cell. It corresponds to that of a diode shifted by a constant amount corresponding to photo generated current in the cell. This characteristic is described by the short circuit current density (V = 0, I = Isc) and the open circuit voltage (V = Voc, I = 0). The product I * V corresponds to the power density supplied by the cell. This product reaches a maximum at the point (Vmax, Imax).This point is related to the maximum power that can be extracted from the cell. Note that the ratio of this product to the Jsc .Voc product is defined as the form factor (FF)

$$FF = (I_{max}.V_{max}) \Big/ (I_{sc}.V_{oc}) \qquad \textbf{(VIII-3)}$$

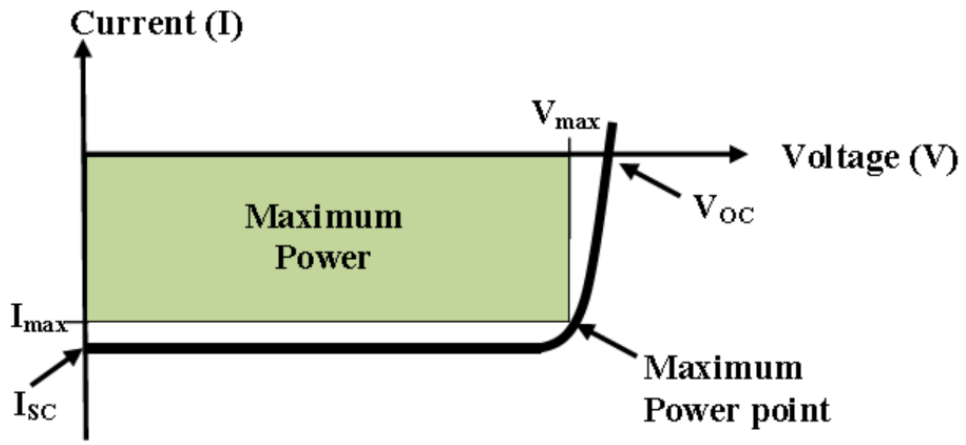

*Figure VIII- 5 : I-V characteristic of p-n junction photovoltaic cell [*462*].*

VIII.3.5 Efficiency of a photovoltaic cell

The efficiency of a cell is quantified by the ratio between the output power and the incident light power. A certain number of losses, which are of optical or electrical origin, can limit the voltage or the current delivered by the cell [460]. A factor of conversion of light energy into electrical energy is given as follow [462]:

$$\eta = \mathbf{P_m} \big/ \mathbf{P_{in}} = I_{\mathbf{m}}.\mathbf{V_m m} \big/ (\mathbf{G.S}) \qquad \textbf{(VIII-4)}$$

Where:

G stands for solar illumination in W / m^2 and S represents surface of the solar cell in m^2.

The yields are then even higher with numerous photo generation processes, lower losses by thermalization, reduced separation and facilitated carriers' collection.

The work of the technologists, engineers and researchers who design and manufacture the cells consists in optimizing each of these parameters. Here are some examples:

To maximize the photo generation, it is necessary to reduce the optical losses due to shading by optimizing the width of the metal contacts, losses due to photon reflection must also be limited by adapting the thicknesses and the optical indices of the materials. To increase yields, we can also combine materials with different gaps in order to make the best use of the entire solar spectrum and thus limit losses by thermalization.

To maximize the collection of carriers, it is important to generate sufficient electric field, by optimizing the band structure and the doping of materials; but it is also essential to reduce the electrical losses due to the recombination of the electrons with the holes during their transport. To do so, it is necessary to maximize the life span of the charge carriers, by optimizing the quality of the materials, interfaces, and adjust the thicknesses accordingly.

Among the various technologies, heterojunction (HET) cells are particularly promising. The laboratory yield record obtained for these cells is currently 24.7 % and it is held by Panasonic [462].

The main advantages of HET compared to conventional homojunction cells are given below [463]:

- Possibility of achieving high yields with large surface cells (150 cm^2).
- Very good passivation levels, which reduces the thickness of the substrates and therefore limits the use of raw materials.
- Compatibility of low temperature processes with the use of thin substrates.
- Use of relatively simple processes from the flat screen industry (thin film transistors (TFT), liquid crystal screens (LCD) ...).

- Symmetrical structure allowing their use in two-sided modules.

VIII.4 Fabrication semiconductor-semconductor junction based on loaded lead phosphate glass with metal particles

VIII.4.1 Reminder of P-N junction

It is a structure which results from the juxtaposition of semiconductor materials of two zones, one of type P (majority in holes, minority in electrons) and the other of type N (majority in electrons, minority in holes) (heterojunction p-n). From the juxtaposition, diffusion currents of holes and electrons develop around the junction and create, in the immediate vicinity of the latter, a potential barrier, which opposes the diffusion currents of the majority carriers in each zone. Each of the regions is connected to a metal electrode by means of an ohmic contact of low resistance. The operating principle can be decomposed into two parts: the absorption of photons and the collection of created charges.

When equilibrium is reached, the electric field created by the potential barrier is sufficient to balance the diffusion currents of majority carriers and minority carriers, due to the very small width of the junction (from 0.2 to a few micrometers [464].

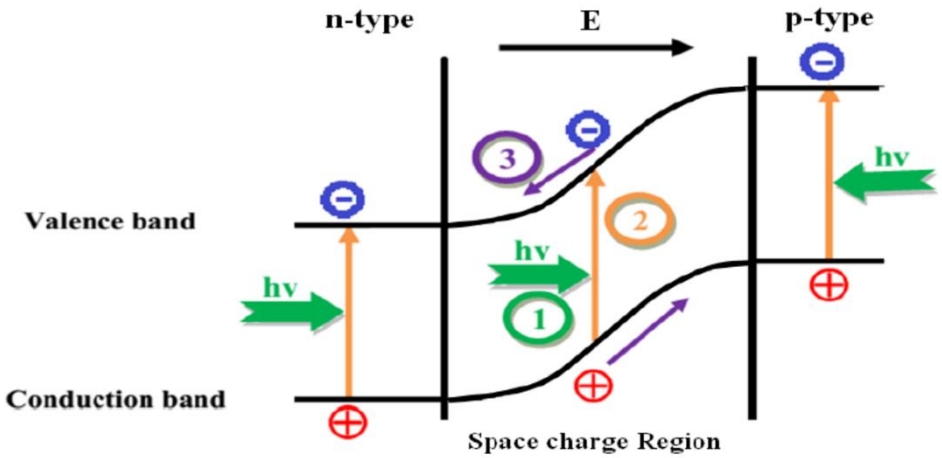

*Figure VIII- 6 : Scheme of p-n junction photovoltaic cell mechanism [*451*].*

VIII.4.2 Solar cell structure

The device structure of a solar cell consists of a) semiconductor which absorbs light and generates electron-hole pairs, b) p-n junction which separates the photo-generated carriers and c) contacts on the front and back of the cell that allow the current to flow in the external circuit.

In order to perform similar structure, we need Indium doped tin oxide glass (1 x 1 cm^2), p-type semiconductor and n-type semiconductor. Hot plate , tap and spatulas .Firstly we have to cover

the two extremities of conducting side of ITO glass so as to make a hole of about 10 mm, then we put the semiconducting glass mixture and flatten it with razor blade on the same side of the ITO glass , the obtained electrode is annealed using a hot plate at 250°C during 10 min. The counter electrode is constituted of n-type semiconductor , it is deposited on the already fabricated electrode to face them each other.

It is worthy to mention that surface preparation, the processing environment and the deposition techniques are essential factors, because it can alter the performance of the produced cells and their reproducibility.

VIII.4.3 The produced P-N junction

In the previous chapter, the structural analysis have led to an optimized composition of 56%PbO-44% P2O5 (in weight percentage). This composition manifests a good transparency and significant electrical conductivity when it is loaded with metal particles. In this chapter, we have decided to use this composition to demonstrate the feasibility of a new type of thin film based solar cells based on PbP/metal nanocomposites. To the best of our knowledge, this is the first time that such kind of composites is proposed for a photovoltaic application.

It is known that a relatively thick film would lead to heterogeneous crystallization. For this reason, we decided to design a PV device with relatively thin films. The basic structure of a photovoltaic cell based on P-N junction composite layer, formed by p-type and n-type, sandwiched between the anode (ITO) and the cathode (tin) is illustrated in Figure VIII- 7.

Photovoltaic cell was fabricated based on the PbP/Ni composite, which is a p-type semiconductor, and PbP/Cr, which is found to behave, as n-type semiconductor. The selected thickness is around 500 nm for both layers. These thin films are heat treated together after the deposition during 20 min at 250 °C.

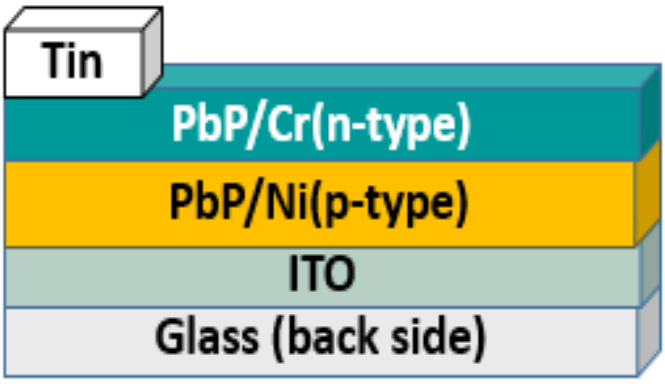

Figure VIII- 7 : Structure of a photovoltaic cell based on homojunction of PbP/metal nanocomposites.

VIII.4.4 Evaluation of PbP/metal composites based P-N junction

Since the main characteristic of solar cell is the contact resistance between metal electrodes and active semiconductor materials. The investigation of our solar cell prototype is restricted on the evolution of resistivity values as function of wavelengths attributed to light intensity.

Note that the conversion efficiency of the thin film solar cells may be remarkably affected by the contact resistance. So far, the highest power conversion efficiency has been obtained with Chalcogenide glass-based composite ,it is about 1%,Thus,more efforts are needed to be in progress to achieve better performance[465,466,467].

Table VIII- 1 : Used Leds and their corresponding wavelength, and resistance response of illuminated cell.

Led colors	wavelength (nm)	Contact Resistance response of illuminated cell (Ohm)
Red	650	17
Yellow	580	31
Blue	445	56

Table VIII-1 represents the resistance response of cell, which is illuminated by leds of three different colors namely red, yellow and blue.

From the measured response of the solar cell junction we concluded that the efficiency would be enhanced by high increasing wavelength, thus by increasing illumination intensity. This finding is in good agreement with previous research results [455-468]. Indeed, performance improvement of solar cell is only possible by reducing the contact resistance.

In order to verify the origin of the photovoltaic effect, two separate junctions, Tin-PbP/Cr and PbP/Ni-ITO have been fabricated.

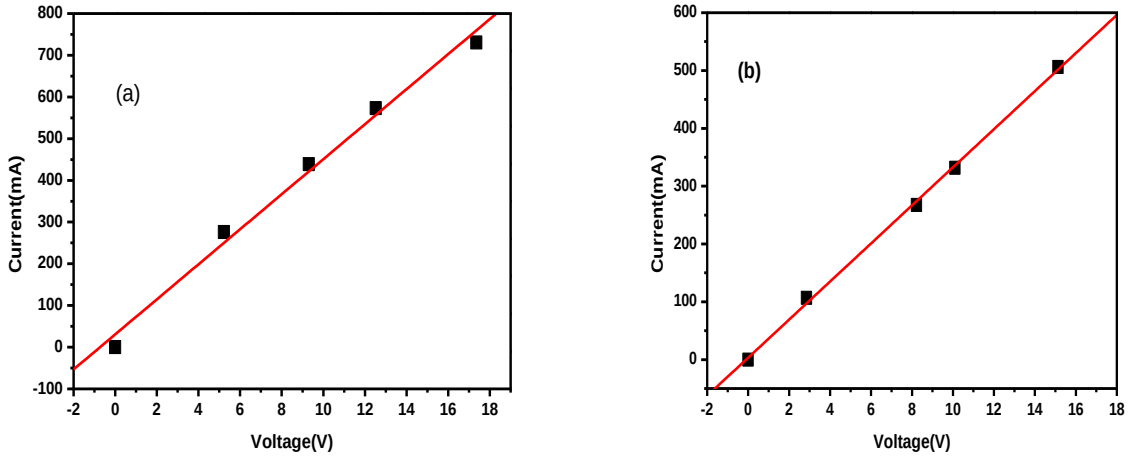

Figure VIII- 8 : (a) Current –voltage profile of PbP/Ni-ITO, (b) Current –voltage profile of Tin-PbP/Cr.

Current-voltage characteristic of these two junctions was measured; it is clearly indicating two ohmic contacts. Similar results have been obtained with chalcogenide glass ceramic/Sb2Se3:I junction by group of researchers [464]. Therefore, we conclude that the junction PbP/Ni-PbP/Cr achieves the photovoltaic effect.

Conclusion

This chapter focuses on the fundamental notions of semiconductors and the P-N junction as well as the different types of recombination and the metal / semiconductor structure. We have discussed the principle of the photovoltaic effect based on the conversion of solar energy into electrical energy. It includes concepts relating to the energy transmitted by the sun, as well as some elements of the physics of semiconductors and the main mechanisms of transport of electrical charges in the P-N junction. We also gave an overview on the basic electrical characteristics such as the voltage, current and conversion efficiency of the photovoltaic device. P-N heterojunction has been fabricated based on the p-type PbP/Ni associated with PbP/Cr, which is n-type semiconductor. For this very new type of solar cell, we have measured the resistance under illumination.Ohmic contact between ITO and p- PbP/Ni and between tin and n-PbP/Cr were confirmed in preliminary experiments using single layer films.

General conclusion

In order to achieve high electrical conductivity and fulfill the requirement of rapid developing science and technology, a new type of high-performance conductive composites is prepared by developing bulk and thin film materials based on matrix of binary phosphate glasses loaded with conductive particles. Thus, the recovery of phosphate materials in the energy sector is ensured by bringing to light their applications in the field of thermoelectricity and photovoltaics.
Firstly, we have synthesized binary phosphate glass matrix and its based composites in bulk form. Then we carried out the characterization of these phosphate glass/conductive fillers composites by different methods such as density measurement, X-ray diffraction (XRD), FTIR, morphological aspects by scanning microscopy (SEM), thermal measurements by DSC and wettability along with surface energy determination by contact angle measurements.

These investigations led to the following results:

- Density measurements have shown that the elaborated composites are binary and do not change over time. They contain very low porosity rates.

-The repeated characterization by XRD showed that the matrix is stable, homogeneous and does not show crystallization. However, diffraction peaks appear in the composites when the fillers content increase. The peaks intensity of crystallized phase increases with filler amount.

- SEM micrographs coupled with EDX, showed that the metallic phase is distributed quite homogeneously within the matrix. The EDX analysis highlighted the presence of the constituents of the composite and very few impurities, thus, confirming density measurements and X-rays.

-Thermal measurements revealed reasonable thermal stability of the studied composites and enabled to determine the glass transition temperatures Tg. The obtained glass phase transitions temperature decreases gradually with fillers loading.

-The FTIR measurements do not show any glass-filler bonding; suggesting that the composite mixture is purely of physical nature.

- Contact angle of the composites was calculated using liquid droplets on the substrate. One of the most common wetting parameters namely total solid surface free energy was calculated. The interaction parameter between the glass matrix and the liquid has been calculated using owns wendt method. The performed calculations revealed the existing of weak matrix-fillers interactions.

Afterward, we carried out electrical and thermoelectric behavior as a function of the volume fraction of the fillers and as a function of temperature; we have highlighted two important types of behavior according to:

Composites with Φ> Φc:

T<Tg, the studied composites expressed an original conducting-insulating transition at accurate temperature value called the CTP transition, observed for the first time in this type of composites.

Composites with Φ ≤ Φc:

The temperature dependences of the electrical conductivity of the samples with fillers below percolation threshold have been reported in the temperature range 370-715K. It has been observed at least two different conduction mechanisms that were attributed to the conduction mode changing from small polaron hopping to variable range hopping with the decrease in temperature.

For thin films studies, we have successfully prepared phosphate glasses loaded with metal precursors as in the case of bulk composites but this time the fillers are in the form of nitrate precursors.

We have carried out structural analysis of samples by different structural characterization such as X-ray diffraction, IR/ATR and Raman spectroscopy. Further investigation of metal particles loading effect were conducted by morphological, optical and electrical measurements such as SEM/EDX analysis, transmission measurement and electrical conductivity measurements at room temperature. Moreover, electrical conductivity measurements versus temperature were carried out.

The obtained results are listed below:

- The structural studies reveal that the obtained films have low and incomplete crystalline nature.
- The UV-Visible transmittance plots have been used to estimate the optical bandgap (E_g) of the glass-based films assuming that these materials as an indirect amorphous semiconductor.
- Further loading concentration leads to a remarkable decrease of optical gap.
- It was found that the electrical conductivity of nanocomposite thin films is increasing with the temperature increase and the conduction mechanism is thermally activated process. This behavior is also characteristic to bulk composites conductivity versus temperature as observed below percolation threshold.

Potentially we consider the most important application of loaded lead phosphate glass in thin film form is the direct conversion of sunlight to electric power, and the prevailing application of bulk composites is

References

References

[1] M. H. Brodsky (ed), Amorphous semiconductors, Springer Verlag (second edition), 1985.
[2] R. Zallen, The physics of amorphous solids, Wiley, 1998.
[3] S.R. Elliott, The physics of amorphous materials, Longman group limited, 1984.
[4] M. H. Cohen, H. Fritzsche and S. R. Ovshinski, Quantum Percolation: Meaning and Results. Phys. Rev. Lett. 22(1969)1065.
[5] J. M. Marshall and A. E. Owen, Drift mobility studies in vitreous arsenic triselenide, Phil. Mag. 24(1971) 1281-1305.
[6] N. Qamhieh, M. L. Benkhedir, M. Brinza and G. J. Adriaenssens, Low temperature steady state photoconductivity in amorphous selenium films,J Optoelectron. Adv. Mater. 7(2005), 1781 - 1784
[7] J. Noolandi, Multiple-trapping model of anomalous transit-time dispersion in a−Se Phys. Rev. B. 16(1977), *4466*-4473.
[8] K. Koughia and S.O. Kasap, Density of states of a-Se near the valence band,J. Non-Cryst. Solids. 352(2006), 1539-1542.
[9] N. Da., M. Peng, S. Krolikowski,L.Wondraczek, Intense red photoluminescence from Mn 2+-doped (Na+; Zn2+) sulfophosphate glasses and glass ceramics as LED converters, Opt. Express. 18 (2010) 2549-2557.
[10] G. Kumar, S.K. Apte, S.N. Garaje, M.V. Kulkarni, S.M. Mahajan, B.B. Kale, Magneto-optic characteristics of ferric oxide quantum-dot-phosphate glass nanocomposite, Appl. Phys. A –Mater. 98 (2010) 531-535.
[11] Z. H. Stachurski, On Structure and Properties of Amorphous Materials, Mater.J,4(2011) 1564-1598.
[12] E. D. Zanotto and J. C. Mauro, The glassy state of matter: Its definition and ultimate fate, J. Non. Cryst. Solids, 471(2017) 490–495.
[13] J. E. Shelby,Introduction to Glass Science and Technology,2nd Ed. R.S.C (2005).
[14] W.H. Zachariasen, J. Chem. Phys. 4 (1936) 618
[15] A. C. Wright and M. F. Thorpe, Eighty years of random networks, Phys. Status Solidi Basic Res., 250(2013) 931–936.
[16] J.R. van Wazer, Phosphorous and Its Compounds, IntersciencePublishers, Inc., New York, 1(1958) 364–367.
[17] A.K. Varshneya, Fundamentals of Inorganic glasses , Academic Press, New York, 1 (1994)112.
[18] M. T. Soltani,Elaboration et étude de nouveaux matériaux pour application optronique dans les systèmes Sb2O3-M2O-XO,Thèse de l'université de Biskra, (2005).
[19] W. H. Zachariasen, The atomic arrangement in glass, J.Am.Chem.Soc., 54 (1932) 3841–3851.
[20] J. Zarzyky, Les verres et l'état vitreux, (Paris ; New York ; Barcelone : Masson) 1982.
[21] T. Kubo, J. Cha, H. Takebe, M. Kuwabara, Thermal properties and structure of zinc phosphate glasses ,Phys. Chem. Glasses 50 (2009) 15-18
[22] F. Kohler, US Patent, 3243753, Resistance element, United States Patent Office,1966.
[23] Masingu A, Piccaluga G, Pinna G. Structural properties of lead-iron phosphate glasses by X-ray diffraction. J Non-Cryst Solids. 122(1990) *52*-56.
[24] Nelson, N.B. and Exarhos, G.J. Vibrational Spectroscopy of Cation-Site Interactions in Phosphate Glasses.J. Chem. Phys., 71(1979) *2739*-2747.
[25] N. H. Ray, Structure and Properties of Inorganic Polymeric Phosphates. Br. Polym. J.,11 (1979) 163–177.

[26] Furdanowiez, W.; Klein, L. C., Viscosities and durabilities of lead phosphate glasses. Glass Technol. 24(1983)198-201.
[27] Van Wazer, J.R., Phosphorus and its Compounds Volume I: Chemistry. New York: Interscience Publishers, 1 (1958), Inc. 954
[28] R. K. Brow, Review: the structure of simple phosphate glasses, J. Non. Cryst. Solids, 263(2000) 1–28.
[29] B.C. Sales, L.A. Boatner, Lead-iron phosphate glass: a stable storage medium for high-level nuclear waste Mater. Lett. 2 (1984) *301*-308
[30] H. S. Liu, P. Y. Shih and T. S. Chin Low melting PbO-ZnO-P_2O_5 glasses., Phys. Chem. Glas., 37 (1996) 227–235.
[31] Y. He, D.E. Day, Glass Technol. 33 (1992) 214.
[32] Y. B. Peng and D. E. Day, High Thermal Expansion Phosphate Glasses. Part 2, Glas. Technol., 32 (1991) 200–205.
[33] G. Guo, Optical and thermal properties of some chemically durable lead phosphate glasses, Glas. Technol., 39 (1998) 138–141.
[34] R. K. Brow, Local Structure of xAl2O3· (1 −x)NaPO3 Glasses: An NMR and XPS Study, J.Am. Ceram. Soc., 73 (1990) 2293-2300
[35] R. Delaval, G.Palavit, Reyc.Patent WO 95/26934 (1995).
[36] H. Tichá, J. Schwarz, L. Tichý, and R. Mertens, Physical properties of PbO-ZnO-P_2O_5 GLASSESII. Refractive indes and optical properties 6 (2020)747–753.
[37] K. El-Egili, H. Doweidar, Y. M. Moustafa, and I. Abbas, Structure and some physical properties of PbO-P_2O_5glasses, Phys. B Condens. Matter,339(2003) 237–245.
[38] L. M. Sharaf El-Deen, M. S. Al Salhi, and M. M. Elkholy, Spectral properties of PbO-P_2O_5 glasses, J. Non. Cryst. Solids,354 (2008)3762–3766.
[39] K. Nakamoto, in: Infrared spectra of Inorganic and Coordination compounds, Wiley-Interscience, New York,1970.
[40] Y.M. Moustafa, A. EL-Adawy, Structural and Physical Properties of Iron Oxychloride Phosphate Glasses , Phys. Stat. Sol. (a) 179(2000) 83-93.
[41] A. Osaka, K. Takahashi, M. Ikeda, Infrared study of trivalent cations B and Fe in amorphous and crystalline phosphates, J.Mater. Sci. Lett. 3 (1984) 36-38.
[42] D.E.C. Corbridge, E.J. Low, The infra-red spectra of some inorganic phosphorus compounds, J. Chem. Soc., 1954, 493-502.
[43] C. Dayanand, G. Bhikshamaiah, V. Jayatyagaraju, M. Salagram, Structural investigations of phosphate glasses: a detailed infrared study of the x(PbO)-(1 - x)P205, vitreous system, J. Mater. Sci. 31 (1996) 1945 - 1967.
[44] J.J. Hudgens, S.W. Martin, Glass Transition and Infrared Spectra of Low-Alkali, Anhydrous Lithium Phosphate Glasses, J. Am. Ceramic. Soc. 76 (1994) 1691-1696.
[45] V. Sudarsan and S. K. Kulshreshtha, Study of structural aspects of PbO - P_2O_5-Sb_2O_3 glasses, J. Non-Cryst. Solids, 286 (2001)99–107.
[46] O. Oabi, Composites des Verres Binaires de Phosphates /Charges Métalliques : MO-P2O 5 (M = Zn , Ca)/(Ni , Co) Élaboration et Caractérisations Physico-chimiques pour des Applications Thermoélectriques, Thèse de doctorat, Faculté des Sciences, Université Mohammed V, Rabat (2017).
[47] A. Maaroufi, O. Oabi, B. Lucas, A. El Amrani, and S.Degot, New composites of ZnO-P_2O_5/Ni having PTC transition and high Seebeck coefficient, J. Non-Cryst. Solids. 358 (2012) 3312–3317.

[48] O.Oabi, a. Maaroufi, B. Lucas, S. Degot, and a. El Amrani, Positive temperature coefficient and high Seebeck coefficient in $ZnO–P_2O_5$/Co composites, J. Non. Cryst. Solids. 385 (2014) 89–94.

[49] A. Maaroufi, O. Oabi, G. Pinto, M. Ouchetto, R. Benavente, J.M. Pereña, electrical conductivity of new zinc phosphate glass/ metal composites, J. Non-Cryst. Solids, 358 (2012) 2764–2770.

[50] M. Hammi, G.Aziate, G. Pinto, A.Maaroufi, Electrical and Thermoelectrical Behavior of Binary Composites of Phosphate Glass Loaded with Zinc Fillers: Promising Materials for Photovoltaic's, Journal of the Chinese chemical Society 62 (2015) 1035-1044.

[51] Deborah D. L. Chung, Composite Materials, Science and Applications, Springer (second edition), 2010.

[52] L.Mascia, The role of additives in plastics, Edward Arnold London, UK (1974).

[53] I. Ahmed, M. Lewis, I. Olsen, J.C. Knowles, Phosphate glasses for tissue engineering: Part 2. Processing and characterisation of a ternary-based P_2O_5-CaO-Na_2O glass fibre system Biomaterials 25 (2004) 501-507.

[54] S. Kirkpatrick, Percolation and conduction, Rev. Mod. Phys. 45 (1973) 574-588.

[55] F. Lux, Models proposed to explain the Electrical Conductivity of mixtures made of Conductive and Insulating Materials, J. Mater. Sci. 28 (1993) 285-301.

[56] D. Staufer, A. Aharony, Introduction to Percolation Theory, second edition, Taylor and Francis, Philadelphia,(Book,1994).

[57] E. P. Mamunya, V. V. Davidenko,E.V. Lebedev, Percolation conductivity of polymer composites filled with dispersed conductive filler, Polym. Compos. 16 (1995) 319–324.

[58] A. Maaroufi, O. Oabi, and B. Lucas, Ac-conductivity and dielectric response of new zinc-phosphate glass / metal composites, Physica B 492 (2016) 31–38.

[59] D. A. Jameel, Thin Film Deposition Processes, Ijmpa, 1(2015)193–199.

[60] S.Shahidi, B. Moazzenchi, M. Ghoranneviss, A review-application of physical vapor deposition (PVD) and related methods in the textile industry Eur. Phys. J. Appl. Phys. 71(2015) 31302-31314.

[61] H.O. Pierson, Handbook of Chemical Vapor Deposition (CVD), Noyes Publications,Westwood, NJ, 1999.

[62] D. B. Chrisey and G. K. Hubler Pulsed Laser Deposition of Thin Films , A Wiley – interscience publication, New York (1994).

[63] Vinay Kumar Singh& Hridaya Nand Sah, Versality of spray pyrolysis technique for the deposition of carbon thin films, JETIR, 4(2017)312-318.

[64] L. Znaidi, Sol gel deposited ZnO thin films Mater. Sci. Eng. B, 174 (2010) 18-30.

[65] D.Carta, Pickup, D.M., Knowles, J.C., Smith, M.E&Newport, R.J, Sol-gel synthesis of the P_2O_5-CaO-Na2O-SiO2 system as a novel bioresorbable glass. J. Mater. Chem., 15(2005) 2134-2140.

[66] Radha Gupta , Ashok Kumar , A. Bioactive materials for biomedical applications using sol-gel technology. Biomed. Mater. 3(2008) 1-15.

[67] Hench, L.L. and West, J.K. The Sol-Gel Process. Chemical Reviews, 90(1990) 33-72.

[68] J.LivageP.BarbouxM.T.VandenborreC.SchmutzF.Taulelle .Sol-Gel Synthesis of Phosphates. J. Non-Cryst. Solids, 147(1992)18-23.

[69] Aronne, A. et al. Synthesis of High Surface Area Phosphosilicate Glasses by a Modified Sol - Gel Method. Chem. Mater. 2005, 17 (2005) 2081–2090.

[70] Tang,A.J.,Hashimoto,T.,Nasu,H.and Kamiya,K., A.,Sol-gel preparation and properties of TiO_2-P_2O_5 bulk glasses. Mater. Res. Bull., 40(2005) 55-66.

[71] Carta, D., Knowels, J. C., Smith, M. E. & Newport, R. J. Synthesis and structural characterization of P_2O_5-CaO-Na2O sol-gel materials. J. Non-Cryst. Solids, 353(2007a) 1141-1149.

[72] Lee, In-Ho; Foroutan, Farzad; Lakhkar, Nilay J.; Gong, MyoungSeon; Knowles, Jonathan C. Sol-gel synthesis and structural characterization of P_2O_5–CaO–Na2O glasses Physics and Chemistry of Glasses - European Journal of Glass Science and Technology Part B,54 3(2013)115-120.

[73] R. J. Pickup, D.M., Knowles, J.C. (2012) Titanium-containing bioactive phosphate glasses. Philosophical Transactions of the Royal Society A: Mathematical, Physical and Engineering Sciences, 370 (1963). pp. 1352-1375.

[74] Daniela Carta, David M. Pickup, Jonathan C. Knowles, I. Ahmed,Mark E. Smith, Robert J. Newport. A structural study of sol–gel and melt-quenched phosphate-based glasses. J. Non-Cryst. Solids 353 (2007) 1759–1765

[75] A. R. Hilton, Optical Properties of Chalcogenide Glasses, J. Non-Cryst. Solids 2(1970)28–39.

[76] A. Crossay, S. Buecheler, L. Kranz, L. Kranz, J. Perrenoud, C.M. Fella, Y.E. Romanyuk, A.N. Tiwari, Spray-deposited Al-doped ZnO transparent contacts for CdTe solar cells Sol. Energy Mate. Sol. Cells 101(2012)283 -288.

[77] P. Lucas, G. J. Coleman, S. Jiang, T. Luo, and Z.Yang, Chalcogenide glass fibers : Optical window tailoring and suitability for bio-chemical sensing, Opt. Mater. (2015)1–7.

[78] Outts T. J, Young D. L, Li X. Characterization of transparent conducting oxides. Mrs Bulletin (2000) 58-65.

[79] A.N. Tiwari, G. Khrypunov, F. Kurdzesau, D. Batzner, A. Romeo, H. Zogg, CdTe solar cell in a novel configuration, Prog. Photovolt. Res. Appl. 12 (2004) 33-38.

[80] A. Feigel, M. Veinger, S: Sfez, A. Arsh, M. Klebanov, and V. Lyubin, Three-dimensional simple cubic woodpile photonic crystals made from chalcogenide glasses, Appl. Phys. Lett. 83(2003) 4480-4482.

[81] M. Katayama, TFT-LCD technology, Thin Solid Films 341(1999)140-147.

[82] A. Porch, D. V. Morgan, R. M. Perks, M. O. Jones, P. P. Edwards, Electromagnetic absorption in transparent conducting films J. Appl. Phys. 95(2004) 4734-4737.

[83] C. G. Granqvist, A. Hultaker, Transparent and conducting ITO films: new developments and applications Thin Solid Films 411, (2002) 1-5.

[84] H. Köstlin, R. Jost, W. Lems, Optical and electrical properties of doped In2O3 films Phys. Status Solidi A 29(1975) 87-93.

[85] T. Minami, Transparent conducting oxide semiconductors for transparent electrodes, Semicond. Sci. Technol. 20 (2005) S35–S44

[86] H. Kim, R. C. Auyeung, Y. Pique, Transparent conducting F-doped SnO2 thin films grown by pulsed laser deposition Thin Solid Films 516(2008) 5052-5056.

[87] G. C. Morris, A. E. McElnea, Fluorine doped tin oxide films from spray pyrolysis of stannous fluoride solutions,Appl. Surf. Sci. 92(1996) 167-170.

[88] J. Keirsse et al., Chalcogenide glass fibers used as biosensors, J. Non-Cryst. Solids, vol. 326–327(2003)430–433.

[89] N. Armaroli and V. Balzani,The Future of Energy Supply: Challenges and Opportunities , Angew.Chem. Int. Ed. 46 (2006)52-66

[90] S.Chu and A. Majumdar, Opportunities and Challenges for a Sustainable Energy Future Nature. 488(2012) 294–303.

[91] Zhang, X. et al. Chalcogenide glass-ceramic with self-organized heterojunctions : application to photovoltaic solar cells. EPJ Photovolt. 9(2018) 1–6.

[92] Corsin Battaglia, Andres Cuevas & Stefaan StefaanDe Wolf.High-efficiency crystalline silicon solar cells :status and perspectives. Energy Environ. Sci., 9(2016) 1552–1576.

[93] H. Joon, H. Kyung, G. Cho, and J. Choi, Construction and characterization of an amorphous silicon flat-panel detector based on ion-shower doping process, Nuclear Instruments and Methods in Physics Research A .505(2003) 155–158.

[94] G. Bracco, B. Holst (Eds), Surface Science Techniques,Springer-Verlag Berlin Heidelberg 2013.

[95] Fowkes F M. Attractive forces at interfaces. Ind. Eng. Chem. 56(1964)40-52.

[96] R. Mevrel, S. Poulard, J. Dumiel, M. Vignollet, Tensions de surface et adhésivité, Rheol. Acta. 13(1974) 318–322.

[97] A. Pegoretti, A. Dorigato, M. Brugnara, A. Penati, Contact angle measurements as a tool to investigate the filler–matrix interactions in polyurethane–clay nanocomposites, Eur. Polym. J., 44 (2008) 1662–1672.

[98] D. O. Njobuenwu, E. O. Oboho, R. H. Gumus, Determination of Contact Angle from Contact Area of Liquid Droplet Spreading on Solid Substrate, Leonardo Electronic Journal of Practices and Technologies, 10 (2007) 29–38.

[99] A. Maaroufi, The determination of some solid polymers surface energies, Travaux pratiques des polymères, Faculté des sciences, Rabat, 2012/2013.

[100] A. Rudawska, E.Jacniacka, Analysis for determining surface free energy uncertainty by the Owen – Wendt method, Int. J. Adhes. Adhes., 29 (2009) 451-457.

[101] Dupré, Athanase, and Paul Dupré. Théorie Mécanique de la Chaleur (Paris: Gauthier-Villars) 1869.

[102] Etzler, Frank Determination of the Surface Free Energy of Solids J. Rev. Adhesion and Adhesives, 1(2013) *3*-45.

[103] K.E. Zhang, Experimental Investigation of Dynamic and Metastable Contact Angles, PhD-thesis, University of Calgary, 2014.

[104] S. Wu, Calculation of Interfacial Tensions in Polymer Systems, J. Polym. Sci., 43 (1971)19-30.

[105] S. Wu, Polar and Nonpolar Interaction in Adhesion, J. Adhes., 5 (1973) 39-55.

[106] F.M. Fowkes, Determination of interfacial tensions, contact angles, and dispersion forces in surfaces by assuming additivity of intermolecular interactions in surfaces, J. Phys. Chem., 66(2) (1962) 382–382.

[107] I. Technologies, On the definition of scales in van oss-chaudhury-good acid-base theory, MATCH Commun. Math. Comput. Chem. 56 (2006) 291-316.

[108] M. Żenkiewicz, Methods for the calculation of surface free energy of solids, J.AMME 24(2007)137–145.

[109] O. Oabi, Composites des Verres Binaires de Phosphates / Charges Métalliques : MO-P 2 O 5 (M = Zn , Ca)/(Ni, Co) Élaboration et Caractérisations Physico-chimiques pour des Applications Thermoélectriques , Thèse de Doctorat, Université Mohammed V, Faculté des Sciences, Rabat, 2017.

[110] A. Maaroufi, O. Oabi, G. Pinto, M. Ouchetto, R. Benavente, J.M. Pereña, Electrical conductivity of new zinc phosphate glass/ metal composites, J. Non. Cryst. Solids. 358 (2012) 2764–2770.

[111] M. Hammi, G.Aziate, G. Pinto, A.Maaroufi, Electrical and Thermoelectrical Behavior of Binary Composites of Phosphate Glass Loaded with Zinc Fillers: Promising Materials for Photovoltaic's, J. Chin. Chem. Soc. 62 (2015) 1035-1044.

[112] A. Maaroufi, K. Haboubi, A. El Amarti, F. Carmona, Electrical resistivity of polymeric matrix loaded with nickel and cobalt powders, J. Mater. Sci., 39 (2004) 265-270.

[113] D. Staufer, A. Aharony, Introduction to Percolation Theory, second edition, Taylor and Francis, Philadelphia (1994).

[114] B. I. Shklovskii and A. L. Efros, Electronic Properties of Doped Semiconductors; Springer-Verlag, New York, 1984 and references therein.

[115] D. J. Bergmann and D. Stroud, Solid State Physics: Advances in Research and Applications 46, ed. by H. Ehrenreich and D. Turnbull (Academic Press, New York, (1992), and the references therein.

[116] E. P. Mamunya, V. V. Davidenko, and E. V. Lebedev, Effect of polymer-filler interface interactions on percolation conductivity of thermoplastics filled with carbon black, Compos. Interface. 4 (1997) 169–176.

[117] C. Chiteme and D. S. Mclachlan, Measurements of universal and non-universal percolation exponents in macroscopically similar systems, Physica B 279(2000) 69–71.

[118] D. S. M. C. Lachlan *et al.*, AC and DC Percolative Conductivity of Single Wall Carbon Nanotube Polymer Composites, nc. J Polym Sci Part B: Polym Phys.43 (2005)3273–3287,

[119] D. S. Mclachlan and G. Sauti, The AC and DC Conductivity of Nanocomposites, J. Nanomater.**2007** (2007)1-9.

[120] J. Wu and D. S. Mclachlan, Percolation exponents and thresholds obtained from the nearly ideal continuum percolation system graphite-boron nitride, Phys. Rev. B.56(1997) 1236–1248.

[121] McLachlan,Electrical resistivity of composites,J.Am.Ceram.Soc.73(1990)2187-2203.

[122] P. J. Flory, Molecular Size Distribution in Three Dimensional Polymers. I. Gelation. Am. Chem. Soc. 63(1941) 3083–3090.

[123] W. H. Stockmayer, Theory of molecular size distribution and gel formation in branched-chain polymers, J. Chem. Phys. 11 (1943) 45; 12(1944) 125.

[124] Ulrich Brauner, Search for critical exponents at the gel-to-sol transition

Macromol. Chem. Phys 180(1979) 251-253.

[125] Xiang et al. The relationship between the degree of branching and glass transition temperature of branched polyethylene : experiment and simulation. Polym. Chem., 5(2014)1305-1312.

[126] D. Stauffer, A. Coniglio and M. Adams, Advances in Polymer Science, 44, Springer, Berlin, 1982.

[127] S. R. Broadbent and J. M. Hammersley, Percolation processes: I. Crystals and mazes, 53(1957) 629-641.

[128] S. Kirkpatrick, Percolation and conduction, Rev. Mod. Phys. 45 (1973) 574-588.

[129] F. Lux, Models proposed to explain the electrical conductivity of mixtures made of conductive and insulating materials, J. Mater. Sci., vol. 28 (1993) 285–301.

[130] E. P. Mamunya, V. V. Davidenko, E.V. Lebedev, Percolation conductivity of polymer composites filled with dispersed conductive filler, Polym. Compos. 16 (1995) 319–324.

[131] M. Panda, V. Srinivas, A.K. Thakur, Non-universal scaling behavior of polymer-metal composites across the percolation threshold, Res. Phys. 5 (2015) 136–141.

[132] M.B. Heaney, Measurement and Interpretation of Nonuniversal Critical Exponents in Disordered Conductor–Insulator Composites, Phys. Rev. B. 52 (1995) 12477-12480.

[133] N. P. Berezina and L. V. Karpenko, Percolation Effects in Ion-Exchange Materials, Colloid J., 62 (2000) 676-684.

[134] I. Balberg, Tunneling and Non-universal Conductivity in Composite Materials, Phys. Rev. Lett. 59 (1987) 1305-1308.

[135] Z. Rubin, S.A. Sunshine, M.B. Heaney, I. Bloom, I. Balberg, Critical Behavior of the Electrical Transport Properties in a Tunneling Percolation System, Phys. Rev. B. 59 (1999) 12196-12199.

[136] F.Carmona, P. Prudhon, F. Barreau, Percolation in Short Fibres Epoxy Resin Composites: Conductivity Behavior and Finite Size Effects near Threshold, Solid. State. Commun., 51 (1984) 255-257.

[137] David Berney Needleman, Optical Design Guidelines for Spectral Splitting Photovoltaic Systems: A Sensitivity Analysis Approach, Master of Science in Mechanical Engineering, University of Oregon,Massachustts Institute of Technology(2014).

[138] Schumacher B., Bach HG. Spitzer P., Obrzut J., Electrical Properties. In: Czichos H., Saito T., Smith L. (eds) Springer Handbook of Materials Measurement Methods. Springer Handbooks. Springer, Berlin, Heidelberg (2006).

[139] J.Tauc, R.Grigorovici, A. Vancu, Optical properties and electronic structure of amorphous germanium, Phys. Stat. Sol., 15 (1966) 627-637.

[140] D. Adler, Theory of Amorphous Semiconductors, Solar Cells, 2 (1980) 199 – 226.

[141] P.W. Anderson, Absence of Diffusion in Certain Random LatticesPhys. Rev., 109 (1958)1492- 1505.

[142] R. Zallen, "Physics of Amorphous Solids", John Wiley & Sons, New York, 1983.

[143] P.M. Kastner Prediction of the influence of additives on the density of valence-alternation centers in ion paire semiconductors, Phil. Mag. B., 37 (1978) 127-133.

[144] P. Nagels, chapter 5 in "Amorphous semiconductors", M.H. Brodsky (ed.), Springer-Verlag (1985).

[145] S. Kasap, P. Capper, Springer Handbook of Electronic and Photonic Materials Amorphous Semiconductors: Structure, Optical, and Electrical Properties, 10.1007/97(2007).

[146] A. Maaroufi, O. Oabi, B. Lucas, A. El Amrani, and S.Degot, New composites of ZnO-P_2O_5/Ni having PTC transition and high Seebeck coefficient, J. Non-Cryst. Solids, 358(2012) 3312–3317.

[147] O. Oabi, a. Maaroufi, B. Lucas, S. Degot, and a. El Amrani, Positive temperature coefficient and high Seebeck coefficient in ZnO–P_2O_5/Co composites, J. Non. Cryst. Solids, 385 (2014) 89–94.

[148] A. Moliton, B. Ratier, Electronic properties and band schemes in amorphous semiconductors.II.Electronic transport,Ann. Phys. Fr. 16 (1991) 305-344.

[149] N. F. Mott and E. A. Davis, Electronic Processes in Non-crystalline Materials; 2nd. ed., Clarendon Press, Oxford (1979).

[150] N. F. Mott, Conduction in glasses containing transition metal ions, J. Non-Cryst. Solids1 (1968) 1-17.

[151] S. R. Elliot, Physics of Amorphous Materials, 2nd. ed., John Wiley and Sons, New York, 1990.

[152] J. Li and A. Drabold, Electron hopping between localized states: A simulation of the finite-temperature Anderson problem using density functional methods, Phys. Rev. B - Condens. Matter Mater. Phys., 68 (2003)1–4.

[153] A. šantić, A. Moguš-Milanković, D.E.Day, The dc electrical conductivity of iron phosphate glasses, J. Non-Cryst. Solids, 296 (2001) 65-73.

[154] Daefalla M. Tawati, M. Jamel Basha Adlan, Mat Johar Abdullah, DC electrical conductivity of semiconducting cobalt–phosphate glasses, J Non-Cryst. Solids, 357 (2011) 2152-2155.

[155] M. M. El-Desoky, I. Kashif, Electrical Conductivity in Mixed Calcium and Barium Iron Phosphate Glasses, Phys. Stat. Sol. (A) 194 (2002) 89-105.

[156] K.V. Ramesh, D.L. Sastry, Transport properties of ZnO substituted lead vanadate glass system at eutectic composition, Mater. Sci. Eng. B 126 (2006) 66-73.

[157] G.D. Khattak, a. Mekki, M.N. Siddiqui, Compositional dependence of DC electrical conductivity of SrO-vanadate glasses, Solid State Ionics. 211 (2012) 5-11.

[158] I.G. Austin, N.F. Mott, Polarons in crystalline and non-crystalline materials,Adv. Phys. 18 (1969) 41-102.

[159] H. Jain,E. I. Kamitsos,W. C. Huang&Y. D. Yiannopoulos, Electrical Conduction in Relation to Local and Intermediate Range Structure of Rubidium Germanate Glasses, Mat.Res,411(1996)143-150.

[160] J. M. Marshall &A. E. Owen, The hole drift mobility of vitreous selenium, physica status solidi (a), 12(1972)181-191.

[161] R.G. Gordon, Criteria for Choosing Transparent Conductors MRS Bull. 25(2000) *52* – 57.

[162] T. Maruyama and R. Kitamura, Transformations of the wavelength of the lightincident upon CdS/CdTe solar cells, Solar Energy Materials and Solar Cells,69 (2001) *61*-68.

[163] T. S. Moss, The Interpretation of the Properties of Indium Antimonide Proc, Phys. Soc. B 67 (1954) 775-782.

[164] W.E. Spear, The hole mobility in selenium, Phys.Stat.Sol. 76 (1960) 826-832.

[165] M. Fox, Optical properties of solids, Oxford University Press, New York (2001).

[166] R. Swanepoel, Determination of the thickness and optical constants of amorphous silicon, J. Phys. E: Sci. Instrum., 16 (1983) 1214-1222.

[167] J. C. Manifacier, D. M. Murcia, J. P. Fillard, E. Vicario, Optical and electrical properties of SnO2 thin films in relation to their stoichiometric deviation and their crystalline structure, Thin solid films, 41 (1977) 127-135.

[168] N. Boumedienne, A. Maaroufi, Structural and opto-electronic properties of epoxy/silver nanocomposite films, Physica B 578 (2020) 411853.

[169] J. Tauc, A. Menth, States in the gap, J.Non-Cryst. Solids, 8 (1972) 569-585.

[170] F. Urbach, The long-wavelength edge of photographic sensitivity and of the electronic absorption of solids, Phys. Rev., 92 (1953) 1324 -1326.

[171] E. Burstein, Anomalous Optical Absorption Limit in InSb, Phys. Rev., 93 (1954) 632-633

[172] A. Maaroufi, O. Oabi, G. Pinto, M. Ouchetto, R. Benavente, J.M. Pereña, Electrical conductivity of new zinc phosphate glass/ metal composites, J. Non. Cryst. Solids. 358 (2012) 2764–2770.

[173] Y. D. Yiannopoulos, C.P.E. Varsamis, E.I. Kamitsos, Density of alkali germinate glasses related to structure, J. Non-Cryst. Solids. 293-295 (2001) 244-249.

[174] H. Doweidar, Density–structure correlations in $Na_2O–CaO–P_2O_5–SiO_2$ bioactive glasses, J. Non-Cryst. Solids. 355 (2009) 577-580.

[175] A. Maaroufi, K. Haboubi, A. El Amarti, F. Carmona, Electrical resistivity of polymeric matrix loaded with nickel and cobalt powders, J. Mater. Sci. 39 (2004) 265-270.

[176] A. El Hadrami, Etude des conditions de confinement du plomb et du cadmium dans desverres à base de méta phosphates de zinc, Thèse de doctorat en cotutelle entre l'Université Cadi Ayyad Marrakech et Université Bordeaux 1, 2003.

[177] T. Kikutani, US Patent 6,309,989, issued Oct. 30, 2001.

[178] T. Yamanaka, US Patent 6,306,783, issued Oct. 23, 2001.

[179] C.L. Buhrmaster, R. Morena, KP Reddy, and RE Youngman, US Patent 6,737,375, issued May 18, 2004.

[180] K. EL Igili, H. Doweidar, Y.M. Mostafa, I. Abbas, Structure and some physical properties of $PbO-P_2O_5$ glasses, Physica B. 339 (2003) 237-245.

[181] C. Dayanand, G. Bhikshamaiah, V. Jayatyagaraju, M. Salagram, Structural investigations of phosphate glasses: a detailed infrared study of the $x(PbO)-(1 - x)P_20_5$, vitreous system, J. Mater. Sci. 31 (1996) 1945 - 1967.

[182] Le Saoût, G.; Vaills, Y.; Luspin, Y. Effects of thermal history on mechanical properties of $(PbO)_x(ZnO)(0.6-x)(P_2O_5)_{0.4}$ glasses using Brillouin scattering, Solid State Commun., 123 (2002) 49-54.

[183] A. Osaka, K. Takahashi, M. Ikeda, Infrared study of trivalent cations B and Fe in amorphous and crystalline phosphates, J.Mater. Sci. Lett. 3 (1984) 36-38.

[184] J. J. Hudgens, S. W. Martin, Glass Transition and Infrared Spectra of low-Alkali, Anhydrous Lithium Phosphate Glasses, J. Am. Ceramic. Soc. 76 (1993) 1691-1696.

[185] M. Hammi, G.Aziate, G. Pinto, A.Maaroufi, Electrical and Thermoelectrical Behavior of Binary Composites of Phosphate Glass Loaded with Zinc Fillers: Promising Materials for Photovoltaic's, J. Chin. Chem. Soc. 62 (2015) 1035-1044.

[186] M. Ganguli, K. J. Rao, Structural Role of PbO in $Li_2O–PbO–B_2O_3$ Glasses, J. Solid State Chem., 145 (1999) 65-67.

[187] N. H. Ray, Structure and Properties of Inorganic Polymeric Phosphates., Br. Polym. J., vol. 11 (1979) 163–177.

[188] A Moguš-Milanković, A Šantić, A Gajović, DE Day, Spectroscopic investigation of $MoO_3–Fe_2O_3–P_2O_5$ and $SrO–Fe_2O_3–P_2O_5$ glasses. Part I J Non-Cryst. Solids, 325 (2003), 76-84.

[189] J. Fortineau, E. Le Clézio, F. Vander Meulen, G. Feuillard, C. E. A. Le Ripault, and A. Samples, Moisture Content Characterization in Composite Materials based on Transmission Measurements, 114911 (2006), 232–235.

[190] O. Zerzouf, A. Elmansouri, Elaboration et caractérisation des verres binaires : PbO-SiO2, $PbO-B_2O_3$, $PbO-P_2O_5$ et $PbO-V_2O_5$, rapport de stage, Université Mohammed V, Laboratoire de chimie de solide appliquée,1995-1996.

[191] T.Sankarappa, G. B.Devidas, M. Prashant Kumar, S. Kumar, and B. Vijaya Kumar, Ac Conductivity Studies in Single and Mixed Alkali Vanadophosphate Glasses, J. AlloysCompd., 469 (2009),576–579.

[192] G. D. L. K. Jayasinghe, M. A. K. L. Dissanayake, M.A. Careem, J.L. Souquet, Electronic to ionic conductivity of glasses in the in the Na2O-V2O5-TeO2 system, Solid State Ionics, 93 (1997) 291-295.

[193] P.Claudy, Analyse calorimétrique différentielle : théorie et applications de la DSC Lavoisier, Paris, (2005).

[194] M.Ouchetto, B.Elouadi, S. Parke, Study of lanthanide zinc phosphate glasses by differential thermal analysis, Phys. Chem. Glasses. 32 (1991) 22-28.

[195] J.S.Hassan and M. Hafid, Properties of vitreous barium zinc mixed metaphosphate,Mater. Res. Bull.39 (2004) 1123-1130

[196] A. Dietzel, Glass structure and glass properties, Glas. tech. Ber. 22 (1968) *41*-50

[197] O. Oabi, Composites des Verres Binaires de Phosphates /Charges Métalliques : MO-P_2O 5 (M = Zn , Ca)/(Ni , Co) Élaboration et Caractérisations Physico-chimiques pour des Applications Thermoélectriques, Thèse de doctorat, Faculté des Sciences, Université Mohammed V, Rabat (2017).

[198] A. Hruby, Czech. , Evaluation of glass-forming tendency by means of DTA,J. Phys. B. 22 (1972) 1187–1193.

[199] N. Syam Prasad, K. B. R., Varma, Crystallisation, dielectric, polar and optical characteristics of Li2B4O7-SrO-Bi2O3-Nb2O5 glasses and glass nanocomposites,Phys. Chem. Glasses. 44 (2003) 365-375.

[200] G. Bascheka, G. Hartwiga, F. Zahradnik, Effect of water absorption in polymers at low and high temperatures, Polym. 40 (1999) 3433-3441.

[201] J.M. Montes, F.G. Cuevas, J. Cintas, Porosity effect on the electrical conductivity of sintered powder compacts, Appl. Phys. A 92 (2008) 375-380.

[202] L.M. Sharaf El-Deen, M.S. Al Salhi, M.M. Elkholy, Spectral properties of PbO–P_2O_5 glasses, J. Non. Cryst. Solids. 354 (2008) 3762–3766.

[203] M. Abid, A. Shaim, M. Et-tabirou, Glass-forming region and electrical properties of Li2O–PbO–P_2O_5 glasses, Mater. Res. Bull. 36 (2001) 2453–2461.

[204] S.S. Das, N.P. Sing, Vibha Srivastava, P.K. Strivastava, Role of Fe, Mn, and Zn ions as dopants on the electrical conductivity behavior of sodium phosphate glass, Ionics,14 (2008) 563-568.

[205] Michael I. Ojovan, Viscosity and Glass Transition in Amorphous Oxides , Advances in Condensed Matter Physics, Article ID 817829,(2008) 1-23

[206] M. V. S. Murty, E. A. Grulke, D. Bhattacharyya, Influence of metallic additives on thermal degradation and liquefaction of high density polyethylene (HDPE), Polym. Degrad. Stabil. 61 (1998) 421-430.

[207] M. Azeem Arshad, A. Maaroufi, R. Benavente, J.M. Pereña, G. Pinto, Thermal Degradation Kinetics of Insulating/Conducting epoxy/Zn Composites under Non-Isothermal Conditions, Polym. Comp. 34 (2013) 2049–2060.

[208] P. Y. Shih, S. W. Yung, and T. S. Chin, Thermal and corrosion behavior of P_2O_5-Na_2O-CuO glasses, J. Non. Cryst. Solids. 224 (1998)143–152.

[209] K. Meyer, A. Barz, and D. Stachel, Effects of atmospheric humidity on the infrared reflectivity of vitreous P205 and ultraphosphate glasses, J. Non. Cryst. Solids.191 (1995) 71–78.

[210] V. Dimitrov, Y. Dimitriev, Structure of glasses in PbO-V_2O_5 system, J. Non. Cryst. Solids. 122 (1990)133–138.

[211] A. Maaroufi, O. Oabi, G. Pinto, M. Ouchetto, R. Benavente, J.M. Pereña, Electrical conductivity of new zinc phosphate glass/ metal composites, J. Non-Cryst. Solids. 358 (2012) 2764–2770.
[212] M. Hammi, G. Aziate, G. Pinto, A. Maaroufi, Electrical and Thermoelectrical Behavior of Binary Composites of Phosphate Glass Loaded with Zinc Fillers: Promising Materials for Photovoltaic's, J. Chin. Chem. Soc., 62 (2015) 1035-1044.
[213] A. Maaroufi, O. Oabi, B. Lucas, A. El Amrani, and S.Degot, New composites of ZnO-P_2O_5/Ni having PTC transition and high Seebeck coefficient, J. Non-Cryst. Solids, 358 (2012) 3312–3317.
[214] O. Oabi, A. Maaroufi, B. Lucas, S. Degot, and A. El Amrani, Positive temperature coefficient and high Seebeck coefficient in ZnO–P_2O_5/Co composites, J. Non-Cryst. Solids, 385 (2014) 89–94.
[215] O. Oabi, Composites des Verres Binaires de Phosphates / Charges Métalliques : MO-P_2O_5 (M = Zn, Ca) / (Ni, Co) Élaboration et Caractérisations Physico-chimiques pour des Applications Thermoélectriques, Thèse de Doctorat, Université Mohammed V, Faculté des Sciences, Rabat (2017).
[216] Y. Yuan and T.R. Lee, Chapter 1: Contact Angle and Wetting Properties in Surface Science Techniques, G. Bracco, B. Holst (eds.), Springer Series in Surface Sciences 51, DOI 10.1007/978-3-642-34243-1_1, Springer-Verlag Berlin Heidelberg 2013.
[217] T. Young, An essay on the cohesion of fluids, Philos. Trans. R. Soc. Lond., 95 (1805) 65.
[218] A. W. Adamson, A. P. Gast, Physical Chemistry of Surfaces; 6th Ed.; Wiley-Interscience, New York, 1997.
[219] A. Lafuma and D. Quéré, Superhydrophobic states, Nature Materials, 2(2003) 457–460.
[220] Dupré, Athanase, and Paul Dupré. *Théorie Mécanique De La Chaleur*. Paris: Gauthier-Villars, 1869. Print.
[221] R.J. Good, Contact angle, wetting and adhesion: a critical review, J. Adhesion Sci. Technol., 6 (1992) 1269-1302.
[222] N. K. Adam, Physics and Chemistry of Surfaces, 3rd edn. Oxford University Press, London (1941). Or N. K. Adam, Nature, 180 (1967) 809.
[223] A. Maaroufi, The determination of some solid polymers surface energies, Travaux pratiques des polymères, Faculté des sciences, Rabat, 2012/2013.
[224] D. K. Owens and R.C. Wendt, Estimation of the surface free energy of polymers,J. Appl. Polym. Sci., 13 (1969) 1741-1747.
[225] R.N., Wenzel, Resistance of Solid Surfaces to Wetting by Water, Ind. Eng. Chem., 28 (1936) 988-994.
[226] A.B.D. Cassie, S. Baxter, Wettability of porous surfaces, Trans. Faraday Soc., 40 (1944) 546-551.
[227] A.B.D. Cassie, S. Baxter, Large Contact Angles of Plant and Animal Surfaces, Nature 155 (1945) *21*–22
[228] A.B. D. Cassie. Contact angles. Discuss. Faraday Soc., 3 (1948) 11–16.
[229] A. Marmur, Wetting on Hydrophobic Rough Surfaces: To Be Heterogeneous or Not To Be?, Langmuir, 19 (2003) 8343-8348.
[230] T. S. Wong, T. Sun, L. Feng, J.Aizenberg, Interfacial materials with special Wettability, MRS Bulletin, 38 (2013) 336-371.
[231] C. Ishino and K. Okumura, Wetting transitions on textured hydrophilic surfaces, Eur. Phys. J. E 25 (2008) 415–424.
[232] D. O. Njobuenwu, E. O. Oboho, and R. H. Gumus, Determination of Contact Angle from Contact Area of Liquid Droplet Spreading on Solid Substrate, Leonardo Electronic Journal of Practices and Technologies, 10 (2007) 29–38.

[233] K.S. Lee, N. Ivanova, V.M. Starov, N. Hilal, V. Dutschk, Kinetics of wetting and spreading by aqueous surfactant solutions, Advances in Colloid and Interface Science 144 (2008) 54–65.
[234] O. Dezellus, N. Eustathopoulos, Fundamental issues of reactive wetting by liquid metals, J. Mater. Sci., 45 (2010) 4256-4264.
[235] P.G. De Gennes, wetting statics and dynamics, Rev. Mod.phys., 57 (1985) 827-863.
[236] C. P. Saini, A. Barman, D. Das, B. Satpati, S. R. Bhattacharyya, D. Kanjilal, A. Ponomaryov, S.Zvyagin, A. Kanjilal, Role of Oxygen Vacancy on the Hydrophobic Behavior of TiO2 Nanorods on Chemically Etched Si Pyramids, J. Phys. Chem. C, 121 (2017) 278–283.
[237] Y. Xia, J. Chen, Z. Zhu, Q. Zhang, H. Yang, and Q. Wang, Significantly enhanced dielectric and hydrophobic properties of SiO_2 @MgO/PMMA composite films, *RSC* Adv., 8 (2018) 4032–4038.
[238] A. Pegoretti, A. Dorigato, M. Brugnara, and A. Penati, Contact angle measurements as a tool to investigate the filler-matrix interactions in polyurethane-clay nanocomposites from blocked prepolymer, *Eur. Polym. J.*, 44 (2008) 1662–1672.
[239] R.Pogreb, G. Whyman, R. Barayev, E. Bormashenko, D. Aurbach, A reliable method of manufacturing metallic hierarchical superhydrophobic surfaces, Appl. Phys. Let., 94 (2009) 221902-1-3.
[240] L. Huang, S. P. Lau, H. Y. Yang, E**.** S. P. Leong, S. F. Yu, Stable Superhydrophobic Surface via Carbon Nanotubes Coated with a ZnO Thin Film, J. Phys. Chem. B 109 (2005) 7746-7748.
[241] J. Rafiee, X. Mi, H. Gullapalli, A.V. Thomas, F.Yavari, Y.Shi, P.M. Ajayan, N. A.Koratkar, Wetting transparency of graphene, Nat. Mater. Lett. 11 (2012) 217-222.
[242] J. Bico, C. Marzolin, D. Quéré, Pearl drops, Europhyis. Lett. 47 (1999) 220- 226.
[243] J. Bico, C. Tordeux, D. Quéré, Rough wetting, Europhys. Lett. 55 (2001) 214–220.
[244] L. Feng, Y. Zhang, J. Xi, Y. Zhu, N.Wang, F. Xia, L. Jiang, Petal Effect: A Superhydrophobic State with High Adhesive Force, Langmuir, 24 (2008) 4114-4119.
[245] X. Chen, R. Ma, J. Li, C. Hao, W. Guo, B. L. Luk, S. C. Li, S.Yao, Z. Wang, Evaporation of Droplets on Superhydrophobic Surfaces: Surface Roughness and Small Droplet Size Effects, Phys. Rev. Lett.,109 (2012) 1-6.
[246] F.M. Fowkes, Determination of interfacial tensions contact angles and dispersion forces in surfaces by assuming additivity of intermolecular interactions in surfaces, J. Phys. Chem., 66 (1962) 382- 382.
[247] F.M. Fowkes, Attractives forces at interfaces, Ind. Eng. Chem., 56 (1964) 40-52.
[248] L.A. Girifalco, R.J. Good, A theory for the estimation of surface and interfacial energies. I. Derivation and application to interfacial tension, J. Phys.Chem., 61 (1957) 904-909.
[249] D. H. Kaelble, Dispersion-Polar Surface Tension Properties of Organic Solids, J. Adhesion, 2 (1970) 66-81.
[250] W. Rabel, Einige Aspekte der Benetzungstheorie und ihre Anwendung auf die Untersuchung und Veränderung der Oberflächeneigenschaften von Polymeren. In: Farbe und Lack, 77 (1971) 997-1005.
[251] B. J. Ryan and K. M. Poduska, Roughness effects on contact angle measurements, *Am. J. Phys.*, 76(2008)1074–1077.

[252] Uri Paz and Hillel Rubin, Surface Tension Observation in Distilled and Saline Water Interface, Ind. Eng. Chem. Fundamen. 9(1970) 509–511.
[253] F. M. Fowkes, Donor-acceptor interactions at interfaces, J. Adhes., 4 (1972) 155–159.

[254] J. Fortineau, E. Le Clézio, F. Vander Meulen, G. Feuillard, C. E. A. Le Ripault, and A. Samples, Moisture Content Characterization in Composite Materials based on Transmission Measurements, 114911 (2006), 232–235

[255] A. Maaroufi, O. Oabi, G. Pinto, M. Ouchetto, R. Benavente, J.M. Pereña, Electrical conductivity of new zinc phosphate glass/ metal composites, J. Non. Cryst. Solids. 358 (2012) 2764–2770.

[256] A. Celzard, Contribution à l'étude du phenomene de Percolation dans des materiauxcomposites à proprietes anisotropes, Thèse de doctorat l'Université Henri Poincaré,Nancy 1(1995).

[257] O. Oabi, Composites des Verres Binaires de Phosphates /Charges Métalliques : MO-P2O 5 (M = Zn , Ca)/(Ni , Co) Élaboration et Caractérisations Physico-chimiques pour des Applications Thermoélectriques, Thèse de doctorat, Faculté des Sciences, Université Mohammed V, Rabat (2017).

[258] A. Maaroufi, K. Haboubi, A. El Amarti, F. Carmona, Electrical resistivity of polymeric matrix loaded with nickel and cobalt powders, J. Mater. Sci. 39 (2004) 265-270.

[259] E. P. Mamunya, V. V. Davidenko, and E. V. Lebedev, Effect of polymer-filler interface interactions on percolation conductivity of thermoplastics filled with carbon black, Compos. Interface. 4 (1997) 169–176.

[260] C. Rajagopal, M. Satyam, Studies on electrical conductivity of insulator-conductor composites, J. Appl. Phys. 49 (1978) 5536-5542.

[261] S. Kirkpatrick, percolation and conduction Rev. Mod. Phys. 45 (1973) 574- 588.

[262] E.P. Mammunya, V. V. Davidenko and E. v. lebedev, Percolation Conductivity of Polymer Composites Filled With Dispersed Conductive Filler, Polym. Comp., 16 (1995) 319-324.

[263] M. Panda, V. Srinivas, A.K. Thakur, Non-universal scaling behavior of polymer- metal composites across the percolation threshold, Res. Phys. 5 (2015) 136–141.

[264] M.B. Heaney, Measurement and Interpretation of Nonuniversal Critical Exponents in Disordered Conductor–Insulator Composites, Phys. Rev. B. 52 (1995) 12477-12480.

[265] I. Balberg, Tunneling and Non universal Conductivity in Composite Materials, Phys. Rev. Lett. 59 (1987) 1305-1308.

[266] I. Balberg, Limits on the Continuum Percolation Transport Exponents, Phys. Rev. B. 57 (1998) 13351-13354.

[267] Z. Rubin, S.A. Sunshine, M.B. Heaney, I. Bloom, I. Balberg, Critical Behavior of the Electrical Transport Properties in a Tunneling Percolation System, Phys. Rev. B. 59 (1999) 12196-12199.

[268] S. Kirkpatrick, Percolation and conduction, Rev. Mod. Phys. 45 (1973) 574-588.

[269] F. Lux, Models proposed to explain the Electrical Conductivity of mixtures made of Conductive and Insulating Materials, J. Mater. Sci. 28 (1993) 285-301.

[270] D. Staufer, A. Aharony, Introduction to Percolation Theory, second edition, Taylor and Francis, Philadelphia, (Book,1994).

[271] F. Carmona, P. Prudhon, F. Barreau, Percolation in Short Fibres Epoxy Resin Composites: Conductivity Behavior and Finite Size Effects Near Threshold, Solid. State. Commun. 51 (1984) 255-257.

[272] N.R. Draper, H.Smith, Applied Regression Analysis, Third Edition. John Wiley & Sons, Inc. 1998.

[273] Y.N. Anisimov, L.P. Dobrova, A.Y. Anisimov, Conducting and Strength Properties of Composites Based on Modified Epoxy and Oligoester Resins Filled with Nickel, Russ. J. Appl. Chem. 71 (1998) 819-822.

[274] W.B. Genetti, W.L Yuan, B.P. Grady, E.A. O'rear, C.L. Lai, D.T. Glatzhofer, Polymer Matrix Composites: Conductivity Enhancement Through Polypyrrole Coating of Nickel Flake, J. Mater. Sci. 33 (1998) 3085-3093.

[275] A. Maaroufi, G. Pinto, I. Paz, Non-Linear Electrical Conductivity of Urea Formaldehyde Cellulose Loaded with Powders of Different Carbon Fillers, J. Appl. Polym. Sci. 98 (2005) 990-996.

[276] J.M. Montes, F.G. Cuevas, J. Cintas, Porosity effect on the electrical conductivity of sintered powder compacts, Appl. Phys. A92 (2008) 375-380.

[277] M. Ni, M.K.H. Leung, D.Y.C. Leung, K. Sumathy, An Analytical Study of the Porosity Effect on Dye-Sensitized Solar Cell Performance, Sol. Energy Mater. and Sol. Cells. 90 (2006) 1331–1344.

[278] M. L. Clingerman, Development and Modelling of Electrically Conductive Composite Materials, PhD Thesis,michigan technological university (1998).

[279] J. M. Keith, J. A. King, and B. A. Johnson, Electrical conductivity modeling of carbon filled polypropylene based resins for fuel cell bipolar plate applications, Journal of New Materials for Electrochemical Systems, 11(2008)253–257.

[280] A. Merzouki, N. Haddaoui,Electrical conductivity modeling of polypropylene composites filled with carbon black and acetylene black,ISRN Polym Sci,4(2012)1-7.

[281] A. Merzouki and N. Haddaoui, Electrical Conductivity Modeling of Polypropylene Composites Filled with Carbon Black and Acetylene Black,*ISRN Polym. Sci.* 2012(2012) 1–7.

[282] M. L. Clingerman, E. H. Weber, J. A. King, and K. H. Schulz, Development of an additive equation for predicting the electrical conductivity of carbon-filled composites, J. Appl. Polym. Sci., 88(2003)2280–2299.

[283] M. L. Clingerman, J. A. King, K. H. Schulz, and J. D. Meyers, Evaluation of Electrical Conductivity Models for Conductive Polymer Composites,(2002) 1341–1356.

[284] A. Šantić, A. Moguš-Milanković, D.E. Day, The dc electrical conductivity of iron phosphate glasses. J. Non-Cryst. Solids 296 (2001)65–73.

[285] J.Castillo, E.M.Materon, R.Castillo, R.A.Vargas, P.R.Bueno, J.A.Varela, Electrical relaxation in proton conductor composites based on $(NH_4)H_2PO_4/TiO_2$, Ionics, 15 (2009) 329–336.

[286] K.V. Ramesh, D.L. Sastry, Transport properties of ZnO substituted lead vanadate glass system at eutectic composition, Mater. Sci. Eng. B 126 (2006) 66-73.

[287] G.D. Khattak, a. Mekki, M.N. Siddiqui, Compositional dependence of DC electrical conductivity of SrO-vanadate glasses, Solid State Ionics. 211 (2012) 5-11.

[288] P. Nagels, in ″Amorphous semiconductors″, M.H. Brodsky, ed. Springer-Verlag (1986).

[289] Daefalla M.Tawati, M. Jamel Basha Adlan, Mat Johar Abdullah, DC electrical conductivity of semiconducting cobalt-phosphate glasses.J.Non-Cryst. Solids 357 (2011) 2152-2155.

[290] A. Maaroufi, O. Oabi, B. Lucas, A. El Amrani, and S.Degot, New composites of ZnO-P2O5/Ni having PTC transition and high Seebeck coefficient, J. Non-Cryst. Solids, 358(2012) 3312–3317.

[291] O.Oabi, a. Maaroufi, B. Lucas, S. Degot, and a. El Amrani, Positive temperature coefficient and high Seebeck coefficient in ZnO–P2O5/Co composites, J. Non. Cryst. Solids, 385(2014) 89–94.

[292] N. F. Mott, E. A. Davis, Electronic process in non-crystalline materials , Oxford, Clarendon Press (1971).

[293] N. F. Mott, Conduction and switching in non-crystalline materials, Contemp. Phys., 10(1969)125–138.

[294] I. G. Austin and N. F. Mott, Polarons in crystalline and non-crystalline materials, Adv. Phys. 50(2001) 757–812.
[295] J. S. Ashwajeet, T. Sankarappa, R. Ramanna, T. Sujatha, N. Nagaraja, and B. Vijayakumar, Electrical Conduction in Borophosphate Glasses Doped With CoO and Li2O, Res. J. Mater. Sci., 3(2015) 1–6.
[296] M. Rudra, S. Halder, S. Saha, A. Dutta, and T. P. Sinha, Temperature dependent conductivity mechanisms observed in Pr2NiTiO6, Mater. Chem. Phys., 3(2019) 1–21
[297] N. F. Mott, Conduction in non-crystalline systems, Philos. Mag., 17(1968) 1259–1268.
[298] B. Indrajit Sharma and A. Srinivasan, Electrical properties of V2O5-CaO-B2O 3 glasses exhibiting majority charge carrier reversal, Phys. Chem. Glas. Eur. J. Glas. Sci. Technol. Part B, 47(2006) 301–309.
[299] N. M. Shash and I. S. Ahmed, Structure and electrical properties of ZnO doped barium-metaphosphate glasses, Mater. Chem. Phys., 137(2013) 734–741.
[300] M. M. El-Desoky, I. Kashif, Electrical Conductivity in Mixed Calcium and Barium Iron Phosphate Glasses, Phys. Stat. Sol. (A) 194 (2002) 89-105.
[301] N.F. Mott, Philos. Mg., Conduction in non-crystalline materials,III. Localized states in a pseudogap and near extremities of conduction and valence bands19 (1969) 835-852
[302] F. K. Tan, J. Hassan, Z. A. Wahab, and R. S. Azis, Electrical conductivity and dielectric studies of MnO2 doped V2O5, Results Phys., 6(2016) 420–427.
[303] E. Asare, J. Evans, M. Newton, T. Peijs, and E. Bilotti, Effect of particle size and shape on positive temperature coefficient (PTC) of conductive polymer composites (CPC) - a model study, Mater. Des., 97(2016) 459–463.
[304] D. Bellucci, V. Cannillo, and A. Sola, Coefficient of thermal expansion of bioactive glasses: Available literature data and analytical equation estimates, Ceram. Int., 37(2011) 2963–2972,
[305] C. Dohare, M. M. A. Imran, and N. Mehta, Study of dielectric relaxation and thermally activated a.c. conduction in glassy Se70Te30and Se70Te28M2(M = Ag, Zn and Cd) alloys, J. Asian Ceram. Soc., 4(2016) 252–258.
[306] W. Heywang, Resistivity Anomaly in Doped Barium Titanate,J Am Ceram Soc, 47 (1964) 484-490.
[307] D.C. Sinclair, A.R. West, Use of Succinic Acid to Test the Stability of PTCR Barium Titanate Ceramics under Reducing Conditions, J Am Ceram Soc, 78 (1995) 241-244.
[308] M. Yethiraj, Pure and doped vanadium sesquioxide: A brief experimental review,J Solid State Chem, 88 (1990) 53-69.
[309] F. Bueche, Electrical resistivity of conducting particles in an insulating matrix, J Appl Phys, 43 (1972) *4837*-4838.
[310] R. Shrout, D. Moffatt, W. Huebner, Composite PTCR thermistors utilizing conducting borides, silicides, and carbide powders,J Mater Sci, 26 (1991) 145–154.
[311] T. Ota, I. Yamai, Positive-Temperature-Coefficient Effect in Graphite–Cristobalite Composites, J Am Ceram Soc, 75 (1992) 1772-1776.
[312] V.E. Gul, L.Z. Shenfil, G.K. Mel'nikova, N.L. Maslennikova, Temperature dependence of electrical conductivity of films prepared from epoxy resin with metallic fillers,Soviet Plastics, 4 (1967) 43-46.
[313] S. Littlewood, B.F.N. Briggs, Investigation of current-interruption by metal-filled epoxy resin, J Phys D Appl phys, 11 (1978) 1457-1462
[314] T. Kubo, J. Cha, H. Takebe, M. Kuwabara, Thermal properties and structure of zinc phosphate glasses, Phys Chem Glasses-B, 50 (2009) *15*-18.

[315] O. Zerzouf & A.Elmansouri,Elaboration et caractérisation des verres binaires :PbO-SiO2,PbO-B2O3,PbO-P2O5 et PbO-V2O5, rapport de stage ,université Mohammed V,Laboratoire de chimie de solide appliquée,1995-1996.

[316] Hun-Gi Jung, Yong Soo Kang, Yang-Kook Sun, Anatase TiO2 spheres with high surface area and mesoporous structure via a hydrothermal process for dye-sensitized solar cells, Electrochimica Acta 55 (2010) 4637–4641.

[317] Natalia Yantara, Nripan Mathews, K.B. Jinesh, Hemant Kumar Mulmudi, S.G. Mhaisalkar, Modulating the optical and electrical properties of all metal oxide solar cells through nanostructuring and ultrathin interfacial layers, Electrochimica Acta 85 (2012) 486– 491.

[318] Anatoli Korkin · Predrag S. Krsti´c · Jack C. Wells Ed., Nanotechnology for Electronics, Photonics, and Renewable Energy, Springer, 2010.

[319] Michael J.Pitkethly, Nanomaterials – the driving force, Mat.today. 7(2004)20-29.

[320] D. R. Kammler et al., Comparison of thin film and bulk forms of the transparent conducting oxide solution Cd1+xIn2-2xSnxO4, J. Appl. Phys.90 (2001) 5979–5985.

[321] W. Nolting and C. Santos, Ferromagnetic Kondo-lattice model: Application to thin ferromagnetic and semiconducting local moment films, Phys. Status Solidi Basic Res. 236(2003) 272–280,.

[322] N. D. Hoa, S. Y. An, N. Q. Dung, N. Van Quy, and D. Kim, Synthesis of p-type semiconducting cupric oxide thin films and their application to hydrogen detection, Sensors Actuators, B Chem.146 (2010) 239–244,.

[323] E. Lee and K. Park, Potential applications of nanoscale semiconductor quantum devices for information and telecommunications technologies, Mat. Sci. and Eng.B.74 (2000) 1–6.

[324] V. Pamukchieva, Z. Levi, and E. Savova, DC electrical conductivity in GexSb40- xS60 glasses and thin films, Semicond. Sci. Technol. 13(1998) 1309–1312.

[325] C. Jagadish and S. Pearton, Zinc Oxide Bulk, Thin Films and Nanostructures, (2006) Elsevier.

[326] Shriram Ramanathan Ed., Thin Film Metal-Oxides Fundamentals and Applications in Electronics and Energy, Springer, 2010.

[327] A. Boulouz, S. Chakraborty, A. Giani, F. Pascal Delannoy, A. Boyer, and J.Schumann, Transport properties of V-VI semiconducting thermoelectric BiSbTe alloy thin films and their application to micromodule Peltier devices, J. Appl. Phys.89(2001) 5009–5014.

[328] M.H. Brodsky, Ed., Amorphous semiconductors, Springer-Verlag, 1985.

[329] A. Klein, Y. Shigesato, and R. Martins, Advances in Transparent Electronics, Phys. Status Solidi Appl. Mater. Sci.214 (2017) 1770112.

[330] E. Fortunato, D. Ginley, H. Hosono, and D. C. Paine, Transparent Conducting Oxides for Photovoltaics, MRS Bull., 32(2007) 242–247.

[331] J. P. Chu et al., Thin film metallic glasses: Unique properties and potential applications, Thin Solid Films, 520(2012) 5097–5122.

[332] M. C. RAO and M. S. Shekhawat, a Brief Survey on Basic Properties of Thin Films for Device Application, Int. J. Mod. Phys. Conf. Ser.22(2013) 576–582.

[333] M.M.Wakkad et al., Optical and electrical properties of Sn-Sb-Se chalcogenide thin films, Eur. Phys. J. Appl. Phys. 43(2008) 23–30.

[334] N. G. Park and K. Kim, Transparent solar cells based on dye-sensitized nanocrystalline semiconductors, Phys. Status Solidi Appl. Mater. Sci., 205(2008) 1895–1904.

[335] M. Ito et al., Amorphous oxide TFT and their applications in electrophoretic displays, Phys. Status Solidi Appl. Mater. Sci., 205(2008)1885–1894.

[336] J. Clatot, G. Campet, A. Zeinert, C. Labrugère, M. Nistor, and A. Rougier, Low temperature Si doped ZnO thin films for transparent conducting oxides, Solar Energy Materials and Solar Cells, 95(2011) 2357–2362.
[337] M. P. Taylor et al., The remarkable thermal stability of amorphous In-Zn-O transparent conductors, Adv. Funct. Mater. 18(2008)3169–3178.
[338] J. Hautala and P. C. Taylor, A review of optical properties of metal chalcogenide glasses, J. Non. Cryst. Solids, 141(1992)24–34.
[339] A. Facchetti and T. J. Marks, Transparent Electronics: From Synthesis to Applications, In book: Transparent Electronics (2010)299-323.
[340] Kotipalli, R., M. Zhukova and D. Flandre. Thin-film solar cells based on chalcogenide (CIGS) and kesterite (CZTS) quaternary semiconducting compounds. (2017).
[341] T. Minami, Transparent conducting oxide semiconductors for transparent electrodes, Semiconductor Science and Technology, 20 (2005)35–44.
[342] W. M. Kim et al., The electromagnetic interference shielding effect of indium-zinc oxide/silver alloy multilayered thin films, Thin Solid Films, 473(2005) 315–320.
[343] D. B. Buchholz, J. Liu, T. J. Marks, M. Zhang, and R. P. H. Chang, Control and characterization of the structural, electrical, and optical properties of amorphous zinc-indium-tin oxide thin films, ACS Applied Materials & Interfaces,1(2009) 2147–2153.
[344] C. G. Granqvist, Transparent conductors as solar energy materials: a panoramic review, Solar Energy Materials and Solar Cells, vol. 91, no. 17, pp. 1529–1598, 2007.
[345] V. S. Shiryaev and M. F. Churbanov, Part I: Preparation and properties of chalcogenide, chalcogenide glasses. In book: Chalcogenide Glasses (2013)3-35
[346] Y. Tveryanovichb and Y. Vlasovb, Ion Conductivity and Sensors (Book,2004)
[347] A. Bornstein, N. Croitoru, and E. Marom, Chalcogenide infrared As 2_ xSe3+ x glass fibers ,J.noncrystalline sol.,74(1985)57–65.
[348] Hongtao Lin, Chalcogenide glass mid-infrared on chip sensor for chemical sensing. A dissertation submitted to the University of Delaware in partial fulfillment of the requirements for the degree of Doctor of Philosophy in Materials Science, 2015.
[349] C. Paper and B. Ambed, Scope of chalcogenide glasses in emerging science &technology[Review Article],Published inI nternational Conference on Advances in Engineering Science and Management, Agra, 08th November, 2015.
[350] P. K. Singh and D. K. Dwivedi, Chalcogenide glass: Fabrication techniques, properties and applications, Ferroelectrics, 520 (2017)256–273.
[351] K. Homma, H. K. Henisch, and S. R. Ovshinsky, New experiments on threshold switching in chalcogenide and non-chalcogenide alloys, J. Non. Cryst. Solids, 35–36, (1980)1105–1110.
[352] S. A. Fayek, M. H. El Fouly, H. H. Amer, A. H. Amar, and M. M. El Ocker, Electrical conductivity of amorphous semiconducting films of system (Ge20As30Se50-xTex), Solid State Commun.93 (1995)213–217.
[353] A. V Priezzhev, G. L. Cote, S. Bockle, L. Rovati, and R. R. Ansari, Proceedings of the Society of Photo-Optical Instrumentation Engineers (Spie), Opt. Diagnostics Sens. Biomed. Iii, 4965(2014) 116–121.
[354] F. Demichelis, G. Kaniadakis, A. Tagliaferro, and E. Tresso, New approach to optical analysis of absorbing thin solid films, Appl. Opt., 26(1987)1737.
[355] N. F. Mott and E. A. Davis, Electronic processes in Non-Crystalline Materials(1979).
[356] A. B. Seddon, Chalcogenide glasses: a review of their preparation, properties and applications, J. Non. Cryst. Solids, 184(1995)44–50.
[357] K. Nomura, H. Ohta, A. Takagi, T. Kamiya, M. Hirano, and H. Hosono, Room-temperature fabrication of transparent flexible thin-film transistors using amorphous oxide semiconductors, Nature, 432(2004)488–492.

[358] D. B. Buchholz, L. Zeng, M. J. Bedzyk, and R. P. H. Chang, Differences between amorphous indium oxide thin films, Prog. Nat. Sci. Mater. Int.23(2013)475–480.
[359] A. A. Volinsky, J. B. Vella, and W. W. Gerberich, Fracture toughness, adhesion and mechanical properties of low-K dielectric thin films measured by nanoindentation, Thin Solid Films,429(2003)201–210.
[360] R. D. Evans, G. L. Doll, P. W. Morrison, J. Bentley, K. L. More, and J. T. Glass, The effects of structure, composition, and chemical bonding on the mechanical properties of Si-aC : H thin films, Surf. Coatings Technol., 157(2002)197–206.
[361] F. U. Hamelmann, Transparent Conductive Oxides in Thin Film Photovoltaics, J. Phys. Conf. Ser., 559(2014).
[362] M. Hammi and A. Maaroufi.On optical properties of phosphate glass thin films, Mater. Lett. 182(2016) 227–230.
[363] M. Hammi, G.Aziate, G. Pinto, A.Maaroufi, Electrical and Thermoelectrical Behavior of Binary Composites of Phosphate Glass Loaded with Zinc Fillers: Promising Materials for Photovoltaic's, Journal of the Chinese chemical Society 62 (2015) 1035-1044.
[364] J.R.Bellingham, W.A.Phillips, C.J.Adkins, Electrical and optical properties of amorphous indium oxide, Journal of Physics: Condensed Matter 2 (1990) 6207–6221.
[365] C. Malibert and S. Bach, Elaboration and characterization of thin films of TiO 2 prepared by sol – gel process, 418 (2002)79–84.
[366] L. Znaidi, Sol-gel-deposited ZnO thin films: A review, Mater. Sci. Eng. B Solid-State Mater. Adv. Technol. 174(2010) 18–30.
[367] T. H. Ioki, M. A. Kiyama, T. U. Eda, Y. O. Nozuka, and K. S. Uzuki, Preparation of Pb (Zr , Ti)O_3 Thin Films by Plasma-Assisted Sputtering, 38(1999)5375–5377.
[368] G. V Ramesh, S. Porel, and T. P. Radhakrishnan, Polymer thin films embedded with in situ grown metal nanoparticles 38(2009) 2646-2656.
[369] Y.-K. Tseng, F.-M. Pai, Y.-C. Chen and C.-H. Wu, Effects of UV assistance on the properties of al-doped ZnO thin films deposited by sol-gel method, Electron. Mater. Lett. 9(2013)771–773.
[370] E. Szalkowska, J. Gluszek, and J. Masalski, Structure and protective properties of TiO2 coatings obtained using the sol-gel technique, J. Mater. (2001) 495–497.
[371] D. Fang, P. Yao, and H. Li, Influence of annealing temperature on the structural and optical properties of Mg-Al co-doped ZnO thin films prepared via sol-gel method, Ceram. Int., 40(2014)5873–5880.
[372] N. Ren, Z. Liu, and Q. Wang, Investigating the effects of microstructure on optical properties of different kinds of polysilicon thin films, Phys. Lett. Sect. A Gen. At. Solid State Phys., 379(2015)1153–1160.
[373] G.KWilliamson,W.HHall, X-ray line broadening from filed aluminium and wolfram Acta Metallurgica,1 (1953) 22-31.
[374] M. Azeem, A. Abdelkrim, and M. Rosario, Kinetics of the thermal degradation mechanisms in urea- formaldehyde cellulose composites filled with zinc particles,*J. Mater. Sci. Mater. Electron.*, 28(2017)11832–11845.
[375] R. Fleming, Nickel-induced crystallization of amorphous silicon, Doctoral thesis, University of Arkansas, Fayetteville (2009).
[376] Ligang Ma Effect of substrate and Zn doping on the structural, optical and electrical properties of CdS thin films prepared by CBD method J. Alloys Compd. 691(2016)
[377] Grdadolnik, ATR-FTIR spectroscopy : Its advantages and limitations, Acta Chim. Slov. 49(2002) 631-642.
[378] M. Abid, A. Shaim, M. Et-tabirou, Glass-forming region and electrical properties of Li_2O–PbO–P_2O_5 glasses, Mater. Res. Bull. 36 (2001) 2453–2461.

[379] S.S. Das, N.P. Sing, Vibha Srivastava, P.K. Strivastava, Role of Fe, Mn, and Zn ions as dopants on the electrical conductivity behavior of sodium phosphate glass, Ionics,14 (2008) 563-568.

[380] Michael I. Ojovan, Viscosity and Glass Transition in Amorphous Oxides, *Advances in Condensed Matter Physics*, Article ID 817829(2008) 23.

[381] P. Y. Shih, S. W. Yung, and T. S. Chin, Thermal and corrosion behavior of P_2O_5-Na_2O-CuO glasses, J. Non. Cryst. Solids. 224 (1998)143–152.

[382] K. Meyer, A. Barz, and D. Stachel, Effects of atmospheric humidity on the infrared reflectivity of vitreous P205 and ultraphosphate glasses, J. Non. Cryst. Solids.191 (1995) 71–78.

[383] V. Dimitrov, Y. Dimitriev, Structure of glasses in PbO-V_2O_5 system, J. Non. Cryst. Solids. 122 (1990)133–138.

[384] M. Ganguli, K. J. Rao, Structural Role of PbO in Li2O–PbO–B_2O_3 Glasses, J. Solid State Chem., 145 (1999) 65-67.

[385] N. H. Ray, Structure and Properties of Inorganic Polymeric Phosphates., Br. Polym. J. 11 (1979) 163–177.

[386] J. Franke, T. Niemczyk, and H. DM, Infrared spectroscopic techniques for quantitative characterization of dielectric thin films on silicon wafers, Part A Mol. Spectrosc., 50(1994) 1687–1723.

[387] K. EL Igili, H. Doweidar, Y.M. Mostafa, I. Abbas, Structure and some physical properties of PbO-P_2O_5 glasses, Physica B. 339 (2003) 237-245.

[388] C. Dayanand, G. Bhikshamaiah, V. Jayatyagaraju, M. Salagram, Structural investigations of phosphate glasses: a detailed infrared study of the x (PbO)-(1- x) P_2O_5, vitreous system, J. Mater. Sci. 31 (1996) 1945 - 1967.

[389] Films: doping effect, microstructure and electrical property, J.Sol-GelTechnol, 49 (2009)238-242.

[390] M. R. Ahsan, M. A. Uddin, and M. G. Mortuza, Infrared study of the effect of P_2O_5 in the structure of lead silicate glasses, Indian J. pure Appl. Phys.43 (2005) 89–99.

[391] V. N. Rai, B. N. R. Sekhar, D. M. Phase, and S. K. Deb, Effect of gamma irradiaton on the structure and valence state of Nd In phosphate glass. J. Lumin .130 (2010) 582–586

[392] J. Hong, M. K. Park, E. J. Lee, D. Lee, D. S. Hwang, and S. Ryu, Origin of new broad raman D and G Peaks in annealed graphene, Sci. Rep.3(2013)1–5.

[393] Z. Jehl et al., Insights on the influence of surface roughness on photovoltaic properties of state of the art copper indium gallium diselenide thin films solar cells, J. Appl. Phys.111 (2012).

[394] K. Roumaih, M. Kaiser, F. H. Elbatal, and I. S. Ali, Transport properties of lead phosphate glass doped by cobalt, vanadium and chromium oxides, Phil. Mag., 91(2011) 3830–3843.

[395] M. Peng and L. Wondraczek, Bismuth-doped oxide glasses as potential solar spectral converters and concentrators, J. Mater. Chem., 19(2009)627–630.

[396] K. Sasaki, H. Takahashi, Y. Kudo, and N. Suzuki, Determining the absorption coefficient of absorbing thin films with optical waveguides. Appl. Opt., 19 (1980) 3018–3021.

[397] S. A. Aly, influence of film thickness on optical absorption and energy gap of thermally evaporated $CdS_{0.1}Se_{0.9}$ thin films, Chalcogenide lett.12(2015) 489–496.

[398] Alan E Owe Electronic and Optical Properties of Amorphous Semiconductors : Their Principles and Applications, Doctoral thesis,University of Edinburgh-UK (1994).

[399] Fridman, Optical Properties and Electronic Structure of Amorphous Germanium, Phys. Status Solidi, 15(1966) 627–637,

[400] Tom Markvart ,LuisCastañer ,Chapter I-1-B - Semiconductor Materials and Modeling,McEvoy's Handbook of Photovoltaics (Third Edition).(2018) 29-57.

[401] N. Boumedienne, A. Maaroufi, Structural and opto-electronic properties of epoxy/silver nanocomposite films, Phys. B 578 (2020) 411853.
[402] J. Tauc, A. Menth, States in the gap, J.Non-Cryst. Solids,10 (1972) 569-585.
[403] Y. M. Galperin, V. G. Karpov, and V. I. Kozub, Localized states in glasses, Adv. Phys. 38(1989) 669–737.
[404] Khawla S. khashan, Jehan A. Saimon , Azhar I. Hassan Optical Properties of CUO Thin Films with Different Concentration by Spray Pyrolysis Method. Eng. &Tech.Journal, 32(2014)86-93
[405] Morigaki K., Ogihara C. (2017) Amorphous Semiconductors: Structure, Optical, and Electrical Properties. In: Kasap S., Capper P. (eds) Springer Handbook of Electronic and Photonic Materials. Springer Handbooks. Springer, Cham.
[406] N. M. Abdul-Ameer and M. C. Abdulrida, Direct Optical Energy Gap in Amorphous Silicon Quantum Dots, J. Mod. Phys.2 (2011)1530–1537.
[407] F. Wooten, Optical properties of solids, Academic Press, New York and London, 1972.
[408] AZakery and S.Elliott, An Introduction to Chalcogenide Glasses, Opt. nonlinearities chalcogenide Glas. Their Appl., (2007)92.
[409] L.K. Yu, H.J. Jae, H.K. Kyung, S.Y. Hyun, S.S. Man, H.B. Se, K. Yong, Nanotechnology 20 (2009) 095605.
[410] J. Tauc, Amorphous and Liquid Semiconductors, New York. Plenum (1974).
[411] K.A. Aly, A.M. Abd Elnaeim, N. Afify, A.M. Abousehly, Improvement of the electrical properties of Se3Te1 thin films by In additions, J.Non-Cryst. Solids 358 (2012) 2759-2763.
[412] H, FRITZSCHE, Optical and electrical energy gaps in amorphous semiconductors, J.Non Cryst. Solids, 6 (1971) 49—71
[413] N. F. Mott, E. A. Davis: Electronic Processes in Noncrystalline Materials, 2nd ed. (Clarendon, Oxford1979)
[414] P.G.LeComber,W.E.Spear,G.Müller,S.Kalbitzer ,Electricalandphotoconductive properties of ion implanted amorphous silicon, 356(1980)327-332
[415] Michelle M. Paquette , Bradley J. Nordell, Anthony N. Caruso, Masanori Sato, Hiroyuki Fujiwara and Sean W. King, Optimization of amorphous semiconductors and low-/high-k dielectrics through percolation and topological constraint theory, MRSBulletin, 42 (2017)39-44.
[416] I. P. Studenyak, M. V Kurik, and M. Kranjc, On the Urbach rule in non-crystalline solids, 355 (2009) 54–57.
[417] F. Urbach, The long-wavelength edge of photographic sensitivity and of the electronic absorption of solids, Phys. Rev. 92 (1953) 1324--1324
[418] S.A. Fayek and Maged A.F., Optical Absorption of. Glasses in the system (As2Se3)1-XTIX, Materials Science &. Engineering B 32 (1995) 47-49. U.K.
[419] C. Manifacier, D. M. Murcia, J. P. Fillard, E. Vicario, Optical and electrical properties of SnO2 thin films in relation to their stoichiometric deviation and their crystalline structure, Thin solid films 41 (1977) 127-135.
[420] R. Swanepoel, Determination of the thickness and optical constants of amorphous silicon, J. Phys. E: Sci. Instrum. 16 (1983) 1214-1222.
[421] M. R. Nenkov and T. G. Pencheva, Determination of thin film refractive index and thickness by means of film phase thickness, Cent. Eur. J. Phys., 6(2008)332–343.
[422] P. S. Nikam, R. Y. Borse, R. R. Pawar, Composition dependence of electrical properties of Al-Sb thin films, Bull. Mater. Sci.20 (1997)1015–1021
[423] Dong Jin Kim et al., Influence of calcination temperature on structural and optical properties of TiO2 thin films prepared by sol–gel dip coating, Materials Letters 57 (2002) 355– 360

[424] Y. Singh, Electrical resistivity measurements:A Review, International Journal of Modern Physics: Conference Series 22 (2013) 745–756

[425] J. Domaradzki, D. Kaczmarek, K. Drabczyk, and P. Panek, Investigations of electrical and optical properties of functional TCO thin films, Mater. Sci. Pol., 33(2015)363–368.

[426] E. Burstein, Anomalous optical absorption limit in InSb, Lett. Editor 93 (1953) 632-633.

[427] T. S. Moss, The interpretation of the properties of indium antimonide, Proc. Phys. Soc. 76 (1954) 755-782.

[428] Sylvie FAŸ, L'oxyde de zinc par dépôt chimique en phase vapeur comme contact électrique transparent et diffuseur de lumière pour les cellules solaires, Ecole polytechnique Fédérale de Lausanne (EPFL), Thèse n0 2899, 2003.

[429] D. B. Fraser and H. D. Cook, Highly Conductive, Transparent Films of Sputtered In_{2-x} Sn x O_{3-y}, J. Electrochem. Soc. 119(1972) *1368*–1374.

[430] G. Haacke, New figure of merit for transparent conductors, Appl. Phys. 47 (1976) *4086*-4089

[431] O.S. Heavens, Optical Properties of Thin Solid Films, Dover, NY, (1965)113.

[432] R. G. Gordon, Criteria for Choosing Transparent Conductors, MRS Bulletin, (2000) 52-57.

[433] N. F. Mott, E. A. Davis, Electronic process in non-crystalline materials, Oxford, Clarendon Press (1971).

[434] Ahmed MISRAR, Jean-Marc SAITER and Claude VAUTIER Dark conductivity or amorphous Ge0.08Te0.92 thin films. J.Non-Cryst. Solids.97&98 (1987) 671-674.

[435] P. Nagels, in ″Amorphous semiconductors″, M.H. Brodsky, ed. Springer-Verlag (1986).

[436] A. Šantić, A. Moguš-Milanković, D.E. Day, The dc electrical conductivity of iron phosphate glasses. J. Non-Cryst. Solids 296 (2001) 65–73.

[437] Daefalla M.Tawati, M. Jamel Basha Adlan, Mat Johar Abdullah, DC electrical conductivity of semiconducting cobalt-phosphate glasses.J.Non-Cryst. Solids 357 (2011) 2152-2155.

[438] A. Maaroufi, O. Oabi, B. Lucas, A. El Amrani, S. DEGOT, New Composites of ZnO-P_2O_5/Ni Having PTC Transition and High Seebeck Coefficient, J.Non-Cryst. Solids, 358 (2012) 3312–3317.

[439] O. Oabi, A. Maaroufi, B. Lucas, S. DEGOT, A. El Amrani, Positive Temperature Coefficient and High Seebeck Coefficient in ZnO-P_2O_5/Co Composites, J.Non-Cryst. Solids, 385 (2014) 89-94.

[440] Adler, D., Yoffa, E. Electronic Structure of Amorphous Semiconductors J., Phys. Rev. Lett. 36 (1976) 1197-1200.

[441] E. Properties *et al.*, Optical and Electrical Properties of the Ge_{10} In, Egypt. J. Phys. 45(2017)39–47.

[442] andey,V. , Tripathi, S.K. and Kumar, Effect of In incorporation on optical properties of amorphous Se–Ge thin films,A Physica B:Condensed Matter, 388(2007)200-205 .

[443] A. Sharma and P. B. Barman, Transport properties of amorphous Ge 20 Te 80-x Bi x glassy alloys,*Phys. Procedia*, 32(2012) 144–151.

[444] J.W. Cook and G.N. Parsons and C. Kusano and G. Lucovsky, Bonding defects in amorphous silicon alloys, Solar Cells, 21(1987) 387 – 397.

[445] ütten, M., Kaes, M., Albert, A. *et al.* Relation between bandgap and resistance drift in amorphous phase change materials. *Sci Rep* **5** (2015)1736

[446] Ben Minnaert and Peter Veelaert, A Proposal for Typical Artificial Light Sources for the Characterization of Indoor Photovoltaic Applications, Energies, 7(2014)1500-1516.
[447] Green, Martin A., *Solar Cells: Operating Principles, Technology, and System Applications*. Englewood Cliffs, NJ: Prentice-Hall, 1982.
[448] M. Zeman, Introduction to photovoltaic solar energy, Delft University of Technology, (2014).
[449] William Shockley and Hans J.Queisser Detailed balance limit of efficiency of P-N junction solar cells, J.Appl.Phys.32 (1961) 510-51.
[450] Koster, L. J. A., Origin of the light intensity dependence of the short-circuit current of polymer/fullerene solar cells, Appl. Phys. Lett.87 (2005) 2035021–20350214
[451] C. Chen, D. C. Bobela, Y. Yang, S. Lu, K. Zeng, C. Ge, B. Yang, L. Gao, Y. Zhao, and M. C. Beard, Characterization of basic physical properties of Sb_2Se_3 and its relevance for photovoltaics,Front, Optoelectron, 10(2017)18–30.
[452] Zhang, X. et al. Chalcogenide glass-ceramic with self-organized heterojunctions : application to photovoltaic solar cells, EPJ Photovolt, 3(2018) 1–6.
[453] M. Salmi. Contribution à la quantification de l'irradiation solaire globale en Algérie et applications aux générateurs photovoltaïques. Thèse de doctorat, Université de Sétif (2012).
[454] Karzazi, Y. & Arbouch, I. Inorganic photovoltaic cells : Operating principles, technologies and efficiencies - Review. JMES,5(2014) 1505–1515.
[455] M. Taguchi *et al*., 24.7% Record Efficiency HIT Solar Cell on Thin Silicon Wafer, in *IEEE Journal of Photovoltaics*, 4(2014) 96-99.
[456] W.G. J. H. M. van Sark et al.(Eds.) Physics and Technology of Amorphous-Crystalline Heterostructure Silicon Solar Cells. Springer-Verlag Berlin Heidelberg 2012.
[457] Ahmed Msrar, Jean-Marc saitier and Claude vautier, Dark conductivity or amorphous Ge0.08Te0.92 Thin films, J. Non-Cryst. Solids.98(1987)671–674.
[458] W. Ma, C. Yang, X. Gong, K. Lee and A. J. Heeger, Thermally Stable, Efficient Polymer Solar Cell with Nanoscale Control of the Interpenetrating Network Morphology, Adv. Funct. Mater. 15 (2005)1617-1662.
[459] G. Li, V. Shrotriya, J. Huang, Y. Yao, T. Moriaty, K. Emery and Y. Yang, High-efficiency solution processable polymer photovoltaic cells by self-organization of polymer blends, Nat.Mater. 4 (2005) 864-868.
[460] J. Y. Kim, K. Lee, N. E. CD. Moses, T.-Q. Nguyen, M. Dante and A. J. Heeger, Efficient Tandem Polymer Solar Cells Fabricated by All Solution Processing, Science 317 (2007) 222-225.
[461] M.-S. Kim, M.-G. Kang, L. J. Guo and J. Kim, Choice of electrode geometry for accurate measurement of organic photovoltaic cell performance, Appl. Phys. Lett. 92 (2008)133301-133303.
[462] W.-J. Yoon and P. R. Berger, 4.8% efficient poly (3-hexylthiophene)- fullerene derivative (1:0.8) bulk heterojunction photovoltaic devices with plasma treated AgO_x/indium tin oxide anode modification, Appl. Phys. Lett. 92 (2008)13306-13308.
[463] A. Cravino, P. Schilinsky and C. J. Brabec, Characterization of Organic Solar Cells: the Importance of Device Layout, Adv. Funct. Mater. 17 (2007)3906-3910.
[464] Irwin MD, Buchholz DB, Hains AW, Chang RPH, Marks TJ. *p*-Type semiconducting nickel oxide as an efficiency-enhancing anode interfacial layer in polymer bulk-heterojunction solar cells. *Proc Natl Acad Sci U S A*. 105(2008)2783-2787.
[465] Y. Lee, S. T. Connor, Y. Cui, and P. Peumans, Solution-Processed Mesh Transparent Electrodes, Nano Lett. 8 (2008) 689-692.

[466] A. Gadisa, K. Tvingstedt, S. Admassie, L. Lindell, X. Crispin, M. R. Anderson, W. R. Salaneck, and O. Inganas, Transparent polymer cathode for organic photovoltaic devices , Synth. Met. 156 (2006)1102- 1107.

[467] T. Aernouts, P. Vanlaeke, W. Geens, J. Poortmans, P. Heremans, S. Borghs, R. Mertens, R. Andriessen, and L. Leenders, Printable anodes for flexible organic solar cell modules , Thin Solid Films 451-452 (2004) 22-25.

[468] K. Tvingstedt and O. Inganas, Electrode Grids for ITO-free Organic ¨ Photovoltaic Devices, Adv. Mater. 19 (2007)2893-2897.

Résumé

Le but de cette thèse est la valorisation éminente des matériaux phosphatés dans le secteur énergétique. Ainsi, des verres à base de phosphate de plomb (PbP) : $PbO\text{-}P_2O_5$ chargés de particules conductrices (Ni, Co, Cr et Zn) ont été élaborés sous forme massive et en couches minces, en utilisant respectivement la technique de trempe et la voie sol-gel.

Pour les composites massives, les propriétés structurales et thermiques ont été étudiées par les mesures de la densité, la diffraction des rayons X (DRX), la microscopie électronique à balayage (MEB), l'analyse calorimétrique différentielle (DSC) et l'angle de contact.

Ensuite, l'évolution de la conductivité électrique en fonction de la charge à l'ambiante a été interprétée par la théorie de la percolation. Les mesures de la conductivité électrique en fonction de la température ($300 \leq T \leq 715$ K) ont été entreprises au-dessus du seuil de percolation indiquant une transition de phase conducteur-isolant, nommée Coefficient de Température Positif (PTC). Enfin un comportement semi-conducteur a été décelé en dessous du seuil de percolation, montrant ainsi des mécanismes de conduction multiples, interprétés par la théorie des polarons à haute température et celle de VRH de Mott (Mott's variable range hopping theory) à basse température.

Les films obtenus ont été caractérisés par DRX, MEB-EDAX, UV-visible et des mesures de résistivité respectivement. De plus, la résistivité électrique des couches minces semi-conductrices a été mesurée en fonction de la température. Tous les résultats ont été décrits en détail et ils ont indiqué que les couches minces préparées dans cette étude sont utiles dans le domaine optoélectronique.

Mots clés : composites ; verres de phosphate ; couches minces ; structure ; optoélectronique ; conductivité électrique ; Angle de contact ; percolation ; PTC ; Polarons ; VRH theory.

Abstract

The aim of this thesis is the eminent valorization of phosphate materials in the energy sector. Thus, lead phosphate glasses ($PbO\text{-}P_2O_5$) filled with conductive particles (Ni, Co, Cr and Zn) were elaborated in bulk and thin film forms, using melt quenching technique and low cost sol gel technique, respectively.

For bulk forms, the structural and thermal properties of the elaborated composites have been studied by density measurements, X-ray diffraction technique (XRD), scanning electron microscopy (SEM) and differential scanning calorimetry (DSC) analysis. Afterward, the electrical conductivity as function of filler content at room temperature were investigated and have been interpreted on the basis of percolation theory framework, the outcomes related to percolative models were assessed by surface analysis trough the calculation of composites' surfaces tension via contact angle measurements.

The electrical conductivity temperature dependence ($300 \leq T \leq 715$K) was undertaken on heating and cooling above the percolation threshold indicating a Positive Temperature Coefficient (PTC). Furthermore, bellow percolation threshold, a semiconducting behavior is fairly discussed in Mott's Variable Range Hopping (VRH) mechanism theory frame. The thin film forms composites were elaborated by filling the matrix with conducting particles ranging from 0 wt % - 16wt %. Then, the effect of fillers on structural, morphological, optical and electrical properties of glass thin films were evaluated by XRD, SEM-EDAX, UV-VIS and DC electrical resistivity measurements respectively. Moreover, electrical resistivity of the semiconducting thin films was measured versus temperature. Taking into account the dc resistivity depending on the concentration of free carriers and the absorption coefficient, the figure of merit was calculated.

All results were described in details and they indicated that the films prepared in this study could be useful for opto-electronic applications.

Key words: composites; phosphate glasses; thin film; structure; opto-electronic; electrical conductivity; contact angle; percolation; PTC; Polarons; VRH theory.

Academic year : 2019-2020